Laboratory Characterization of a Highly Weathered Old Alluvium in San Juan, Puerto Rico

by

Guoping Zhang

B.Eng., Hydraulic and Hydropower Engineering
B.Eng., Precision Instruments and Mechanology
Tsinghua University, China
(1991)

M.Eng., Geotechnical Engineering
Tsinghua University, China
(1994)

Submitted to the
Department of Civil and Environmental Engineering
in Partial Fulfillment of the Requirements for the Degree of

Doctor of Philosophy in Geotechnical and Geoenvironmental Engineering

at the

MASSACHUSETTS INSTITUTE OF TECHNOLOGY

February 2002

Signature of Author: _____
Department of Civil and Environmental Engineering
January 19, 2002

Certified by: _____
Dr. John T. Germaine, Thesis Co-supervisor

Certified by: _____
Professor Andrew J. Whittle, Thesis Co-supervisor

Accepted by _____
Professor Oral Buyukozturk
Chairman, Departmental Committee on Graduate Studies

Laboratory Characterization of a Highly Weathered Old Alluvium in San Juan, Puerto Rico

by
Guoping Zhang

Submitted to the Department of Civil and Environmental Engineering on January 19, 2002
in Partial Fulfillment of the Requirements for the Degree of
Doctor of Philosophy in Geotechnical and Geoenvironmental Engineering

ABSTRACT

The *old alluvium* underlying much of metropolitan San Juan was formed in early Pleistocene and has undergone substantial post-depositional weathering in the tropical climate of Puerto Rico, resulting in a special combination of soil mineralogy and structure, with very unusual engineering properties.

The soil mineralogy was determined both qualitatively and quantitatively by a series of analytical techniques, consisting of X-ray diffraction, thermal analysis, X-ray fluorescence, and chemical analyses including cation exchange capacity (CEC), soil pH, and selective chemical dissolutions (SCD). Results show that the old alluvium contains: (1) two most weathering resistant primary minerals: quartz and orthoclase; (2) kaolinite and smectites as major clay minerals; and (3) Fe-oxides (goethite and hematite) as special fine-grained minerals, which give the soil distinct red, brown, and yellow coloration. The subsequent quantitative analysis yields high accuracy results, such that the identified mineral phases account for 94-95% of the bulk material.

Characterization of soil microstructure also used a variety of techniques including environmental scanning electron microscope (ESEM), slaking tests, CEC, and SCD of Fe-oxides. The results reveal an aggregate structure comprising groups of clay platelets, which each consist of clay particles associated with face-to-face contact. Cementation and aggregation agents are positively identified by SCD as Fe-oxides, which form coatings over clay platelets and aggregates, and bridge bonding between aggregates. These results were confirmed by slake tests in water and glycerol.

Index properties vary due to the microstructure. Particle size distribution and Atterberg limits are affected by remolding energy and drying conditions, resulting in difficulties for soil classification. The combination of mineralogy and structure, cause the consolidation behavior to differ from conventional sedimentary soil behavior in the following aspects: (1) the coefficient of consolidation decreases by four orders of magnitude as the sample is compressed to 300ksc; (2) the swelling strains increase significantly with maximum past consolidation pressure; (3) the intact soil exhibits an exceptionally high yield stress ($\sigma_y \approx$ 8ksc); and (4) vertical consolidation strains can be completely recovered upon unloading when samples are pre-loaded above the yield stress. Triaxial compression and extension shear tests on intact samples suggest that the intact shear strength can be described by a conventional Mohr-Coulomb criterion with an isotropic cohesive strength component. The current conceptual models of microstructure offer a framework for developing realistic constitutive models to describe the complex mechanical behavior of this complex residual soil.

Thesis Co-Supervisor: Dr. John T. Germaine
Title: Principal Research Associate in Civil and Environmental Engineering

Thesis Co-Supervisor: Professor Andrew J. Whittle
Title: Professor of Civil and Environmental Engineering

ACKNOWLEDGEMENTS

This work was supported by the KKZ/CMA Consortium in conjunction with the underground construction of Tren Urbano in Rio Piedras, Puerto Rico.

First of all, I am greatly indebted to my thesis committee members:

Dr. John T. Germaine, my thesis supervisor, always brought me superior intellectual challenges and genius ideas, and enlightened me to continue the research in new directions. Everyone in the laboratory knows he has a large pool of knowledge. He has been a mentor for me for the last 5.5 years.

Professor Andrew J. Whittle, my thesis co-supervisor, provided me his brilliant advice on the interpretation of experimental results and his intuition on soil modeling. His constructive comments and encouragement are very valuable to the completion of this thesis.

Professor Charles C. Ladd offered me invaluable scientific knowledge on soil behavior. It is my great honor to have him in my thesis committee and to be able to receive his enthusiastic encouragement to the thesis, from which I benefit throughout my life.

Professor Herbert H. Einstein offered me expertise on geology, soil formation, and weathering. I would especially like to thank him for his successful guidance throughout this research.

Dr. R. Torrence Martin is a world-famous clay mineralogist, who offered me his "golden" experience on X-ray diffraction and clay mineralogy. His help is gratefully acknowledged.

My particular thanks are expressed to:

Professor Patricia J. Culligan, for her interest in my research and for her supporting my second year study at MIT.

Mr. Stephen W. Rudolph, who helped numerous times in providing me the in-time apparatus and tools so that my work could be continued. This work would have not been possible without his many helps.

These successful colleagues, *Dr. Catalina Marulanda (my sister), Dr. Greg Da Re, Dr. Kurt Sjoblom, Dr. Liangyang Zhang, Doctor-to-be Laurent Levy, Doctor-to-be Suchatvee Suwansawat, Carlos Regalado, Yun-Sung Kim*, and many other labmates and classmates.

The four nice ladies, *Alise Kalemkiarian, Carolyn Jundzilo, Shila Fay, and Marry Elliff.*

I would like to dedicate this dissertation to my mother in memory and my father, from whom I inherit enthusiasm and persistence to knowledge and work.

Finally, I heartily thank my wife for her love and her support to my study at MIT.

Table of Contents

List of Figures

List of Tables

Chapter 1 INTRODUCTION

1.1 Project Description

With the economic development and population growth in the past decades, the Puerto Rican capital of San Juan is demanding new solutions to mobility problems. The San Juan metropolitan region, which includes 13 municipalities covering 400 square miles along the island's northeastern coast, is a densely populated urban area with heavy traffic congestion and no existing subway or other rail transit systems (Figure 1-1). The 1.3 million residents of greater San Juan, 37% of Puerto Rico's total population, generate about 3.2 million trips daily, producing traffic congestion on expressways and major roads. To reduce this congestion and the anticipated future increases in congestion levels, the Puerto Rico Department of Transportation and Public Works (DTPW), through its Highway and Transportation Authority (PRHTA), is constructing a 10.7-mile (17.2-km) double-track guideway between Bayamon Centro and the Sagrado Corazon area of Santurce in San Juan (Figure 1-2). This project constitutes the first phase of a rapid rail transit system referred to as Tren Urbano. The original capital cost for the project as specified in the Full Funding Grant Agreement totaled $1.25 billion, and the latest cost estimate is $1.55 billion. The Tren Urbano project is expected to carry 113,300 riders per day in 2010 (FTA, 1998).

The line of Tren Urbano is being built with total grade separation and high-level platforms. Of the 16 stations, 10 are elevated, 4 are at grade or in open cut, and two are

constructed underground. Section 7 of the alignment is linked by the two underground stations, Río Piedras and Universidad, and runs through the densely populated area and the business district of Río Piedras (RT, 1999). Early in the planning and design process, local agencies and citizens requested that the historic Río Piedras section of the city be protected during and after construction by putting the alignment underground. Therefore, to minimize construction impact on the community and minimize disturbance to the community in future operation, Section 7 must be constructed underground for a length of 1500m.

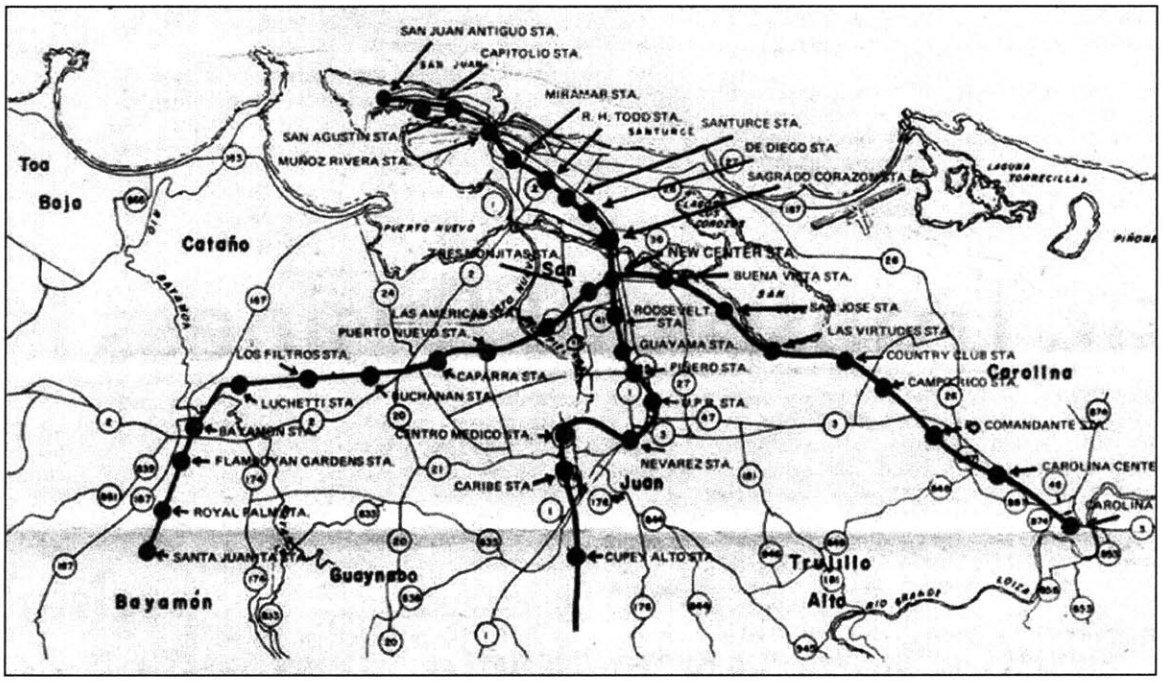

Figure 1-1. Schematic map showing the major expressways in the San Juan metropolitan area.

The underground construction of Section 7 started in 1996 and was expected to be completed by December 2001. Four different tunneling techniques were used in the construction of the tunnel (Figure 1-3): (1) boring of twin, 6.3m diameter tunnels with conventional segmental concrete lining using an EPBM (Earth Pressure Balance) tunnel

boring machine; (2) Open cut & cover (with excavations supported by cross-lot bearing); (3) four short sections of NATM (New Australia Tunneling Method) tunnel, constructed with top heading and bench and supported by lattice girders and shotcrete lining; (4) hand mining of a series of stacked drifts (3m square) that form the structural arch for the station cavern (19m wide by 16m high) (Figure 1-4). The cavern and much of the running tunnel alignment pass 5m-10m below fragile masonry buildings in the historic district of Río Piedras.

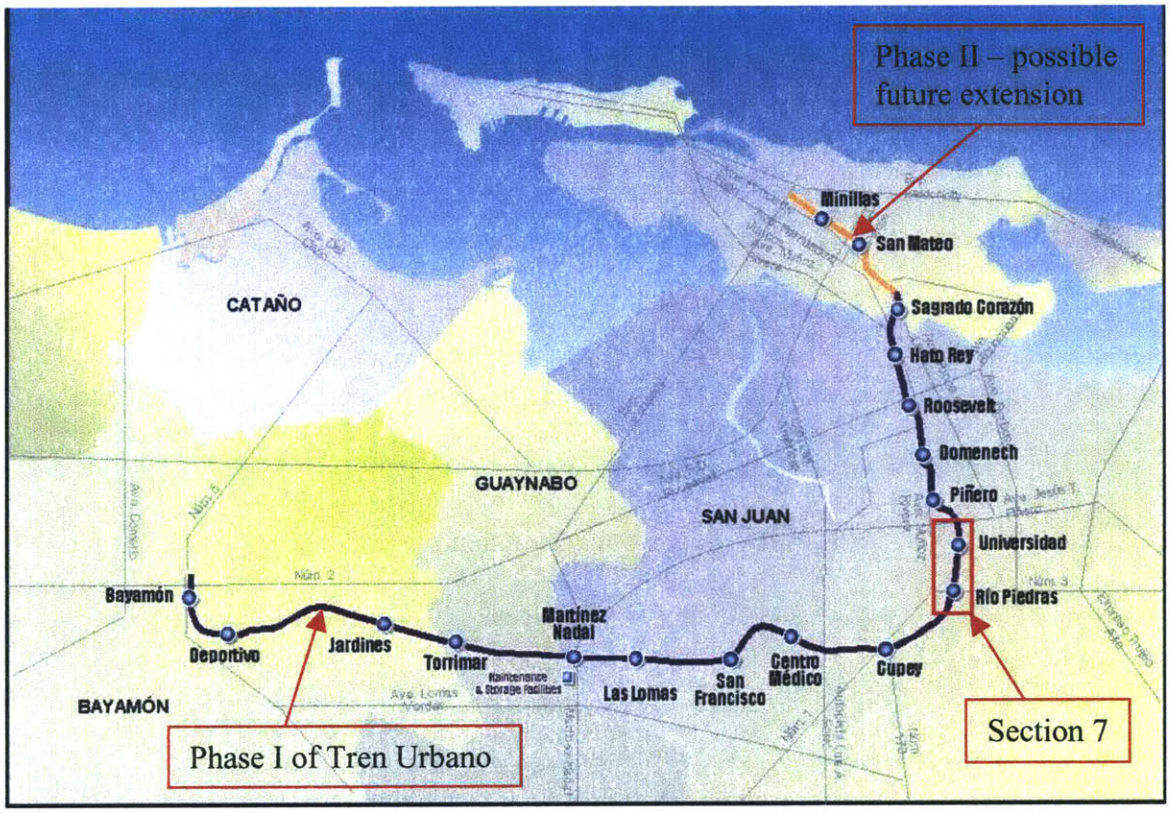

Figure 1-2. The alignment of Tren Urbano project.

As always, the complexity and difficulty of underground construction near or through the foundations of existing buildings deserve the special attention of geotechnical engineers. Ground movements induced by underground excavation are always of critical

concern, particularly in urban areas. In view of the unusual range of tunneling activities and their close proximity to existing buildings, a research contract for the "Prediction of Ground Deformations Caused by Underground Construction of The Tren Urbano in Río Piedras" was initiated between MIT and KKZ/CMA Consortium. Among the many important issues involved in the design and construction of a tunnel, the measurement and understanding of the behavior and engineering properties of the soils encountered in tunneling are the most critical. The research work described in this thesis is one of several tasks undertaken as part of this research, and focuses on the soil behavior and engineering properties of the old alluvium soils that occur throughout Section 7 in the construction site.

The 1500m-long Río Piedras segment (Section 7) of the Tren Urbano project has been designated by Federal Transit Administration (FTA) one of five turnkey demonstration projects for testing procurement procedures which shorten schedules and control costs. Three joint ventures bid on the project. The bid of KKZ-CMA of USD $225 million was deemed the best value and an award and notice to proceed was given in April 1997. The joint venture constructors, KKZ-CMA are comprised of Kiewit Construction; Kenny Construction; and H.B. Zachry Company; CMA Architects & Engineers, a San Juan based engineering design firm. Kiewit is the leading company for the construction of the tunnel. Other engineering firms include Jacobs Associates, Sverdrup and Woodward Clyde. Jacobs Associate is providing all tunnel design as part of the design-build team. Woodward Clyde Consultants (WCC) is the main geotechnical consultant. In addition, Bachy Soletanche, Ltd. provides all grouting work.

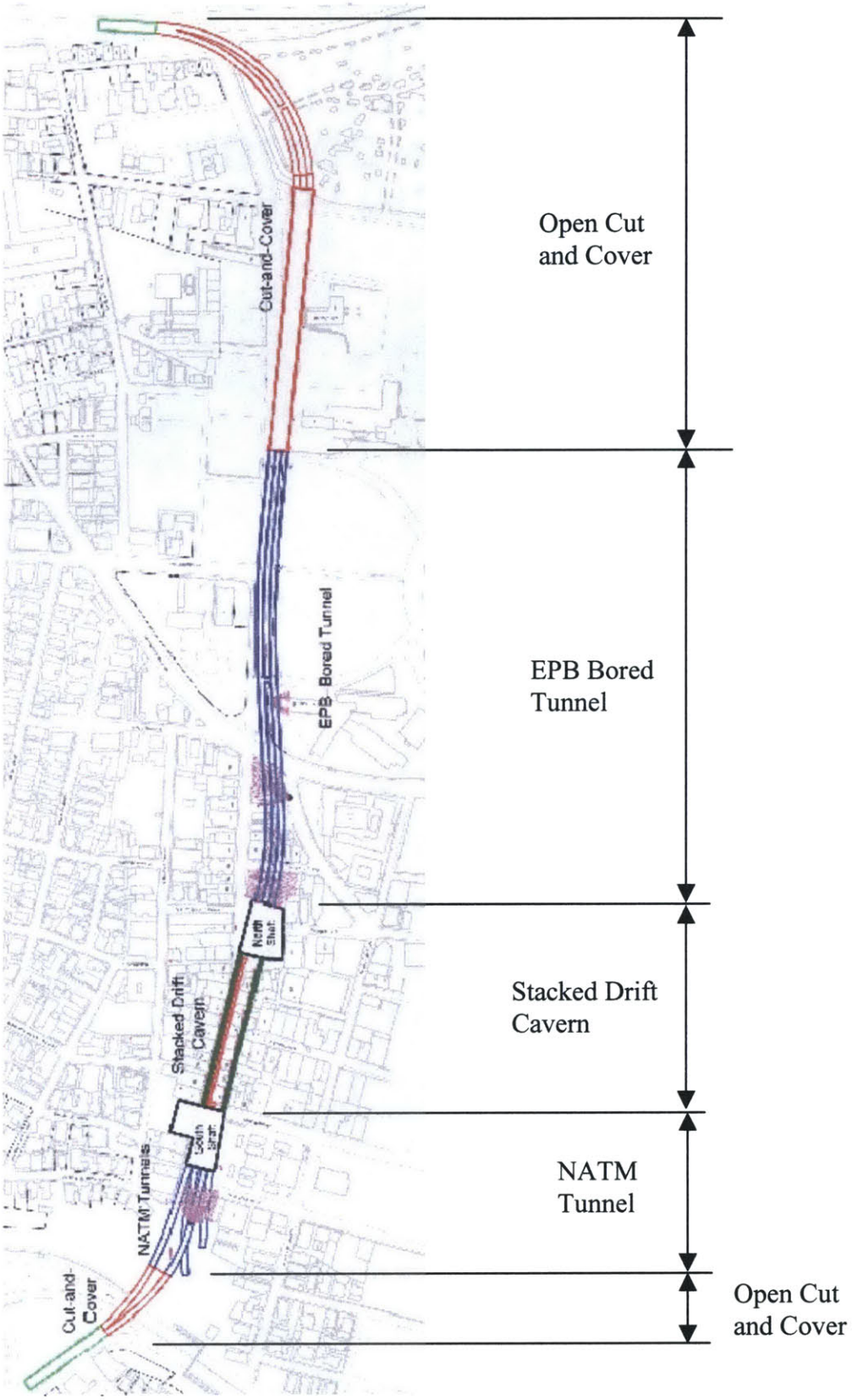

Figure 1-3. Schematic map showing the four tunneling techniques.

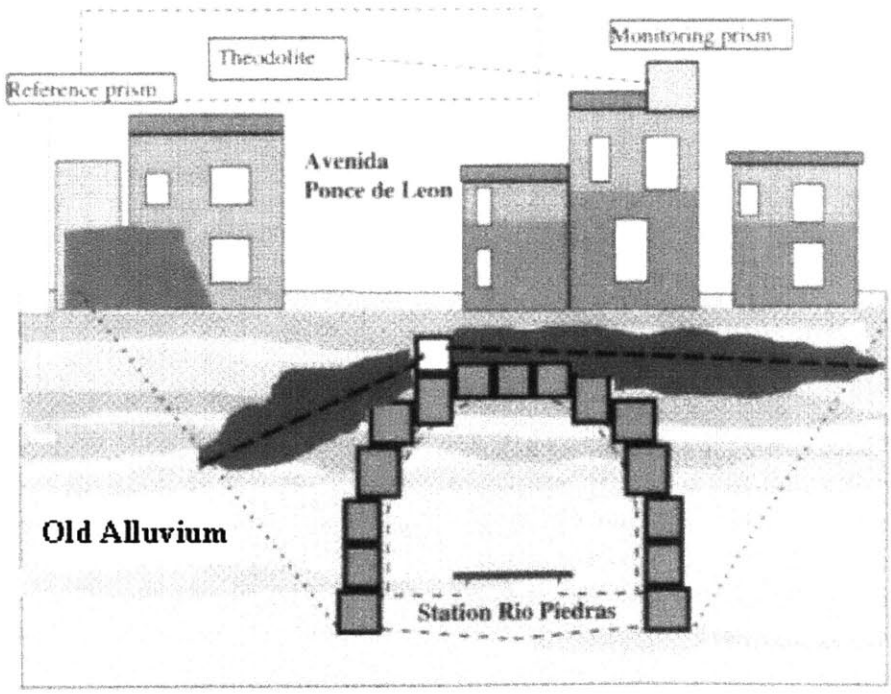

Figure 1-4. Station cavern formed by the stacked drifts.

1.2 Problem Statement

Before the design and construction of the tunnel, a series of site investigations and laboratory testing programs had been conducted to characterize the soil and to obtain soil properties. However, the underground construction has encountered a series of problems, which, of course, require investigation and hence the need for the considerable research. This thesis will only focus on the soil materials in the construction site. Other problems involved in the design processes and construction activities are the focuses of other tasks.

In fact, there are difficulties and problems involved in all phases of the Tren Urbano project, ranging from site characterization and sampling, soil classification and identification, laboratory measurement of soil parameters for design, and field construction. All site investigations have found that the geomaterial has an alluvial origin

and the soil deposit is quite heterogeneous in both coloring and stratifications (CSTC, 1996; WCC, 1997; WCC; 1998). The intact soil mass is stiff and firm, indicating that the material seems to be cemented. Experience with tube sampling showed that it is difficult to obtain high quality undisturbed samples (see Section 3.7 for further information). Fookes et al. (1997) also pointed out that tube samples are not usually suitable for the laboratory determination of strength and stiffness of residual soils.

For both field and laboratory identification and classification, one found the misleading appearance of the deposit. Geologists termed the deposit an "old alluvium" and already described the alteration or weathering of the original coarse sand grains which were deposited through rainfall or streams. Without remolding, the deposit appears to consist of coarse grains visible to the naked eye, in spite of its high clay fraction, which is very confusing and misleading. In fact, some layers in the deposit have been misclassified as sands. Therefore, the problem arises on how to classify the deposit and how to measure its index properties, such as Atterberg limits and grain size distribution.

The real-time field construction has also found the material problematic, i.e., it is difficult to deal with this deposit. Although it has a sand-like appearance, it becomes very plastic after disturbing and remolding under drilling head and hence sticks to construction tools, resulting in difficulties in digging, dumping, and transportation. In addition, one found that the cutting heads in all construction tools were worn down quickly.

Another important problem is the ground settlement caused by tunneling. In order to mitigate the potential damage to overlying buildings in the historic area of Río Piedras due to tunneling induced ground movements, the design incorporated a compensation grouting scheme. During early stages of construction it became clear that ground movements were generally much larger than expected, and a secondary system of "consolidation" or permeation grouting was installed to stabilize soils ahead of the advancing tunnel face. Initial estimates of settlements ranged from 25mm to 50mm, while measured data for the EPB tunnel bores without grouting or overlying structures ranged from 60mm to 90mm. In the stacked drifts section, despite extensive compensation grouting and permeation grouting of the deposits, movements have exceeded 140-160mm in many locations over the centerline of the stacked drifts section, resulting in cracking damage to several buildings.

1.3 Research Objectives

The above discussion points out that this soil deposit is not a common geomaterial, as reflected by the fact that the field performance is quite different from previous expectations, even though an intensive geotechnical site investigation has been conducted prior to the design and construction. Moreover, the current understanding of the old alluvium behavior is not adequate for effective design. In fact, early conventional laboratory testing at MIT has found difficulties in characterizing the consolidation and shear behavior of the deposit. For example, oedometer tests found that the coefficient of consolidation decreases dramatically when the soil was consolidated to a vertical stress of 300ksc such that the coefficient must be plotted with a logarithmic scale.

Therefore, the primary objective of this research is to characterize the material and provide the framework to understand its engineering behavior. A soil is an earth particulate material formed in the complex and uncontrollable environment. By treating the old alluvium as an unknown geomaterial, complete understanding its engineering properties requires systematic approaches of characterization, which include depositional history, post-depositional weathering or alteration, qualitative and quantitative soil composition, microcharacterization of soil structure. As residual soils are formed through weathering, during which different chemical and physical reactions take place and hence new minerals may be formed, it seems necessary to identify the soil minerals in the deposit qualitatively and quantify each phase in the material. Knowledge of soil composition or mineralogy is helpful in understanding the engineering behavior. The macroscopic engineering behavior also depends on the arrangement of the individual soil particles, i.e., soil structure and hence, a complete microstructure characterization is desirable.

The second objective is to investigate the physical and chemical behaviors of the old alluvium. These physical and chemical behaviors depend on both the soil composition and structure. For example, cation exchange capacity of a soil depends directly on both the type and the amount of clay minerals present. In turn, the engineering properties are also influenced by the chemistry of pore fluid and the different cations adsorbed on surfaces of clay minerals.

The third objective is to measure the index properties, including the sensitiveness of the index properties to remolding. The interpretation of these parameters is based on the soil composition and structure of the deposit. Measurements of these parameters also serve as an indirect way to the understanding of the soil composition and soil structure. For example, the variety in clay fraction obtained by grain size analysis also reflects the degree of destructuring of a cemented soil.

The fourth objective is devoted to measuring and understanding the mechanical behavior of this geomaterial. After knowing the soil composition, soil structure, and index properties, the interpretation of its engineering properties becomes possible. This research does not aim to develop a constitutive soil model, but rather to establish a conceptual model based on the observed soil composition and structure.

General speaking, the final objective of this research is to accumulate research experience for the MIT Geotechnical Group. In addressing the above objectives, this research has proven very useful in the development of new techniques and methods (e.g., microcharacterization of a new soil material) for testing weathered soils, and for providing data for future constitutive model development.

1.4 Organization of the Thesis

The research presented in this thesis comprises an intensive experimental investigation for the characterization of the old alluvium in San Juan, Puerto Rico. This thesis starts with Chapter 1, the introduction to the project background, problems to be

solved, and research goals. Since the subject of this research is a special highly weathered old alluvium (see Section 2.4 for discussion on "old alluvium"), the basic background information and concepts on residual soils and tropical weathering are required before the presentation of the experimental program. Therefore, Chapter 2 provides a literature review on fundamental information about residual soils and tropical weathering, so that the experimental results on soil mineralogy and structure presented in subsequent chapters can be easily understood. This information provides a basic context for defining the scope and focus of the current studies on the old alluvium.

Chapter 3 is devoted to the detailed information on the site characteristics associated with Section 7 of the Tren Urbano project, including both the geographical and geological settings and the geological origin of the old alluvium. This chapter also includes site-specific information related to the soil which was used for the research, including the soil profile and sampling locations.

Chapter 4 gives an overview of the experimental test methods that are available for examining the mineralogy and soil structure of the old alluvium. It also gives a summary of the entire experimental program used in the subsequent chapters. This chapter seems necessary to explain the research methodology before the detailed presentation of the testing methods and results.

Chapter 5 presents the study of the mineralogy and composition of the old alluvium, including both qualitative and quantitative mineralogical analyses. In addition,

the analytical results are discussed with the tropical weathering process and the soil formation environment.

Chapter 6 describes the particle arrangement or soil structure of the old alluvium at both the micro and macro scale. This chapter also gives a detailed account of the variability of index properties, including Atterberg limits and grain size distributions, and shows how these parameters reflect changes in the soil microstructure.

Chapter 7 presents data on the engineering properties of the old alluvium, based principally on laboratory compression and shear tests on intact samples of the soil. This chapter also postulates how these engineering properties can be related to the microstructure and mineralogy of the deposit. The objective of this chapter is to investigate the effects of the soil mineralogy and micro and macro structure on the mechanical behavior by some routine laboratory measurements of engineering properties.

Finally, at the end of this thesis, Chapter 8 presents a summary of the research, the results, conclusions, and recommendations for future research.

References

Alba-Carbo, A.L. (1998) *Prediction of Ground Deformations Caused by Underground Construction of the Tren Urbano in* Río *Piedras.* M.S. Thesis, Massachusetts Institute of Technology, Cambridge, MA.

AUA – American Underground-construction Association (1999) *Featured Project – Tren Urbano*. http://www.auca.org/month/trenurbano.html

CSTC (Caribbean Soil Testing Co., Inc.) (1996) *Geotechnical Data Report* – Río Piedras Contract.

Fookes, P.G. (1997) *Tropical Residual Soils.* Geological Society Professional Handbooks. The Geological Society, London.

FTA – Federal Transit Administration (1998) *Tren Urbano.* http://www.fta.dot.gov/library/policy/ns/trenurbano.html

RT – Railway Technology (1999) *Tren Urbano – Rapid Transit System, Puerto Rico.* http://www.railway-technology.com/projects/tren/

WCC (Woodward Clyde Consultants, Inc.) (1997) *Supplemental Site Investigation Reports for Tren Urbano Section 7 – Vol. 1.*

WCC (Woodward Clyde Consultants, Inc.) (1998) *Supplemental Site Investigation Reports for Tren Urbano Section 7 – Vol. 2.*

Chapter 2 BACKGROUND ON RESIDUAL SOILS AND TROPICAL WEATHERING

2.1 Introduction

Based on its formation method, a soil can be classified as sedimentary (or transported), residual, or fill (Lambe and Whitman, 1969). Most residual soils are the products of rock weathering that are not transported as sediments but accumulate in place. However, there is a kind of soil which has been transported in history and then weathered after sedimentation or deposition. This kind of soil should also be classified as residual despite of its sedimentary origin. The particular formation process of residual soils affects their composition, structure, and corresponding engineering behavior. Although the weathering and soil formation processes are not the main focus of this thesis, an understanding of the basic concepts of weathering is of great importance for geotechnical engineers to appreciate the typical soil composition, structure, and engineering properties of residual soils.

This chapter serves as a fundamental and brief overview of tropical weathering and soil formation, and aims to provide sufficient background for subsequent discussions on soil mineralogy and soil fabric of the old alluvium. It begins with a very general description about the concepts of residual soils in Section 2.2; following by a discussion of weathering as the main soil formation process in the tropics in Section 2.3. Finally, the basic concepts on old alluvium are discussed in Section 2.4.

2.2 Residual Soils

A residual soil is one formed in place by the weathering of the rock at the location, with little or no movement of the individual soil particles (Lambe and Whitman, 1969). Much notably information on residual soils has been published in numerous journal articles (e.g., Townsend et al., 1971; Vaughan and Kwan, 1983; Townsend, 1985; Vaughan, 1985 and 1988; Nishida, 1999), several conference proceedings (e.g., two conferences organized by ASCE, 1982 and 1999; two International Conferences on Geomechanics in Tropical Soils, 1985 and 1988), and in recent monographs edited by Blight (1997) and Fookes (1997).

Besides "residual soils", several other terms are widely used in literature to stand for soils weathered in subtropics or tropics, including "tropical soils", "tropical residual soils", "laterites", "transported residual soils", etc. The first two terms are equally used to designate the residual soils in the tropical regions, while the term "laterite" is widely used for ferruginous types, but has also been applied both to soft, clay-rich soils showing marked iron segregation or mottling and to loose gravelly materials comprising mainly iron oxide concretions (Fookes, 1997). Since most laterites are basically formed through tropical weathering, they are essentially residual soils with distinctive red coloration and high concentrations of Fe. The last term "transported residual soils" is seldom used and lacks of a clear definition, except that the term was used by Fookes (1997) to point out the necessity of considering the different properties imparted to this kind of tropical soil by processes of transportation and deposition. In addition, Mitchell (1993, p.79) also uses

a term "post-depositional weathering" to designate any possible alteration that has taken place in a transported sediment after deposition.

In some particular cases, weathering occurs and new soil-forming processes are initiated in new sedimentary deposits after exposure to the atmosphere, just as they are on freshly exposed rock. If a deposit in a tropical zone consists of mainly coarse grains which are primarily rock minerals and exposes to the atmosphere, the post-depositional weathering essentially converts the rock minerals into clays and oxides. Although strictly speaking, the altered material is not weathered in situ from rock mass, the final residues are the same as that transformed from rock mass through the same changing processes. Therefore, the final product weathered post-depositionally from a coarse deposit is essentially a residual soil. As discussed later in Chapter 3, the old alluvium in San Juan, Puerto Rico is one of such materials that have undergone intensive post-depositional weathering.

Residual soils differ from transported soils which are principally derived from coastal, alluvial, wind blown, or glacial processes. In the tropics, residual soils probably form the largest group with which the engineer has to deal. Due to their in situ formation, these soils have particular characteristics which distinguish them from material deposited from a fluid medium such as wind or water. The processes forming residual soils include (Fookes, 1997):

- Incorporation of humus (decaying vegetation);

- Physical and chemical degradation (i.e., alteration of mineralogy derived from parent rocks);
- Leaching of insoluble materials;
- Accumulation of insoluble residues;
- Downward movement of fine particles (lessivage);
- Disturbance by root penetration, animal burrowing, free fall and desiccation.

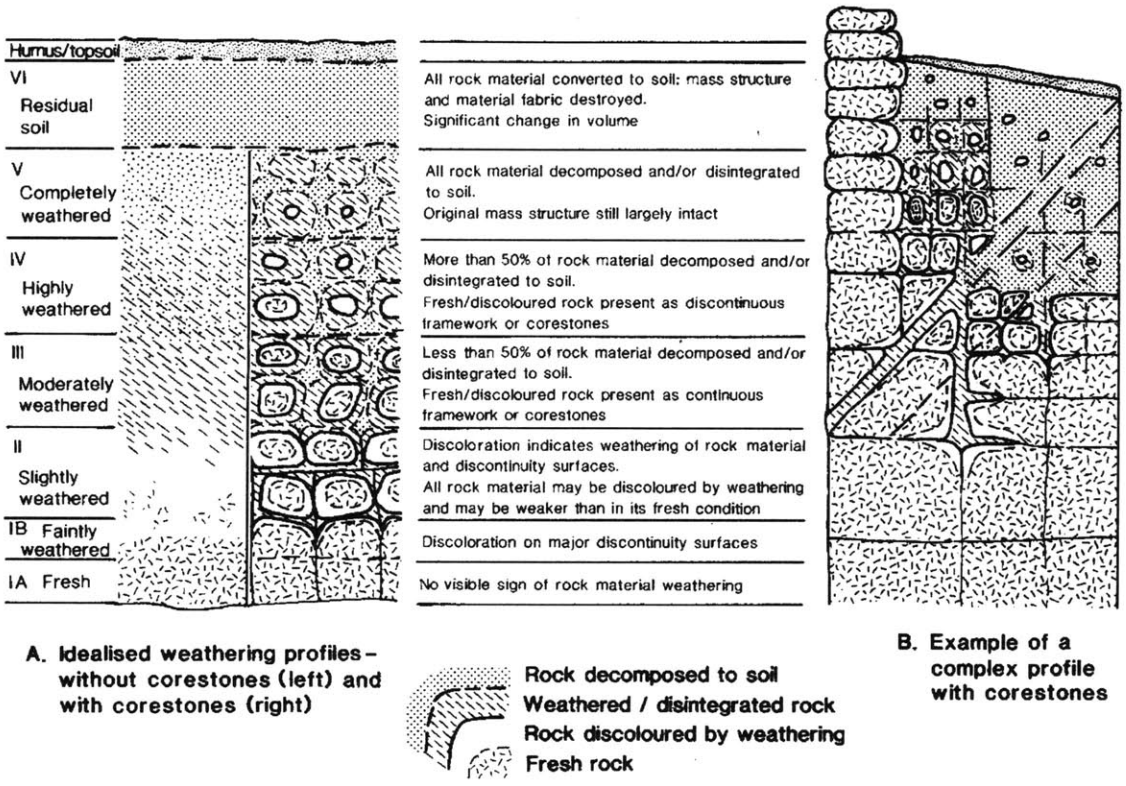

Figure 2-1. Typical profile of an in-situ weathered rock showing the six weathering grades (Fookes, 1997).

As weathering is strongly dependent on climatic conditions (including primarily precipitation and temperature), residual soils are mainly distributed in Mediterranean, subtropical, or tropical regions, where the mean annual temperature is usually greater

than 20°C and the annual rainfall is greater than 1.0m with or without a dry season. The typical profile of a weathered rock is shown in Figure 2-1, where different weathering grades are proposed and introduced to differentiate the soil-like and rock-like materials. Usually, residual soil includes the three weathering Grades VI – IV, since to the base of weathering grade IV, most of the soils in the weathering profile are included and the mass and material properties are still soil-like. Below, in weathering Grade III, rock-like characteristics begin to dominate both the mass and the material.

2.3 Tropical Weathering

Tropical weathering processes have been extensively studied by soil scientists and geochemists. Here it is appropriate to briefly summarize some fundamental concepts about weathering based mainly on information from Velde (1992, 1995), Righi and Meunier (1997), and Fookes (1997) to assist the understanding and clarification of the formation processes that are likely to have taken place in the formation of the old alluvium in San Juan.

2.3.1 Basic Process

In the tropics, weathering is a complex interaction of aqueous solution with rocks at the earth surface, during which different physical, chemical, and biological processes continuously transform organic and non-organic materials into soils. The overall reaction of weathering is:

rock minerals + water → soil minerals

Water mainly from rainfall is essential for the chemical reactions during weathering and soil formation. When large amounts of water are present, the solid minerals in the rocks tend to be very unstable and can dissolve for the most part. The greater the renewal of the water input (rainfall or fluid circulation), the more dissolution occurs, resulting in large amounts of cations being lost through dissolution to the relatively dilute solution. Therefore, the amount of drainage from rainfall is a very important parameter in rock weathering and soil formation.

The energy state of water varies from place to place in a soil or a weathered rock, between a minimum value, in the absorbed layer on the solid surfaces, to a maximum value which is that of free water in large voids. This is important for chemical reactions at the solid-fluid interface. In fact, the interaction between rock minerals and water consists of two opposing chemical reactions: dissolution and recrystallization. *Dissolution* is the first step of most water-rock interactions or weathering. More specifically, when water flows through rocks, water-rock interaction leads to dissolution of cations (e.g., Na^+, K^+, Ca^{2+}, Mg^{2+}), i.e., leaching of cations by drainage water. During the dissolution of pre-existing crystalline phases of silicates, cations will

- Detach from the oxygen bonds in most silicates;
- Diffuse away from their site in the crystalline lattice;
- Desorb from the crystal surface;
- Diffuse into the bulk solution of water.

With progressive leaching of soluble cations, the chemical concentrations of the solutions change and the primary minerals lose some components and corrode (Figure

2-2). Silicates dissolve and release some cations into solution in the order of their ionic bonding strength, i.e., the most weakly bonded cations can be released first, while others cannot be dissolved or dissolve very slowly. The ionic bond ranking for the common cations is as follows:

$$Si^{4+} = Ti^{4+} > Fe^{3+} > Al^{3+} > Fe^{2+} = Mg^{2+} > Ca^{2+} > Na^{+} > K^{+}$$

Therefore, K^+, Na^+, Ca^{2+}, Mg^{2+}, Fe^{2+} ions are dissolved before Al^{3+} and Fe^{3+} dissolve. Silicon ions are generally dissolved as SiO_2. After leaching of some cations, these primary silicates may either transform their crystal lattice structure to form new minerals (usually clays) or continue leaching until completely dissolved. For example, smectites can be formed from mica through the leaching of the interlayered K^+. This process can be illustrated by the following reaction (Fanning et al., 1989):

$$\text{Micas} \xrightarrow[\text{Incorporating new exchangeable cations}]{\text{Removing } K^+ \text{ through dissolution and leaching}} \text{Expandable 2:1 minerals, smectites}$$

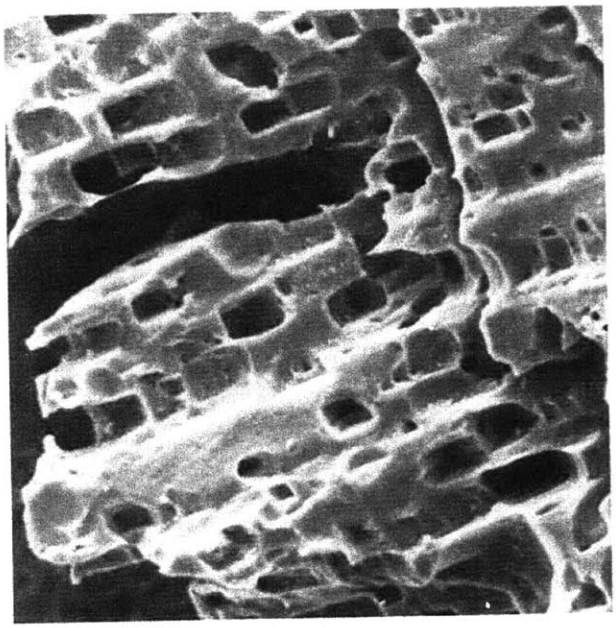

Figure 2-2. SEM micrograph of a feldspar particle etched by weathering. Picture width is 100μm (Press and Siever, 1998).

In addition to the transformation of the parent crystal lattice by dissolution and diffusion, there is a concurrent process of reprecipitation from solution enriched in dissolved components (i.e., cations or anions) that form secondary minerals in the voids or contacts of primary minerals. For example, during weathering dissolution, the ferrous iron in pyroxene ($FeSiO_3$) is released to the solution and oxidized to the ferric form when meeting with oxygen, and finally insoluble Fe-oxides (hematite) precipitate from the solution, as illustrated by the following reaction (Figure 2-3):

$$\underset{\text{Pyroxene}}{FeSiO_3} + \underset{\text{Oxygen}}{O_2} + \underset{\text{Water}}{H_2O} \rightarrow \underset{\text{Hematite}}{Fe_2O_3} + \underset{\text{solid or dissolved Silica}}{SiO_2} + H_2O$$

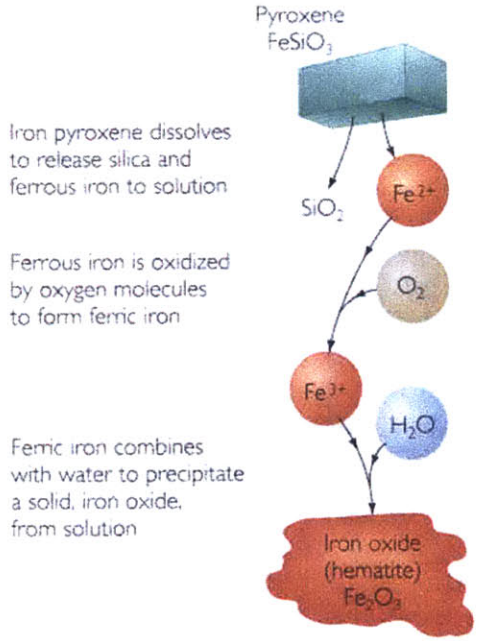

Figure 2-3. Hematite formation through weathering of a Fe rich pyroxene (Press and Siever, 1998).

In other words, the secondary minerals are formed through either transformation of the crystal lattice of primary minerals or recrystallization of cations in solution dissolved from primary minerals during weathering.

Dissolution of primary minerals as well as growth of secondary ones are controlled by the differences in chemical concentrations of the solutions far away and adjacent to the surface of the solids. Therefore, the circulation of water and dissolved components is the decisive parameter which controls mineral reactions. Whether dissolution or precipitation occurs depends on the local chemical composition of the solutions which in turn depend on the renewal rate of water flow.

In summary, the dissolution-recrystallization processes which occur at the mineral-aqueous solution interface can be reduced to an exchange of protons (i.e., H^+) for soluble cations. For example,

K-feldspar + H^+ → kaolinite + K^+ + Si^{4+}

Or more specifically,

Feldspar + hydrogen ions → clay (kaolinite) + cations, solids, water

$2KAlSi_3O_8 + 6\,H^+ \rightarrow Al_2Si_2O_5(OH)_4 + 2K^+ + 4SiO_2 + H_2O$

In most clay-forming reactions, several phases are produced from primary minerals and water. The reaction produces clays and other minerals. Silica is a common by-product of mineral-water reactions. It can go into aqueous solution or be formed a solid phase such as quartz or amorphous silica.

It should be pointed out that not all silicates weather to form clay minerals. For example, quartz, one of the silicate minerals with the slowest weathering rate, dissolves

without forming any clay minerals. In addition, silicate weathering can also form materials other than clay minerals. Bauxite, a mineral composed of aluminum hydroxide ($Al(OH)_3$), is one such product. Bauxite forms when clay minerals derived from the weathered silicates continue to weather until they have lost all their silica (SiO_2) and ions other than aluminum. Bauxite is found in hot and humid tropical regions where rainfall is heavy and weathering is very intense.

2.3.2 Factors Controlling Weathering

The end product (i.e., soils) of the weathering process is determined by many factors, of which climate, parent rocks, vegetation, age, and topography are dominant over others. Climate and vegetation are active factors of soil genesis. They act on the parent rocks and slowly change it to clays or other fine-grained particles. The effects of climate and vegetation are conditioned by topography, including the drainage conditions of the soil. In fact, climate and vegetation are relevant to the distribution of soils on a worldwide scale. However, within a smaller area, topography strongly perturbs the spatial distribution of soils. The parent material also affects the kind of soil profile that can be formed and, in some cases, determines it almost entirely. Finally, the time scale, or age of the soil, is required for the change of the parent material into a mature or well-developed soil. During the formation process of a soil, age is also a relative measurement of the status of the maturity.

(a) Climate

Climate is mainly defined by temperature and rainfall. Different types of soils form within different climatic zones of the world (Blight, 1997; Fookes, 1997). The amount of rainfall and its distribution over the year determine the intensity of weathering and hence, the type of soils formed. In tropical wet zones without a dry season, rainfall is plenty and the renewal rate of water flow is fast. Thus, the aqueous solution is rather dilute and kaolinites are the main clay minerals formed. In tropical zones with a dry season, high evaporation rate causes a high concentration of dissolved components in solution. In this case, mainly smectites are formed. On the other hand, temperature increases the kinetics of chemical reactions, i.e., weathering is fast and intensive under higher temperature. Moreover, hot and humid conditions favor biological activity and, thereby, the quick transformation of organic matter into acids which affect weathering. In addition, the climate also affects the soil composition. For instance, in tropical wet climate, residual soils generally have low organic matter content and little calcium carbonate ($CaCO_3$), simply because of the availability of microorganisms that decompose the organic matter, while $CaCO_3$ is dissolved by the abundant water from rainfall.

(b) Parent rocks

Soil formation is strongly dependent on rock compositions (i.e., parent primary minerals). For example, soils with contrasting properties develop in granitic areas and areas of calcareous deposit. The parent rock composition is a determinative parameter for clay chemistry in the early stages of weathering. However, for a well-developed mature soil, the effect of climate on the final weathering products is much more dominate than the composition of the parent rocks. In fact, so long as sufficient time has elapsed, the

mineralogical composition of soils depends more on climate than on the chemical composition of the parent rock. This situation is enhanced in humid tropical climates where the rock composition does not control the types of clay minerals that are formed. For example, basalt and granitic rocks, can both produce soils which contain the same kaolinite and oxides assemblages (Velde, 1995).

(c) Vegetation and soil organic matter

Organic matter is added to the soil system through vegetation. Most soil organic matter comes from the remains of dead plants falling on the soil. Organic compounds from plant remains may be involved in two major processes: mineralization and humification. Mineralization is the transformation of organic molecules by microbes into CO_2, NH_4 and H_2O. It is fast typically in warm climates. In this case, the contribution of organic matter to weathering is achieved through the production of CO_2, which reacts with water to give carbonic acid. Humification leads to more complex organic polymers, typical of the soil system, so called humic compounds. It is a slow process in which both biological and physico-chemical reactions are involved. It is well known that soils of the warmer climatic zones generally have a low organic matter content, despite the large quantity of plant material produced and returned to the soil. This is attributed to the high activity of micro-organisms in the warmer temperature (Velde, 1995).

On the other hand, recent research has found that live vegetation also affects the weathering processes (White and Brantley, 1995) and the type of clay minerals formed (Dixon & Weed, 1989). This mechanism is called localized weathering by live roots.

Vascular plants affect the weathering in numerous ways. White and Brantley (1995) summarize the new effects of live roots as follows:

- Rootlets with high surface area secrete organic acids/chelates which attack minerals in order to gain nutrients;
- These acids, besides providing extra H^+ ions for the attack on minerals, are also able to complex and dissolve otherwise insoluble elements such as Fe and Al. This helps to further dissolve minerals containing Al and Fe;
- On a regional scale, plants recirculate water via transpiration followed by rainfall and thereby increase water/mineral contact time. There is a greater rainfall in forested regions than there would be in the absence of trees;
- Plants anchor clay-rich soil against erosion allowing retention of water and continued weathering of primary minerals between rainfall events.

(d) Topography

Topography determines the flow channel and hence the depositional characteristic of sediments. It should be expected that different size fractions deposit in different terraces of a river channel. Moreover, in a smaller area under the same climate and vegetation conditions, topography strongly affects the local distribution of soils in the following ways by translocations and accumulations:

- Topography (slope) changes the direction of the water flow which may not be only vertical, but also laterally along a slope. Lateral transfer of clays through solution or suspension may occur from the higher to the lower part of the slope: soils at the higher parts become impoverished in clays whereas soils lower down are enriched.

As a result, a rather impermeable layer may be formed by clay translocation and accumulation, and hence drainage water may be kept above this layer. This is the reason why perched ground water table has been found in residual soils formed in footslope.

- Slope controls the effective water-rock ratio which is defined as the ratio of the amount of renewal water to the amount of rock. The flow of the aqueous solution over soil profile is more rapid if the slope is greater. This shortens the solution residence time and prevents extensive water-rock interaction, thus the soil solution chemistry appears to be one of a high water/rock ratio. In a flatter areas, the residence time of solutions increases and low water/rock ratio is reached.

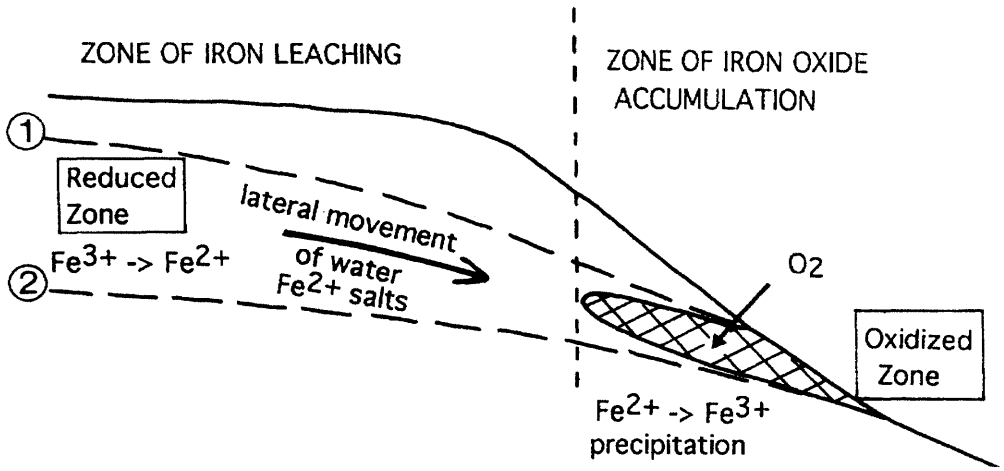

water has a higher ion concentration and the dissolution of primary minerals is slow. While in the intermittent slope, water drains laterally and vertically, resulting in that water has a low ion concentration and dissolution of rocks is always fast. Different ion concentrations in solution may favor different clay minerals. A typical example is the lateral translocation of Fe ions along a slope (Figure 2-4), resulting in a red zone rich in Fe-oxides at lower part of the slope.

(d) Time and soil age

Time is needed for changes to take place in the parent material during soil formation, since weathering of rocks is a slow process that requires hundreds, thousands or even millions of years. Moreover, periodic changes of climate and vegetation have often occurred which have changed the original pathways of soil development. Consequently, soils should be regarded as the result of a developmental sequence which exhibits not only the present-day factors and processes of soil formation, but also many preceding phases. In most cases the interpretation of soil features, such as the type of clay present, as being the result of interactions under present-day environmental conditions would be erroneous.

2.3.3 Minerals in Tropical Residual Soils

In residual soils, minerals derived from parent rocks include primary ones which are inherited and more weathering resistant or stable, and neo-formed secondary ones which are recrystallized or transformed during weathering. As a general rule proposed by soil scientists (Velde, 1995; Righi and Meunier, 1995; Fookes, 1997), the minerals

present in a soil, including clay and non-clay minerals, are determined mainly by climatic conditions. In tropical areas the tendency is to produce simple clay assemblages made of only one or two clay mineral phases. The clays are controlled for a large part by the chemistry of the soil solution, which itself depends on the prevailing climatic conditions, especially the amount of rainfall and its distribution throughout the year. High rainfall, regularly distributed throughout the year induces soil solutions with low concentrations of silica and basic cations: this favors the formation of kaolinite. Low rainfall, followed by a dry period with intense evaporation, induces soil solutions concentrated in silica and basic cations. In this latter environment, smectite is formed (Velde, 1995). Table 2-1 summarizes both the primary and neoformed minerals in different climates.

Table 2-1. The dependence of weathered products on the climate (summarized from Fookes, 1997).

Climate type	Mean annual temperature (°C)	Annual rainfall (m)	Dry Season	Primary minerals	Neoformed minerals[#]
Mediterranean, or subtropical	13-20	0.5-1.0	Yes	Quartz Alkali feldspars Muscovite	Smectites Fe-oxides Kaolinite* Imogolites[a] Halloysite[a]
Subtropical	20-25	1.0-1.5	Sometimes	Quartz Orthoclase Muscovite	Kaolinite Fe, Al-oxides Smectites*
Tropical	>25	>1.5	No	Quartz	Kaolinite Fe-oxides Gibbsite

[#] The mineral listed first is dominant;
* designates the occasional occurrence;
[a] developed from volcanic ashes.

However, the mineral formation is also conditioned by underground drainage, topography, and time duration of weathering. Poor drainage tends to accumulate more silica and basic cations, and hence promote the formation of smectite. In addition, smectite could be the intermediate mineral in the weathering pathways of kaolinite

formation if weathering time is not long enough. With more dissolution and weathering in tropical wet climate, smectites can be further weathered into kaolinites (Wilson, 1999).

The types of minerals present in the clay fraction have also been proposed as an index for approximately measuring soil development or maturity by soil scientists (Table 2-2). Since kaolinite and halloysite are 1:1 type minerals, they are the most stable clay minerals in the weathering environment. If the whole soil mineralogy is concerned, the inherited primary minerals must be considered with their stability or weathering resistance (Figure 2-5). Those with highest stability would be left behind after weathering, if the weathering duration is not long enough to completely alter the weathering resistant minerals. A mature soil developed in the hot and humid tropical climate may only contain kaolinite, Fe-oxides, and gibbsite (Al-oxide) (Table 2-1).

Table 2-2. Types of minerals as indicators for relative degree of soil development (the higher the number, the higher the degree of development) (from Dixon & Weed, 1989)

Degree of soil development	Prominent minerals in soil clay fraction
1	Gypsum, and other soluble salts
2	Calcite, dolomite, and apatite
3	Olivine-hornblende minerals
4	Biotite, glauconite, ferromagnesian chlorite
5	Feldspars
6	Quartz
7	Muscovite-illite
8	Interstratified 2:1 layer silicates and vermiculite
9	Montmorillonites
10	Kaolinite and halloysite
11	Gibbsite and allophane
12	Hematite-goethite
13	Anatase-leucoxene

For geologically brief periods, the soils on young landscapes or recently deposited pyroclastic or alluvial sediments are rich in minerals that are found throughout the world. But with time and the effect of warm and humid conditions, these minerals rapidly decompose, leaving on the landscape the insoluble residue of highly weathered materials, rich in the oxides and hydrous oxides of iron and aluminum (Figure 2-5).

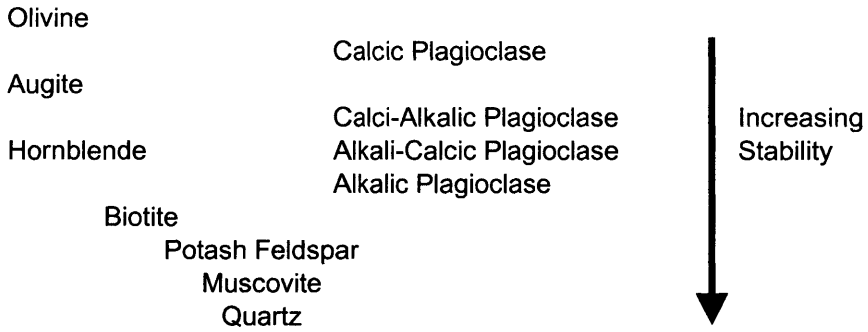

Figure 2-5. Mineral stability sequence. Stability of minerals increases as one proceeds towards quartz, and as a group, salic minerals (plagioclases, feldspars, etc.) are more stable than mafic minerals (olivine, augite, etc.) (from Dixon & Weed, 1989).

2.4 Old Alluvium

"Alluvium" is a general term for all detrital material deposited permanently or in transition by streams. It includes gravel, sand, silt, and clay, and all variations and mixtures of these (Stokes and Varnes, 1955). It is usually applied to the unconsolidated deposits of streams in their channels and over their flood plains and deltas. Through this definition, the term is used in two different meanings by geologists:

a. deposited by water;

b. from the youngest geological period, also called Holocene.

In soil science the term "alluvium" or "alluvial soil" is generally used for young (undeveloped) soils in alluvial plains (Edelman and van der Voorde, 1963). Following

this definition, alluvium is often used for young and unconsolidated soils deposited in Holocene age.

On the other hand, soils on river terraces are often called alluvial too. However, since most river terraces are of Pleistocene age, such soils are normally rather well-developed, especially in the tropics, where weathering is intensive. Therefore, strictly speaking, these alluvial deposits of Pleistocene age do not belong to alluvium, and hence geologists often term such materials as "old alluvium".

Table 2-3 summarizes the occurrence of old alluvia in the world. Although it is not inclusive of all formations of old alluvium, it is clear that the old alluvium has a great coverage on earth. However, there are not enough publications about research on the geotechnical characteristics of old alluvia.

Table 2-3. Typical occurrence of old alluvia throughout the world (except noted, all are from Edelman and van der Voorde, 1963).

Africa	Asia	South America
Nigeria, Niger River; Tanganyika, Great Ruaha River; Belgian Congo, Lufira Valley; Northern Rhodesia, Kafue Flats; Nyasaland, Shire Valley;	Indonesia: Java, Borneo, Sumatra; Burma, Irriwaddy Delta; India: Ganges, Brahmaputra River; Pakistan; New Guinea; Singapore[b]; Malaysia[b];	Venezula, Orinoco; Guianas; Colombia; Puerto Rico[a];

[a] Kaye (1959);
[b] Gupta et al. (1987); Shirlaw et al. (2000).

Depending upon the geographical location where the old alluvium was deposited, it may undergo further alteration under different climates after the exposure to the atmosphere. In the tropics, weathering is intensive and the original grains of the old alluvium may partially or totally convert to clays and oxides, resulting in significant changes of composition, soil structure or texture, and behavior of the old alluvium; while in temperate zones, the alteration process is inactive and slow and the deposit of the old alluvium may not change significantly. The following lists some important differences between old alluvia in tropical and temperate regions, which are mainly summarized from Edelman and van der Voorde (1963):

- Natural fertility

In temperate regions alluvial soils are generally rich in nutrients. This fact is due to the glaciations, during which physical weathering prevailed. Most river-laid alluvial soils in temperate regions contain a substantial quantity of pulverized fresh mineral grains. However, many rivers in the tropics originate from deeply weathered areas and their deposits consist mainly of quartz and other resistant minerals. Through further post-depositional weathering, more cations or salts are leached with water, thus the natural fertility of the sediments is low.

- Clay minerals

In temperate regions the clay fraction of alluvial soils is complicated and can vary widely, but illites are the most important clay minerals; while smectites and kaolinites are of minor importance. In the tropical regions, provenance has apparently a much greater influence on clay minerals. Some deposits contain only kaolinites, while others have smectites as the principal clay minerals.

- $CaCO_3$

The deposits of big rivers in temperate regions often contain $CaCO_3$, but in the wet tropics many alluvial soils do not contain $CaCO_3$ and may be quite acidic.

- Organic matter

Under comparable conditions alluvial soils in temperate regions have a higher content of organic matter than in tropical areas. The reason is that there is rapid decomposition of organic matter at higher temperatures.

- Gley Phenomena

When oxidation of alluvial soils takes place, gley phenomena can be observed in that layer of the soil where oxidation and reduction alternate. Often these mottlings are clearly recognizable, because they are found at a rather shallow depth.

In summary, "old alluvium" is generally used as a term to describe the alluvial deposits of Pleistocene age. Depending on the geographical location (and hence the climate type) where the old alluvium is formed, post-depositional exposure to the active atmosphere may alter the composition and structure of the deposit. In the tropics, weathering is intensive and the old alluvium may form as well-developed (mature) soils. Therefore, soil composition and structure of such weathered old alluvium may require attention and research. In fact, the old alluvium in the San Juan area, Puerto Rico is one of the post-depositional weathered deposits. The next chapter will provide detailed information about the site characteristics and the geological history of this deposit.

References

Blight, G.E. (ed.) (1997) *Mechanics of Residual Soils*. A. A. Balkema, Rotterdam.

Committee of 1 ICOTS (eds.) (1985) *Geomechanics in Tropical Soils.* Proceedings of the 1st International Conference on Geomechanics in Tropical, Lateritic, Saprolitic Soils, Brasilia.

Committee of 2 ICOTS (eds.) (1988) *Geomechanics in Tropical Soils.* Proceedings of the 2nd International Conference on Geomechanics in Tropical Soils, Singapore.

Geotechnical Engineering Division (eds.) (1982) *Engineering and Construction in Tropical and Residual Soils*. Proceedings of the ASCE Geotechnical Engineering Division Specialty Conference.

Edelen, B. (1999) (ed.) Behavioral Characteristics of Residual Soils. Geotechnical Special Publication No.92. American Society of Civil Engineers.

Fanning, D.S., Keramidas, V.Z., and El-Desoky, M.A. (1989) Micas. In J.B. Dixon and S.B. Weed (eds.), *Minerals in Soil Environments,* 2nd Edition, 551-634. Published by Soil Science Society of America, Madison, Wisconsin, USA.

Edelman, C.H. and van der Voorde, P.K.J. (1963) Important characteristics of alluvial soils in the tropics. *Soil Science*, **95**, 258-263.

Fookes, P.G. (ed.) (1997) *Tropical Residual Soils*. Geological Society Professional Handbooks. The Geological Society, London.

Gupta, A., Rahman, A., Wong, P.P., and Pitts, J. (1987) The old alluvium of Singapore and the extinct drainage system to the South China Sea. *Earth Surface Processes and Landforms*, **12**, 259-275.

Kaye, C.A. (1959) *Coastal Geology of Puerto Rico: (A) Geology of the San Juan Metropolitan Area*. Geological Survey Professional Paper 317. US Government Printing Office, Washington, D.C.

Lambe, T.W. and Whitman, R.V. (1969) *Soil Mechanics*. John Wiley & Sons, Inc.

Mitchell, J.K. (1993) *Fundamentals of Soil Behavior*. 2nd Edition. John Wiley & Sons, Inc., 437pp.

Nishida, K. (1999) Peculiarities of properties and problematic behavior of residual soils. *Problematic Soils*, Vol. 2, Proceedings of the international symposium of problematic soils IS-TOHOKU'98, Japan, Oct. 28-30, 1998, pp.865-884.

Press, F. and Siever, R. (1998) *Understanding Earth*. 2nd Edition. W.H. Freeman & Company.

Rahardjo, H., Toll, D.G., and Leong, E.C. (eds.) (2000) *Unsaturated Soils for Asia*: Proceedings of the Asian Conference on Unsaturated Soils, Singapore.

Righi, D. and Meunier, A. (1995) Origin of clays by rock weathering and soil formation. In: B. Velde (ed.), *Origin and Mineralogy of Clays*, 43-161. Springer-Verlag Berlin.

Shirlaw, J.N., Hencher, S.R., and Zhao, J. (2000) Design and construction issues for excavation and tunneling in some tropically weathered rocks and soils. In: H. Rahardjo, D.G. Toll, and E.C. Leong (eds.), *Unsaturated Soils for Asia*. Proceedings of the Asian Conference on Unsaturated Soils, Singapore.

Stokes, W.L. and Varnes, D.J. (1955) *Glossary of Selected Geologic Terms*. Colorado Scientific Society Proceedings, Vol.16, Denver, Colorado. 165pp.

Townsend, F.C. (1985) Geotechnical characteristics of residual soils. *Journal of Geotechnical Engineering*, **111**, 77-94.

Townsend, F.C., Manke, P.G., and Parcher, J.V. (1971) The influence of sesquioxides on lateritic soil properties. *Highway Research Record*, **374**, 80-92.

Vaughan, P.R. and Kwan, C.-Y. (1983) Weathering, structure and in-situ stress in residual soils. *Geotechnique*, **34**, 43-59.

Vaughan, P.R. (1985) Mechanical and hydraulic properties of tropical, lateritic and saprolitic soils. *General report: Session 2, Proceedings of the 1st International Conference on Geomechanics in Tropical, Lateritic, Saprolitic Soils, Brasilia*. Vol. 3, 231-263.

Vaughan, P.R. (1988) Keynote lecture: Characterising the mechanical properties of residual soils. *Proceedings of the 2nd International Conference on Tropical Soils*. Singapore. Vol.2, 469-487.

Velde, B. (1992). *Introduction to Clay Minerals*. Chapman & Hall.

Velde, B. (ed.) (1995) *Origin and Mineralogy of Clays*. Springer-Verlag, Berlin. 334pp.

White, A.F. and Brantley, S.L. (eds.) (1995) *Chemical Weathering Rates of Silicate Minerals*. Mineralogical Society of America, Washington, D.C.

Wilson, M.J. (1999) The origin and formation of clay minerals in soils: past, present and future perspectives. *Clay Minerals*, **34**, 7-25.

Chapter 3 SITE CHARACTERISTICS AND SAMPLING PROGRAM

3.1 Introduction

Chapter 2 introduced the weathering and soil formation processes in tropics. Soil formation is a complex process which is affected by its surrounding environment, including geographical location, geological settings and origin, climate, surrounding soils and rocks, groundwater and drainage conditions, etc. These important factors that influence the behavior and properties of a soil usually result in site specific soil characteristics. This chapter mainly provides information on these factors and their potential influence on the characteristics of the old alluvium in Rio Piedras. Sections 3.2 and 3.3 describe the geographical location and the climate of San Juan, respectively, while Section 3.4 focuses on the geological settings of the site. The geological origin of the earth material at the site is summarized from the literature and presented in Section 3.5. Based on the site investigation and geotechnical exploration reports, Section 3.6 summarizes the soil profile. Finally, the soil sampling program is presented in Section 3.7.

3.2 Geographical Location

As discussed in Chapter 2, the weathering process is highly dependent on climatic conditions. In turn, climate depends upon the latitude on earth. Therefore, the

geographical location of the construction site of the Tren Urbano project needs to be addressed first.

Puerto Rico is the easternmost and the smallest island of the Greater Antilles in the northeastern part of the Caribbean Sea (Figure 3-1). The Greater and Lesser Antilles enclose the Caribbean Sea, while waters outside this great island arc are referred to as the Atlantic Ocean. Puerto Rico and its offshore islands all lie in the area between latitudes 17°37' and 18°31' N., and longitudes 65°14' and 67°56' W. (Figure 3-2). The island of Puerto Rico is almost rectangular in shape, extending 175 km (110 mile) east-west and 65 km (40 mile) north-south and covering an area of 8,497 km^2. The town of Rio Piedras, where the project is located, is a southern suburb of the San Juan metropolitan area, and lies in the eastern part of the north coast of Puerto Rico (Figure 3-2).

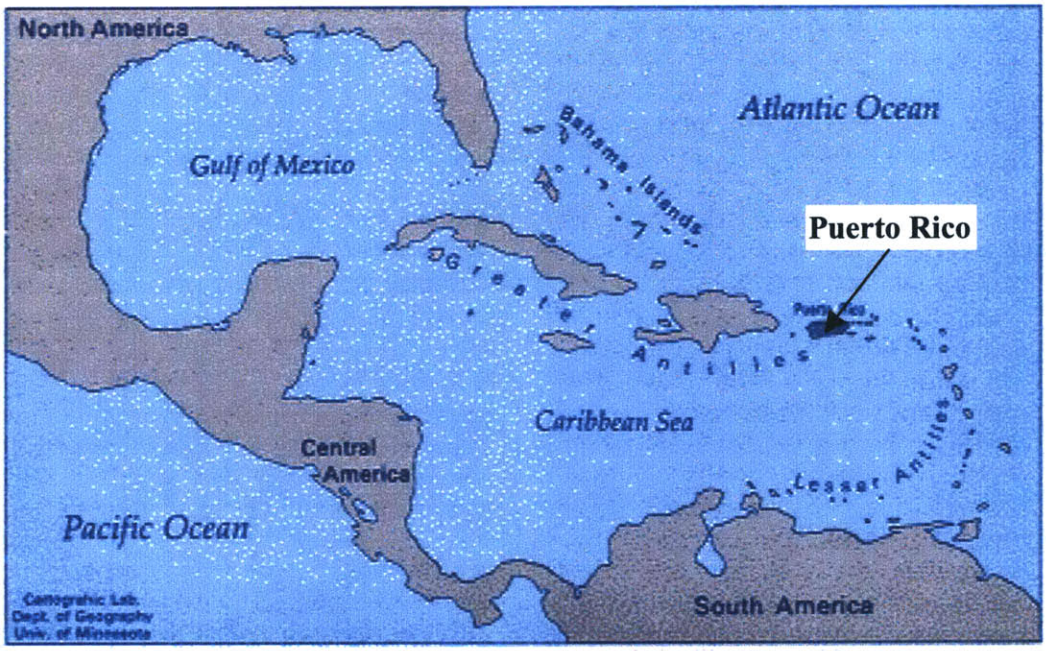

Figure 3-1. Map showing the location of the Puerto Rico Island.

Figure 3-2. Geographical location of the Puerto Rico Island with the distribution of rivers and streams.

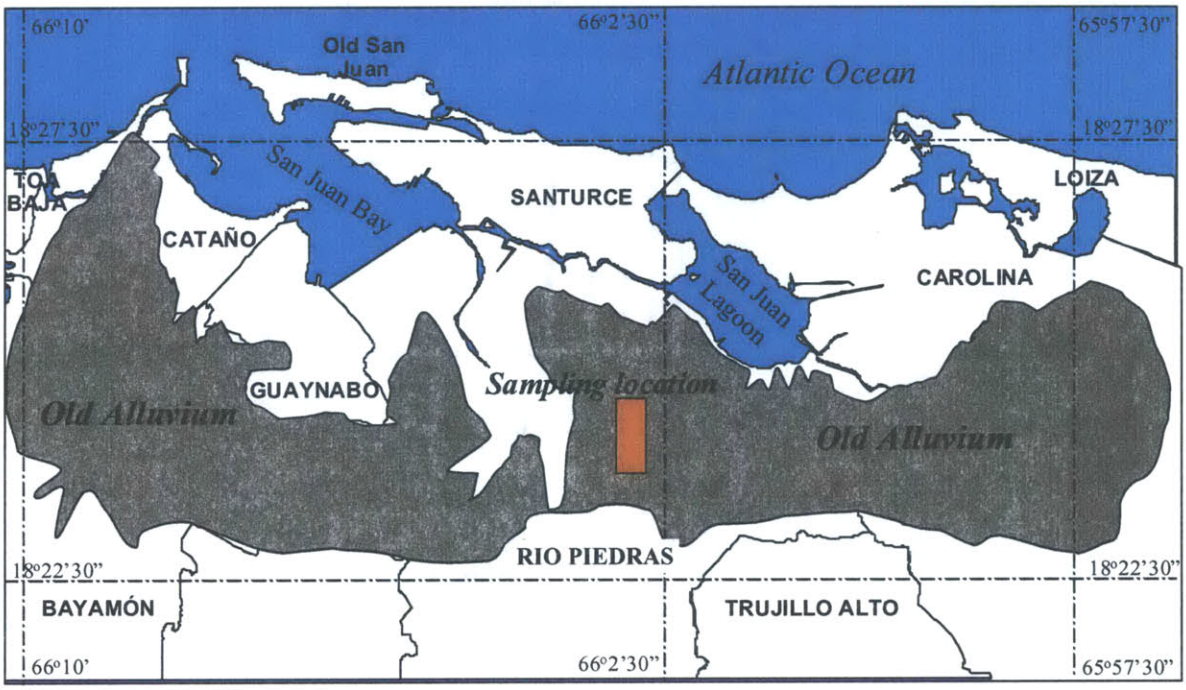

Figure 3-3. Schematic map showing the coverage of the old alluvium in the San Juan area.

Figure 3-3 shows the geographical distribution of the old alluvium in the San Juan area. It blankets much of the coastal plain, higher stream terraces, and part of the upland. In fact, most of the present-day flood plain sediments distributed in Santurce and around the lagoons (Figure 3-3) (e.g., recent littoral deposits and recent alluvium) of Holocene age are underlain by the old alluvium. Therefore, the old alluvium has a great coverage beneath the coastal plains.

3.3 Climate

As reflected by its smaller latitude, the climate of Puerto Rico is subtropical marine and is largely controlled by the northeast trade winds, which not only provide a nearly constant breeze that makes high temperatures comfortable, but also the constant direction has had a noticeable effect on precipitation.

In Puerto Rico, seasons are poorly defined, both as to temperature and rainfall. The temperature range is small and commonly less than 10°C in San Juan. The mean maximum is 30°C and the mean minimum is 21°C (USDA, 1978). Rainfall in Puerto Rico is fairly well distributed throughout the year, though in general about twice as much as rain falls per month from May through October as does from January through March. Precipitation varies from high on the windward (north) side of the main insular divide to relatively low on the lee (south) side of the divide, such that the north side of the island is humid while the south side is semiarid (Monroe, 1976). In the San Juan area, the mean annual precipitation is 193 cm, while the relative humidity averages about 80% throughout much of the year. The rate of evaporation is very high. In San Juan, the long-

term average annual rate of evaporation is 207 cm, which is even higher than the annual precipitation. Such a high evaporation rate greater than precipitation sometimes causes an upward movement of the groundwater, which also probably brings fine clay particles and dissolved Fe^{2+} to the upper layer of the subsurface. This is probably another reason why the upper layer has more Fe-oxides than in depth, as well as the lateral translocation mechanism described in Section 2.3.

3.4 Geological Settings

The territory of Puerto Rico can be divided into three main geographic divisions (Figure 3-4): (1) a mountainous core that makes up the southern two-thirds of the island, also known as the central upland province; (2) a belt of rugged karst topography in the north-central and northwestern parts of the island; and (3) a discontinuous fringe of relatively flat coastal plains distributed along the coastal shores of the island.

The central mountainous area has been deeply eroded by streams into valleys several hundred meters deep with steep valley sides and the slopes of 30^{o} to 45^{o} are not uncommon. The rocks in the central upland are predominantly volcanic, including lava and tuff, sedimentary rocks derived from volcanic rocks, intrusive rocks, and discontinuous beds of limestone, ranging in age from Early Cretaceous to middle Eocene (Monroe, 1976). The karst region is an area underlain mostly by limestone of Oligocene and Miocene age, in which the topography is chiefly formed by solution. The coastal plains are nearly flat having a slight slope upward from the shore to the foothills, through which isolated hills of bedrock materials (such as limestone) are projected at places. The

deposits are mostly of Quaternary age (including Pleistocene and Holocene epochs) and consist of sand, clay, and gravel deposited in flood plains and alluvial fans of rivers, in coastal and river swamps, and on beaches.

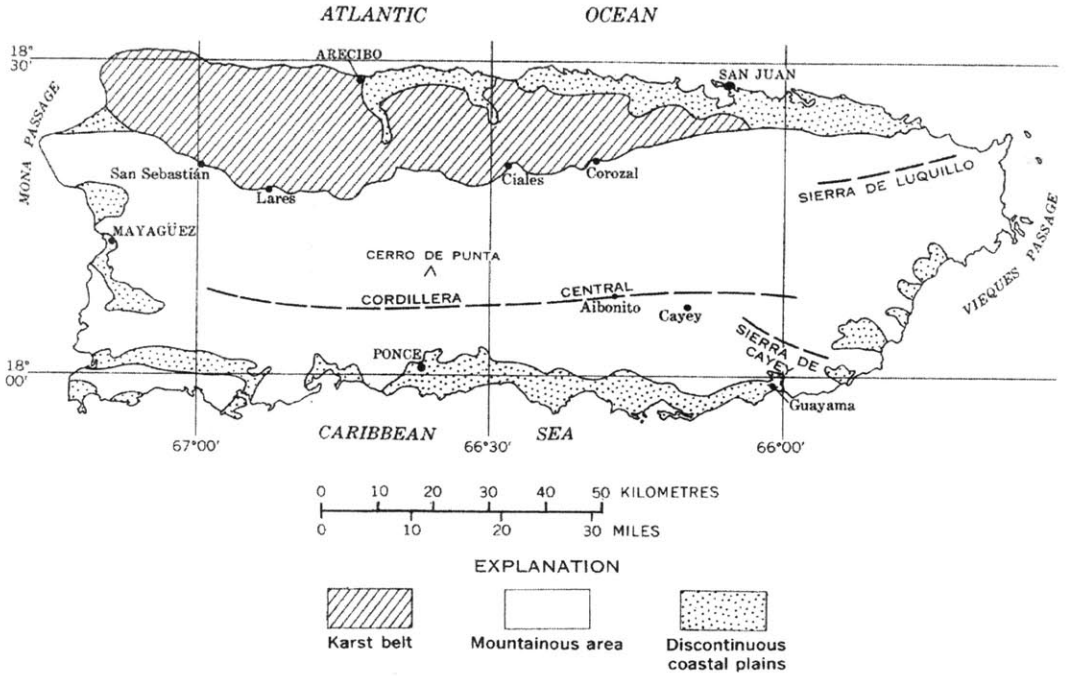

Figure 3-4. Map of Puerto Rico showing principal physiographic divisions (Monroe, 1976).

The investigated deposit in the construction site in Rio Piedras is named "old (or older) alluvium" by geologists (Deere, 1955; Kaye, 1959; Pease & Monroe, 1977), in order to differentiate it from the more recent lagoonal or flood plain sediments. It has also been referred to as the Hato Rey formation by the local practicing foundation engineers in Puerto Rico, because the deposit is exceedingly well exposed at the surface in the Hato Rey district. As part of the coastal plains, this area slopes very gently at 5~12% with surface elevation between 22 m to 28 m in the town of Rio Piedras and rises gently southward from the lagoons and swamps on the north and terminates to the south against hills of the central uplands. Figure 3-5 shows the cross-section of the San Juan area along with the construction site on the coastal plain.

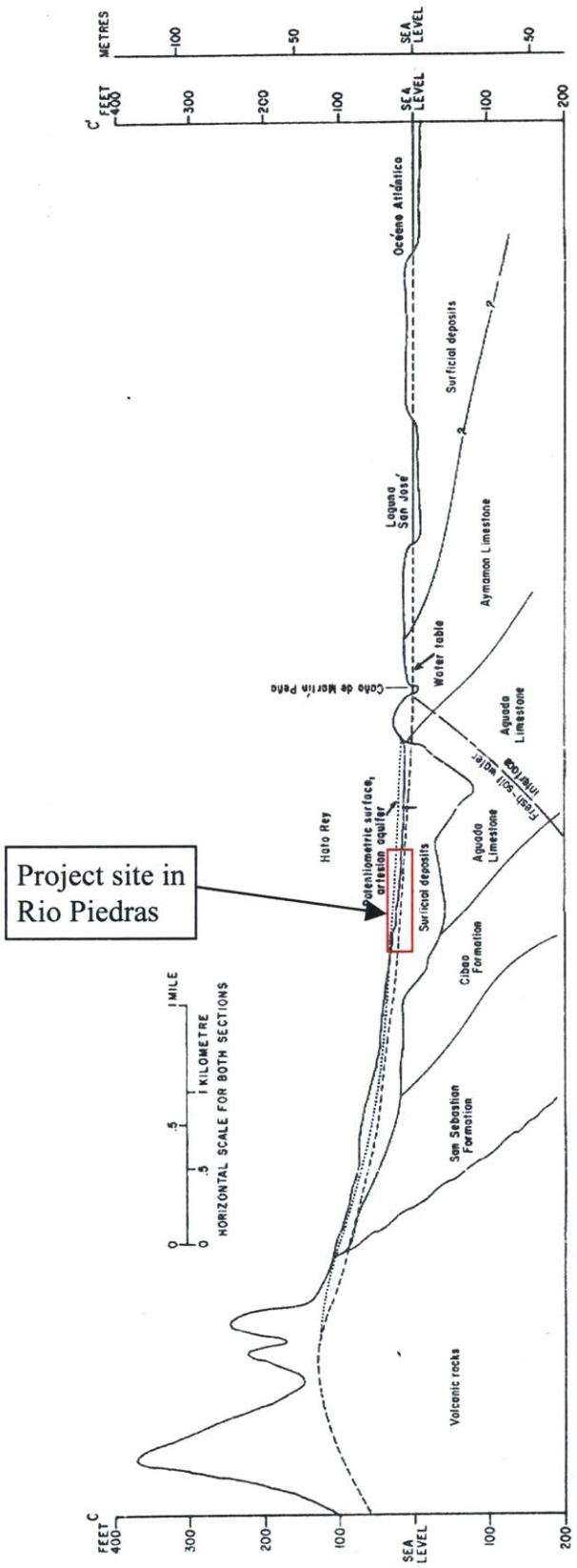

Figure 3-5. Cross-sectional sketch showing the geological settings of the old alluvium.

The contact between the old alluvium and the underlying bedrock is generally sharp. As Kaye (1959, p.35) described, "a thin pavement of pebbles and cobbles, among which fragments of vein quartz are particularly conspicuous, commonly marks the base of the older alluvium." It is believed that the old alluvium is generally underlain at depth by an eroded peneplain of middle Tertiary (early Miocene) limestone of Aguada formation (Kaye 1959; Anderson, 1976; Monroe, 1980a) with a complex erosional surface characterized by isolated conical-shaped pinnacles of more resistant limestone (CSTC, 1996). At several places isolated ridges and bosses of Miocene rock even project through or break the old alluvium (Pease & Monroe, 1977).

3.5 Geological Origin

The geology of the San Juan area has principally been studied by Deere (1955), Kaye (1959), Pease & Monroe (1977), and Monroe (1976, 1980a, 1980b). The top surfacial layer in this area has also been investigated by U.S. soil survey (USDA, 1978). US geological surveys focus mainly on the underlying bedrock in depth or on a very broad scope, while USDA soil surveys only concentrate on the surfacial layer at shallower depth. A knowledge of geologic origin including parent materials and soil development history helps understand the possible weathering paths and the final weathering products and minerals at present. Therefore, this section is a synthesis of several sources of the literature by summarizing the geologic origin of the deposit of the old alluvium based on U.S. geological surveys and soil surveys.

3.5.1 Alluvial Depositing

First of all, it is claimed that the structural and stratigraphic complexities in the San Juan area are too great to permit one to obtain a satisfactory synthesis of the geological history on the basis of reconnaissance or small-scale mapping (Kaye, 1959). In fact, the island of Puerto Rico has a very complex geologic history and the San Juan area encompasses nearly the full range of geology known on Puerto Rico. However, there is a generally consistent agreement about the geological origin of the old alluvium in the coastal plain. It has been built up by the accumulation of alluvial and colluvial sediments derived from the uplands to the south. According to Kaye (1959), the old alluvium was formed as a series of coalesced alluvial fans which are slightly dissected by small streams.

Based on field observations and boring logs, Deere (1959) concluded that: "the presence of the occasional stratification, sand pockets and lenses; the lack of marine fossils; and the areal relationship with the definitely fluvial type of deposits where the Hato Rey formation overlaps the Cretaceous rocks to the south, suggest very strongly that the Hato Rey formation is fluvial in origin, probably having been deposited as a piedmont alluvial plain." USDA (1978) also classifies the old alluvium as "soils formed in transported materials" within the area consisting of "deep, gently sloping to sloping, well-drained soils on terraces and alluvial fans of the coastal plain".

Moreover, other geological and geotechnical field investigations (CSTC, 1996) show that the deposition of the old alluvium on the coastal plain varies from sub-aqueous

to terrestrial and includes the development of complex stream systems subject to meandering of stream channels during numerous sea level fluctuations at the Pleistocene glacial epoch. During periods of glacial retreat, sea level rose and finer grained deposition generally occurred. During periods of glacial advance, sea level fell as water was taken up in expanding glacial ice sheets. During these times, stream gradient and energy increased resulting in down-cutting through and reworking of previously deposited coastal plain sediments. Consequently, the deposit is highly variable both horizontally and vertically.

3.5.2 Parent Rocks

As described above, the old alluvium is derived from the decomposed grains of the central upland to the south. The rocks in the upland are obviously the parent materials of the old alluvium. Basically, this deposit formed from sediments of mixed origin (USDA, 1978), which are the pre-weathered fragments (mainly sand and gravel) of the rocks in the surrounding uplands that are washed to the coastal plain from the hills. The major rocks are:

- Intrusive rocks, mainly granodiorite and quartz-diorite;
- Extrusive basic volcanic rocks, such as lava, tuff, breccia (USDA, 1978);
- Sedimentary rocks, such as limestone, tuffaceous sandstone and siltstone (Kaye, 1959).

The following lists the main rock-forming minerals which are contained in these rocks in the central upland (summarized from Kaye, 1959):

- Sedimentary rocks: calcite, marly clay, quartz, kaolinite;

- Intrusive rocks: albite, quartz, calcite, augite, chlorite;
- Volcanic rocks: feldspar, quartz, mica, pyroxene, albite, hornblende, chlorite, zeolite.

With the knowledge of the types of the parent rocks and the corresponding rock-forming minerals, it is possible to infer the possible residues left behind tropical weathering. For example, quartz and K-feldspar which are quite weathering resistant may still exist even the deposit has undergone long-term alteration, while other minerals, such as pyroxene and albite may be completely decomposed either into clays or other secondary minerals.

3.5.3 Post-depositional Weathering

The alluvial origin of the old alluvium may be misleading to geotechnical engineers if no further investigation is conducted. Weathering occurs and new soil-forming processes are initiated in deposits after exposure to the atmosphere, just as they are on freshly exposed rock (Mitchell, 1993). According to Deere (1955), the old alluvium was deposited in early Pleistocene, indicating that the soil has been deposited in place for 1~1.6 million years. Although there is no indication about when the deposit was exposed to the atmosphere, the old alluvium at present days is not submerged in rivers or oceans.

On the other hand, the current old alluvium consists of thoroughly decomposed sands and gravels. The most characteristic features of the deposit are (1) the lack of

relationship to present stream alluviation; and (2) The extensive conversion of non-quartz components to clays (Kaye, 1959). The weathered soil grains and aggregates, which visually look like sand or silt, can be broken down by finger pressure. As the soil is remolded between fingers, the soil becomes more plastic, very creamy and sticky. It implies that the deposit has undergone intense post-depositional weathering. Therefore, this deposit is a residual soil which is evolved from alluvial sediments through alteration or post-depositional weathering.

In summary, the old alluvium, originating from weathered rocks in central upland, deposited in an old coastal plain in early Pleistocene (1 to 1.6 million years ago). Originally it consisted of mainly sand and gravel grains as it deposited in the middle river terraces. Since deposition, the sand and gravel particles have undergone further alteration or post-depositional weathering, due to exposure to such humid tropical climate in San Juan. Fundamental changes with mineralogy, structure, and properties must have taken place. Therefore, the old alluvium is a special residual soil with alluvial origin, i.e., a highly weathered old alluvium, or sometimes a "transported residual soil".

3.6 Soil Profile

This section presents the general characteristics of the soil profile of the old alluvium in the San Juan area. Part of the information is obtained from the literature and some geotechnical data reports (CSTC, 1996; WCC, 1998), while other information is based on the author's first-hand experience obtained from field observations, field sampling, and the laboratory testing of the soil samples.

First of all, since the deposit was transported to the current location through variable stream channels, it has the following characteristics: weak stratification, absence of the parent rock structure, high vertical and lateral variability. The heterogeneity causes difficulties in defining the soil profile precisely.

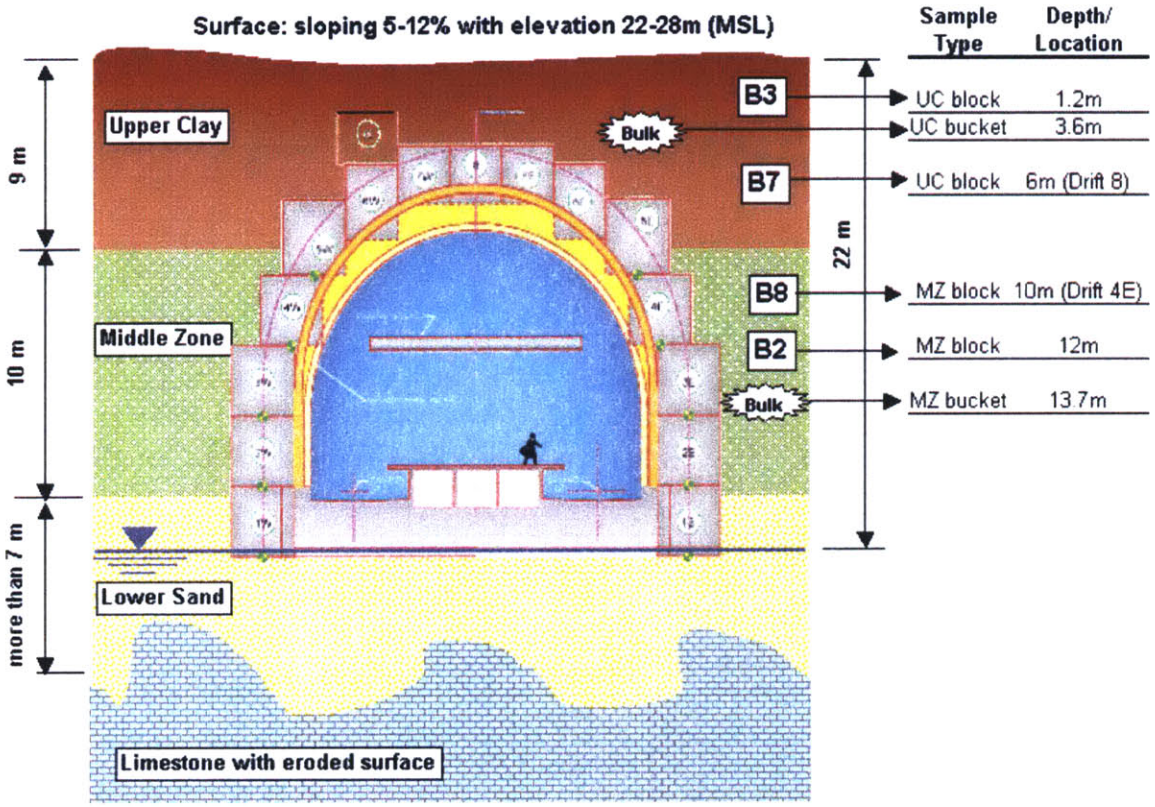

Figure 3-6. Soil profile of the old alluvium and sampling locations.

The old alluvium, consisting of thoroughly decomposed sands and gravels, is highly variable in thickness and may have a depth of at least 25m, in some places the thickness may exceed 30m (Kaye, 1959; Pease and Monroe, 1977). The variability in thickness may derive from the dissolved or eroded peneplain surface of the limestone

bedrock on which the old alluvium rests unconformably (Figure 3-6). As proposed by Woodward Clyde Consultants, Inc. (WCC, 1997), the deposit can be broadly classified into three main layers (Figure 3-6):

1. **Upper Clay (UC),** which is a medium stiff, brittle, red or reddish brown clay. This layer, with an average thickness of 8-9 m, consists mostly of red, or mottled red and white, silty clays with complex patterns of white veins. These light gray or white reticulations are rather characteristics and seem to be due to leaching by acidic subsurface water along fractures and roots (Kaye, 1959).
2. **Stratified Middle Zone (MZ),** 10 m thick, is a very stiff, brittle, light brown to yellowish sandy clay, silt or clayey sand with inter-bedded layers of sand. It seems less weathered than and denser than the UC layer, and contains more abrasive quartz grains which has a very high hardness (Mohs scale 7).
3. **Lower Sand (LS),** which is a layer containing quite extensive of relatively clean sand and silty sand. It is light gray when moist and becomes white after dried. The sand particles are mainly white quartz. Notice that this layer is within the range of groundwater fluctuations and weathering is not as intense in depth as in surface, hence LS is less weathered and the alteration is not so advanced. Therefore, for a well-drained sand layer within ground water fluctuations, possibly all weathered fine particles have been transported away by groundwater flow, and only coarse particles are left in place.

The above stratification is of great convenience for engineering design and construction. However, geotechnical investigations (CSTS, 1996; WCC, 1997) have also shown that the boundaries and transitions between these layers are not very clear and vary with

locations and depths, which are introduced through the complex depositional processes mentioned above.

The measured groundwater table is in the Lower Sand layer and is at 22m below surface (Figure 3-6). Notice that the ground water table is just 3 to 5 m higher than the mean sea level at this site. Therefore, both the UC and MZ are partially saturated. However, due to the effect of perched ground water and surface water percolation, the water content is very erratic over depth. Perched groundwater table conditions have been found locally in individual boring logs (CSTS, 1996). As discussed in Section 2.3, perched groundwater is mostly caused by the re-deposition of fine clay particles through illuviation and translocation with groundwater flow from the upper layer or the upper slope.

Based on field observations and boring logs, a general trend over depth is that the soil color changes from bright red to brown, to yellowish brown, and to yellowish gray with increasing depth, i.e., the red color decreases with depth. The clay fraction decreases with depth, whereas the fraction of sand (mostly quartz) and the average particle size increase. The UC has some fine sand particles of quartz, MZ fine to medium, and LS contains mostly medium quartz grains. Also, soil becomes denser and stiffer with increasing depth down to the LS layer.

Finally, the special soil profile of the old alluvium is quite different from that of common residual soils derived from in situ weathered rocks. The latter consists of several

weathering grades (Figure 2-1). The classification system based on these grades for in-situ weathered residual soils cannot be used for this alluvial residual soil in San Juan.

3.7 Soil Samples

Block samples, tube samples, and bucket material have been taken from the old alluvium at various depths in the construction site of Tren Urbano (Figure 3-6). Since the Lower Sand (LS) layer consists mainly of sands, only bucket sample was taken from this layer, while all three kinds of samples were obtained from both the UC and MZ layers.

Since bucket samples are disturbed and no intact structure is preserved, their main usage is to obtain the intrinsic properties of the particulate assemblage of the soil material. For example, soil composition (e.g., mineralogical and chemical analyses), index properties (including particle size distribution and Atterberg limits), and certain physical or chemical properties (e.g., cation exchange capacity, organic matter and water contents, soil pH, etc.) can be measured directly on bucket samples. Table 3-1 summarizes some basic information for the bucket samples taken from the old alluvium.

To assure the small amount of tested material to be highly representative, each bucket sample was totally homogenized by mixing and quartering before any utilization, during which caution was taken to prevent samples from drying, since drying may alter its mineralogical contents and physico-chemical properties (Fookes, 1997). Some basic chemical and physical properties of the two layers are presented in Table 3-2.

Table 3-1. Summary of the bucket samples taken from the old alluvium.

Sample ID#	Layer	Location	Depth (m)	Water content	Quantity (gallon)	Description	Utilization
Bucket1	UC	South shaft	3.6	44%	5	Reddish brown clay with white inclusions	Mineralogy Particle size Atterb. limits Soil pH Soluble salt SEM/ESEM
Bucket2	MZ	North shaft	13.7	34%	5	Yellowish gray, with sand particles	
Bucket3	LS	Drift 1E, Set 65	20.5	26.9%	5	White gray sands with quartz	Particle size SEM/ESEM

Table 3-2. Some basic physical and chemical properties of the old alluvium.

Parameter	Upper Clay	Middle Zone	Method
1:1 water pH	4.90	5.38	Soil reaction (pH) (SSL, 1996)
1:2 $CaCl_2$ (0.01M) pH	4.03	4.48	
1:1 KCl (1.0N) pH	3.48	3.84	
Water content (wt.%)	44.3	34.1	ASTM D2216 (1997)
Specific gravity	2.68	2.67	ASTM D854 (1997)
Soluble salt (wt. ppt)	0.086	0.048	KCl equivalent salt (SSL, 1996)
Carbonate (wt.%)	N.D.*	N.D.*	ASTM D4373 (1997)
Organic matter (wt.%)	0.1	0.0	Modified Walkley-Black (SSL, 1996)
Clay (<2μm) (wt.%)	38.1	20.5	ASTM D422 (1997)
Silt (2-75μm) (wt.%)	49.0	53.9	
Sand (>75μm) (wt.%)	12.9	25.6	
Plasticity Index (%)	32.2	22.3	ASTM D4318
Activity	0.84	1.09	Based on the above results

All data is measured from natural wet sample with in-situ water content.
*N.D. – not detectable.

High-quality undisturbed samples are essential to measure reliable and accurate data on the engineering properties of intact soils. Efforts have been made to obtain both tube samples and block samples. However, all 10 Shelby tube samples recovered from the site were totally disturbed, according to the sample quality evaluation by transmission X-ray radiography, and thus have not been utilized in any laboratory testing. As pointed

out by Fookes (1997), Shelby tubes are generally not recommended to obtain undisturbed samples from residual soils and block samples are preferred.

The recovery of block samples is generally difficult, especially at depths greater than a few meters. However, the open excavation of the tunnel at the Tren Urbano construction site provided much advantage in obtaining block samples, and enabled recovery of block samples from three site visits in January 1999, May 1999, and June 1999, respectively. In the field, immediately after excavating, each block sample was carefully selected and trimmed into rectangular shape and wrapped with 8-10 layers of plastic film to protect them from disturbance and drying during shipping and storage. Table 3-3 summarizes the location and quantity of these block samples.

Table 3-3. Summary of all block samples taken from the old alluvium.

Boring site	Sampling time	Layer	Depth (m)	Quantity	Utilization
B1	Jan 99	MZ	10.7	2 blocks	Consolidation behavior Shear strength Intact microstructure Macro-structure Slaking
B2	Jan 99	MZ	12	4 blocks	
B3	Jan 99	UC	1.2	8 blocks	
B4	May 99	UC	3.5	2 blocks	
B5	May 99	UC	9.0	2 blocks	
B6	May 99	MZ	15.3	1 blocks	
B7	Jun 99	UC	6	15 blocks	
B8	Jun 99	MZ	10	11 blocks	

In fact, subsequent assessment of the sample quality by transmission X-ray radiography indicated that the majority of these large blocks have little disturbance, while others have cracks or fissures imparted through shipping, which have not been used in laboratory testing. These intact samples also provide the advantage of imaging both the micro- and the macro-structure of these two layers, as well as measuring the intact soil properties.

References

Anderson, H.R. (1976) *Ground water in the San Juan metropolitan area, Puerto Rico.* U.S. Geological Survey, Water-Resources Investigations 41-75.

Blight, G.E. (ed.) (1997) *Mechanics of Residual Soils.* A. A. Balkema, Rotterdam.

CSTC (Caribbean Soil Testing Co., Inc.) (1996) *Geotechnical Data Report* – Rio Piedras Contract.

Deere, D.U. (1955) *Engineering properties of the Pleistocene and recent sediments of the San Juan Bay area, Puerto Rico.* Ph.D. thesis, University of Illinois Urbana.

Dixon, J.B. and Weed, S.B. (ed.) (1989) *Minerals in Soil Environments.* 2nd Edition. SSSA Book Series 1. Soil Science Society of America, Wisconsin, USA.

Fookes, P.G. (ed.) (1997) *Tropical Residual Soils.* Geological Society Professional Handbooks. The Geological Society, London.

Kaye, C.A. (1959) *Coastal Geology of Puerto Rico: (A) Geology of the San Juan Metropolitan Area.* Geological Survey Professional Paper 317. US Government Printing Office, Washington, D.C.

Martini, J.A. and Mosquera, L. (1972) Properties of five tropepts in a toposequence of the humid tropics in Costa Rico. *Soil Science Society of America Proceedings*, **36**, 473-477.

Mitchell, J.K. (1993) *Fundamentals of Soil Behavior.* 2nd edition. John Wiley & Sons, Inc.

Monroe, W.H. (1976) *The Karst Landforms of Puerto Rico.* Geological Survey Professional Paper 899. US Government Printing Office, Washington, D.C.

Monroe, W.H. (1980a) *Geology of the Middle Tertiary Formations of Puerto Rico.* Geological Survey Professional Paper 953. US Government Printing Office, Washington, D.C.

Monroe, W.H. (1980b) *Some Tropical Landforms of Puerto Rico.* Geological Survey Professional Paper 1159. US Government Printing Office, Washington, D.C.

Moore, D.M. and Reynolds, R.C., Jr. (1997) *X-Ray Diffraction and the Identification and Analysis of Clay Minerals.* 2nd Edition. Oxford University Press.

Pease, M.H., Jr. and Monroe, W.H. (1977) *Geologic Map of the San Juan Quadrangle, Puerto Rico.* US Geological Survey.

Paterson, E. & Swaffield, R. (1987) Thermal analysis. In: M.J. Wilson (ed.), *A Handbook of Determinative Methods in Clay Mineralogy*, Blackie & Son Ltd.

SSL – Soil Survey Laboratory (1996) *Soil Survey Laboratory Methods Manual.* Soil Survey Investigations Report No. 42, Version 3.0.

Stucki, J.W., Goodman, B.A., and Schwertmann, U. (ed.) (1985) *Iron in Soils and Clay Minerals.* NATO ASI series. D. Reidel Publishing Company.

Uhlik, P., Sucha, V., Eberl, D. D., Puskelova, L., & Caplovicova, M. (2000) Evolution of pyrophyllite particle sizes during dry grinding. *Clay Minerals*, **35**, 423-432.

USDA (United States Department of Agriculture) (1978) *Soil Survey Of San Juan Area of Puerto Rico.*

Velde, B. (1992) *Introduction to Clay Minerals.* Chapman & Hall.

Velde, B. (ed.) (1995) *Origin and Mineralogy of Clays.* Springer-Verlag, Berlin.

WCC (Woodward Clyde Consulting, Inc.) (1997) *Geotechnical Data Report* – Rio Piedras Contract.

Wilson, M.J. (ed.) (1987) *A Handbook of Determinative Methods in Clay Mineralogy.* Blackie & Son Ltd.

Wilson, M.J. (1999) The origin and formation of clay minerals in soils: past, present and future perspectives. *Clay Minerals*, **34**, 7-25.

Chapter 4 OVERVIEW OF RESEARCH METHODOLOGY

4.1 Introduction

This research comprises an extensive experimental characterization of soil composition, structure, and behavior (including some physico-chemical properties, index properties, and engineering properties) for the old alluvium in the Tren Urbano construction site in Rio Piedras. The previous chapters have provided sufficient background information on weathering and soil formation in tropical climates, geological history and site characteristics of this deposit. Starting with this chapter, the laboratory experimental research program will be discussed. Before a detailed description of each experiment and its related results is presented in the following chapters, it is necessary to give a general overview of the methodology adopted for this research.

To emphasize the reasons why so much effort has been taken and so much time has been spent on the soil composition determination and the microstructure characterization, Chapter 4 begins with a general introduction to the inter-relationships between soil composition, structure, and soil behavior (Section 4.2), followed by a discussion of the central theme of the adopted experimental research program in Section 4.3. Section 4.4 serves as an introduction to those techniques for determination of soil composition and for characterization of soil microstructure, most of which are available in the Center for Materials Science and Engineering (CMSE) at MIT. Finally, this chapter

ends with Section 4.5, which briefly summarizes the entire experimental research program presented in subsequent chapters.

4.2 Soil Composition, Structure, and Soil Behavior

Without doubt, the macroscopic mechanical properties of a common material (e.g., steels, plastics, or wood) are predetermined by the chemical or elemental compositions and the microstructure at the molecular or atomic level. Any changes in mechanical properties must be caused by certain alterations in chemical compositions or microstructure or both. For instance, an aluminum alloy has different mechanical properties from the pure aluminum since it contains some extra elements (such as Ni, Cr) added to improve its performance; Stainless steel is more resistant to corrosion than a common steel since it contains other metal elements in its composition. On the other hand, even without any change in chemical compositions, a material may behave differently through changing its internal microstructure. A simple example is that a common steel bar gains a higher yielding stress simply by strain-hardening or prestressing, due to the strain-induced reorientation of dislocations existing in the polycrystalline steel.

Soil mechanics deals with the naturally occurring soil, a particulate earth material consisting of hard particles with no or weak cohesion or cementation. One of the fundamental assumptions used to develop many theories in soil mechanics is that these individual soil particles are not compressible compared to the stress level that the soil skeleton can sustain, resulting in the main focus of soil mechanics is the individual

particles. In general, stresses are transmitted between particles, shear strength is generated though particle contacts, and the volume change reflects the relatively movements between particles or particle groups. Therefore, the soil composition simply means the solid particles or mineral phases, but not the elemental chemical compositions; and soil microstructure describes the arrangement and association between particles or particle groups, but not the atomic or molecular structure (crystal structure) of minerals in a soil.

The particles existing in a soil can comprise crystals or amorphous minerals, whose properties (mainly crystal structure and surface properties) also affect the macroscopic mechanical properties of the soil. For example, kaolinite and smectite are the two most common clay minerals in soil environments. A soil consisting dominantly of smectites behaves totally different from one which only contains kaolinite, if they are subjected to same wetting and drying cycles; under the same conditions and stress state, the former has a much low effective friction angle ϕ' than the latter (Ladd, 2001). Therefore, knowledge of the soil composition is important for understanding the mechanical properties of a soil material.

However, only knowing the soil composition is far from enough for a thorough understanding of engineering properties. A simple example used by Mitchell (1993) to illustrate the importance of soil structure to its properties is the strength loss of a quick clay caused by the disturbance or remolding at constant water content (Figure 4-1). Clearly, disturbance or remolding does not change the soil composition and water

content, but only the soil fabric. However, the quick clay with certain strength becomes fluid on remolding. Other familiar examples include that: (1) disturbed samples generally show smaller compression indexes and lower preconsolidation stresses than the original intact soil. The difference is also caused by disturbing or changing the initial intact soil structure; and (2) the anisotropic properties of some sedimentary soils are the macroscopic reflection of particle orientations or interparticle contact orientations in the soil's microstructure. These examples clearly show that soil microstructure plays an important role in understanding engineering properties of the soil.

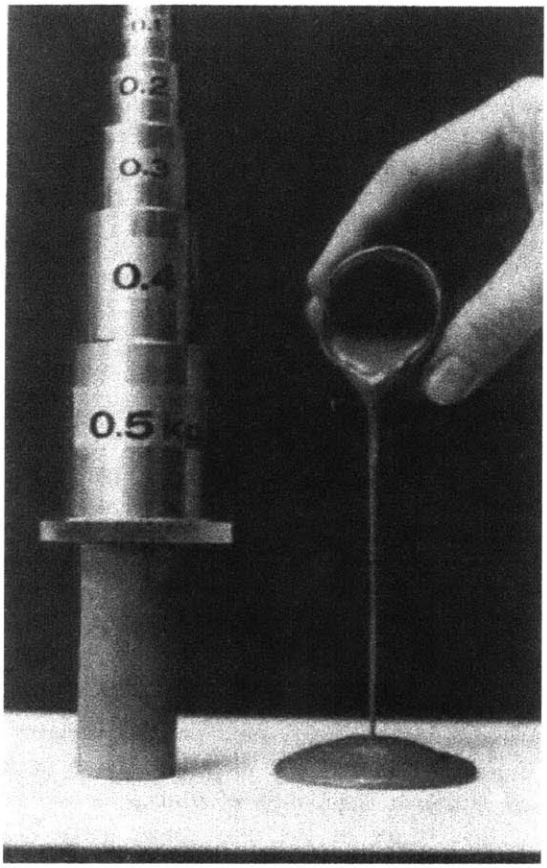

Figure 4-1. Strength loss of a quick clay that is extremely sensitive to remolding. (Photograph courtesy of Haley and Aldrich, Inc.) (Mitchell, 1993)

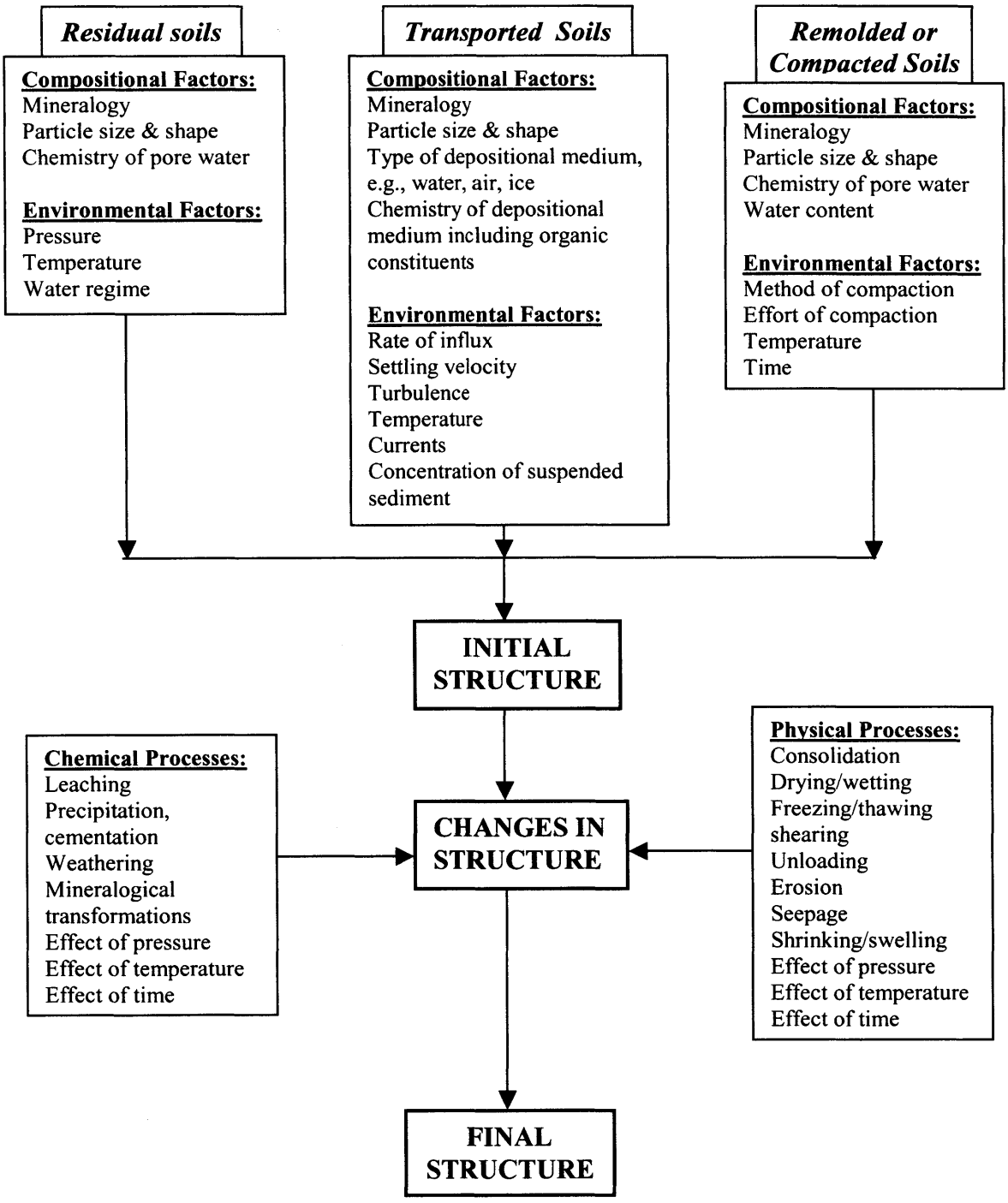

Figure 4-2. Structure-determining factors and processes (Mitchell, 1993).

The previous discussions of weathering processes have also shown that the composition and structure of the residual soils are likely changing over time. In comparison, leaching of salt or changes in pore water chemistry of transported soils can

also alter the soil structure. Furthermore, any changes in the stress state to which the deposit is subjected may introduce new structural features in the soil fabric. Mitchell (1993) states that the current structure of soil is composed of its fabric and interparticle force system that reflect all facets of the soil composition, history, present stress state, and environment. To completely understand the current structure which determines the current properties of a soil deposit, both the initial structure developed in a young deposit and any changes in structure caused by any geological, physical, or chemical processes should be taken into account. For purposes in both research and engineering practice, these structure-determining factors and processes shown in Figure 4-2 should be investigated as thoroughly as possible.

In summary, soil composition, structure, and soil behavior are interrelated. Certain changes in soil composition can alter the soil structure, while soil behavior depends directly upon mineralogical and chemical compositions, the current state of soil structure, and the historical effects of the environment (Mitchell, 1993, p.84). Indeed, "the effects of structure are as important in determining engineering behavior as are the effects of initial porosity and stress-history, which are the basic concepts of soil mechanics" (Leroueil and Vaughan, 1990).

4.3 Central Theme of the Experimental Research Program

Now that the inter-relationships between soil composition, structure, and properties have been discussed, it is clear that both the soil composition and soil structure should be determined. This requires the application of materials characterization

techniques. The importance of materials characterization in geotechnical engineering was also pointed out by Mitchell (1993): "To properly deal with the earth materials (i.e., soils and rocks) associated with any project requires knowledge, understanding, and appreciation of the importance of geology, materials science and testing, and mechanics." However, due to difficulties involved in the compositional analysis and soil microstructure characterization, the long time needed to perform the analyses, their cost, and lack of background knowledge of most practical engineers, these investigations are rarely performed in most practical construction projects.

Fortunately, before sophisticated materials characterization techniques were available, the pioneering research of geotechnical engineers and soil scientists who already recognized the importance of soil composition and soil structure to the mechanical properties produced some simple methods to indirectly estimate the soil composition and structure. Of all these techniques, index property measurement is widely used and well developed. For example, clays with exceptional high liquid limit (say, >400%) and/or very high activity (activity, A = plasticity index/%<2μm) can be expected to contain smectites. In addition, the concept of sensitivity (defined as the ratio of the undisturbed to remolded strength) can be used to estimate the fragility of the situ soil structure. However, difficulties rise with these simple index properties when a soil is a mixture of several minerals. Moreover, the above empirical estimation on soil composition and structure is not positive and diagnostic. Therefore, positive determination of soil composition and microstructure is still a prerequisite for a thorough understanding of engineering properties.

The importance of direct measurement of engineering properties should not be underestimated. In fact, many successful projects have relied only on direct measurements on compressibility, permeability, and shear strength. However, for many other situations, knowledge of soil composition and structure may be more critical than the direct measurement of engineering properties, since the selection and design of the laboratory or field testing program (including methods and procedures) to measure the engineering properties require the knowledge of soil composition and soil structure. Without an appreciation of soil structure, misleading results may be obtained using inappropriate experimental methods. A simple and familiar example is that, for the strength measurement of a sedimentary soil with cementation or high sensitivity, the recompression technique is preferred over SHANSEP. Therefore, the soil composition and soil structure also affect the design and selection of laboratory testing methods and procedures for the measurement of engineering properties.

Therefore, the central theme of this thesis research is to give equal importance to geology, materials characterization, and engineering properties measurement and to follow the sequence of investigations: from geology, surrounding environment, and soil formation, to soil composition, to soil structure, to index and physico-chemical properties, and finally to engineering properties, as illustrated in Figure 4-3.

The main difference between the research methodology adopted here and the conventional soil mechanics approach is that much more effort has focused on the two

main tasks, i.e., determination of soil composition and characterization of soil microstructure. Although index properties are routinely measured in conventional site investigation, this research program includes a detailed investigation of the relationship between Atterberg limits, particle size distributions, and the energy used to break down the intact soil structure.

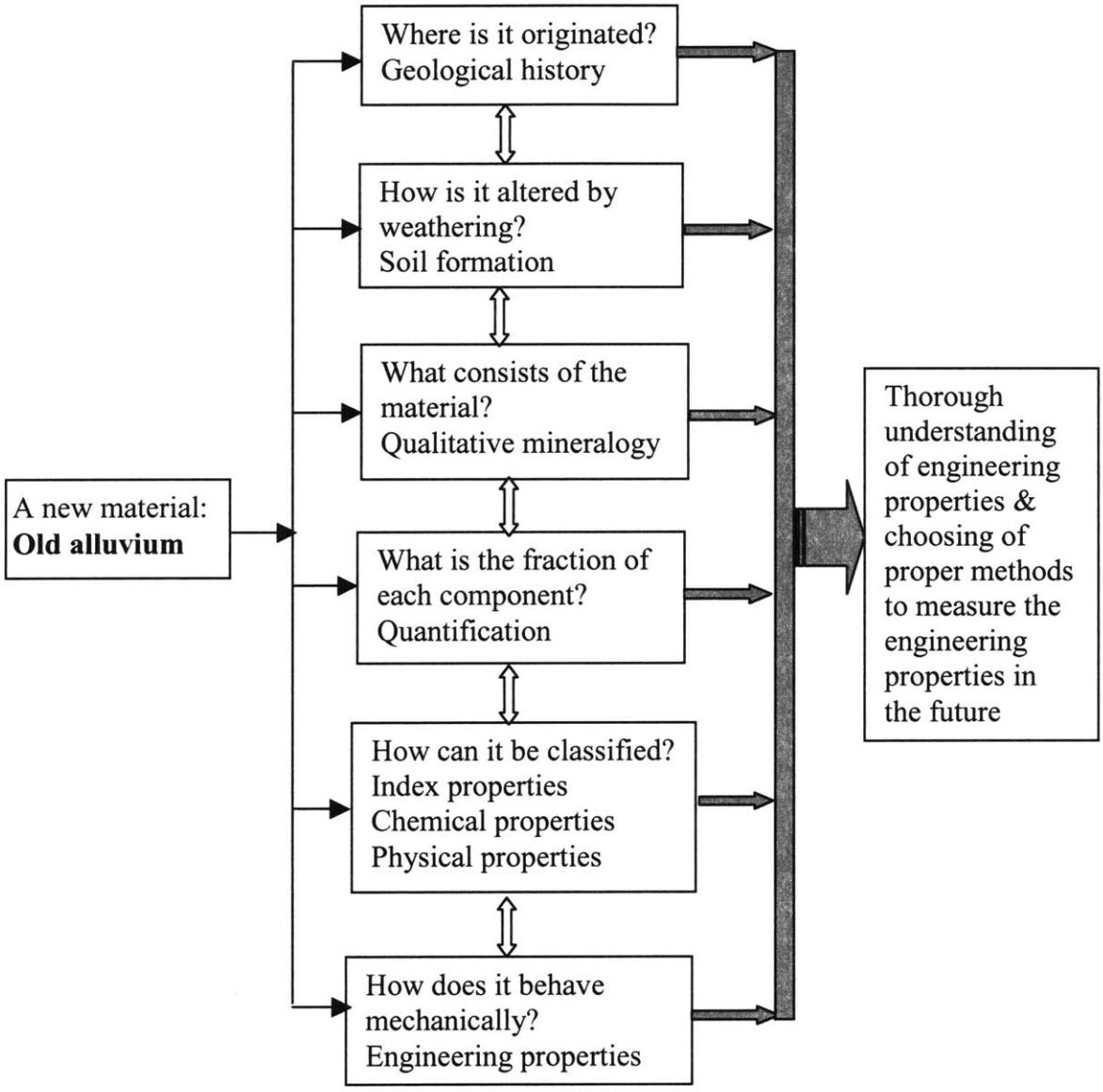

Figure 4-3. Flow chart showing the central theme of the thesis research.

Another reason why this methodology is adopted here is that the investigated material is a special residual soil with alluvial origin, or a weathered old alluvium. As the behavior of residual soils, especially tropical residual soils, is governed at the microscopic and mineralogical levels and influenced by environmental factors (rainfall, temperature, vegetation, etc.), their behavior is sufficiently different from other sedimentary soils that they require special attention, it is necessary to delve into the science and chemistry of these soils in order to better understand their behavior for engineering and construction purposes.

4.4 Overview of Techniques for Soil Characterization

Various experimental techniques are required in order to implement the research methodology depicted in Figure 4-3. In this section, a general overview of techniques for soil characterization is provided for understanding what approaches are available and why they are chosen to characterize the old alluvium. It should be pointed out that most of them, which are available in the Center for Materials Science and Engineering (CMSE) at MIT, are more frequently used for materials analysis and characterization. These techniques are the main concerns of this section; while others are more routine methods used extensively in geotechnical laboratory, and will not be addressed here.

In addition, a thorough treatment on each technique includes the fundamental principles, instrument, sample preparation, operation and procedures, and data processing. It is out of the scope of the thesis to delve deeply into all aspects of these

experimental techniques. Therefore, only the physical principles lying behind these techniques are presented here, focusing exclusively on their applications for soils.

Techniques for determining soil composition

Numerous approaches have been adopted from materials microcharacterization techniques to identify soil minerals. The traditional and well-established tools include X-ray powder diffraction (XRD), thermal analysis, and chemical analysis (Wilson, 1987), while electron microscopy equipped with energy-dispersive X-ray spectroscopy (EDXS) can provide useful information on micromorphology and chemical constituents of individual particles. Mitchell (1993) gave a systematic summary of these methods and techniques that may be employed for determination of soil composition:

a) Particle size analysis and separation;
b) Various pretreatments prior to mineralogical analysis;
c) Chemical analysis for oxides, hydroxides, amorphous constituents, carbonates, and organic matter;
d) Electron microscopy;
e) X-ray diffraction (XRD) for identification of crystalline minerals;
f) Thermal analysis;
g) Determination of specific surface area;
h) Chemical analysis for layer charge, cation exchange capacity (CEC), exchangeable cations, pH, and soluble salts.

Of all techniques listed above, only are XRD, thermal analysis, and chemical analysis (including X-ray fluorescence (XRF), CEC, and selective chemical dissolution (SCD))

presented here, since this research employs these methods to determine the composition of the old alluvium. Although scanning electron microscopy (SEM) is also used to study soil composition, its advantage is to study soil structure of this deposit. Therefore, SEM is discussed in the next section.

X-ray diffraction (XRD)

XRD is a method most commonly used to study crystalline minerals, including the minerals in soil environments. XRD derives its strength from the direct measurement of the size and shape of crystal structure of minerals. The physics behind this technique is that:

1) As part of the electromagnetic spectrum, X-rays have properties of both waves and particles;
2) As one form of solid matter, crystalline minerals (or simply crystals) are comprised of millions of regularly arranged unit cells (consisting of atoms);
3) The distance between atoms in crystals is about the same as the wavelength of X-rays (i.e., 10^{-10} m = 1 Å);
4) Atoms in a crystal interact with X-ray waves by scattering. An array of atoms arranged regularly scatter X-ray waves instantaneously, producing either constructive or destructive interferences between these scattered waves;
5) Constructive interference occurs between these scatted waves only when $n\lambda = 2d\sin\theta$ (in which, λ is the wavelength of the X-ray, n is an integer,

d is the distance between two atomic planes in the crystal, and θ is the diffraction angle between the incident X-ray and the atomic plane), resulting in a strong peak (amplitude) in the diffracted beam formed by summing the amplitudes of all scattered X-rays (Figure 4-4). This principle is well known as Bragg's Law (the Braggs, father and son, shared the 1915 Nobel Prize for this work).

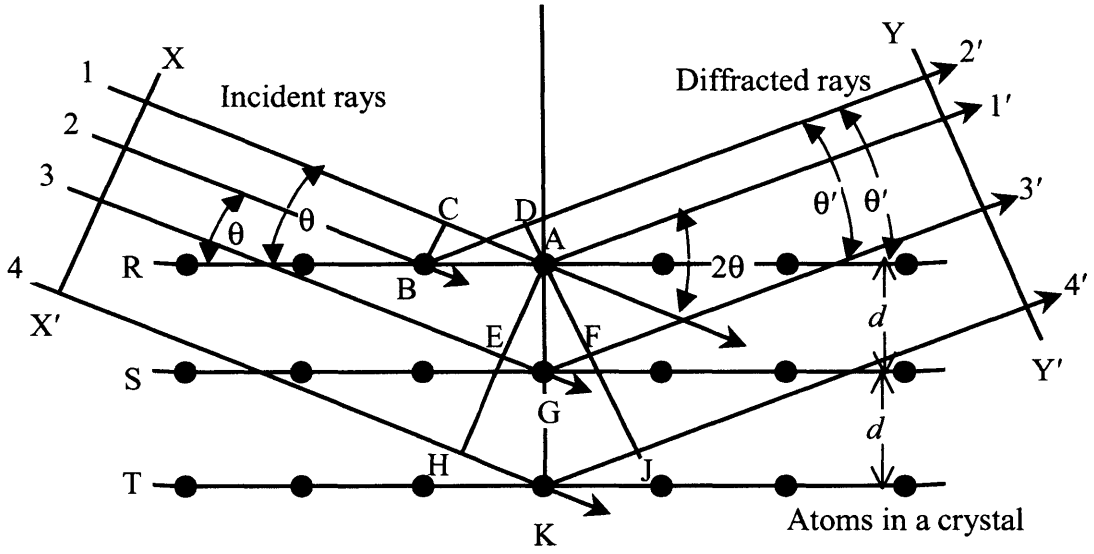

Figure 4-4. Schematic illustration of Bragg's Law (Moore and Reynolds, 1997).

[Note: constructive interference of diffracted rays 1′ and 2′ from a single row of atoms (e.g., atom row R) is satisfied only when $\theta = \theta'$. For diffraction from more than one row of atoms, constructive interference of diffracted rays 1′, 3′, and 4′ occurs only when $EG + FG = n\lambda$, i.e., $2d\sin\theta = n\lambda$.]

Clay minerals are hydrous aluminum silicates and are classified as phyllosilicates, or layered silicates, most of which are crystalline. The classification of clay minerals is based on the unique crystal structure of each mineral. Therefore, XRD is the most powerful technique to positively identify clay minerals with crystalline state. Other non-clay minerals, such as quartz, feldspars, mica, calcite, can also be positively identified if they are in crystalline state. However, amorphous minerals, including both clays and non-

clays, cannot be readily identified by XRD. For instance, the existence of allophane (a clay mineral) or Opal-A (an amorphous silica, like glass) cannot be determined by XRD and other techniques, such as NaF pH measurement, may be required.

Besides its strength in qualitative analysis, XRD can also be used for quantitative estimation of the fraction of the crystalline minerals in a soil, since the X-ray intensities (amplitudes) diffracted by components in mixtures are obviously related to the proportions of the components. Brindley (1980) provids a good summary for quantification of soil minerals. However, difficulties rises with the number of the types of different minerals present in a soil. When a soil contains several mineral phases, reflections from different minerals may coincide or overlap, and hence it is difficult to precisely measure the intensity of each reflected peak.

Thermal Analysis

The basis that minerals can be identified by thermal analysis is that different minerals exhibit different physical and chemical properties upon heating, i.e., certain reactions take place within the minerals upon heating. These reactions usually cause either the weight loss (e.g., dehydration) of the sample or temperature changes associated with the reactions. Thermogravimetric analysis (TGA) involves the measurements of the sample weight during the heating process, while differential thermal analysis (DTA) measures the temperature difference between the analyzed sample and a thermally inert substance (usually alumna (Al_2O_3) or platinum as a reference material).

The important thermal reactions that generate peaks on the recorded thermogram are listed as follows:

- **Dehydration.** This is a process of losing water upon heating. In addition to free pore water, a soil or a mineral may also contain the other three forms of water: adsorbed water or cation-hydrated water on mineral outer surface; absorbed water or interlayered water such as in the tubular halloysite and expandable smectites. This water may also be hydrated with cations, but it exists in the inner space of clay minerals; and the crystalline water in the form of (OH^-) hydroxyls, the removal of which is called dehydroxylation.
- **Recrystallization.** By heating to a higher temperature, new crystals can form either from amorphous minerals or from another crystal destroyed at a lower temperature. For example, goethite (FeOOH) usually dehydroxylates at 300-350°C and recrystallizes as hematite (Fe_2O_3) at higher temperatures (>500 °C).
- **Crystal structure transformation.** Some crystals simply change their structure from one form to another at a specific temperature without weight change. For example, quartz changes from the α (low or hexagonally closed packed, hcp) to β (high) form (reversible) exactly at 573°C, showing a sharp peak in the DTA curve but no peak in the TGA curve.
- **Oxidation.** Such reactions as oxidation may take place when temperature is increased, e.g., the combustion of organic matter, oxidation of Fe^{2+} to Fe^{3+}, and the loss of CO_2 from calcium carbonate.

The results of thermal analysis are usually plotted as weight versus temperature (TGA) or differential temperature versus heating temperature (DTA). Depending on the position (i.e., the temperature), the direction (upward, exothermic with energy loss; downward, endothermic with energy gain), and the shape (sharp or broad) of the peaks in the recorded DTA or TGA curves, the mineral species can be identified. Moreover, if the peak height or area can be measured and calibrated, quantitative thermal analysis can also be performed. For example, the loss of weight accompanied with the dehydroxylation of kaolinite or goethite can be used to estimate the amount of kaolinite or goethite in a soil.

Chemical analysis by X-ray fluorescence (XRF)

XRF is a broadly employed technique to analyze both qualitatively and quantitatively the elemental composition of bulk material. Indeed, this technique is well developed and has high accuracy of results. However, the results obtained by XRF only reflect the total concentration of the chemical elements in a given mixture, while the mineral phases or species are unknown. The great importance of this analysis can be exhibited with qualitative XRD or thermal analysis to perform quantitative analysis of a soil whose mineral phases have already been identified.

The basic principle lying behind XRF is that different chemical elements have unique X-ray emissions, characterized by a constant wavelength or energy ($E = h\upsilon = hc/\lambda$, in which, E is the energy of X-rays; h is Planck's constant; υ and λ are frequency and wavelength of X-rays, respectively; c is the speed of light). By bombarding a sample with high-energy X-radiation, X-ray emission can be generated from the chemical

elements in the sample. By measuring the wavelength or energy of the emitted X-rays, all elements within the sample can be identified. In turn, by recording the amplitude or the intensity of the X-rays, the concentration of each element can be estimated. Depending on which parameter, i.e., either wavelength or energy, of the X-rays is measured, the detection method is called either wavelength dispersive X-ray spectroscopy (WDXS) or energy dispersive X-ray spectroscopy (EDXS).

Other chemical analyses

Other analyses on the chemistry of soils include CEC (cation exchange capacity), selective chemical dissolution (SCD), pH, soluble salts, organic matter, carbonates, oxides and hydroxides, and amorphous minerals, most of which influence the soil behavior either through direct interaction with clay minerals or through the pore water chemistry. Most of these methods can be found in ASTM Standard Methods Manuals (ASTM, 1997) and Soil Survey Laboratory method manuals (SSL, 1996). However, CEC and SCD deserve further discussion. CEC measures the total negative charges on the faces of clay minerals, which is caused by isomorphous substitutions in the tetrahedral or octahedral sheets in clay minerals. Each clay mineral has a specific range of CEC. The CEC of a clay mixture is the weighted average of the CEC of each component, therefore, CEC can also be used to identify and quantify clay minerals (Mitchell, 1993).

SCD is a technique widely used by soil scientists. Basically, SCD uses one or more specific chemicals to treat a soil sample to dissolve only one special mineral

component. For example, the determination of organic matter, carbonate, and Fe-oxides can all be obtained by SCD techniques.

Techniques for microstructure characterization

Although soils are composed of discrete soil particles and particle groups, a soil mass is almost always treated as a continuum for analysis and design. Nonetheless, the values of properties such as strength, permeability, and compressibility are determined directly by the size and shape of the particles, their arrangements, and the forces between them. As mentioned previously, the soil microstructure, referring to the arrangement of particles, particle groups, pore spaces, and interparticle forces (e.g., bonds, cementation), is an important characteristic of an intact soil. Techniques used in this research for microstructure characterization include scanning electron microscopy (SEM), environmental SEM, slaking, transmission X-ray radiography, and mechanical property measurements.

Electron microscopy

The electron microscope is a valuable tool for the study of soils, because of its much higher magnification than optical microscopes, its larger depth of field, its ease of operation, and the simplicity of sample preparation. In addition, the built-in facilities, consisting usually of energy dispersive X-ray spectrometers (EDXS) and electron diffraction, improve the usefulness of the electron microscopes.

Two types of electron microscope are widely used to study minerals: scanning electron microscopy (SEM) and transmission electron microscope (TEM). Recently developed environmental SEM (ESEM) is fundamentally the same as the conventional SEM, except that it is capable of imaging and analyzing the sample in low vacuum pressures, which should be avoided in a conventional SEM. As a result, samples in an ESEM can be observed in wet mode. This is a great advantage for the study of soil microstructure, since intact soils are usually wet in situ and drying may significantly destroy the soil fabric, especially for soft clays. Although different techniques have been developed to minimize the disturbance to the intact structure and to remove the pore fluid from soils so that the sample can be examined in a conventional SEM, such as freeze-drying, critical-point drying, or pore fluid replacement (McHardy and Birnie, 1987), it is difficult to keep the soil fabric intact and almost impossible to estimate the degree of any possible disturbance.

SEM/ESEM is an indispensable tool for studying the soil micromorphology (particle size, shape, and surface features), soil fabric (particle orientation, texture, particle associations, pore size and distribution), and interparticle bonds or cementation. With the add-on tools, such as EDXS or electron diffraction, microanalysis (usually elemental analysis or crystal orientation) can be performed on single particles over a small area (<1μm). Therefore, SEM can reveal both the soil microstructure and soil composition. The chemical analysis performed by EDXS is different from XRF, since the results of XRF are obtained from a bulk material, whereas EDXS under SEM can accurately reveal the chemical composition of single grains or a small area. It should be

pointed out that, although the EDXS on a SEM employs the same principle to detect the X-rays as XRF, the X-ray emission in XRF is caused by high energy X-rays while in EDXS under SEM the emission is produced by the high energy electron beam.

The physics employed by electron microscope is listed as follows:

- By bombarding the sample (essentially atoms) with high energy electron beam accelerated through high voltage, several quantum processes can take place: part of the original electrons re-bounce back as backscattered electrons; these low-energy electrons in atoms of the sample are ejected out by the original electrons as secondary electrons; X-rays are produced accompanied with the loss of an electron in atoms (basically a drop of a high energy electron in the outer shell of atom to fill the empty space previously occupied by the ejected electron in the inner shell of an atom). By focusing on either backscattered electrons, secondary electrons, or X-rays, the sample can be analyzed by imaging or microanalysis.
- Imaging generally uses secondary electrons, and sometimes backscattered electrons. Through a specially designed integration circuit, these electrons can be detected or collected to form a current, whose intensity can be used as a base to form an image. In addition, the electron beam or the electron gun is controlled to move very quickly in a zigzag pattern over the sample as scanning, so that each point on the sample surface can be scanned. By putting together these signals scanned on each point, an image of the sample is formed. Because of their low energy, only those secondary electrons generated within a few nm of the specimen surface will escape and contribute to the

signal; their yield is little affected by the chemistry of the specimen material and is almost entirely related to topography.

- Microanalysis employs either X-rays by EDXS or backscattered electrons. As mentioned before, each element produces characteristic X-ray emissions which can be used to identify the element and to estimate its concentration. Since backscattered electrons have higher energy and the yield of such electrons is strongly dependent on atomic number, they can be used for both imaging or chemical analysis. In addition, electron backscatter diffraction allows precise measurement of crystal orientation or texture.

While SEM focuses on the observation on topography of samples and on the large depth of field, TEM is more useful to observe thin particles with a much higher magnification. In TEM, electrons transmit or penetrate through the sample so that an image can be obtained. Of course, backscattered electrons can also be used for imaging. Therefore, TEM is more valuable to observe the individual dispersed particles, but not the soil intact structure.

Slaking

Most fine-grained soils slake after exposure to air and subsequent immersion unconfined in water; that is, an initially intact piece of soil will disintegrate into a pile of pieces or sediment of small particles. This disintegration may begin immediately upon immersion or develop slowly with time.

Slaking usually is more rapid and vigorous in materials that have been dried prior to immersion as compared to the same material immersed at its initial water content. Whether a material slakes or not has been proposed as a basis for distinguishing between soil and rock. The following four modes of disintegration have been identified during slaking:

- Dispersion slaking. Particles of clay detach from the surface of the intact clay by dispersion into the adjacent water.
- Swelling slaking. Water is adsorbed by the clay and the material swells and softens.
- Surface slaking. Aggregates of clay particles spall off the surface and accumulate as a sediment in the adjacent water.
- Body slaking. The material splits and disintegrate into pieces, and the failure appears to develop from the inside out.

There are three mechanisms that are responsible for these modes of failure. Dispersion slaking is dependent on the clay and water chemistry; Swelling slaking can be explained by stress relief and water intake due to water adsorption and osmotic forces. In addition, the swelling force from expandable minerals in soils tends to split the samples; Compression of entrapped air in partially saturated soils is responsible for body slaking and, to some extent, for surface slaking. Rapid water absorption into the material compresses the air, which, in turn, exerts tensile stresses on the soil structure. If the structural strength is insufficient to withstand these stresses, then the material splits apart.

Transmission X-ray radiography

This method is a useful and nondestructive tool for the study of soil stratigraphy, homogeneity, and macrofabric. In addition, sample disturbance, inclusions of shells, sand lenses, and big voids can also be detected while sample is still in tubes. However, due to its low resolution, it is not a good tool for microstructure analysis.

Mechanical properties

The mechanical properties of any soil, including stress-deformation behavior, strength, compressibility, and permeability, depend on fabric in ways that are reasonably well understand. It follows, therefore, that information about fabric can be deduced from measurement of these properties. For instance, the sensitivity is developed to depict that the structure features of intact soils.

4.5 Summary of Experimental Program

As mentioned previously, this entire research is an extensive characterization of the old alluvium in San Juan, consisting of the following different individual phases:

A. Geological origin and deposition history
B. Tropical weathering and soil formation processes
C. Qualitative mineralogical analysis
D. Quantitative mineralogical analysis
E. Soil structure determination
F. Physical, chemical, and index properties
G. Consolidation behavior
H. Triaxial shear behavior of intact soils

Table 4-1. Summary of experimental program for characterization of the old alluvium.

Phase	Focus	Methods & techniques	Main knowledge required
A	Geological origin & deposition history	Literature review	Geology or engineering geology
B	Tropical Weathering & soil formation	Literature review	Geochemistry, soil science
C	Qualitative mineralogy	XRD	X-ray physics and crystallography Clay mineralogy
		Thermal analysis	Clay mineralogy
		XRF	General soil chemistry
		SEM/ESEM	Electron optics, soil micromorphology
		EDXS	X-ray physics
D	Quantitative mineralogy	QXRD	XRD & clay mineralogy
		Thermal analysis	Clay mineralogy
		SCD	General chemistry
E	Soil structure	SEM/ESEM	Electron optics, soil micromorphology
		CEC	Clay mineralogy
		Slaking	Clay mineralogy
		SCD and particle size analysis	General soil chemistry
F	Physico-chemical & Index properties	ASTM standards and modifications	General soil science or soil physics
G	Consolidation behavior	Oedometer	Soil mechanics (compressibility & permeability)
H	Intact triaxial shear behavior	Triaxial testing	Soil mechanics (theory of strength generation and deformation)

Although each phase focuses on a special facet of the old alluvium, all of them are inter-dependent and serve for one main objective, that is, to characterize this deposit for the best understanding of the soil behavior used in geotechnical engineering practice. Phases A and B emphasize the importance of geological history and soil formation, and rely heavily on the literature from US Geological Surveys and USDA Soil Surveys and

on the basic knowledge about soil science and geochemistry (mainly tropical weathering). Little laboratory testing was performed to acquire further information. However, for a residual soil evolved from the weathering of an old alluvium, the importance of geology and weathering process should not be neglected.

Except Phases A and B, all other phases involve in the laboratory experimental research for the characterization of the old alluvium and for the measurement of its engineering properties. As seen in later chapters, various direct techniques and indirect methods have been adopted and modified to characterize this old alluvium. Table 4-1 summarizes the experimental program comprising this research.

References

ASTM – American Society for Testing and Materials (1997) *Annual Book of ASTM Standards*. Vol.04.08. 970pp.

Bain, D.C. and Smith, B.F.L. (1987) Chemical analysis. In M.J. Wilson (ed.), *A Handbook of Determinative Methods in Clay Mineralogy*, 248-274. Blackie & Son Limited, 308pp.

Bish, D.L. and Post, J.E. (eds.) (1989) *Modern Powder Diffraction*. Reviews in Mineralogy, Vol. 20, published by the Mineralogical Society of America, Washington, D.C., 369pp.

Borchardt, G. (1989) Smectites. In J.B. Dixon and S.B. Weed (eds.), *Minerals in Soil Environments*, 2nd Edition, 675-727. Published by the Soil Science Society of America, Madison, Wisconsin.

Brindley, G.W. (1966) Invited Review: ethylene glycol and glycerol complexes of smectites and vermiculites. *Clay Minerals*, **6**, 237-259.

Brindley, G.W. (1980)

Brindley, G.W. (1980) Quantitative X-ray mineral analysis of clays. In G.W. Brindley and G. Brown (eds.), *Crystal Structures of Clay Minerals and Their X-ray Identification*, 411-438. Mineralogical Society Monograph No.5, Mineralogical Society, London, 495pp.

Brindley, G.W. and Brown, G. (eds.) (1980) *Crystal Structure of Clay Minerals and Their X-Ray Identification*. Mineralogical Society Monograph No.5, Mineralogical Society, London, 495pp.

Brindley, G.W. and Kurtossy, S.S. (1961) Quantitative determination of kaolinite by X-ray diffraction. *The American Mineralogist*, **46**, 1205-1215.

Brindley, G.W. and Lemaitre, J. (1987) Thermal, oxidation and reduction reactions of clay minerals. In A.C.D. Newman (ed.), *Chemistry of Clays and Clay Minerals,* 319-370. Mineralogical Society Monograph No.6, Mineralogical Society, London.

Carter, J.R., Hatcher, M.T., and Di Carlo, L. (1987) Quantitative analysis of quartz and cristobalite in bentonite clay based products by X-ray diffraction. *Analytical Chemistry*, **59**, 513-519.

Davis, B.L., Smith, D.K., and Holomany, M.A. (1989) Tables of experimental reference intensity ratios – Table No.2, December, 1989. *Powder Diffraction*, **4**, 201-205.

Deere, D.U. (1955) *Engineering Properties of the Pleistocene and Recent Sediments of the San Juan Bay Area, Puerto Rico*. Ph.D. thesis, University of Illinois, Urbana.

Dixon, J.B. (1989) Kaolin and serpentine group minerals. In: J.B. Dixon and S.B. Weed (eds.), *Minerals in Soil Environments*, p.467-525. Published by Soil Science Society of America, Madison, Wisconsin, USA.

Dixon, J.B. and Weed, S.B. (eds.) (1989) *Minerals in Soil Environments*. 2nd Edition. Published by Soil Science Society of America, Madison, Wisconsin, 1244pp.

Emig, J.A. and Smith, D.K. (1989) The detection and quantification of low concentrations of quartz in dolostone by X-ray powder diffraction. *Powder Diffraction*, **4**, 209-213.

Fookes, P. G. (ed.) (1997) *Tropical Residual Soils*. Geological Society Professional Handbooks. The Geological Society, London.

Greene-Kelly, R. (1953) Identification of montmorillonites. *Journal of Soil Science*, **4**, 233-237.

Gupta, A. Rahman, A., Wong, P.P., and Pitts, J. (1987) The Old Alluvium of Singapore and the extinct drainage system to the South China Sea. *Earth surface Processes and Landforms*, **12**, 259-275.

Hayashi, S. and Toraya, H. (2000) Quantitative phase analysis of natural products using whole-powder-pattern decomposition. *Powder Diffraction*, **15**, 86-90.

Hendershot, W.H. and Duquette, M. (1986) A simple barium chloride method for determining cation exchange capacity and exchangeable cations. *Soil Science Society of America Journal*, **50**, 605-608.

Hermann, H. and Ermrich, M. (1989) Microabsorption correction of X-ray intensities diffracted by multiphase powder specimens. *Powder Diffraction*, **4**, 189-195.

Hinckley, D.N. (1963) Variability in "crystallinity" values among the kaolin deposits of the coastal plain of Georgia and South Carolina. *Clays and Clay Minerals*, **11**, 229-235.

Huang, P.M. (1989) Feldspars, olivines, pyroxenes, and amphiboles. In: J.B. Dixon and S.B. Weed (eds.), *Minerals in Soil Environments*, p.975-1050. Published by Soil Science Society of America, Madison, Wisconsin, USA.

Hubbard, C.R. and Snyder, R.L. (1988) RIR – measurement and use in quantitative XRD. *Powder Diffraction*, **3**, 74-77.

JCPDS (1993) *Mineral Powder Diffraction File Databook*. Joint Committee on Powder Diffraction Standards, Swarthmore, PA.

Kaye, C.A. (1959) *Coastal Geology of Puerto Rico: (A) Geology of the San Juan Metropolitan Area*. Geological Survey Professional Paper 317. US Government Printing Office, Washington, D. C.

Keeling, J.L., Raven, M.D., and Gates, W.P. (2000) Geology and characterization of two hydrothermal nontronites from weathered metamorphic rocks at the Uley Graphite Mine, South Australia. *Clays and Clay Minerals*, **48**, 537-548.

Klug, H.P. and Alexander, L.E. (1974) *X-ray Diffraction Procedures*. 2nd Edition. John Wiley & Sons, Inc. 966pp.

Ladd, C.C. (2001) *Soil Behavior Class Notes*.

Lim, C.H. and Jackson, M.L. (1986) Expandable phyllosilicate reactions with lithium on heating. *Clays and Clay Minerals*, **34**, 346-352.

MacEwan, D.M.C. and Wilson, M.J. (1980) Interlayer and intercalation complexes of clay minerals. In *Crystal Structure of Clay Minerals and Their X-Ray Identification*, G.W. Brindley and G. Brown (eds.), 197-248. Mineralogical Society Monograph No.5, Mineralogical Society, London.

Martin, R.T. (2000) Personal communications, together with his unpublished CEC determination method.

Mitchell, J.K. (1993) *Fundamentals of Soil Behavior*. 2nd Edition. John Wiley & Sons, Inc. 437pp.

Monroe, W.H. (1980) *Geology of the Middle Tertiary Formations of Puerto Rico*. Geological Survey Professional Paper 953. US Government Printing Office, Washington, D. C.

Moore, D.M. and Reynolds, R.C., Jr. (1997) *X-Ray Diffraction and the Identification and Analysis of Clay Minerals*. 2nd Edition, Oxford University Press, 378pp.

Newman, A.C.D. (ed.) (1987) *Chemistry of Clays and Clay Minerals*. Mineralogical Society Monograph No.6, Mineralogical Society, London, 480pp.

Novich, B.E. and Martin, R. T. (1983) Solvation methods for expandable layers. *Clays and Clay Minerals*, **31**, 235-238.

Ottner, F., Gier, S., Kuderna, M., and Schwaighofer, B. (2000) Results of an inter-laboratory comparison of methods for quantitative clay analysis. *Applied Clay Science*, **17**, 223-243.

Paterson, E. and Swaffield, R. (1987) Thermal analysis. In: M.J. Wilson (ed.), *A Handbook of Determinative Methods in Clay Mineralogy*, p.99-132. Blackie & Son Limited, London.

Pease, M.H., Jr. and Monroe, W.H. (1977). *Geologic Map of the San Juan Quadrangle, Puerto Rico*. US Geological Survey.

Pevear, D.R., Dethier, D.P., and Frank, D. (1982) Clay minerals in the 1980 deposits from Mount St. Helens. *Clays and Clay Minerals*, **30**, 241-252.

Raab, G.A. (1988) Semiquantitative analysis by X-ray powder diffraction (SQXRD) of the <2mm to 0.002mm and <0.002mm fractions of soil. *Powder Diffraction*, **3**, 144-152.

Rai, D. and Kittrick, J.A. (1989) Mineral equilibria and the soil system. In: J.B. Dixon and S.B. Weed (eds.), *Minerals in Soil Environments*, 161-198. Published by Soil Science Society of America, Madison, Wisconsin, USA.

Righi, D. and Meunier, A. (1995) Origin of clays by rock weathering and soil formation. In B. Velde (ed.), *Origin and Mineralogy of Clays*, 43-161. Springer-Verlag, Berlin.

Schwertmann, U. and Taylor, R.M. (1989) Iron Oxides. In J.B. Dixon and S.B. Weed (eds.), *Minerals in Soil Environment*, 2nd Edition, 379-438. Published by Soil Science Society of America, Madison, Wisconsin, 1244pp.

Shirlaw, J.N., Hencher, S.R., and Zhao, J. (2001) Design and construction issues for excavation and tunneling in some tropically weathered rocks and soils.

Smith, B.F.L. (1994) Characterization of poorly ordered minerals by selective chemical methods. In: M.J. Wilson (ed.), *Clay Mineralogy: Spectroscopic and Chemical Determinative Methods*. p.333-357. Chapman & Hall, UK.

Smith, D.K. (1997) Evaluation of the detectability and quantification of respirable crystalline silica by X-ray powder diffraction methods. *Powder Diffraction*, **12**, 200-227.

Snyder, R.L. and Bish, D.L. (1989) Quantitative analysis. In D.L. Bish and J.E. Post (eds.), *Modern Powder Diffraction,* 101-144. Reviews in Mineralogy, Vol. 20, published by the Mineralogical Society of America, Washington, D.C., 369pp.

SSL – Soil Survey Laboratory (1996) *Soil Survey Laboratory Method Manual*. Soil survey investigation report No.42, Version 3.0, 693pp.

Szabo, P. (1980) Optimization of quantitative X-ray diffraction analysis. *Journal of Applied Crystallography*, **13**, 479-485.

Taylor, R.M. (1987) Non-silicate oxides and hydroxides. In A.C.D. Newman (ed.), *Chemistry of Clays and Clay Minerals*, 129-201. Mineralogical Society Monograph No.6, Mineralogical Society, London.

USDA (1978) *Soil Survey of San Juan Area of Puerto Rico*. United States Department of Agriculture.

Velde, B. (ed.) (1995) *Origin and Mineralogy of Clays*. Springer-Verlag Berlin. 334pp.

Wang, H. (1988) A method for quantitative X-ray phase analysis without standards. *Powder Diffraction*, **3**, 165-167.

Whittig, L.D. and Allardice, W.R. (1986) X-ray diffraction techniques. In A. Klute (ed.) *Methods of Soil Analysis. Part 1. Physical and Mineralogical Methods*. 2nd ed. Agronomy 9, 331-362.

Wilson, M.J. (1987) X-ray powder diffraction methods. In *A Handbook of Determinative Methods in Clay Mineralogy*, edited by M.J. Wilson, 26-98. Blackie & Son Limited, 308pp.

Wilson, M.J. (ed.) (1987) *A Handbook of Determinative Methods in Clay Mineralogy*. Blackie & Son Limited, London. 308pp.

Winburn, R.S., Grier, D.G., McCarthy, G.J., and Peterson, R.B. (2000) Rietveld quantitative X-ray diffraction analysis of NIST fly ash standard reference materials. *Powder Diffraction*, **15**, 163-172.

Zangalis, K.P. (1991) A standardless method of quantitative mineral analysis using X-ray and chemical data. *Journal of Applied Crystallography*, **24**, 197-202.

Zelazny, L.W. and White, G.N. (1989) The pyrophyllite-talc group. In J.B. Dixon and S.B. Weed (eds.), *Minerals in Soil Environments*, 527-550. Published by Soil Science Society of America, Madison, Wisconsin, USA.

Zevin, L.S. and Zevin, S.L. (1989) Standardless quantitative X-ray phase analysis – estimation of precision. *Powder Diffraction*, **4**, 196-200.

Wilson, M.J. (ed.) (1987) *A Handbook of Determinative Methods in Clay Mineralogy*. Blackie & Son Limited, London, 308.

Chapter 5 QUALITATIVE AND QUANTITATIVE MINERALOGICAL ANALYSIS

5.1 Introduction

A soil is a natural particulate earth material. By being a particulate system, an element of soil is inherently "multiphase": *solid* (mineral particles), *gas*, and *liquid* (usually water). Of all three distinct phases, the solid minerals are the most important for geotechnical engineers since they control the fundamental behavior and engineering properties of relating to strength, deformation, and flow. In fact, a soil's physical and chemical behavior on which engineering properties depend are controlled to a very large degree by its mineralogy, especially by those minerals consisting of the clay fraction (Whittig and Allardice, 1986; Mitchell, 1993). Therefore, it is of great importance for geotechnical engineers to understand the detailed mineralogy of soil deposits.

The mineralogy of the old alluvium in San Juan, Puerto Rico has not been investigated either by USDA soil surveys or by US geological surveys, and there is no documentation available in the literature covering the mineralogy of this deposit. Indeed, other old alluvia with similar geological history have a large coverage on earth in the world, such as in Singapore (Gupta *et al.*, 1987; Shirlaw *et al.*, 2001), Columbia, Brazil, and New Zealand (Table 2-3). Though the original purpose of this mineralogical analysis is to provide detailed mineralogy for understanding the engineering behavior, the data will also be of essential interest for clay scientists, geologists, and agriculturists. For

example, knowledge of the mineralogy of the old alluvium in San Juan helps geologists to compare the weathering and soil development process with other similar deposits in the world.

This chapter is entirely devoted to the solid phase of the old alluvium, i.e., the mineralogical composition of the soil material. Both qualitative and quantitative mineralogical analyses were performed on samples taken from the old alluvium. In other words, this chapter presents the mineralogical analysis for the old alluvium, including both positive identification of all minerals in the deposit in Section 5.2 and quantitative estimation of each mineral phase in Section 5.3. Each of these two sections provides a summary of the results and discusses the relationship between soil mineralogy and soil formation processes which are affected by tropical weathering.

5.2 Qualitative Analysis

5.2.1 Introduction

With the advancement of the instrumental analysis in materials science, numerous techniques have become available to soil microanalysis and microcharacterization. Many of these techniques have also been adopted or modified by soil scientists and clay mineralogists to identify soil minerals. It is important to realize that clay minerals are naturally formed colloidal particles that possess some special properties different from these of man-made or synthetic materials. Therefore, special or unique techniques may be required to characterize clay or soil minerals. The traditional techniques for qualitative

analysis include X-ray powder diffraction (XRD), thermal analysis, and chemical analysis (Wilson, 1987), while electron microscopy equipped with energy-dispersive X-ray spectroscopy (EDXS) can provide useful information on micromorphology and chemical constituents of individual particles. Indeed, a positive identification of mineral phases requires a combination of several techniques which may be complementary to each other. For example, XRD derives its strength from the direct measurement of the absolute crystal structure of minerals, while the background of thermal analysis lies in that different minerals exhibit different physical and chemical properties upon heating (Paterson and Swaffield, 1987).

Both crystalline and noncrystalline or amorphous minerals may be present in a soil. Though XRD is the most powerful technique to identify crystalline minerals, it is not effective for the identification of amorphous phases. The latter can be identified by chemical methods of hydroxyl release (Smith, 1994, p.343) or soil NaF pH measurement (SSL, 1996). The reaction of NaF with noncrystalline soil material releases hydroxide ions (OH^-) to the soil solution and increases the pH of the solution. The amount of amorphous materials in the soil controls the release of OH^- and the subsequent increase in pH. The following reactions illustrate this action:

$$Al(OH)_3 + 3F^- \rightarrow AlF_3 + 3OH^-$$

$$Si(OH)_4 + 4F^- \rightarrow SiF_4 + 4OH^-$$

Most soils contain components that react with NaF and release OH^-. However, a NaF pH>9.4 is a strong indicator that amorphous material dominates the soil exchange complex (SSL, 1996).

Smectites are expandable minerals in soils. The detection of smectites is a key issue in this research due to the occurrence of unexpectedly large ground settlements during construction of Tren Urbano in Rio Piedras (see Section 1.2). Due to its negative layer charge, smectite can incorporate different cations (*e.g.*, Mg^{2+}, K^{+}, Li^{+}, Ca^{2+}) and organic molecules (*e.g.*, ethylene glycol, glycerol) together with H_2O between the structural layers and hence, form various interlamellar complexes with different interlayer spacings, *d*. This characteristic is used to identify smectites in soils. Brindley (1966) and MacEwan and Wilson (1980) provided a complete review on the formation of smectite-organic complexes with different interlayer cations and hydration, while Novich and Martin (1983) systematically evaluated various organic solvation methods used to investigate the expandable nature of smectites.

However, only knowing the presence of smectites is not enough, since this 2:1 mineral group consists of montmorillonite, beidellite, and nontronite as dioctahedral subgroup and hectorite (Li-rich), saponite (Mg-rich), and sauconite (Zn-rich) as trioctahedral subgroup (Borchardt, 1989). The two subgroups can be distinguished by observing the (060) reflection in random powder diffraction patterns. The dioctahedral smectites produce a peak near 1.50Å, whereas the trioctahedral smectites near 1.54Å (Pevear *et al.* 1982; Moore & Reynolds, 1997). Further differentiation of smectites within one subgroup requires more complicated techniques. For dioctahedral smectites, Mg^{2+}-saturated montmorillonite expands to 18Å with glycerol vapor solvation, whereas beidellite and nontronite give peaks at ~15Å (Brindley, 1966; Borchardt, 1989). Another way to identify montmorillonite is based on the Hofmann-Klemen effect or Li-fixation

(Greene-Kelly, 1953; Lim and Jackson, 1986), which means that by heating Li^+ cations enter vacant dioctahedral sites where tetrahedral sheet is neutral as in montmorillonite. Li-fixation causes a loss of the expandable nature of montmorillonite by neutralizing the negative charge of octahedral sheet, hence subsequent glycerol solvation results in a 9.5Å peak.

5.2.2 Materials and Methods

Materials and Size Fractioning

Only homogenized bucket samples have been used to perform the mineralogical analyses in this section. Identification of clay minerals by XRD usually requires a pure clay fraction or a clay suspension for making samples of *oriented clay aggregates* or *random powder*, in which nonplaty minerals (e.g., quartz) should be eliminated. The former requires all platy clay particles have perfect preferred orientation in the XRD samples, while a perfect random orientation of the particles is the goal for the latter case.

Two methods were used to extract the clay fraction: one for oriented aggregates and the other for random powder. For the clay suspensions used to prepare oriented clay aggregates, the homogenized wet bulk sample was first dispersed by sodium hexametaphosphate $(NaPO_3)_6$ and stirred for 1 minute in a blender as specified in ASTM D422 (ASTM, 1997), then the clay suspension (<2μm fraction) was extracted by sedimentation according to Stoke's law. The clay fraction used in random powder XRD was obtained by drying a large amount of the clay fraction which was extracted from the

soil suspension dispersed by adjusting the pH to 9 using NaOH solution (Martin, 2001), followed by wet grinding the dried clay fraction with alcohol

Sample Preparation for XRD

Although oriented aggregates which enhance the basal (00*l*) reflections are the most effective method to identify clay minerals, random powder of clay fraction is used to differentiate dioctahedral from trioctahedral subgroups of phyllosilicates and to identify other auxiliary minerals in the clay fraction. Therefore, both oriented aggregates and random powder of clay fraction were prepared for XRD analysis, while only was random powder of the total bulk samples used to identify other primary minerals.

Oriented aggregates. Oriented aggregates were prepared by following the procedures provided by SSL (1996, p.351-361). The dispersed clay suspension obtained by the method described above was drawn into a syringe loaded with pretreated cation-saturated exchange resin, Rexyn 101(H), to exchange cations between clays and resin, then the suspension was dropped onto a glass slide and dried at room temperature. The cations used to saturate clays include K^+, Mg^{2+}, and Li^+. If required, additional treatments were performed by heating air-dried sample slides at 250°C, 300°C, 500°C, or even 600°C.

Organic solvation and Li-fixation were performed on oriented clay aggregates to identify smectite and its species. For organic solvation, glycerol was used to solvate the expandable clays by the liquid or slurry method, vapor method, and towel method (Novich and Martin, 1983). To identify smectite species, clay suspensions were first

saturated with Li^+, then air dried, and heated overnight at 250°C in a muffle furnace. Such samples were designated as "Li-fixed" clays. After cooling in a desiccator, the Li-fixed clay slides were solvated by glycerol with liquid, vapor, or towel methods. Detailed procedures about Li-fixation can be found in Greene-Kelly (1953) and Lim and Jackson (1986). Table 5-1 summarizes all the different treatments performed on oriented clay aggregates of UC and MZ samples.

Table 5-1. Various treatments performed on oriented aggregates of clay fraction.

Cation saturation or organic solvation	Drying or heating
Mg^{2+} (r = 0.65Å)*	Room temperature (RT)
Mg^{2+}-glycerol	RT (liquid method), 100°C (vapor method$^+$)
K^+ (r = 1.33Å)	RT, 300, 500, 600°C (at least 2 hours)
K^+-glycerol	RT
Li^+ (r = 0.60Å)	RT
Li^+-glycerol	RT
Li^+-fixation	250°C
Li^+-fixed & glycerol	RT (liquid method), 100°C (vapor method$^+$), RT (towel method)

* r: ionic radius.
$^+$ Vapor method: heating at 100°C the previously dried clay slides for 16-24 hours over the glycerol liquid in a sealed container.

Random powder. The dry sample powder was obtained by wet grinding with alcohol the air-dried bulk samples and the air-dried clay fraction obtained by the fractioning method described above. All soil grains were ground until they pass through a #325 mesh (<44μm). All random powder mounts were prepared by the RTS method described in Zhang *et al.* (2001) (see Appendix).

X-ray Powder Diffraction

XRD patterns were obtained in a Rigaku Rotaflex 180mm diffractometer equipped with a graphite diffracted beam monochromator, using CuKα (λ=1.5418Å) radiation generated at 18 kW (60kV, 300mA). All scans used a 1° divergence slit, 1° scatter slit, 0.3mm receiving slit, a speed of 1° 2θ/min, and a step size of 0.02° 2θ. For oriented aggregates, a continuous scan range of 2-34° 2θ was adopted, while random powder used a scan range of 2-64° 2θ in order to get the (060) reflection of clay minerals (Moore & Reynolds, 1997, p.244-255).

Iron Oxides Removal

Air-dried UC and MZ bulk samples were treated with sodium dithionite, sodium citrate, and sodium bicarbonate (DCB) to achieve complete dissolution of all iron oxides and oxyhydroxides. The procedure of Mehra and Jackson (Schwertmann & Taylor, 1989; Smith, 1994, p.339-340; SSL, 1996) was performed 4-5 times by using 1.0g of sodium dithionite in 80°C sodium citrate solution buffered with sodium bicarbonate to assure the complete removal of all iron oxides and oxyhydroxides.

Chemical Analysis

The elemental chemical analysis was performed on a Spectro X-Lab 2000 energy dispersive X-ray fluorescence (XRF) spectrometer. Both air-dried samples and iron oxides-removed samples from UC and MZ were analyzed.

Environmental Scanning Electron Microscopy (ESEM)

The micromorphology of clay minerals were observed under a FEI/Philips XL30 FEG ESEM featured with an energy dispersive X-ray spectrometer (EDXS). Fine particles of iron oxides are generally believed to act as binding or coating agents among other soil particles (Schwertmann and Taylor, 1989, p.416). Therefore, to see clearly the clay particles, samples were treated with DCB to remove iron oxides. Chemical analysis was also performed by EDXS on individual clay particles under the electron microscope.

Hydroxyl Release

A 1.000g sample was mixed with 50.0ml of 1.0N NaF solution and stirred for 2min. While the sample is being stirred, the pH is read at exactly 2min in the upper solution. An Orion Model 250A pH/ISE meter was used to measure the soil NaF pH. The initial pH of the 1.0N NaF solution was adjusted to 7.2-8.1 with HF acid.

Differential Thermal Analysis (DTA)

DTA was performed in a Seiko dual TG/DTA 320 thermogravimetric/differential thermal analyzer with heating temperature ranging from 25°C to 1000°C at a rate of 20°C/min in a pure N_2 atmosphere. Both the bulk samples and clay fractions were wet ground with alcohol to pass through a #325 (44μm) mesh and then equilibrated overnight over a saturated magnesium nitrate ($Mg(NO_3)_2$) solution which produces a constant relative humidity of 55% in a sealed glass container.

5.2.3 Results and Discussion

Soil NaF pH

Table 5-2 summarizes the soil NaF pH values of both UC and MZ samples together with the initial and adjusted pH of 1.0N NaF solution. Since the reaction of amorphous minerals with NaF is pH dependent, the pH of NaF solution was adjusted by HF acid to be 7~8 before the addition of soil samples. With the addition of 1.0g soil sample to the adjusted NaF solutions, the pH of the solutions do not go up to 9.4, which means that no detectable amount of amorphous materials are present in either layers.

Table 5-2. Soil pH in 1.0N NaF solution.

Soil Sample	Initial pH of 1.0N NaF solution	Adjusted pH of 1.0N NaF by HF acid	Soil pH in adjusted 1.0N NaF
Air-dried UC	9.70	7.55	7.67
Air-dried MZ	9.70	7.33	7.53

Minerals in Clay Fraction

Oriented Aggregates. Figure 5-1 summarizes the XRD patterns of oriented clay aggregate with various treatments for both UC and MZ layers. These results show that both kaolinite and smectite are present in the two layers, which is explained as follows:

1. The first peak, d = ~14.5Å in samples saturated with Mg^{2+} shifts to ~18Å with glycerol solvation (Figure 5-1 (a) & (c)), and collapses to ~11Å and ~10Å with K^+ saturation and heating at 300°C and 500°C, respectively (Figure 5-1 (b) & (c)). Therefore, smectite is present in both layers.
2. The peak, d = ~7.2Å, does not change position with K^+ or Mg^{2+} saturation, or with glycerol solvation, or with heating to 300°C. However, it starts to disappear when samples are heated to 500°C (Figure 5-1 (b) and (d)), indicating the presence of kaolinite in the two layers.

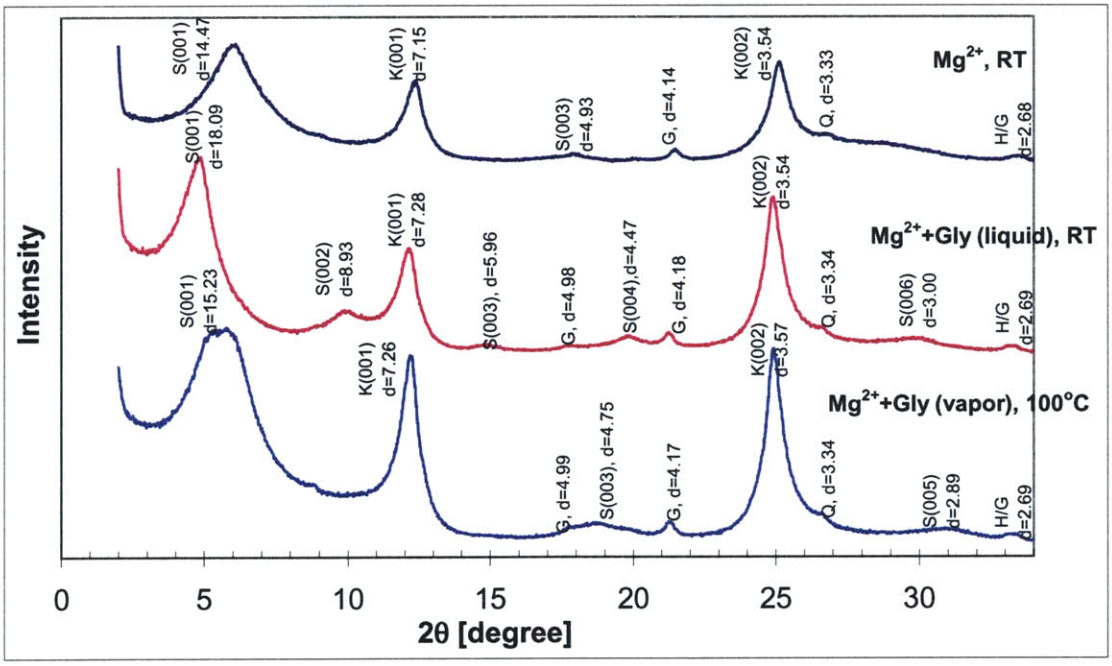

(a) Mg^{2+}-saturated UC clays.

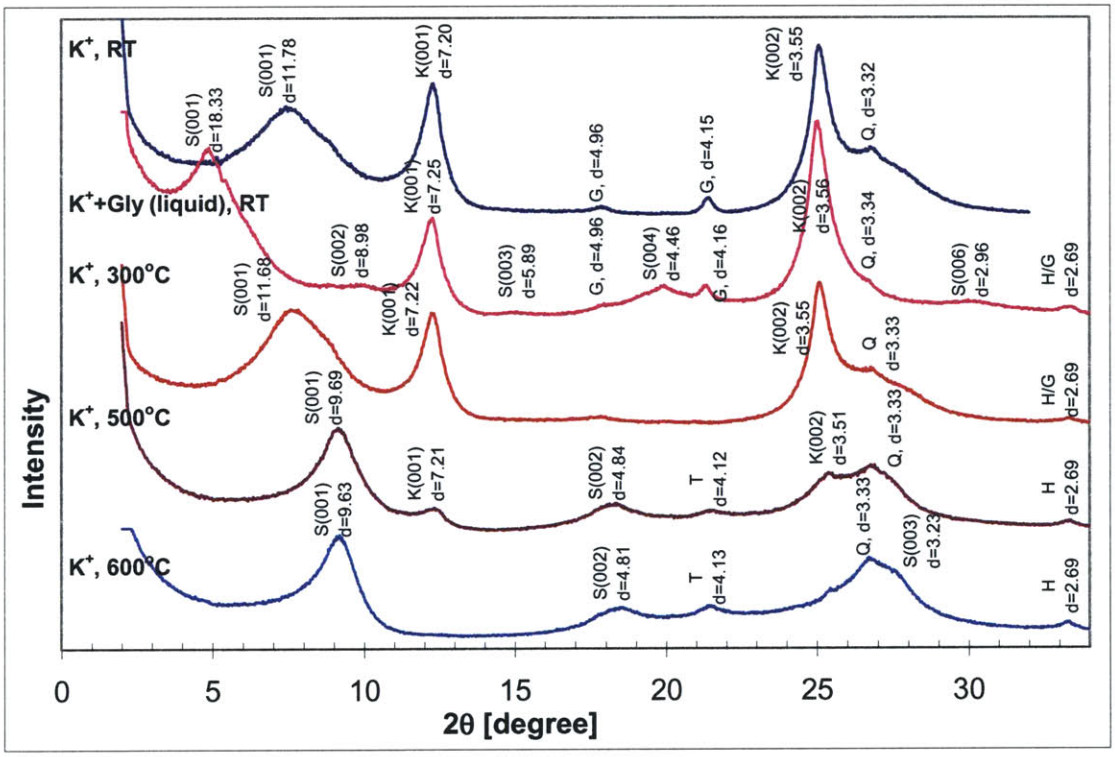

(b) K^{+}-saturated UC clays.

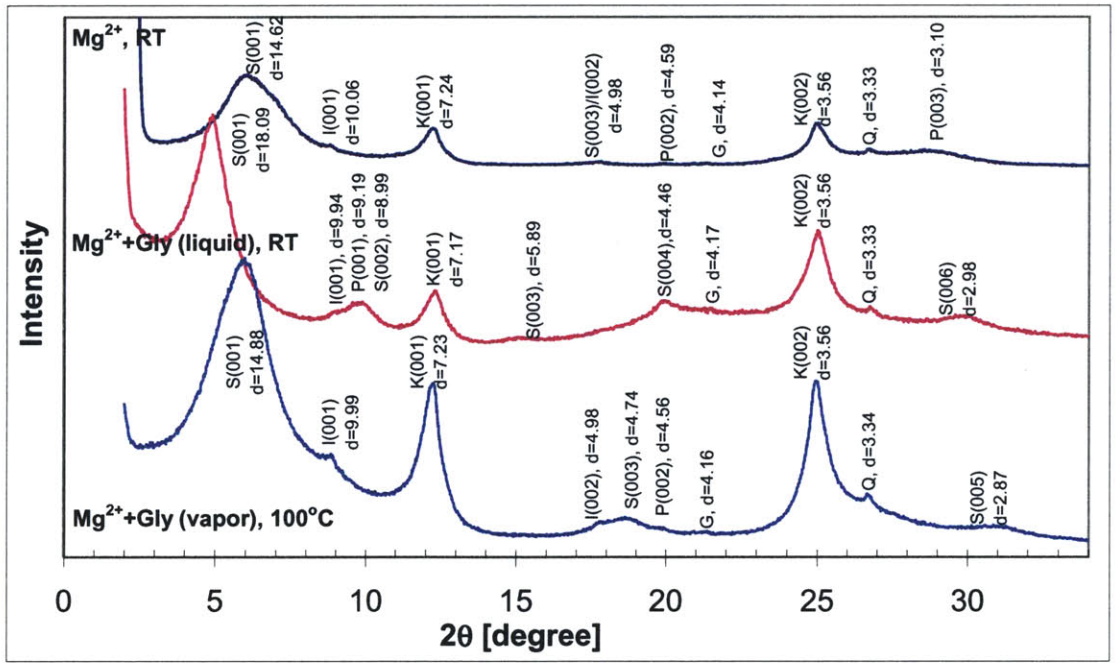

(c) Mg^{2+}-saturated MZ clays.

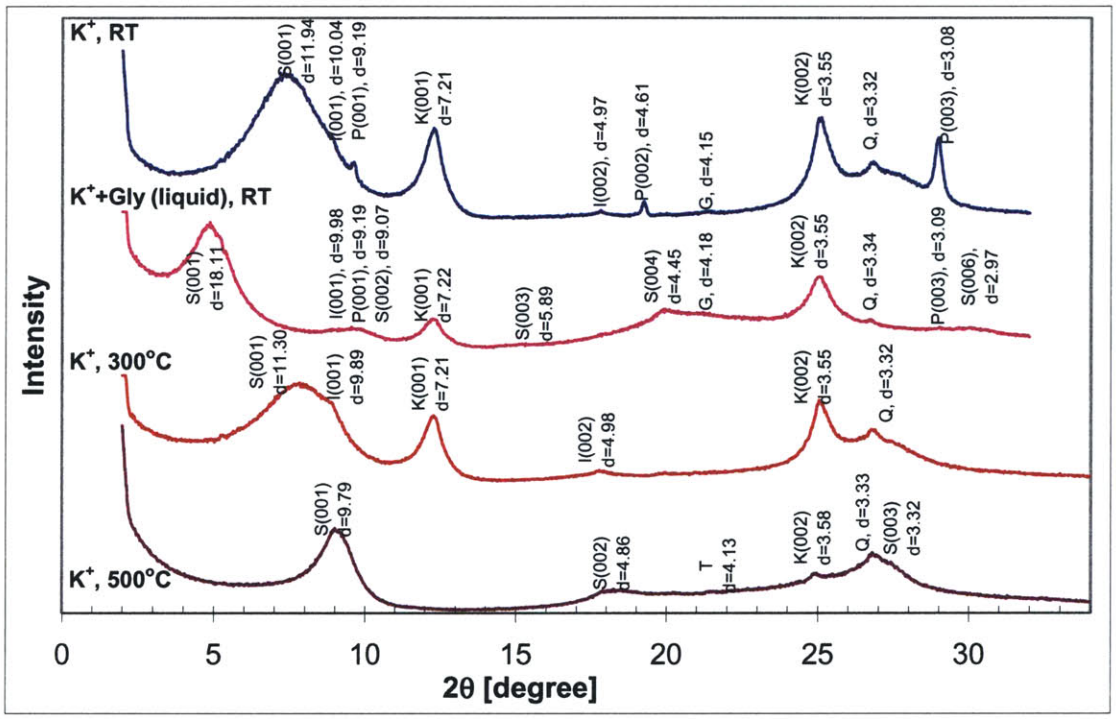

(d) K^{+}-saturated MZ clays.

Figure 5-1. XRD patterns of oriented clay aggregates of the two layers. RT = room temperature, Gly = glycerol, S = smectite, K =kaolinite, G = goethite, Q = quartz, H = hematite, T = tridymite, I = illite, P = pyrophyllite. Tridymite is possibly produced by the dehydroxylation of kaolinite by heating.

3. The UC sample requires 600°C heating to collapse all kaolinites, while heating at 500°C totally removes the kaolinite peaks in MZ. Therefore, the kaolinite in the UC material is more stable than that in the MZ soil.

In Figure 5-1, besides the peaks of kaolinite and smectite, other minerals can be identified easily by their diagnostic reflections. Fine quartz in the <2μm fraction can be identified by its peak d = ~3.34Å presented in both UC and MZ. However, this peak is very weak, indicating that quartz is present in a minor fraction (which can be neglected) in the extracted clay fractions. The presence of goethite can be verified by the peak at 4.17Å, which disappears after heating to 300°C and 500°C. Hematite is identified with the peak at 2.69Å, which is not present in the MZ samples. Therefore, goethite is present in both UC and MZ (though MZ goethite has a weaker peak at 4.18Å), while hematite is present in UC only.

The MZ samples contain two additional clay minerals, illite and pyrophyllite which are present in small amounts, as indicated by the two weak peaks at ~10Å and ~9.2Å (Figure 5-1 (c) and (d)), respectively. The unsymmetrical shoulder of the peak at ~11Å for MZ sample with K^+ saturation and 300°C heating shows that illite is probably present as smectite/illite interstratified minerals.

Random Powder. XRD patterns of random powder of the clay fractions (Figure 5-2) clearly show the three-dimensional reflections (*hkl*) of clay minerals identified by oriented aggregates described above. The presence in UC and absence in MZ of the two

strongest peaks of hematite (104) at 33.3° 2θ and (110) at 35.8° 2θ clearly indicate that hematite is present in UC but not in MZ soil. Peaks of quartz and goethite are present in both UC and MZ, while illite and pyrophyllite are present in MZ only.

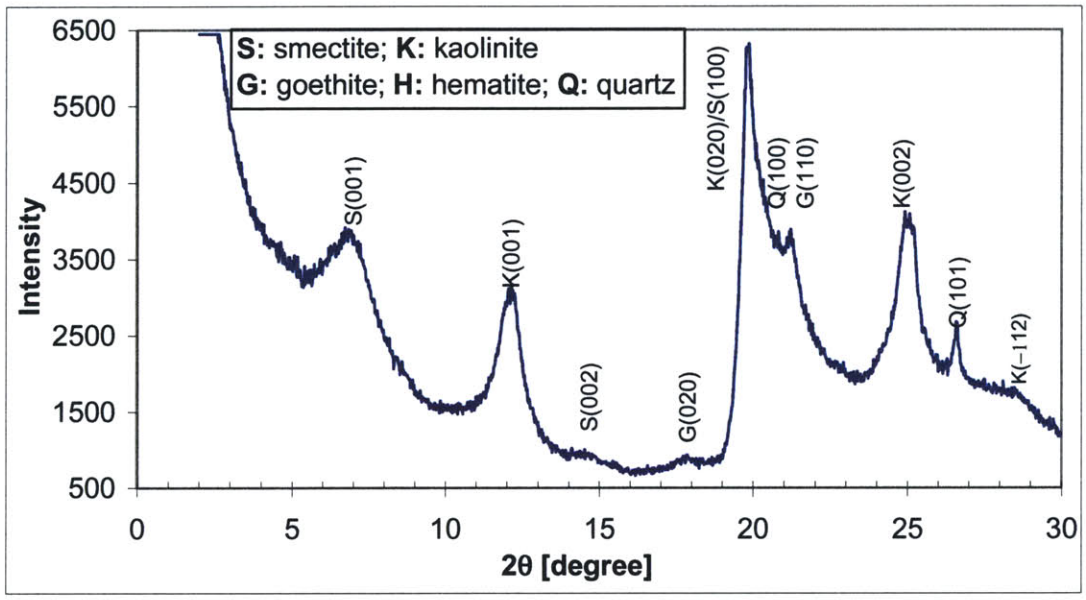

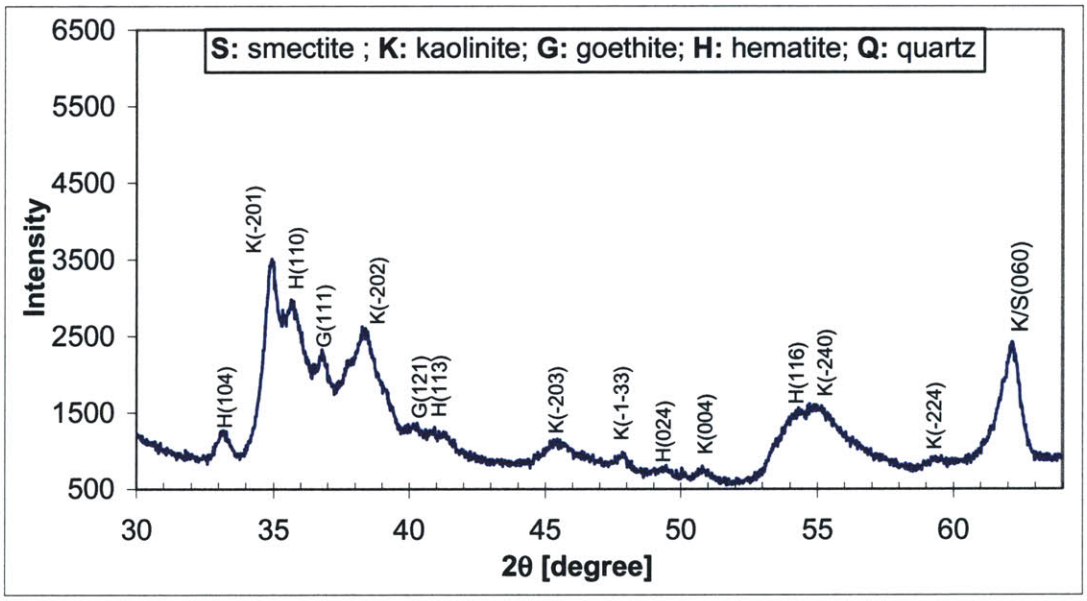

(a) UC clay fraction.

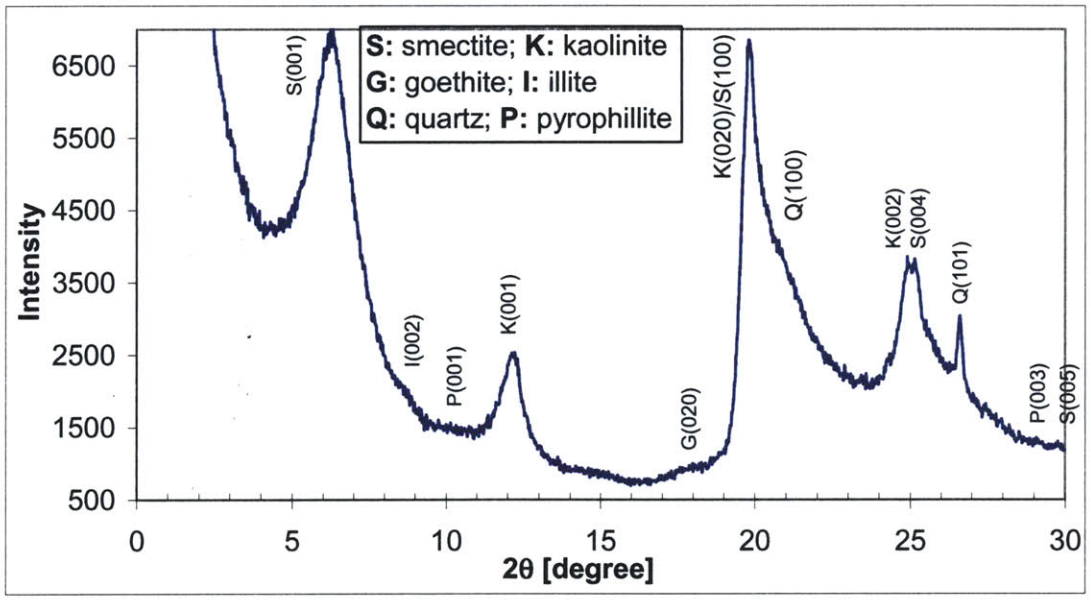

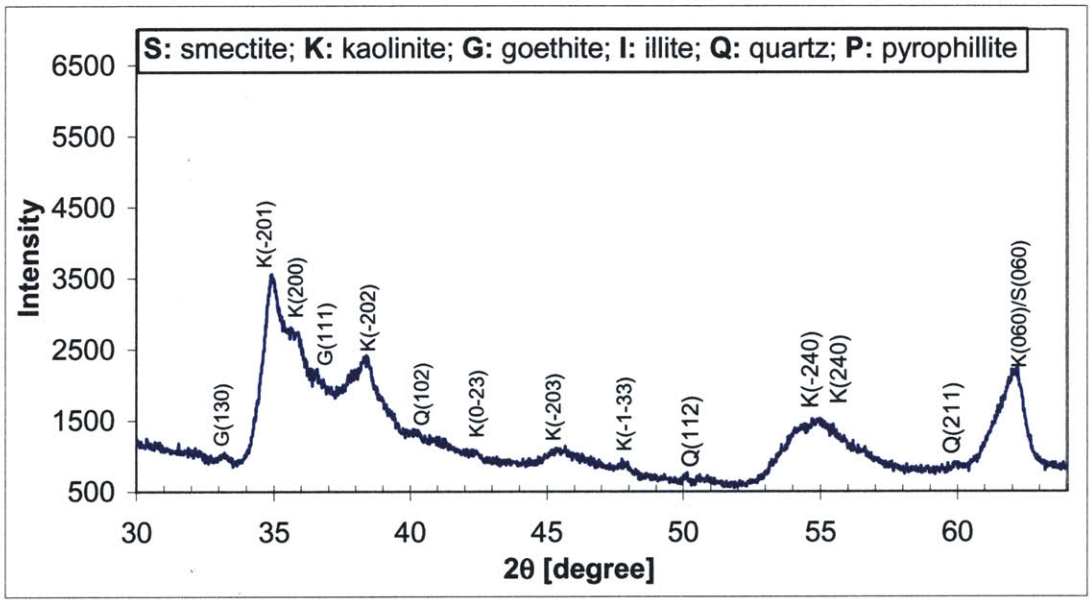

(b) MZ clay fraction.

Figure 5-2. XRD patterns of random powder of clay fraction of the two layers.

Since all clay minerals are positively identified by oriented aggregates with various treatments, the major purpose of XRD with random powder of clay fractions is the (060) reflections and structural disorder of clay minerals. As seen in Figure 5-2, a

strong peak is present at 1.49Å (62.3° 2θ), while there are no other peaks around it, indicating that only dioctahedral subgroups (e.g., kaolinites and dioctahedral smectites) of clay minerals are present in the two layers (Moore and Reynolds, 1997). With respect to kaolinite in both layers, there are no clear peaks seated on the (020) prismatic reflection scattered diffusely in the range of 20° to 33° 2θ, and hence the Hinckley index (Hinckley, 1963) can not be obtained, indicating that kaolinite has a high stacking disorder (Dixon, 1989, p495-496).

Identification of Smectite Species

Smectite species can be identified by the following three different methods:

(1) Differentiating different subgroups of smectites by (060) reflection;

(2) Identifying montmorillonite by (a) Li-fixation and glycerol solvation and (b) Mg^{2+} saturation and glycerol liquid and glycerol vapor solvation; and

(3) Elemental chemical analysis of smectite minerals.

As described above, the strong (060) reflections at 1.49Å (Figure 5-2) indicate that only dioctahedral smectites (including montmorillonite, beidellite, and nontronite) are present. There are no peaks showing the presence of trioctahedral smectites (comprising hectorite, saponite, and sauconite). Therefore, the smectites in the old alluvium belong to the dioctahedral subgroup. From Figure 5-1 (a) & (c), the Mg^{2+} saturated smectite swells to different d-values d = ~18Å and ~15Å with glycerol liquid and glycerol vapor solvations, respectively, indicating that the dioctahedral smectites other than montmorillonite may be present (Brindley, 1966; Borchardt, 1989).

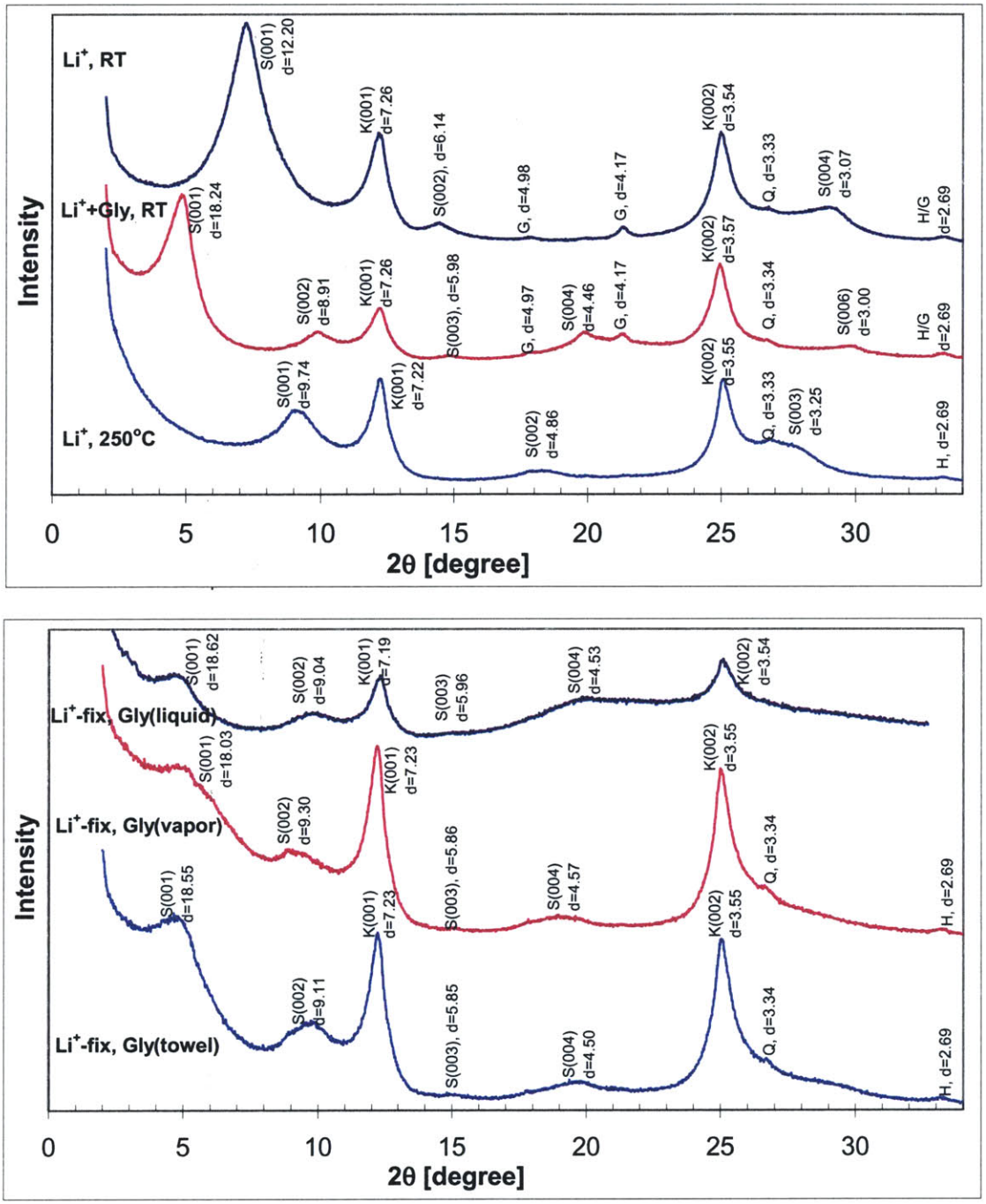

(a) Oriented aggregates of clays from UC

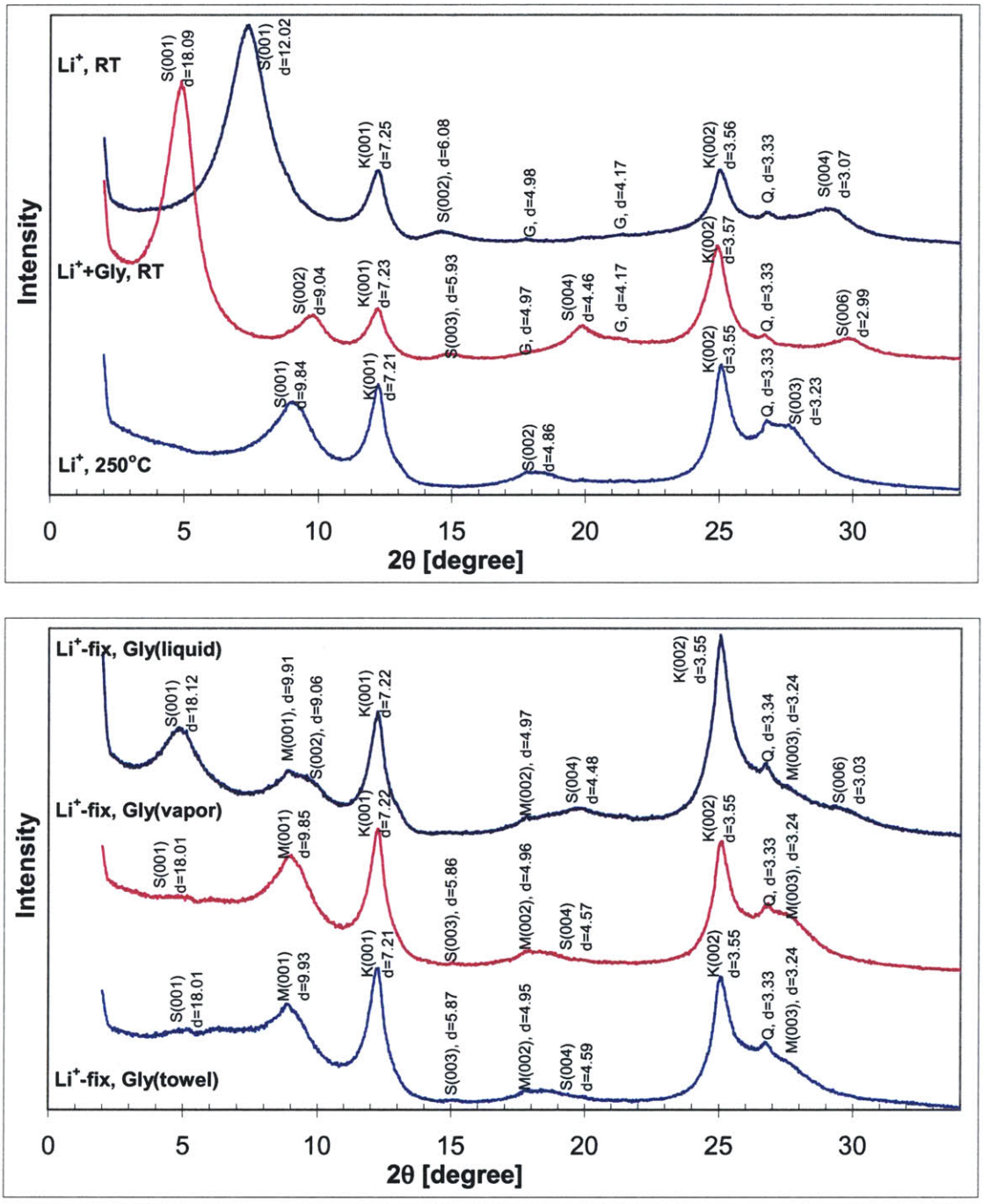

(b) Oriented aggregates of clays from MZ

Figure 5-3. XRD patterns of oriented clay aggregates saturated by Li^+.

The absence or presence of montmorillonite can be further evaluated by Li-fixation. After Li-fixation, *i.e.*, heating Li^+-saturated clay overnight at 250°C, the smectites in both the UC and MZ collapse to 9.7-9.8Å (Figure 5-3). Subsequent glycerol liquid, glycerol vapor, and glycerol towel solvations of UC Li-fixed clays cause smectite to swell to ~18Å. This indicates that montmorillonite is not the smectite species in the UC. For the Li-fixed MZ clay, the peak at 9.8Å is still present for subsequent glycerol liquid, glycerol vapor, and glycerol towel solvations. This indicates that montmorillonite is present in MZ. However, there is also a peak at 18Å present (Figure 5-3 (b)), although this peak is not very strong or obvious for the glycerol vapor and glycerol towel salvations. If the Lorentz-polarization factor is considered (Moore and Reynolds, 1997, p.89-94), which gives a gradually decreasing general background for small 2θ angles, it becomes clear that a broad peak centered around 18Å is still present for glycerol vapor and glycerol towel salvations (Figure 5-3 (b)). Therefore, montmorillonite (ideal formula: $Ca_{0.25}Si_4Al_{1.5}Mg_{0.5}O_{10}(OH)_2$) is present as part of the smectites in the MZ soil. In addition, other dioctahedral smectites are present, as indicated by the presence of a peak at 18Å.

At this point, it is not clear about the other species of dioctahedral smectite, *i.e.*, is it beidellite ($Ca_{0.25}Si_{3.5}Al_{0.5}Al_2O_{10}(OH)_2$) or nontronite ($Ca_{0.25}Si_{3.5}Al_{0.5}Fe_2O_{10}(OH)_2$) (ideal formula) (Borchardt, 1989)? With the realization of the difference of chemical elements between these two smectites, *i.e.*, beidellite is Al rich while nontronite is Fe rich, detailed chemical analysis can differentiate these two smectite species. The results of XRF analysis on the bulk samples which have been treated by DCB to remove iron

oxides show that the two samples still contain a lot of Fe (Table 5-3). The Fe in UC decreases from 9.17 wt.% to 4.10 wt.%, while the Fe in MZ from 4.64 wt.% to 3.13 wt.%. As discussed later, all minerals except smectites in the two layers should have a very low concentration of Fe after Fe-oxides are removed by DCB treatment. Therefore, the high Fe concentration in the DCB-treated samples must be contained in the smectites. Further evidence is provided by the EDXS analysis under ESEM performed on samples after DCB treatment. The results show that a significant amount of Fe is present (Figure 5-4) in the curved and delicately thin flakes, which are usually considered as smectite particles (Borchardt, 1989; Keeling *et al.*, 2000). Therefore, the iron-rich nontronite is the most likely species of smectites present in both UC and MZ, while the MZ also contains montmorillonite.

Table 5-3. Results of chemical analysis performed on the bulk samples with and without DCB pretreatment (unit: wt.%).

Element	UC without treatment	UC with DCB treatment	MZ without treatment	MZ with DCB treatment
Fe	9.17	4.10	4.64	3.13
Na	0.06	0.1	0.19	0.14
Mg	0.81	0.75	0.58	0.58
Al	8.23	12.38	8.04	8.81
Si	23.75	24.83	31.88	29.14
K	1.15	1.10	2.17	1.78
Ca*	0.16	0.01	0.29	0.03
Ti	0.50	0.56	0.32	0.35
Ba	0.46	0.43	0.92	1.09

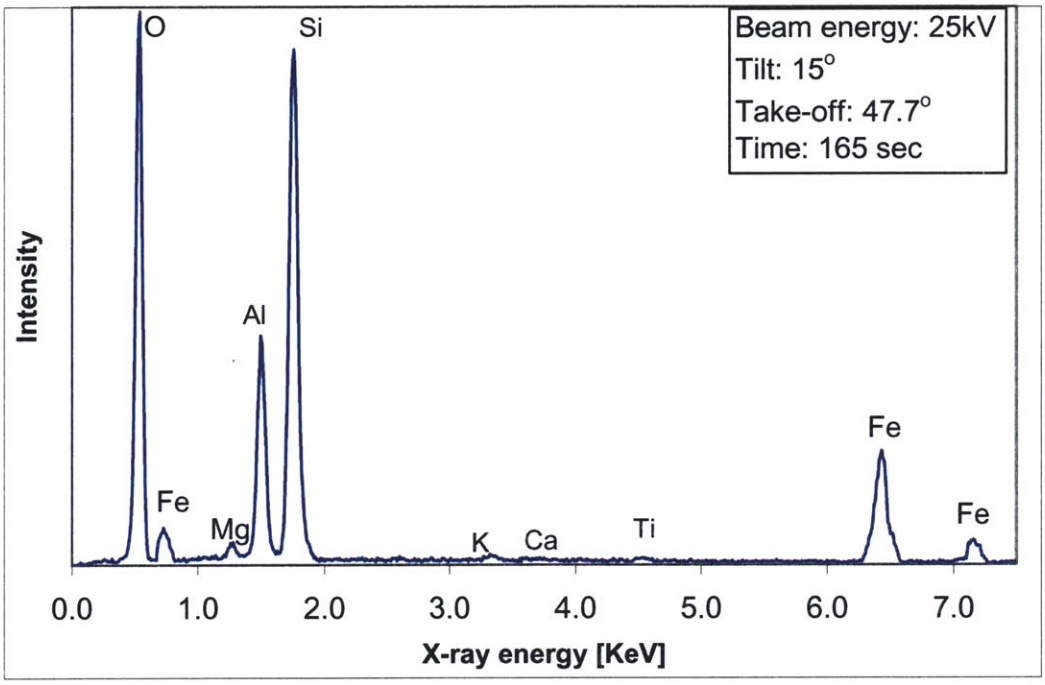

Figure 5-4. Spectrum of EDXS analysis performed on a curved and very thin clay particle after treated with DCB.

ESEM

Observations of the intact soil samples at natural water content under ESEM found no individual clay particles (see Section 6.4). All platy clay particles appear to be grouped and covered with a thin coating, and form stable microaggregates, which are typical of residual soils in tropical wet zones. It is believed that these fine-grained iron oxides act as coatings or binding agents among clay particles (Schwertmann and Taylor, 1989; Righi and Meunier, 1995, p.150). Samples with Fe-oxides removed after DCB treatment clearly show individual clay particles. Delicately thin and curved flakes with size of a few microns are smectites, some may be 5-20μm in size. Although no hexagonal platy thick particles of kaolinites were found, there are thick flat plates existing in both

the UC and MZ samples. More detailed description on the micromorphology of clay minerals can be found in Chapter 6.

Primary Minerals

Primary minerals were identified by XRD measurements on random powder samples of the unfractionated samples. The XRD patterns of the UC and MZ random powder in Figure 5-5 show that quartz is present in both layers, as indicated by the 11 strong and sharp peaks between 2-62° 2θ, which are compared and verified by PDF#33-1161 (JCPDS, 1993).

The identification of feldspar requires more effort. Since feldspars have complex diffraction patterns due to their low symmetry, and the coincidence of some peaks of feldspar with quartz, the identified peaks of K-feldspars have been compared to microcline (triclinic, PDF#19-0926), orthoclase (monoclinic, PDF#31-0966), sanidine (PDF#25-0618 & #19-1227). For triclinic feldspar, the (130) and $(1\bar{3}0)$ reflections and the (131) and $(13\bar{1})$ reflections do not coincide, *i.e.*, these planes are symmetrically nonequivalent. Monoclinic K-feldspar produces a single peak from each of the above sets of planes (Huang, 1989). As shown in Figure 5-5, only (131) (29.84° 2θ) and (130) (23.58° 2θ) reflections are present. Therefore, the XRD data confirm that orthoclase is the kind of feldspar present in both UC and MZ. Besides quartz and orthoclase, traces of muscovite (white mica), though not shown in XRD patterns, were observed during wet sieving in grain size analysis.

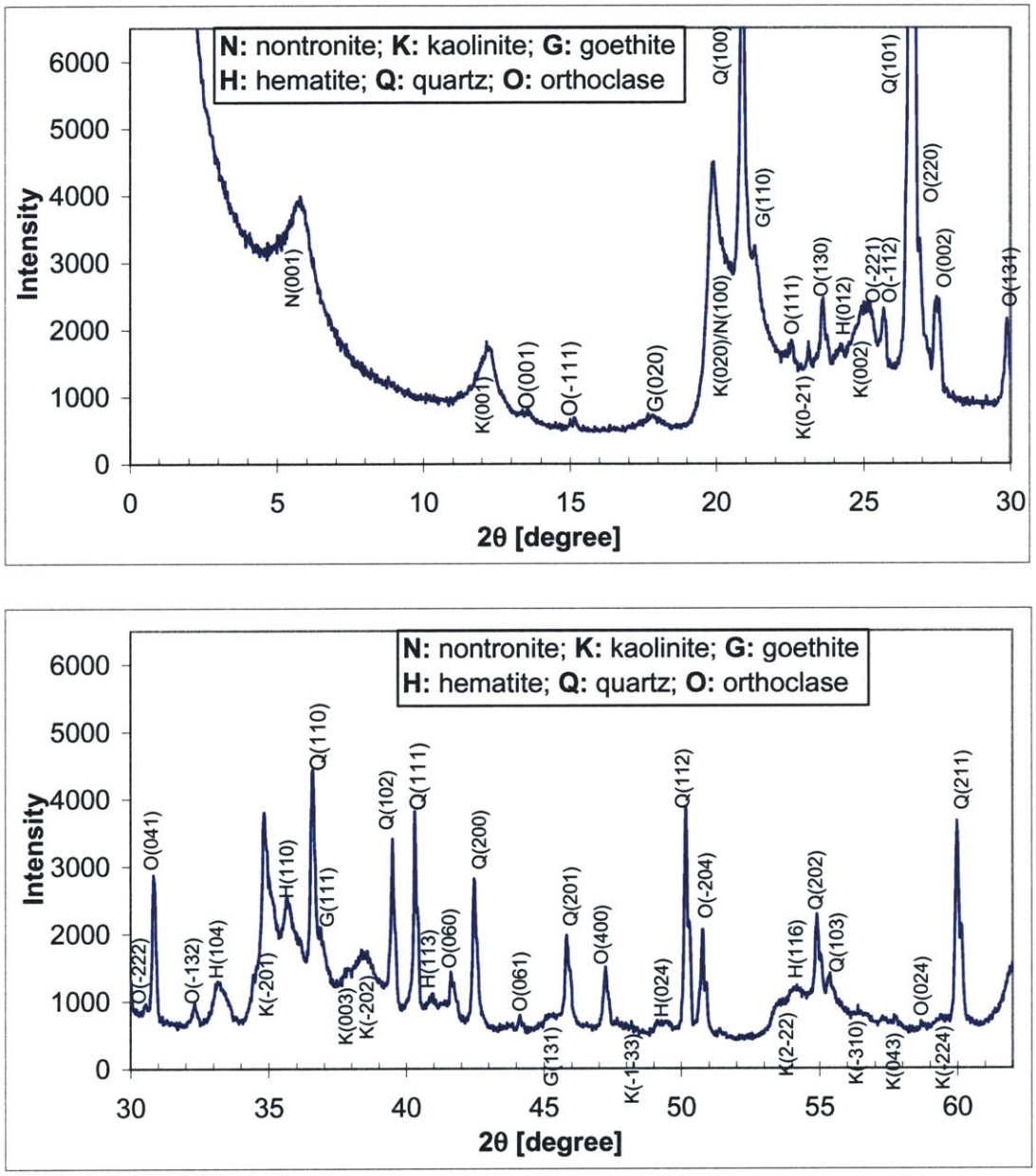

(a) UC bulk sample

Figure 5-5. XRD patterns of random powder from total bulk samples.

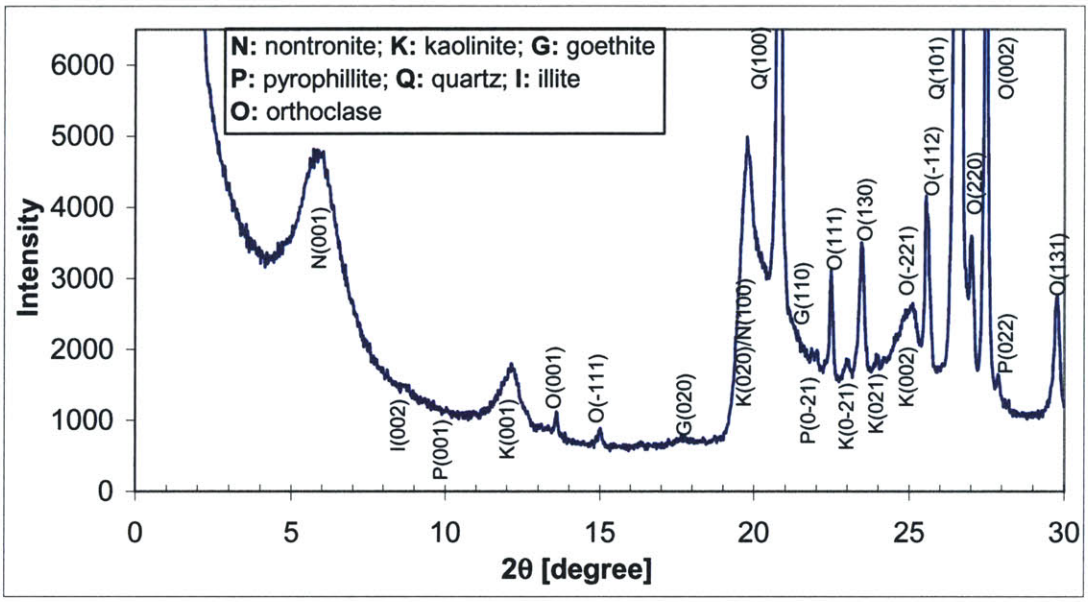

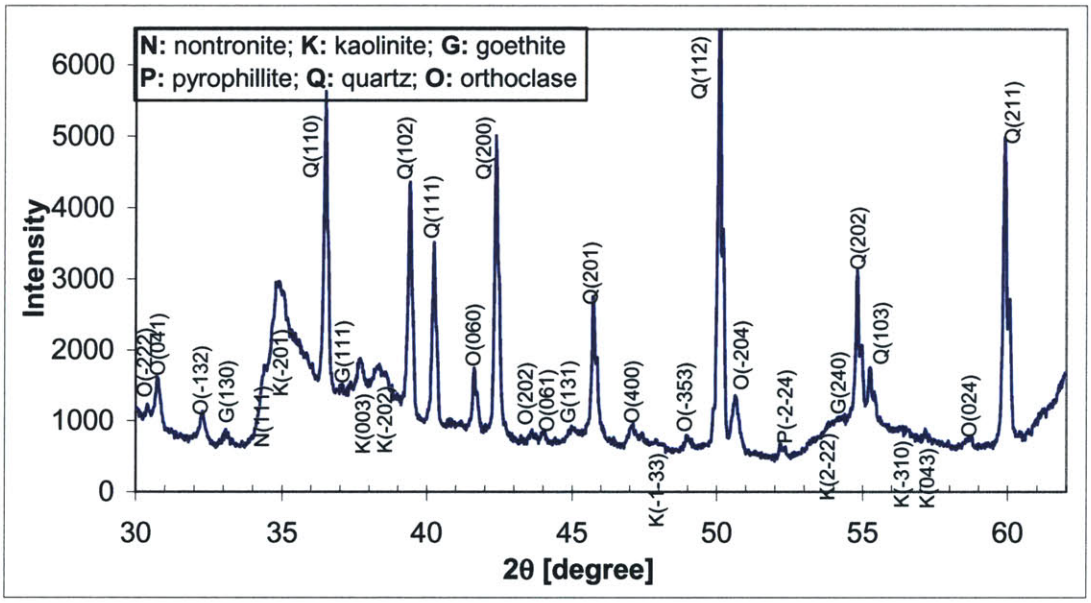

(b) MZ bulk sample

Figure 5-5 (continued). XRD patterns of random powder from total bulk samples.

Differential Thermal Analysis

The DTA results of both unfractionated bulk samples and clay fraction samples are shown in Figure 5-6. Table 5-4 lists the minerals identified by the reactions during heating. Therefore, the presence of smectite, kaolinite, goethite, and quartz in the two

layers is further confirmed by thermal analysis. Notice the difference of temperature for the loss of interlayer water from smectite between the clay fraction (~100°C) and the bulk samples (~80°C), which may be caused by the different interlayer cations in smectites, since the clay fraction is extracted from the clay suspension dispersed by $(NaPO_3)_6$, which caused previously existing cations in smectites to be exchanged with Na^+ ions. It is worthy pointing out that many reactions at very high temperatures may interfere and thus make difficult interpretation of the DTA curves at high temperatures. Since hematite and feldspars are relatively inert thermally, there is no thermal reactions related to hematite and feldspars in the DTA curves.

Table 5-4. Minerals identified by the DTA reactions related to their thermal properties.

Temperature Range [°C]	Thermal Peaks	Minerals Identified	Reactions	Samples
70-80	Endothermic	smectite	Loss of interlayer or adsorbed water	UC bulk MZ bulk
~100	Endothermic	smectite	Loss of interlayer or adsorbed water	UC clay MZ clay
300-310	Endothermic	goethite	dehydroxylation	All samples, but weak in MZ
~500	Endothermic	kaolinite	dehydroxylation	All samples
573	Endothermic (sharp)	quartz	Conversion from low to high quartz	UC and MZ bulk
~650	Endothermic	smectite	dehydroxylation	All samples
870	Endothermic	quartz	Conversion from high quartz to high tridymite	UC and MZ bulk
940	Exothermic	kaolinite	Recrystallization of dehydroxylates	All samples

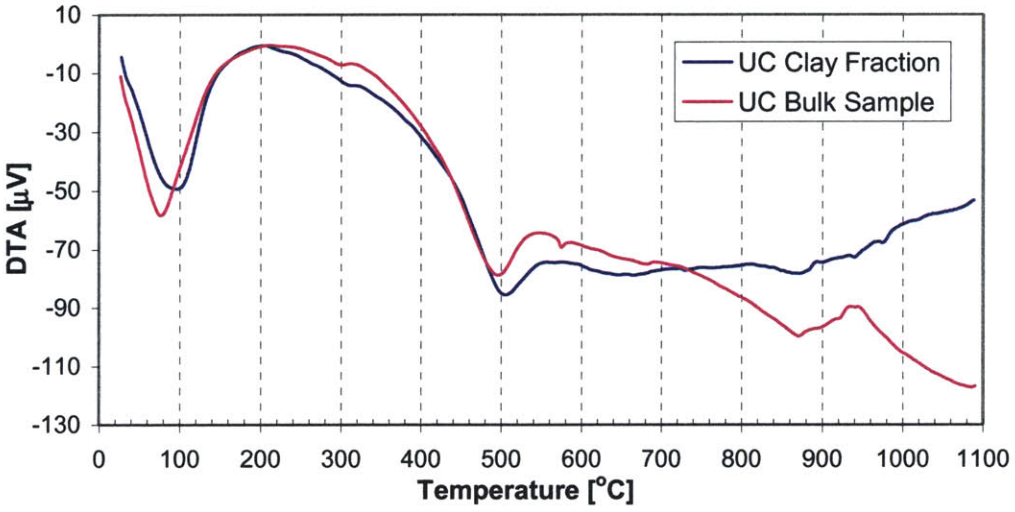

(a)

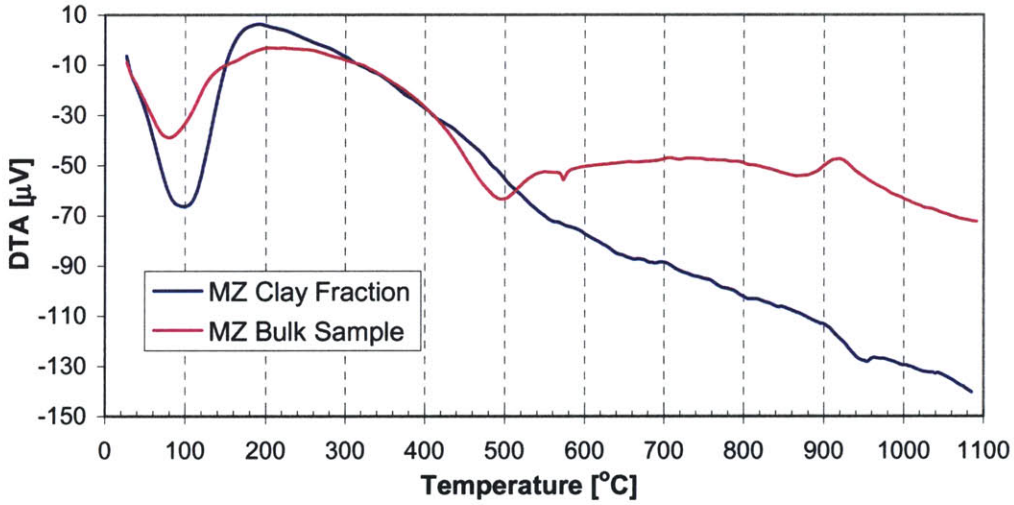

(b)

Figure 5-6. DTA curves for both clay fraction and bulk samples of (a) UC and (b) MZ layers.

Discussion

In the old alluvium, the two abundant clay minerals are kaolinite and nontronite, though MZ also has small amount of pyrophyllite, montmorillonite, and illite. The presence of smectites was not previously known for the old alluvium and can have

significant impact in construction due to its swelling potential. Table 5-5 summarizes the d-values of these two clays with different treatments. Kaolinite in the UC has a d-value of 7.228 ± 0.035 Å which remain invariant for all of the imposed treatments, while kaolinite in MZ has 7.218 ± 0.020 Å. The nontronite in the UC and MZ swells to approximately 18Å for all cations (Mg^{2+}, Li^{+}, K^{+} with different radius) when solvated with glycerol (MacEwan and Wilson, 1980). As shown by the Hinckley index of random powder XRD patterns and the micromorphology , *i.e.*, the non-hexagonal shape of flat plates, the kaolinite is not well crystallized or has a high structural disorder in the two layers. Furthermore, kaolinites in the UC is more stable than that in the MZ, as indicated by the higher temperature required to collapse all kaolinite particles in the UC. The ESEM observations on DCB treated samples found smectite present as curved and delicately thin flakes. The presence of pyrophyllite in the MZ, a 2:1 phyllosilicate with zero layer charge, is quite rare in soils. However, it has previously been found in fair amount in weathered alluvial terrace deposits in the upper Amazon basin of Colombia and Brazil (Zelazny & White, 1989). Therefore, it is not totally surprising to find pyrophyllite in the deep layer of the old alluvium of San Juan, which has a similar climate and geological history.

Iron oxides are the minerals giving the primary coloration of the deposits. Although both hematite and goethite are present in the UC layer, the high pigmenting power of hematite masks the color of goethite. Only goethite is present in the MZ layer, which gives the soil a brown to yellowish color. The soil fabric or texture is strongly affected by the iron oxides, which act as coating or binding agents among other soil

particles. Observations of micromorphology under the ESEM found no individual clay particles (either as plates or flakes) with clear particle edges and boundaries (see also Chapter 6). However, the DCB treatment which removes all iron oxides exposed the curved flakes as smectite particles and flat plates as kaolinite particles, both with clear edges and boundaries. The active physical and chemical properties of kaolinite and smectite, if coated by iron oxides, may not be apparent, *i.e.*, the associated matrix is quite rigid and has inactive physico-chemical properties. Further investigations on the soil structure of the old alluvium and the effect of iron oxides are presented in Chapter 6.

Table 5-5. Summary of d-values (unit: Å) of clay minerals with various treatments.

Saturating cation (radius, Å)	Kaolinite		Smectites	
	UC	MZ	UC	MZ
Mg^{2+} (0.66) & RT	7.15	7.24	14.47	14.62
Mg^{2+} & glycerol (liquid)	7.28	7.17	18.09	18.09
Mg^{2+} & glycerol (vapor)	7.26	7.23	15.23	14.88
K^+ (1.33) & RT	7.20	7.21	11.78	11.94
K^+ & glycerol (liquid)	7.25	7.22	18.33	18.11
K^+ & 300°C	7.22	7.21	11.68	11.30
K^+ & 500°C	7.21	collapsed	9.69	9.79
K^+ & 600°C	collapsed	No test	9.63	No test
Li^+ (0.60) & RT	7.26	7.25	12.20	12.02
Li^+ & glycerol (liquid)	7.26	7.23	18.24	18.09
Li^+ & 250°C (Li-fixation)	7.22	7.21	9.74	9.84
Li-fixed & glycerol (liquid)	7.19	7.22	18.62	18.12 & 9.91
Li-fixed & glycerol (vapor)	7.23	7.22	18.03	18.01 & 9.85
Li-fixed & glycerol (towel)	7.23	7.21	18.55	18.01 & 9.93

Regarding the origin of these mineral phases, the clays and iron oxides are neoformed minerals that are recrystallized or transformed by weathering, while the three primary minerals (*i.e.*, quartz, K-feldspar, and muscovite) are inherited from parent

materials, and are the most weathering resistant in the mineral stability sequence (Rai and Kittrick, 1989, p.180; see Section 2.3). Therefore, it is not surprising to find quartz, muscovite, and K-feldspar in the old alluvium, which has been weathered in a tropical marine climate. Since orthoclase is the characteristic K-feldspar of igneous rocks, part of the parent materials of the old alluvium may derive from igneous rocks. Indeed, this deposit forms in sediments of mixed origin, including plutonic rocks (granodiorite and quartz-diorite), extrusive basic volcanic rocks (lava and tuff), and sedimentary rocks (limestone and siltstone) (USDA, 1978).

Regarding the difference in soil mineralogy between the UC and MZ, the UC layer has hematite and more goethite, while the MZ has pyrophyllite, montmorillonite, and illite. Therefore, the UC layer is more weathered or developed than the MZ material. However, the presence of smectites indicates that neither layer has reached their final weathering stages, since the ultimate weathering products of a very mature soil in a tropical wet zone are essentially kaolinite and iron oxides (hematite) and oxyhydroxides (goethite), plus some gibbsite (Righi and Meunier, 1995).

5.3 Quantitative Analysis

5.3.1 Introduction

Quantitative mineral phase analysis is a nearly well established field and sufficiently advanced for practical use. Of all the techniques currently available for quantification of mineral phases, X-ray powder diffraction (XRD), thermal analysis, and

chemical analysis are the most widely used and well developed methods, each of which has its own strength and limitations. Quantitative XRD (QXRD) analysis is generally good and quick for the determination of certain crystalline minerals. However, it is still difficult to estimate the fraction of amorphous materials and some crystalline minerals with variable structural disorder and unknown amounts of isomorphous substitutions (Brindley, 1980), since the equivalent standard is hardly obtainable except the mineral itself from the bulk sample, provided that the phase separation is very tedious or almost impossible. For example, Brindley and Kurtossy (1961) pointed out it is advisable when selecting a standard kaolinite to choose one with approximately the same angular reflection breadth as the kaolinite to be quantified. Thermal analysis cannot reveal the thermally inert phases, such as hematite (Paterson and Swaffield, 1987); Chemical analysis, including the elemental analysis by X-ray fluorescence (XRF) and the determination of cation exchange capacity (CEC), can provide indirect information about the phases present in the mixture. Therefore, a comprehensive whole sample analysis may require a combination of several techniques that are complementary to each other.

Much has been published about QXRD analysis, among which are an excellent summary for clay minerals by Brindley (1980); a systematic review for many mineral systems by Snyder and Bish (1989); and detailed experimental techniques for clay minerals using oriented clay aggregates by Moore and Reynolds (1997). In addition, numerous publications dealing with the theoretical and mathematical models about QXRD are also available in literature, such as Szabo (1980), Hubbard and Snyder (1988),

Wang (1988), Davis et al. (1989), Hermann and Ermrich (1989), Zevin and Zevin (1989), Zangalis (1991), and Hayashi and Toraya (2000).

Here it is worthwhile to briefly introduce the method of known additions, as described in Brindley (1980, p.418). The basic equation giving the intensity of a reflection by a component P in a mixture is given by (Klug and Alexander, 1974, p.533; Brindley, 1980):

$$I_p = \frac{K_p w_p}{\overline{\mu}} \qquad (1)$$

where w_p is the weight fraction of P in the mixture, K_p is a constant which depends on the nature of the component, the particular reflection considered, and the experimental arrangement; $\overline{\mu}$ is the average mass absorption coefficient (AMAC) of the mixture. In the method of known additions, a known weight of a pure component is added to a mixture containing that component and the diffracted intensities from that component are measured before and after the addition. In its simplest form, the method measures a single component and the standard is the pure component which is added. Consider the determination of w_p, the weight proportion of P in a mixture. Let w_t be the additional amount of P added to 1g of the bulk sample. The resulting weight proportion will be $(w_p + w_t)/(1 + w_t)$. Application of Equation (1) leads to the following result:

$$\frac{I_1}{I_2} = \frac{w_p(1+w_t)\overline{\mu_2}}{(w_p + w_t)\overline{\mu_1}} \qquad (2)$$

where I_1 and I_2, $\overline{\mu_1}$ and $\overline{\mu_2}$ refer to the intensities and AMACs before and after the addition. If w_t is sufficiently small so that $\overline{\mu_2}/\overline{\mu_1}$ does not depart appreciably from unity, then

$$w_p = \frac{w_t(I_1/I_2)}{1+w_t-(I_1/I_2)} \qquad (3)$$

Due to its essentially constant chemical composition and little disorder in crystal structure, quartz usually gives least trouble in QXRD analysis (Brindley, 1980). Indeed, even low concentrations of quartz in soils and rocks can be readily quantified (Carter et al., 1987; Emig and Smith, 1989; Smith, 1997).

As the complementary methods to QXRD, both thermal analysis and chemical analysis are also widely used in quantitative determination of minerals. Thermogravimetric analysis (TGA) is a technique for determining weight loss of a sample as it is being heated at a controlled rate without access to O_2. While the TGA curve is monotonic decreasing with temperature, the peaks in the derivative thermogravimetric (DTG) curve obtained by taking the derivative of TGA data indicate the rate change of water loss with temperature. Upon heating, kaolinite and goethite lose 13.96 wt.% and 10.14 wt.% hydroxyl (OH) water, respectively, as illustrated by the following reactions (Brindley and Lemaitre, 1987; Taylor, 1987):

$Al_2Si_2O_5(OH)_4$ (kaolinite) → $Al_2Si_2O_7$ (metakaolin) + $2H_2O$ (450-550°C)

2α-FeOOH (goethite) → α-Fe_2O_3 (hematite) + H_2O (250-350°C)

The three dioctahedral smectite species common in soils, i.e., montmorillonite, beidellite, and nontronite, lose OH water at ~550-750°C by 4.88 wt.%, 4.87 wt.%, and 4.21 wt.%, respectively (Borchardt, 1989), which are approximately equal to each other. Therefore, no matter what kind of species or a mixture of these phases is present in a soil, the estimation of smectites fraction based on the water loss recorded by TGA will not differ too much from the actual value. In summary, the amount of goethite, kaolinite, and smectites, which lose OH water by 10.14%, 13.96%, and 4.21%, respectively, can be determined based upon the weight loss recorded at specific temperature ranges by TGA.

Among various chemical analyses, CEC is an indirect method and can be used to estimate the proportion of certain clay minerals which have appreciable CEC values, such as smectites (Borchardt, 1989; Mitchell, 1993). In addition, the determination of certain minerals can also be based upon the elemental analysis of the bulk sample, since the concentration of each element in the bulk sample should be in equilibrium with that summed over all individual phases containing that element. Quite often, the chemical data are available and are usually accurate. In fact, many theoretical and mathematical development of quantitative analysis combining both QXRD and chemical data can be found in the literature, such as Snyder and Bish (1989) and Zangalis (1991). The former also pointed out that a quantitative analysis combining the QXRD and chemical or thermal results with a knowledge of the composition of the individual phases can yield results of higher precision and accuracy than is generally possible with only one kind of observation.

All major mineral phases in the old alluvium in San Juan, Puerto Rico, were positively identified in Section 5.2. Of course, quantitative phase analysis is logically the next step. The quantitative determination of the proportion of each phase in the bulk samples can help in understanding the geological development and weathering process having taken place in the old alluvium. In addition, this knowledge may prove critical in subsequent efforts to formulate physically sound constitutive models for this material. For example, the amount of smectites present in the soil controls the magnitude of swelling and hence the potential maximum heave movement of the ground. This section continues with the previous one and describes the quantitative analysis of all identified mineral phases present in the UC and MZ layers of the old alluvium using QXRD, TGA, XRF, and CEC.

5.3.2 Materials and Methods

Materials

Sample size fractionating, sample preparation for XRD, and the removal of iron oxides by sodium dithionite, sodium citrate, and sodium bicarbonate (DCB) treatment were described in the previous section. Since the method of known additions presented above was used to quantify quartz in the old alluvium, a pure quartz powder passing through #325 mesh (<44μm) was added to the bulk sample powder of the UC and MZ as an internal standard. Also, SWy-1 (Na-Montmorillonite, Wyoming) from the Clay Minerals Society Source Clay Repository was used to check the accuracy of the QXRD method.

XRD

XRD patterns were obtained in a Rigaku Rotaflex 180mm diffractomemter with a graphite bean monochromator, using CuKα (λ=1.5418Å) radiation generated at 18 kW (60kV, 300mA). All scans used 1° divergence slit, 0.3mm receiving slit, a speed of 1° 2θ/min, a step size of 0.02° 2θ, and a scan range of 10°-64° 2θ. For the method of known additions, complete mixing was achieved by lightly grinding the quartz and the bulk sample powder with a mortar and pestle. To minimize the preferred orientation of clay minerals, the dry powder mixture was mounted onto the sample holder using the RTS method (see Appendix). A total of 6 samples were analyzed, including bulk UC and MZ, pure quartz, quartz-spiked UC and MZ, quartz-spiked SWy-1.

CEC

The determination of CEC was performed on UC and MZ bulk samples which were previously treated with DCB to remove iron oxides. The procedures of Hendershot and Duquette (1986) and Martin (2000) were followed here:

1. Treat the bulk sample with DCB to dissolve completely Fe-oxides (see Section 5.2.2);
2. Wash 3 times the treated sample with distilled and deionized water by centrifugation to remove all dissolved iron ions and other salts;
3. Wash the sample 4 times with 0.5N $BaCl_2$ solution (ph = 8.0) and shake it in a mechanical shaker to accelerate cation exchange for 20 min;
4. Wash the sample again twice with distilled water, and finally wash it twice with 0.0007N $BaCl_2$ solution

5. The difference of Ba concentrations measured by XRF in samples before and after cation exchange is the CEC of clays in the old alluvium.

XRF

Elemental chemical analyses was performed on air-dried bulk samples, iron-oxide removed samples, and cation-exchanged samples with a Spectro X-Lab 2000 energy-dispersive X-ray fluorescence spectrometer. After different treatments, samples were air dried, ground in a ball mixermill, and then pressed to make the standard pellets readily scanned by the XRF spectrometer.

Thermogravimetric Analysis

Thermogravimetric analysis (TG) was performed in a Seiko dual TG/DTA 320 thermogravimetric/differential thermal analyzer with heating temperature ranging from 25°C to 1000°C at a rate of 20°C/min in a pure N_2 atmosphere. Both the bulk sample and clay fraction were wet ground with alcohol to pass through a #325 mesh (<44μm) and then equilibrated in a sealed container overnight over a saturated $Mg(NO_3)_2$ solution which produces a constant relative humidity of 55%.

5.3.3 Results and Discussion

Direct Quantification of Mineral Phases

Quartz. The amount of quartz in the old alluvium was determined by the method of known additions of QXRD described above.

MZ bulk samples, the quartz-spiked UC and MZ samples. Also included are the peak intensities from a pure quartz powder and quartz-spiked SWy-1. Figure 5-7 shows the diffraction patterns of all these samples. Only 12.5 wt.% and 13.7 wt.% of quartz was added to the bulk UC and MZ, respectively. Based upon Equation (3), without considering peak interferences from other minerals, the average quartz fractions in the bulk UC and MZ samples can be easily calculated as 18.0 wt.% and 28.0 wt.%, respectively (Table 5-6). However, orthoclase and goethite interfere with quartz in the diffraction patterns. Therefore, the quartz peaks interfering with these minerals should be excluded from calculation, resulting in quartz fractions of 19.4 wt.% in the UC and 29.0 wt.% in the MZ. Notice that these values are based on the mass of air-dried bulk samples, which contain a significant amount of adsorbed water on smectites and iron oxides (Schwertmann and Taylor, 1989) or interlayer water in smectites.

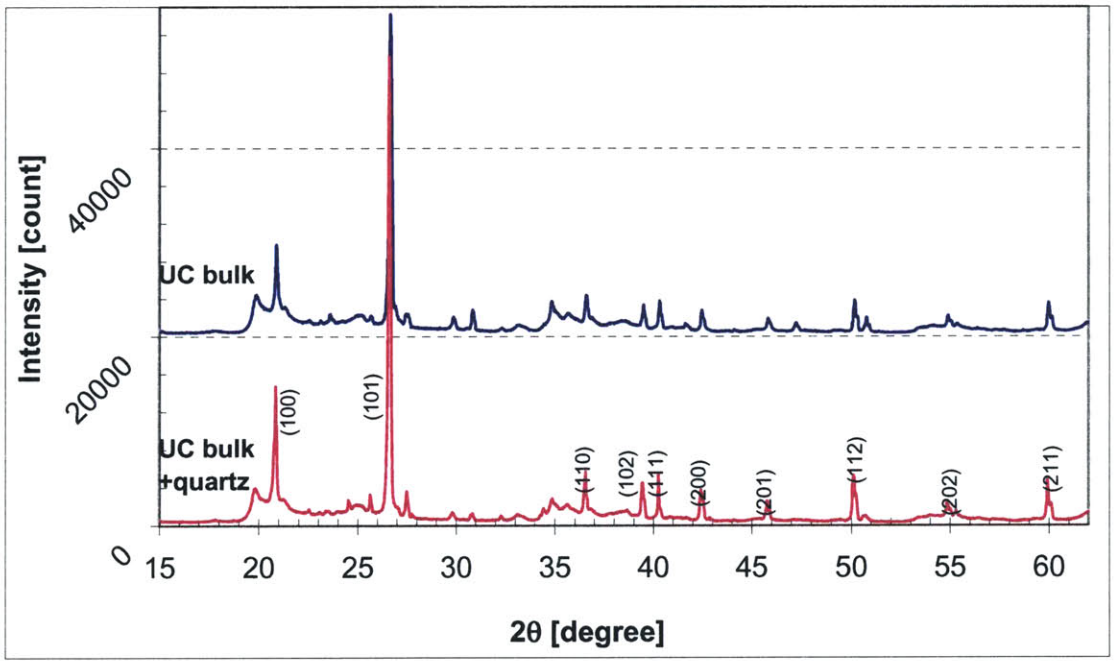

(a)

Figure 5-7. XRD patterns of (a) bulk UC and quartz-spiked UC.

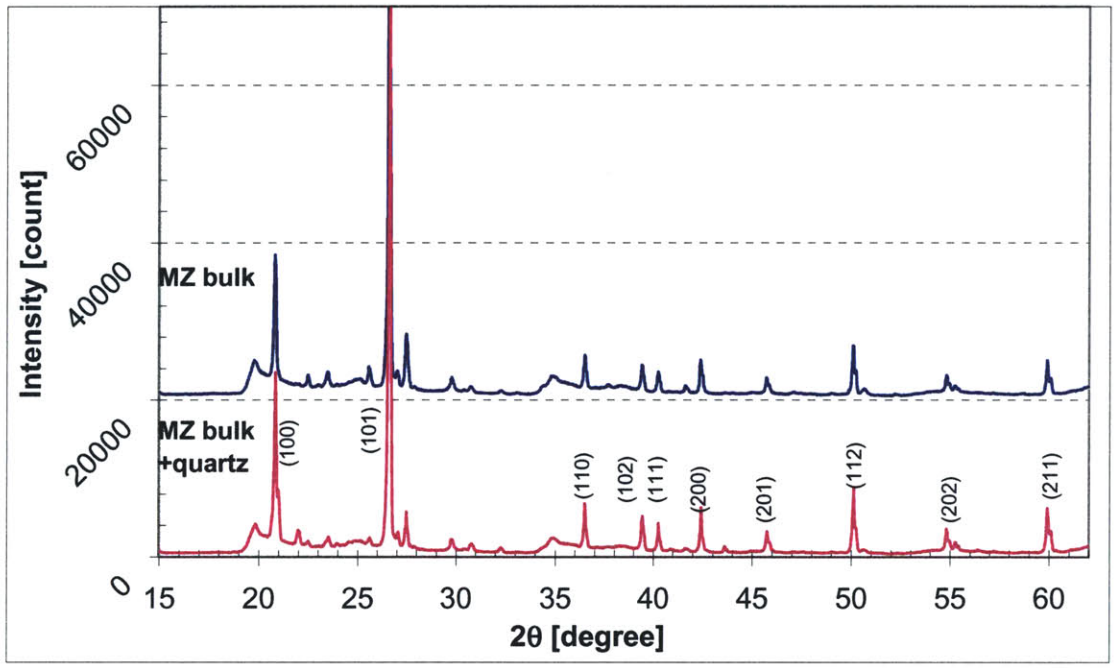

(b)

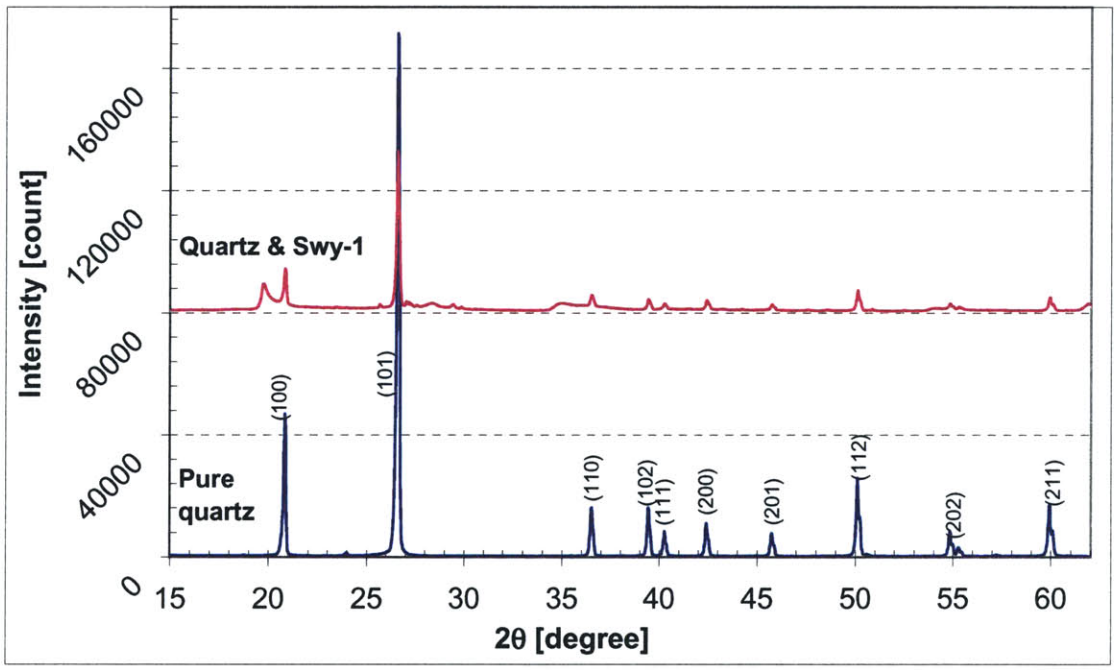

(c)

Figure 5-7 (continued). XRD patterns of (b) bulk MZ and quartz-spiked MZ; and (c) pure quartz powder and quartz-spiked SWy-1.

Table 5-6. Quantification of quartz in UC, MZ, and a mixture of quartz and SWy-1. Qz = quartz.

Quartz Peaks		Intensity (count)		Qz fraction in UC[&]	Intensity (count)		Qz fraction in MZ[&]	Minerals interfering with Qz	Intensity (count)		Qz fraction in SWy-1
$2\theta^{o}$	*hkl*	UC	UC + Qz		MZ	MZ + Qz			Pure Qz	SWy-1 + Qz	
20.85	100	7376	12647	0.135	15797	21232	0.259	Orthoclase	46318	11751	0.254
26.65	101	32921	48435	0.191	60837	78265	0.296		171096	50885	0.297
36.54	110	2986	4636	0.167	4144	5517	0.267	Goethite	15782	3535	0.224
39.46	102	2356	3631	0.170	3209	4282	0.265		15764	3395	0.215
40.28	111	2954	4705	0.158	2573	3446	0.262	Goethite	8022	1971	0.246
42.47	200	2171	3286	0.178	4226	5573	0.274		10779	3082	0.286
45.81	201	1361	1942	0.207	1941	2536	0.282	Orthoclase	7465	1760	0.236
50.14	112	3297	4789	0.197	6197	8066	0.285		25678	6576	0.256
54.87	202	1144	1663	0.197	2127	2685	0.315		8048	1673	0.208
59.95	211	2988	4285	0.204	4290	5532	0.294		16788	4227	0.252
Average including interferences				0.180			0.280				0.247
Average without interferences				0.194			0.290				
Amount of Qz actually added				0.125			0.137				0.222

[&] the quartz fraction measured by QXRD is based on the mass of air-dried bulk samples.

The mass absorption coefficient (μ) of quartz (for CuKα radiation, μ = 36.4 cm^2/g) is nearly equal to that of montmorillonite (μ = 33.4 cm^2/g) (Brindley, 1980). Therefore, the addition of different amounts of quartz to SWy-1 will not change the average mass absorption coefficient of the mixture, as used in Equation (2). The measurement of quartz fraction added to SWy-1 can be used to check the accuracy of the method. In fact, the difference between the amounts of quartz actually added (22.2 wt.%) and the measured one (24.7 wt.%) is very small, i.e., only 2.5 wt.%. The error may be caused by the size of quartz particles, which should have sizes near 1μm for more accurate measurement (Brindley, 1980, p.430).

Orthoclase. Illite (ideal formula: $K_{0.75}(Al_{1.75}Mg_{0.25})(Si_{3.5}Al_{0.5})O_{10}(OH)_2$) and muscovite (ideal formula: $K(Si_3Al)Al_2O_{10}(OH)_2$) have 7.55 wt.% and 9.82 wt.% of K in their chemical structure, respectively. Illite is not present in UC and is present only in small quantities in MZ, as reflected by its very weak peaks in the XRD patterns. In addition, the proportion of muscovite in both layers is negligible since the muscovite peaks are not shown in all XRD patterns (see Section 5.2). Therefore, orthoclase is the only major mineral phase containing K (14.05 wt.% based on its ideal formula, $KalSi_3O_8$) and contributing K to the bulk samples. The amount of orthoclase can be easily computed based on the K concentrations of the bulk samples. Table 5-7 lists the K contents measured by XRF and the calculation of K-feldspar fractions for the two layers. Indeed, UC has 9.35 wt.% and MZ 16.86 wt.% orthoclase based on the oven-dried bulk samples without including adsorbed or interlayer water.

Table 5-7. Quantification of orthoclase based on K concentrations of the bulk samples.

Sample	Adsorbed water (wt.%)	K concentration (wt.%)	Orthoclase (wt.%)
Air-dried UC	12.43	1.15	8.19
Oven-dried UC	0.0	1.31	9.35
Air-dried MZ	8.39	2.17	15.44
Oven-dried MZ	0.0	2.37	16.86

Kaolinite, smectite, and goethite. The three major minerals which have hydroxyls in their structure, i.e., kaolinite, smectite, and goethite, were quantified by thermal analysis. Figure 5-8 presents the plot of weight loss during the thermal reaction including both the TGA and DTG results. These show that no weight loss takes place after 800°C. From Figure 5-8, the dehydroxylation of kaolinite takes place at 400-550°C and smectites at 550-800°C, while goethite at 250-350°C. Taking into account that the adsorbed water in goethite is only totally driven off at about 200°C (Schwertmann and Taylor, 1989, p.407), and the temperature for desorption of adsorbed or interlayered water in smectites can be nearly 220-250°C, the oven-dried mass of the bulk samples is taken at 220°C, which is also shown by the minimum values around 220°C in the DTG curves (Figures 2 (b) and (d)). Table 5-8 summarizes the quantification of kaolinite, smectites, and goethite based on water losses at specific temperature ranges.

Table 5-8. Quantification of kaolinite, smectites, and goethite based on thermal analysis.

Sample	Mineral	Ideal water loss (wt.%)	Dehydroxylation temperature	Weight loss* (wt.%)	Mineral fraction (wt.%)
UC bulk	Goethite	10.14	250-350°C	0.59	5.83
	Kaolinite	13.96	400-550°C	4.70	33.64
	Smectites	4.21	550-800°C	0.85	20.16
MZ bulk	Goethite	10.14	250-350°C	0.26	2.61
	Kaolinite	13.96	400-550°C	3.20	22.93
	Smectites	4.21	550-800°C	0.65	15.32

* The percentage of weight loss is based on the mass dried at 220°C.

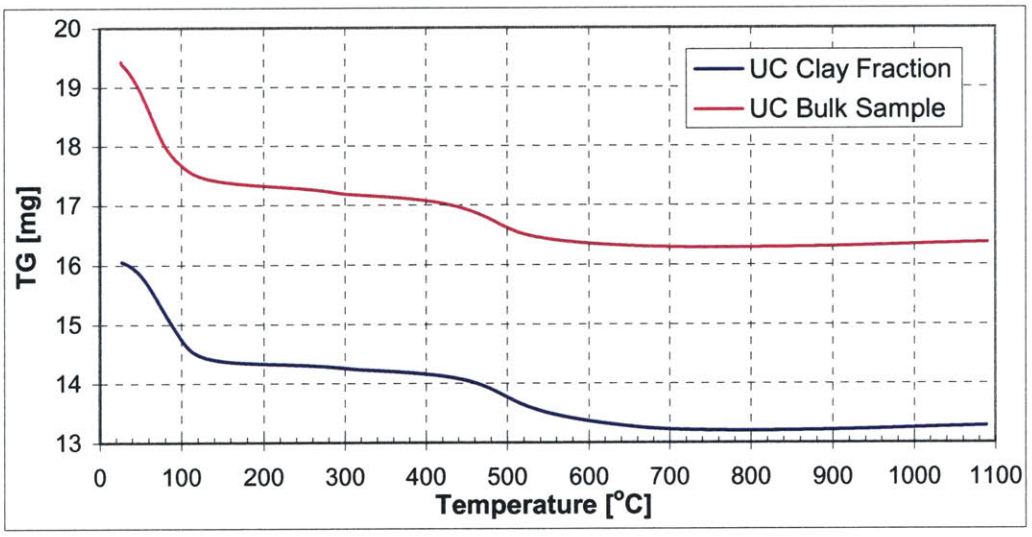

(a)

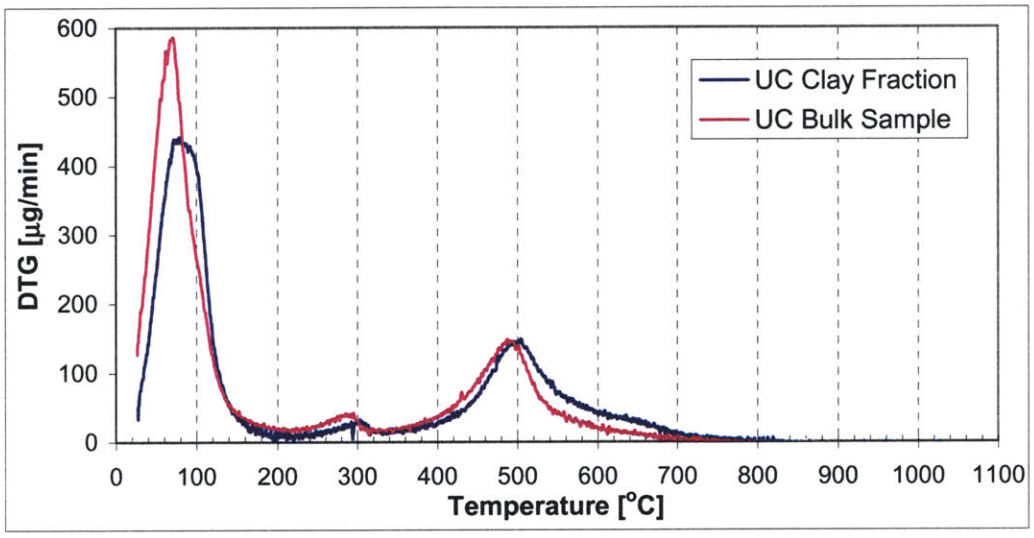

(b)

Figure 5-8. TGA and DTG curves for UC and MZ bulk samples and clay fractions.

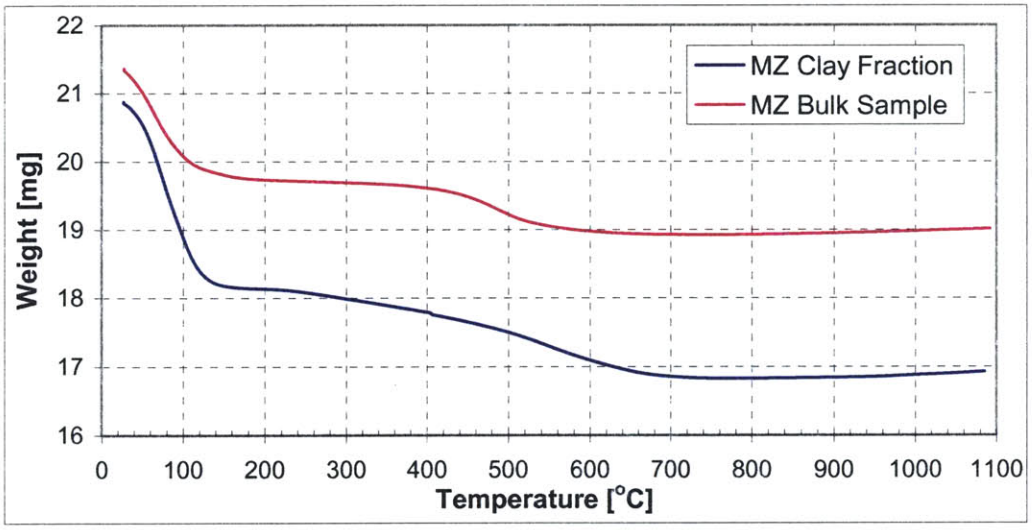

(c)

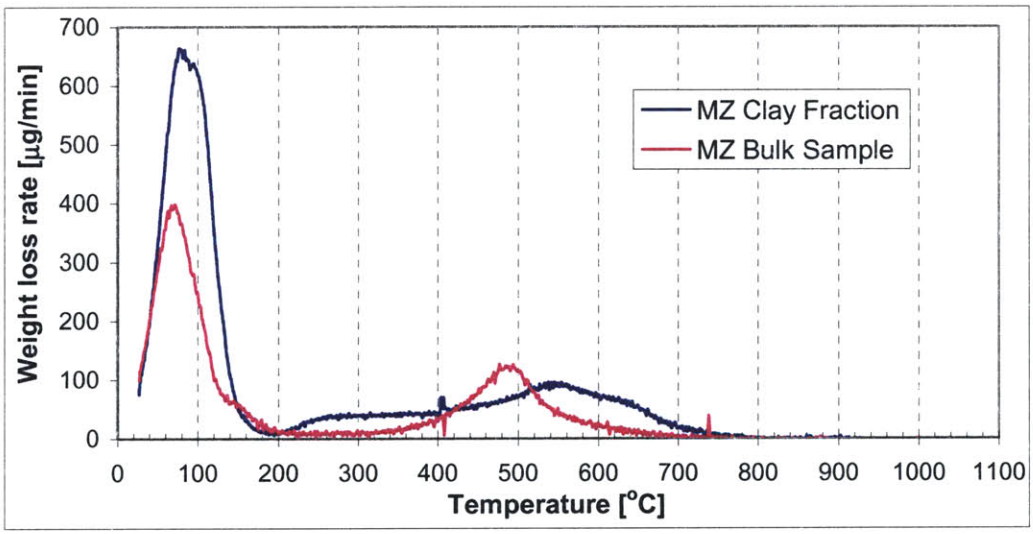

(d)

Figure 5-8 (continued). TGA and DTG curves for UC and MZ bulk samples and clay fractions.

Nontronite and hematite. The quantification of nontronite takes more effort. The above determination of the smectites fraction was based on the water loss during heating at 550-800°C and did not differentiate the water loss from different smectite species. In fact, the UC sample only contains nontronite, while both nontronite and montmorillonite exist in the MZ. Though montmorillonite generally loses its hydroxyls at higher temperatures than nontronite, smectites display a wide range of compositions due to the presence of different exchangeable cations between layers, variable amounts of isomorphous substitutions in both octahedral and tetrahedral sheets, and the resultant different layer charges. Therefore, the thermoanalytical behavior of smectites is quite complex (Paterson and Swaffield, 1987), and it is inadequate to quantify one phase simply based on thermal analysis when two or more smectite species are present in a sample.

However, Fe is the specific element present in the nontronite structure (the simplified ideal formula: $Ca_{0.25}Si_{3.5}Al_{0.5}Fe_2O_{10}(OH)_2$). Based on qualitative analysis, nontronite, hematite (α-Fe_2O_3), and goethite (α-FeOOH) are the only minerals present in the old alluvium and contain Fe in their structural formula. The DCB treatment can dissolve and remove both hematite and goethite, such that the remaining Fe in the DCB-treated samples must be supplied by nontronite. Therefore, the weight fraction of nontronite can be based from the Fe concentrations in the DCB-treated samples. Table 5-9 lists the calculation of nontronite fraction and the distribution of Fe in oxides and nontronite. As a result of the total Fe equilibrium, hematite in the UC can be easily determined by the difference of total Fe concentration in the bulk sample and the Fe

contained in both goethite and nontronite. As there is no detectable amount of hematite in the MZ (based on XRD), the hematite fraction in the MZ was assigned as zero.

Table 5-9. Quantification of nontronite and hematite based on the Fe concentrations in the bulk and DCB-treated samples. All values have a unit of wt.%.

Mineral or element	Ideal Fe Concentration	Amount in air dried UC	Amount in oven dried UC	Amount in air dried MZ	Amount in oven dried MZ	Measuring method
Adsorbed water		12.43	0.0	8.39	0.0	TGA
Total Fe		9.24	10.55	4.52[a]	4.93	XRF
Fe in nontronite		4.10	4.68	3.13	3.42	DCB XRF
Nontronite	26.13	15.69	17.92	11.98	13.08	
Fe in oxides		5.14	5.87	1.51	1.64	
Goethite	62.85	5.11	5.83	2.39	2.61	TGA
Fe in Goethite		3.21	3.66	1.50	1.64	
Fe in hematite		1.93	2.21[b]	0.0	0.0	
Hematite	69.94	2.76	3.15	0.0	0.0	
Smectites			20.16		15.32	TGA Table 4

[a] This value was from XRF on bulk UZ sample, while the summation of Fe in nontronite and Fe in oxides in MZ is 4.63, which is quite close to this value;
[b] This value = [Fe in hematite] = [total Fe] – [Fe in nontronite] – [Fe in goethite].

For comparison, the smectites fractions estimated by TGA (see Table 5-8) are also listed in Table 5-9. Since only nontronite exists in the UC, the smectites fraction in the UC by TGA and that by XRF should be equal or close to each other. Indeed, the difference between these two values is quite small, i.e., 20.16 wt.% versus 17.92 wt.%, respectively. Both montmorillonite and nontronite are present in the MZ, the difference

between the smectites fraction by TGA and that of nontronite by XRF, i.e., 2.24 wt.%, can be assigned to the fraction of montmorillonite.

Pyrophyllite, illite, and muscovite. Pyrophyllite and illite exist in MZ only as a small amount, while muscovite is present in both UC and MZ in an amount which was not detectable by XRD but was seen during wet sieving. Here no specific effort was taken to measure the amount of pyrophyllite, illite, and muscovite. Only semi-quantitative values were chosen based on the detection limits of XRD. Many crystalline substances give such sharp peaks that they are detectable when present to the extent of 1-2% or less in a mixture. Other materials give such poor patterns that, although they can be readily identified when alone, they may not be detected when present in a mixture even to the extent of 50% (Klug and Alexander, 1974). For example, the lower detection limits for quartz has been found as 0.01 wt.% in bentonites (Carter et al., 1987; Snyder and Bish, 1989) to 0.03 wt.% (Emig and Smith, 1989; Smith, 1997). For common silicate mixtures, a conservative estimation of 3-5 wt.% should be appropriate for the amount of detectable clays present in a soil. Therefore, pyrophyllite and illite are assigned to 3 wt.% in the bulk MZ sample.

Summary. Table 5-10 summarizes the fractions of all minerals present in the old alluvium, which account for 94.31% of the UC and 95.38% of the MZ samples. It is quite clear that the UC has more kaolinite and smectites than the MZ, while quartz and orthoclase are more abundant in the MZ, indicating that the UC layer is more weathered than the MZ. Furthermore, the UC has a higher Fe concentration and more iron oxides,

which means that the soil structure in the UC is more affected by iron oxides than the MZ.

Table 5-10. Summary of the fractions of all minerals in the old alluvium.

Mineral	Fraction in air-dried UC (wt.%)	Fraction in oven-dried UC (wt.%)	Fraction in air-dried MZ (wt.%)	Fraction in oven-dried MZ (wt.%)
Adsorbed water	12.43	0.0	8.39	0.0
Quartz	19.42	22.18	29.0	31.66
Orthoclase	8.19	9.35	15.44	16.86
Kaolinite	29.46	33.64	21.01	22.93
Nontronite	17.65	20.16	11.98	13.08
Goethite	5.11	5.83	2.39	2.61
Hematite	2.76	3.15	0.0	0.0
Montmorillonite	0.0	0.0	2.05	2.24
Illite	0.0	0.0	2.75	3
Pyrophyllite	0.0	0.0	2.75	3
Muscovite	trace	trace	trace	trace
Total	95.02	94.31	95.76	95.38

Independent Evaluation of the Results

Total Si and Al concentrations. The direct quantification of the minerals described previously does not use any chemical information on the total Si and Al concentrations in the bulk samples. Hence, these data can be used to provide an independent check on the balance on the Al and Si concentrations. Table 5-11 compares the Al and Si concentrations measured by XRF and that calculated from all individual phases in the bulk samples. It is noted that the Si concentrations match very well, while the Al concentrations have some errors. However, Al concentrations does not vary significantly for all data. The error might be caused by the incomplete isomorphous substitutions of Al by Fe or more substitutions of Si by Al in nontronite, as well as the substitutions of Si or Fe by Al in quartz or iron oxides. Nevertheless, the difference in Al concentrations is still small, i.e., 1.18 wt.% for the UC and 0.83 wt.% for the MZ.

Table 5-11. Balance of total Si and Al concentrations in the bulk samples.

Mineral	Ideal formula	Ideal Si concen. (wt.%)	Ideal Al concen. (wt.%)	Fraction in UC* (wt.%)	Fraction in MZ* (wt.%)
Quartz	α-SiO_2	46.74	0.0	22.18	31.66
Orthoclase	$KAlSi_3O_8$	30.27	9.69	9.35	16.86
Kaolinite	$Al_2Si_2O_5(OH)_4$	21.76	20.90	33.64	22.93
Nontronite	$Ca_{0.25}Si_{3.5}Al_{0.5}Fe_2O_{10}(OH)_2$	22.99	3.16	20.16	13.08
Goethite	α-FeOOH	0.0	0.0	5.83	2.61
Hematite	α-Fe_2O_3	0.0	0.0	3.15	0.0
Illite	$K_{0.75}(Al_{1.75}Mg_{0.25})(Si_{3.5}Al_{0.5})O_{10}(OH)_2$	25.31	13.89	0	3
pyrophyllite	$Al_2Si_4O_{10}(OH)_2$	31.18	14.98	0	3
montmorillonite	$Ca_{0.25}Si_4Al_{1.5}Mg_{0.5}O_{10}(OH)_2$	30.45	10.97	0	2.24

Total Si summed over all mineral phases		25.15	30.27
Total Al summed over all mineral phases		8.57	7.95
Si concentration from XRF	Based on air-dried sample mass	22.34	28.08
	Based on oven-dried sample mass	25.51	30.65
Al concentration from XRF	Based on air-dried sample mass	8.54	8.04
	Based on oven-dried sample mass	9.75	8.78

* based on the mass of oven-dried samples.

CEC. Cation exchange capacity is an indirect way to check the fraction of clays present in the bulk samples. Of all minerals present in UC and MZ, kaolinite, nontronite, illite, and montmorillonite have the ability to exchange cations. Iron oxides have zero CEC (SSL, 1996). Now that the amount of each clay is known, the CECs of the clay fractions in the bulk UC and MZ samples can be calculated. Table 5-12 compares the calculated CECs with the measured ones. Since CEC is generally expressed as milliequivalent charge per 100g of clays, the concentrations of clay minerals based on the total mass of oven-dried bulk samples were converted to that based on the total clays. From Table 5-12, it can be seen that the discrepancy between the calculated and the measured CECs is very small, i.e., 4.1% for UC clays and 6.9% for MZ clays.

Table 5-12. Comparison of calculated and measured CECs of clays in Old Alluvium.

Mineral	CEC (meq/100g)			Fraction in bulk UC (wt.%)	Fraction in UC clays (wt.%)	Fraction in bulk MZ (wt.%)	Fraction in MZ clays (wt.%)
	Ideal[a]	Literature[b]	Selected				
Kaolinite	0	3-15	8	33.64	62.53	22.93	55.59
Nontronite	117	110-150	120	20.16	37.47	13.08	31.71
Mont.[+]	135.5	60-150	90	0	0	2.24	5.43
Illite		10-40	15	0	0	3	7.27
Total clays				53.8	100	41.25	100
Calculated CEC (meq/100g)					49.97		48.48
Measured CEC (meq/100g)					52.12		45.34
Difference					4.1%		6.9%

[+] Montmorillonite;
[a] data from Borchardt (1989);
[b] data from Bain and Smith (1987), except nontronite from Mitchell (1993).

Average mass absorption coefficients (AMACs). Mass absorption coefficients (MACs) for minerals can be calculated from the coefficients for the individual atoms when the compositions are known. For a mixture of substances, the AMAC can also be summed over all components as a weighted average of the MACs of individual substances. Now that the weight proportion of each phase in both the UC and MZ bulk samples is known, their AMACs can be computed. Table 5-13 lists the calculation of AMACs for both UC and MZ bulk samples.

Since quartz is present in both the UC and MZ, from Equation (1), the ratio of the peak intensity of a quartz peak in UC, I_u, to the one in MZ, I_m, can be calculated as follows:

$$\frac{I_u}{I_m} = \frac{w_u \overline{\mu_m}}{w_m \overline{\mu_u}} \qquad (4)$$

where w_u and w_m, $\overline{\mu_u}$ and $\overline{\mu_m}$ refer to the weight fractions of quartz in UC and MZ, and the AMACs of UC and MZ, respectively. By using Equation (4), the ratios of the intensities of each quartz peak from two samples should be equal to the ratio of weight fractions in UC and MZ divided by the ratio of the AMACs of the two samples. Table 5-14 calculates the ratios of the intensities of 10 quartz peaks. It should be noticed that the ratios of peaks (101), (200), (112), and (202) are equal to 0.53-0.54, which is the ratio of $(w_u\overline{\mu_m})/(w_m\overline{\mu_u}) = 0.54$. This further proves that the AMACs, based on the weight proportions of all phases present in bulk UC and MZ, meet the measured peak intensities of quartz peaks.

Table 5-13. Calculation of the average mass absorption coefficients (AMAC) of UC and MZ bulk samples for CuKα radiation.

Mineral	Mass absorption coefficients* (cm^2/g)	Fraction in UC (wt.%)	Fraction in MZ (wt.%)
Quartz	36.4	22.18	31.66
Orthoclase	50.6	9.35	13.08
Kaolinite	30.8	33.64	22.93
Nontronite	105.2	20.16	13.08
Goethite	195	5.83	2.61
Hematite	215.9	3.15	0.0
Illite	40.9	0	3
Pyrophyllite	33.7	0	3
Montmorillonite	37.1	0	2.24
Average mass absorption coefficients (AMACs) (cm^2/g)		62.55	48.21

* MACs are calculated based the ideal formulas of the minerals.

Discussion of the Accuracy

The quantification processes described in this section account for 94.31 wt.% for all minerals in UC and 95.38 wt.% for MZ. The results have been checked independently by considering total Si and Al concentrations, CECs, and the AMACs. Moore and

Reynolds (1997) report that QXRD has a very good precision and that a set of replicate analyses should provide a standard deviation of ±5% of the amounts present if the constituent minerals are all present in reasonably large quantities, say 20% or more. However, accuracy should be considered good if errors amount to ±10% of the amounts present for major constituents, and ±20% for minerals whose concentrations are less than 20%.

Table 5-14. Calculation of the ratios of peak intensity of quartz in UC and MZ.

Quartz peaks		Intensity (count)		Intensity	Peak interfering
$2\theta^{o}$	hkl	Peaks in UC	Peaks in MZ	ratios	with other minerals
20.85	100	7376	15797	0.47	Yes
26.65	101	32921	60837	0.54	
36.54	110	2986	4144	0.72	Yes
39.46	102	2356	3209	0.73	
40.28	111	2954	2573	1.14	Yes
42.47	200	2171	4226	0.51	Yes
45.81	201	1361	1941	0.70	
50.14	112	3297	6197	0.53	
54.87	202	1144	2127	0.54	
59.95	211	2988	4290	0.69	

The amounts of nontronite are estimated by the TGA as 20.16% in the UC and 12.32% in the MZ. Since the dehydroxylation of nontronite, a Fe-rich dioctahedral smectite may interfere with kaolinite identification and measurement (SSL, 1996), the amount of smectites is underestimated, while kaolinite is overestimated. In addition, the possible incomplete isomorphous substitution of Fe in octahedral sheets in nontronite also leads to an underestimating of nontronite.

Weathering is a process of dissolution and leaching of certain cations. For K-feldspar, K is the first element leached out during weathering. Since the old alluvium has

undergone substantial post-depositional weathering, therefore, the K-feldspar in the old alluvium is probably underestimated. The accuracy of quartz concentrations is unknown, since the quartz added to the bulk samples as a standard may have different origin from that present in bulk samples, and the size of quartz particles is not small enough as near 1μm (Snyder and Bish, 1989). The evaluation of the accuracy for the quantification of other minerals present in the old alluvium is difficult and may require much more efforts. Nevertheless, for the engineering purpose, the relative amount of each mineral compared to other minerals may be more important than the accuracy of the value of the mineral fraction.

References

Anderson, H.R. (1976) Ground Water in the San Juan Metropolitan Area, Puerto Rico. US Geological Survey, Water Resources Investigations 41-75.

ASTM – American Society for Testing and Materials (1997) *Annual Book of ASTM Standards*. Vol.04.08. 970pp.

Bain, D.C. and Smith, B.F.L. (1987) Chemical analysis. In M.J. Wilson (ed.), *A Handbook of Determinative Methods in Clay Mineralogy*, 248-274. Blackie & Son Limited, 308pp.

Bish, D.L. and Post, J.E. (eds.) (1989) *Modern Powder Diffraction*. Reviews in Mineralogy, Vol. 20, published by the Mineralogical Society of America, Washington, D.C., 369pp.

Borchardt, G. (1989) Smectites. In J.B. Dixon and S.B. Weed (eds.), *Minerals in Soil Environments*, 2nd Edition, 675-727. Published by the Soil Science Society of America, Madison, Wisconsin.

Brindley, G.W. (1966) Invited Review: ethylene glycol and glycerol complexes of smectites and vermiculites. *Clay Minerals*, **6**, 237-259.

Brindley, G.W. (1980) Quantitative X-ray mineral analysis of clays. In G.W. Brindley and G. Brown (eds.), *Crystal Structures of Clay Minerals and Their X-ray Identification*, 411-438. Mineralogical Society Monograph No.5, Mineralogical Society, London, 495pp.

Brindley, G.W. and Brown, G. (eds.) (1980) *Crystal Structure of Clay Minerals and Their X-Ray Identification*. Mineralogical Society Monograph No.5, Mineralogical Society, London, 495pp.

Brindley, G.W. and Kurtossy, S.S. (1961) Quantitative determination of kaolinite by X-ray diffraction. *The American Mineralogist*, **46**, 1205-1215.

Brindley, G.W. and Lemaitre, J. (1987) Thermal, oxidation and reduction reactions of clay minerals. In A.C.D. Newman (ed.), *Chemistry of Clays and Clay Minerals*, 319-370. Mineralogical Society Monograph No.6, Mineralogical Society, London.

Carter, J.R., Hatcher, M.T., and Di Carlo, L. (1987) Quantitative analysis of quartz and cristobalite in bentonite clay based products by X-ray diffraction. *Analytical Chemistry*, **59**, 513-519.

Davis, B.L., Smith, D.K., and Holomany, M.A. (1989) Tables of experimental reference intensity ratios – Table No.2, December, 1989. *Powder Diffraction*, **4**, 201-205.

Deere, D.U. (1955) *Engineering Properties of the Pleistocene and Recent Sediments of the San Juan Bay Area, Puerto Rico*. Ph.D. thesis, University of Illinois, Urbana.

Dixon, J.B. (1989) Kaolin and serpentine group minerals. In: J.B. Dixon and S.B. Weed (eds.), *Minerals in Soil Environments*, p.467-525. Published by Soil Science Society of America, Madison, Wisconsin, USA.

Dixon, J.B. and Weed, S.B. (eds.) (1989) *Minerals in Soil Environments*. 2nd Edition. Published by Soil Science Society of America, Madison, Wisconsin, 1244pp.

Emig, J.A. and Smith, D.K. (1989) The detection and quantification of low concentrations of quartz in dolostone by X-ray powder diffraction. *Powder Diffraction*, **4**, 209-213.

Fookes, P. G. (ed.) (1997) *Tropical Residual Soils*. Geological Society Professional Handbooks. The Geological Society, London.

Greene-Kelly, R. (1953) Identification of montmorillonites. *Journal of Soil Science*, **4**, 233-237.

Gupta, A. Rahman, A., Wong, P.P., and Pitts, J. (1987) The Old Alluvium of Singapore and the extinct drainage system to the South China Sea. *Earth surface Processes and Landforms*, **12**, 259-275.

Hayashi, S. and Toraya, H. (2000) Quantitative phase analysis of natural products using whole-powder-pattern decomposition. *Powder Diffraction*, **15**, 86-90.

Hendershot, W.H. and Duquette, M. (1986) A simple barium chloride method for determining cation exchange capacity and exchangeable cations. *Soil Science Society of America Journal*, **50**, 605-608.

Hermann, H. and Ermrich, M. (1989) Microabsorption correction of X-ray intensities diffracted by multiphase powder specimens. *Powder Diffraction*, **4**, 189-195.

Hinckley, D.N. (1963) Variability in "crystallinity" values among the kaolin deposits of the coastal plain of Georgia and South Carolina. *Clays and Clay Minerals*, **11**, 229-235.

Huang, P.M. (1989) Feldspars, olivines, pyroxenes, and amphiboles. In: J.B. Dixon and S.B. Weed (eds.), *Minerals in Soil Environments*, p.975-1050. Published by Soil Science Society of America, Madison, Wisconsin, USA.

Hubbard, C.R. and Snyder, R.L. (1988) RIR – measurement and use in quantitative XRD. *Powder Diffraction*, **3**, 74-77.

JCPDS (1993) *Mineral Powder Diffraction File Databook.* Joint Committee on Powder Diffraction Standards, Swarthmore, PA.

Kaye, C.A. (1959) *Coastal Geology of Puerto Rico: (A) Geology of the San Juan Metropolitan Area.* Geological Survey Professional Paper 317. US Government Printing Office, Washington, D. C.

Keeling, J.L., Raven, M.D., and Gates, W.P. (2000) Geology and characterization of two hydrothermal nontronites from weathered metamorphic rocks at the Uley Graphite Mine, South Australia. *Clays and Clay Minerals*, **48**, 537-548.

Klug, H.P. and Alexander, L.E. (1974) *X-ray Diffraction Procedures.* 2nd Edition. John Wiley & Sons, Inc. 966pp.

Lim, C.H. and Jackson, M.L. (1986) Expandable phyllosilicate reactions with lithium on heating. *Clays and Clay Minerals*, **34**, 346-352.

MacEwan, D.M.C. and Wilson, M.J. (1980) Interlayer and intercalation complexes of clay minerals. In *Crystal Structure of Clay Minerals and Their X-Ray Identification*, G.W. Brindley and G. Brown (eds.), 197-248. Mineralogical Society Monograph No.5, Mineralogical Society, London.

Martin, R.T. (2000) Personal communications, together with his unpublished CEC determination method.

Mitchell, J.K. (1993) *Fundamentals of Soil Behavior.* 2nd Edition. John Wiley & Sons, Inc. 437pp.

Monroe, W.H. (1980) *Geology of the Middle Tertiary Formations of Puerto Rico.* Geological Survey Professional Paper 953. US Government Printing Office, Washington, D. C.

Moore, D.M. and Reynolds, R.C., Jr. (1997) *X-Ray Diffraction and the Identification and Analysis of Clay Minerals.* 2nd Edtion, Oxford University Press, 378pp.

Newman, A.C.D. (ed.) (1987) *Chemistry of Clays and Clay Minerals.* Mineralogical Society Monograph No.6, Mineralogical Society, London, 480pp.

Novich, B.E. and Martin, R. T. (1983) Solvation methods for expandable layers. *Clays and Clay Minerals*, **31**, 235-238.

Ottner, F., Gier, S., Kuderna, M., and Schwaighofer, B. (2000) Results of an inter-laboratory comparison of methods for quantitative clay analysis. *Applied Clay Science*, **17**, 223-243.

Paterson, E. and Swaffield, R. (1987) Thermal analysis. In: M.J. Wilson (ed.), *A Handbook of Determinative Methods in Clay Mineralogy*, p.99-132. Blackie & Son Limited, London.

Pease, M.H., Jr. and Monroe, W.H. (1977). *Geologic Map of the San Juan Quadrangle, Puerto Rico*. US Geological Survey.

Pevear, D.R., Dethier, D.P., and Frank, D. (1982) Clay minerals in the 1980 deposits from Mount St. Helens. *Clays and Clay Minerals*, **30**, 241-252.

Raab, G.A. (1988) Semiquantitative analysis by X-ray powder diffraction (SQXRD) of the <2mm to 0.002mm and <0.002mm fractions of soil. *Powder Diffraction*, **3**, 144-152.

Rai, D. and Kittrick, J.A. (1989) Mineral equilibria and the soil system. In: J.B. Dixon and S.B. Weed (eds.), *Minerals in Soil Environments*, 161-198. Published by Soil Science Society of America, Madison, Wisconsin, USA.

Righi, D. and Meunier, A. (1995) Origin of clays by rock weathering and soil formation. In B. Velde (ed.), *Origin and Mineralogy of Clays*, 43-161. Springer-Verlag, Berlin.

Schwertmann, U. and Taylor, R.M. (1989) Iron Oxides. In J.B. Dixon and S.B. Weed (eds.), *Minerals in Soil Environment*, 2nd Edition, 379-438. Published by Soil Science Society of America, Madison, Wisconsin, 1244pp.

Shirlaw, J.N., Hencher, S.R., and Zhao, J. (2001) Design and construction issues for excavation and tunneling in some tropically weathered rocks and soils.

Smith, B.F.L. (1994) Characterization of poorly ordered minerals by selective chemical methods. In: M.J. Wilson (ed.), *Clay Mineralogy: Spectroscopic and Chemical Determinative Methods*. p.333-357. Chapman & Hall, UK.

Smith, D.K. (1997) Evaluation of the detectability and quantification of respirable crystalline silica by X-ray powder diffraction methods. *Powder Diffraction*, **12**, 200-227.

Snyder, R.L. and Bish, D.L. (1989) Quantitative analysis. In D.L. Bish and J.E. Post (eds.), *Modern Powder Diffraction,* 101-144. Reviews in Mineralogy, Vol. 20, published by the Mineralogical Society of America, Washington, D.C., 369pp.

SSL – Soil Survey Laboratory (1996) *Soil Survey Laboratory Method Manual.* Soil survey investigation report No.42, Version 3.0, 693pp.

Szabo, P. (1980) Optimization of quantitative X-ray diffraction analysis. *Journal of Applied Crystallography*, **13**, 479-485.

Taylor, R.M. (1987) Non-silicate oxides and hydroxides. In A.C.D. Newman (ed.), *Chemistry of Clays and Clay Minerals*, 129-201. Mineralogical Society Monograph No.6, Mineralogical Society, London.

USDA (1978) *Soil Survey of San Juan Area of Puerto Rico*. United States Department of Agriculture.

Velde, B. (ed.) (1995) *Origin and Mineralogy of Clays*. Springer-Verlag Berlin. 334pp.

Wang, H. (1988) A method for quantitative X-ray phase analysis without standards. *Powder Diffraction*, **3**, 165-167.

Whittig, L.D. and Allardice, W.R. (1986) X-ray diffraction techniques. In A. Klute (ed.) *Methods of Soil Analysis. Part 1. Physical and Mineralogical Methods*. 2nd ed. Agronomy 9, 331-362.

Wilson, M.J. (1987) X-ray powder diffraction methods. In *A Handbook of Determinative Methods in Clay Mineralogy*, edited by M.J. Wilson, 26-98. Blackie & Son Limited, 308pp.

Wilson, M.J. (ed.) (1987) *A Handbook of Determinative Methods in Clay Mineralogy*. Blackie & Son Limited, London. 308pp.

Winburn, R.S., Grier, D.G., McCarthy, G.J., and Peterson, R.B. (2000) Rietveld quantitative X-ray diffraction analysis of NIST fly ash standard reference materials. *Powder Diffraction*, **15**, 163-172.

Zangalis, K.P. (1991) A standardless method of quantitative mineral analysis using X-ray and chemical data. *Journal of Applied Crystallography*, **24**, 197-202.

Zelazny, L.W. and White, G.N. (1989) The pyrophyllite-talc group. In J.B. Dixon and S.B. Weed (eds.), *Minerals in Soil Environments*, 527-550. Published by Soil Science Society of America, Madison, Wisconsin, USA.

Zevin, L.S. and Zevin, S.L. (1989) Standardless quantitative X-ray phase analysis – estimation of precision. *Powder Diffraction*, **4**, 196-200.

Chapter 6 SOIL STRUCTURE AND INDEX PROPERTIES

6.1 Introduction

After the soil composition of the old alluvium was analyzed both qualitatively and quantitatively, the next logical step was to determine how these minerals are arranged and associated to form the intact soil structure. This information must be supplemented by a description of the particulate system or an assemblage of particles themselves. This is accomplished through measurements of the particle size distribution and Atterberg limits obtained from soil samples that have been thoroughly reworked into a uniform soil-water mixture (Lambe and Whitman, 1969). Unfortunately, the methods of sample preparation and preprocessing can destroy the initial soil fabric or bonds between particles. Therefore, the measured index properties determined on a more or less remolded soil reflect both the initial intact soil structure and effects of sample preparation methods. It has been reported in the literature (e.g., Townsend et al., 1971; Mitchell and Sitar, 1982; Fookes, 1997) that most residual soils have variable index properties, i.e., both particle size distribution and Atterberg limits change with remolding energy, drying condition, etc. Although no specific efforts have been made to relate the variability of index properties to the soil structure, it is generally believed that the changes in index properties reflect the alteration of soil microstructure by remolding or drying. Hence, the determination of index properties by using controlled sample preparation methods can be an indirect method for evaluating the initial intact soil structure.

This chapter gives a unified presentation of the experimental investigation into the intact soil structure and index properties for the old alluvium. Section 6.2 introduces the basic concepts of dispersion, cementation, and aggregation that are used extensively in subsequent discussions. Sections 6.3 and 6.4 focus on direct observations of the macrostructure and microstructure, respectively, while Sections 6.5 and 6.6 present measurements of the particle size distribution and Atterberg limits. Finally, Section 6.7 proposes a conceptual model of the soil structure of the old alluvium based on these data.

6.2 Background on Dispersion, Cementation, and Aggregation

This chapter refers extensively to concepts of dispersion, aggregation, and cementation. These terms have very specific and distinct meaning which is seldom appreciated by geotechnical engineers. In contrast, soil scientists and clay mineralogists are very careful in distinguishing concepts of aggregation and cementation. The following definitions are derived mostly from van Olphen (1987), Schwertmann and Taylor (1989), Mitchell (1993), and Righi and Meunier (1995).

Dispersion

Dispersions of clay particles in water are complex systems involving the principles of colloidal stability. The stability of a colloidal clay suspension is mainly determined by the two competing particle interaction forces: an electrical double layer repulsion force on charged clay surfaces and an attractive force due to the van der Waals' attraction between the atoms of the two particles approaching each other by diffusion. In order to be reasonably stable (i.e., no flocculation between colloidal particles in the

suspension), a colloidal clay system should be rather clean, i.e., containing only small amount of electrolytes. In general, the addition of any inert electrolyte (one which does not react chemically with the particles, such as sodium chloride, NaCl) promotes flocculation in the clay suspension (van Olphen, 1987).

Clay minerals are characterized by the large negative face charges due to ion substitutions and small positive edge charges caused by broken atomic bonds, resulting in an overall shortage of positive charges. This deficit of charge within the crystal is compensated by the adsorption of cations on the negatively charged faces of clay minerals, thus a diffusive electrical double layer is created. This negative double layer has a constant charge independent of the composition of the equilibrium solution of the colloidal suspension. On the other hand, the situation at the edge of clays is quite different from that on the faces. The positive double layer on these edges is dependent on pH, or the activity of H^+ or OH^- ions in solution. In the presence of a negative face double layer and a positive edge double layer, edge to face flocculation must occur in a clean suspension. Therefore, a clean neutral or acidic clay suspension cannot be stable or the colloidal particles tend to flocculate. By increasing pH (e.g., pH = 9) or adding OH^-, the clay suspension may become stable since the excessive OH^- ions in solution reverse the positive edge double layer into a negative double layer.

The principle of stabilizing clay suspensions by double layer modification involves eliminating flocculation by reversing either the face or edge charge, and the building up the reversed charge to a level sufficient to prevent flocculation by van der

Waals' attraction forces (van Olphen, 1987). The most common procedures are based on reversing the edge charge for the relatively small area of the edge surfaces, as edge charge reversal is usually more economical than face charge reversal.

Generally, there are two ways to reverse the edge charge. One is to increase the concentration of OH^- ions by adding alkali and raising the pH. The other is to add electrolytes (acting as dispersants) containing anions which can be chemisorbed to form complex anions with Al^{3+} or other cations exposed at the broken bond edges of clay minerals. Examples of the latter are the fluoride ions (F^-), hydroxyls (OH^-), polymetaphosphate ions (e.g., PO_3^-), and many other inorganic and organic anions, all of which have one feature in common, they produce a buffered pH from neutral to high (Moore and Reynolds, 1997). The most effective dispersants have phosphate ions that promote dispersion by the adsorption of the phosphate ions on clay edges where they reverse normally positive edge charges and thus, help prohibit flocculation.

The amount of dispersant added to a clay suspension depends on the total amount of positive charges on the clay edges. Usually a concentration of 10^{-3} to 10^{-4} M is suitable for most clays or clay mixtures. A clay suspension with too much dispersant may promote flocculation again because of an increase in the concentration of salts in the suspension (Moore and Reynolds, 1997, p.211). In summary, in order to obtain stable clay dispersions, an effective dispersing agent with proper concentration should be used to reverse the positive double layer on clay edges.

Aggregation and Cementation

The previous chapters have shown that Fe-oxides are present in the deposit. Finely divided Fe-oxides usually are believed to act as binding agents among other soil particles. This may result in *cementation* or *aggregation* of the primary soil particles into larger units.

In *cementation*, the Fe-oxides fill significant proportions of the pores between the matrix particles. These cemented masses may form through the growth of Fe-oxide crystals in place between matrix particles, similar to the growth of Ca-silicate crystals in concrete or in soils treated with CaO for stabilization. Mitchell (1993) pointed out that during tropical weathering, the recrystallization or reprecipitation of silica, oxides, and other minerals reprecipitated from aqueous solution (such as carbonates), can form coatings over particles or form bridge connections between particle contacts. Crystal growth may lead to a very stable, nondispersible association of matrix particles. For instance, calcium carbonate usually connects clays, silts, or sands together by cementation to form sedimentary rocks, which cannot be readily dispersed in water. The common cementing agents in soil environments include carbonates, silica, organic matter, and Fe or Al oxides.

On the other hand, aggregates may form not so much through crystal growth but more through an attraction between positively charged Fe-oxide particles and negatively charged matrix particles, particularly clay minerals. In particular, *Aggregation* is understood as the association of soil-matrix particles into small aggregates or clusters by

minute particles of Fe-oxides. The charge of Fe-oxide particles is pH dependent and hence, their aggregation effect should also be pH-dependent. Thus, the mechanism causing aggregation in soils is similar to that of flocculation, except that flocculation is generally used for colloidal suspensions, which of course have much higher water contents than the solid state of in situ intact soils. The two most common Fe-oxides, i.e., goethite (FeOOH) and hematite (Fe_2O_3), behave differently in binding particles together. Although there are some controversy in the literature (Schwertmann and Taylor, 1989), it is generally believed that goethite acts mainly as a cementation agent while hematite causes aggregation (Righi and Meunier, 1991).

Although different mechanisms are involved in the formation of cementation and aggregation on the microscopic scale, they both produce larger aggregates (i.e., clusters of particles) which may be visible macroscopically. In addition, they also increase the initial stiffness and strength of the intact soils. However, the bonds caused by cementation are much stronger than those caused by aggregation. A good example is that the cementation by Ca-silicate crystal growth gives very high strength to concrete.

Chemical and Mechanical Dispersion

The above discussion differentiates cementation from aggregation. Based on the principles of the stability of clay suspensions, the positive charges on both the surfaces of Fe-oxides particles and the edges of clay particles are pH-dependent and can be reversed by dispersants, hence the attraction between the negatively charged faces of clay particles and the positively charged Fe-oxides can be eliminated. Aggregation caused by Fe-oxides

can be dispersed by certain effective dispersants (*chemical dispersion*). However, soils with Fe-oxides cementation do not readily disperse in water with or without dispersants (SSL, 1996), since cementation is developed through recrystallization of Fe-oxides minerals, and the bonds (possibly atomic bonds) caused by cementation cannot be eliminated or cancelled by charge reversal. In order to disperse a soil with Fe-oxides cementation, either mechanical force must be applied to break the cementation bonds (which is called *mechanical dispersion*), or the cementation minerals must be dissolved and removed by treating the soil with certain chemicals. For example, SSL (1996) suggested that Fe-oxides, including both hematite and goethite, be dissolved by sodium dithionite, sodium citrate, and sodium bicarbonate solutions (DCB). Usually, the dispersion method by dissolving the cementation agents is not preferred, since the original soil composition is altered by removing the cementing minerals, or certain soil minerals may be affected by the chemicals added to treat the sample.

However, in order to obtain a stable dispersion from a soil with clays and Fe-oxides, both mechanical and chemical dispersions are required. Cementation can't be reversible if it is broken down by mechanical dispersion, while aggregation is reversible if only mechanical dispersion is used. Therefore, a soil with both cementation and aggregation bonds requires both mechanical and chemical dispersions. A mechanically dispersed soil suspension may become flocculated again if no dispersant is used to reverse the edge charges of clays and the surface charges of Fe-oxides. Examples will be discussed in Section 6.5.

6.3 *Macrostructure*

6.3.1 Introduction

This section discusses the macrostructure of the old alluvium obtained by observational methods. Here macrostructure refers to the features of soil structure at the macroscopic level, i.e., those that can be identified with the naked eye.

6.3.2 Materials and Methods

Some characteristics of macrostructure can be obtained by observing the in situ soil profile exposed on the excavation walls and by examining the large intact block samples, while others are extracted from the geotechnical site investigation reports (CSTC, 1996) and US geological surveys (Kaye, 1959). Of course, only intact high quality big block samples were utilized in the laboratory to record the macrostructure.

Methods involved consist of imaging with an optical computer scanner and chemical analysis of the elemental composition of the samples by X-ray fluorescence (XRF) spectroscopy. It is surprisingly easy to obtain the true-color image with layers, coloration, and soil macro texture by simply putting a piece of soil block on an optical scanner. In order to examine the difference of chemical constituents between the white-colored inclusions and red-colored matrix as described in Section 3-6, XRF tests were performed using a Spectro X-Lab 2000 energy dispersive spectrometer on both the bulk material and the material carefully picked up from white veins.

6.3.3 Results

Mottling and Soil Color

Figure 6-1 shows the images of typical block samples from different depths obtained by an optical scanner. The most striking features of the old alluvium (especially the UC layer) are its coloring and the reticulated mottling. The UC layer consists mostly of red, or mottled red and white, silty clays, with a somewhat crisscross pattern of white and buff clay veins. Another important visual characteristic is the change of soil color with depth. The UC and MZ samples look very different in color. In places, the shallow UC samples include pure red or bright red soil matrix with occasional dark-red nodules. As depth increases, the soil becomes dark or bright red, brown in the UC layer, and light brown and yellowish brown or gray in the MZ layer.

From the results of mineralogical analysis, the bright red color comes from hematite (α-Fe_2O_3, or Fe-sesquioxide), while light brown to yellowish color from goethite (α-FeOOH, or Fe oxyhydroxide) (Schwertmann and Taylor, 1989). Due to the higher pigmenting power of hematite, the presence of goethite (brown color) in UC may be masked by only a small amount of hematite. In addition, the brown to yellowish color of MZ samples also reflects the absence of hematite (pure red color), which is consistent with the mineralogical analysis.

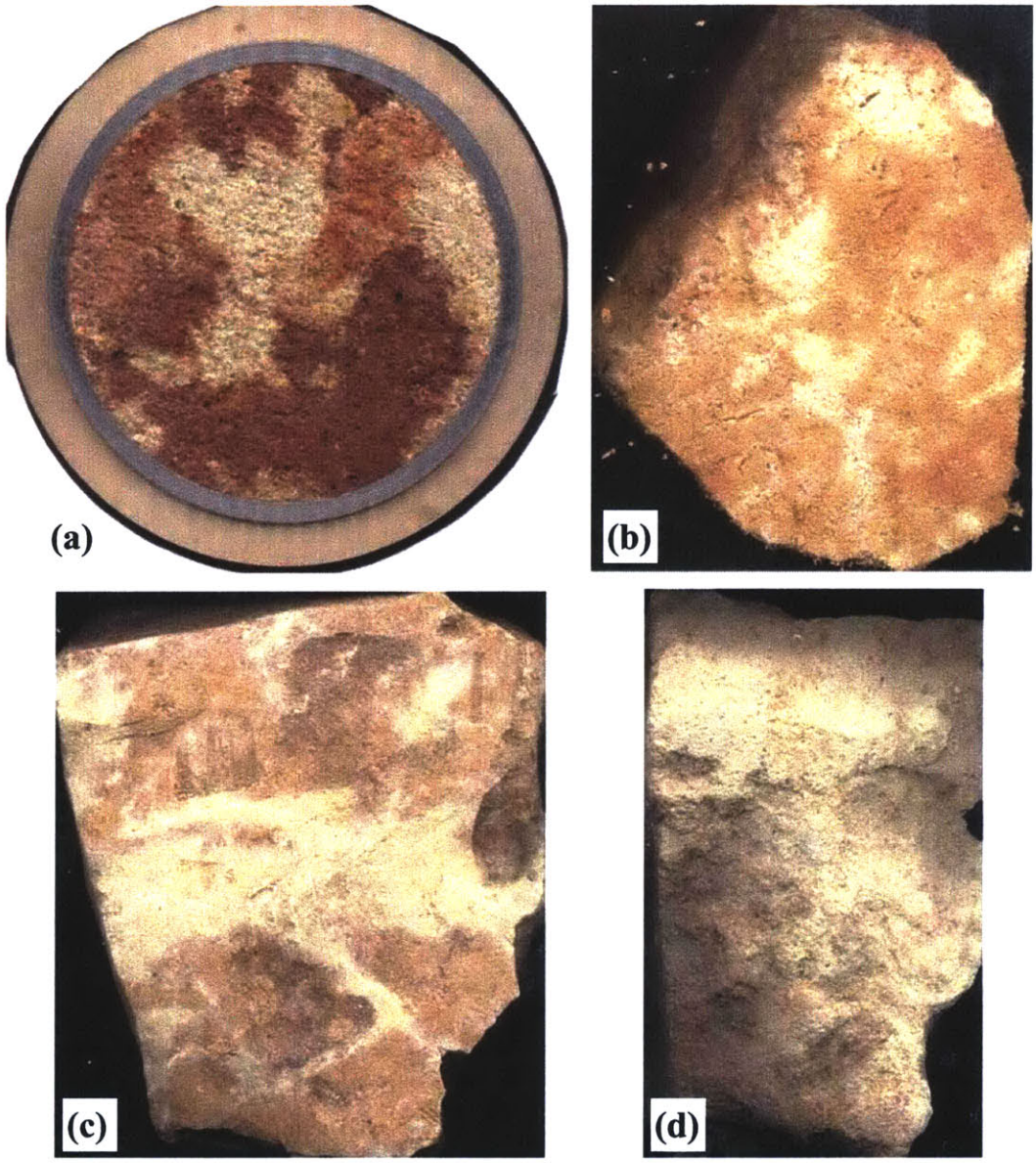

Figure 6-1. Images showing the macrostructure of the old alluvium. (a) and (b), UC; (c) and (d), MZ. Each image is typical of the intact soil block samples taken from the four locations, as shown in Figure 3-6 (see Chapter 3, p.69)

Venation

White veins through both UC and MZ can be seen in Figure 6-1 (a) - (c) and Figure 6-2. These veins have a somewhat crisscross pattern, an inch or less in width. Most veins are more or less circular in cross-section. The central part of a typical vein

consists of the white (light gray when moist) clay, with the buff clay forming an intermediate zone separating the white clay from the red matrix. Notice that Figure 6-2 (a) and (b) are taken from samples in shallow depth where shrinkage may occur, while Figure 6-2 (c) and (d) from a deeper location in UC. In the latter case, it is apparent that roots are located in the center of the white veins.

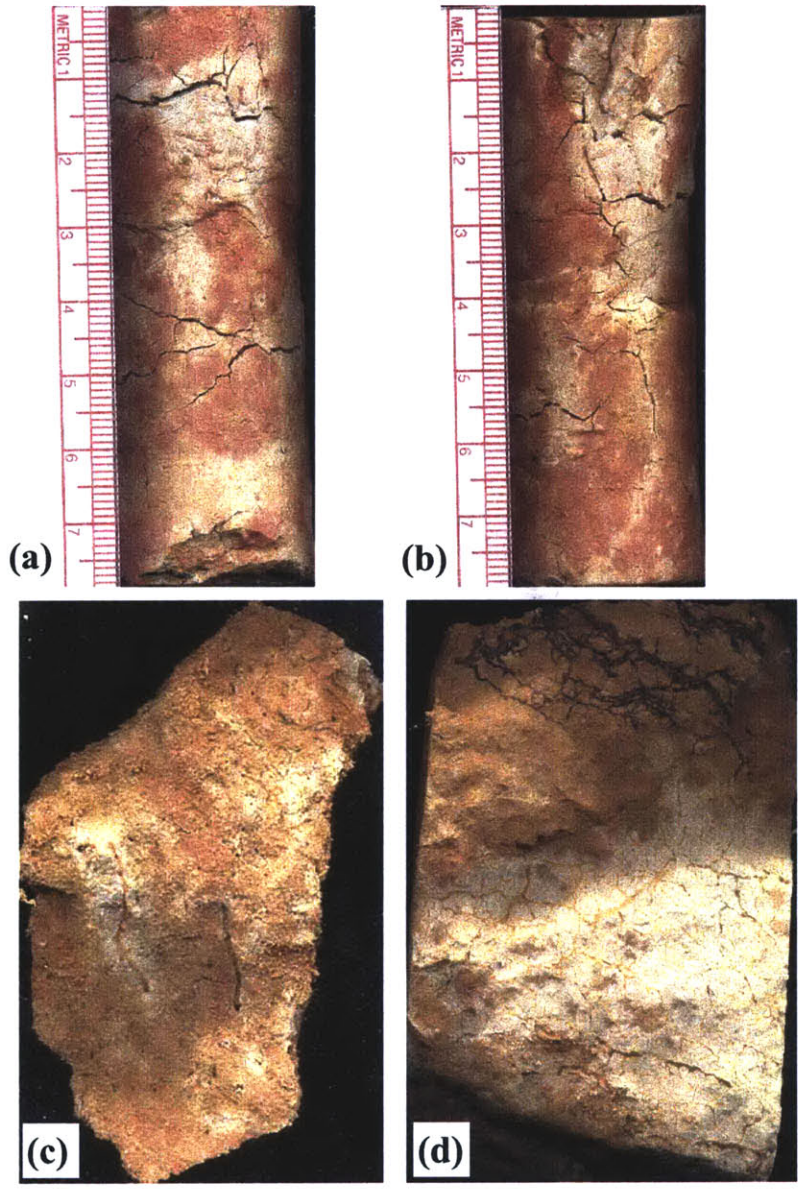

Figure 6-2. Images of white veins in UC caused by localized weathering. (a) and (b) white veins along shrinkage cracks; (c) and (d) white veins along root paths.

Stratification

Stratification is a typical feature of all alluvial deposits. As the old alluvium is formed through a series of coalesced alluvial fans which were slightly dissected by small streams (Kaye, 1959), the non-uniform stratification distributes randomly almost everywhere within the deposit. Occasionally, depositional stratifications and sand pockets and lenses can still be observed on the soil profile. However, due to the long-term alteration caused by tropical weathering, stratification is not apparent in places where intensive weathering has converted sand and gravel grains into clays and tends to homogenize the alluvial deposit.

6.3.4 Discussion

It is clear that the heterogeneity of macrostructure is introduced into the old alluvium through the historical deposition, subsequent soil formation processes, and the environments, e.g., roots from vegetations, dissolution of the limestone bedrock, high evaporation at hot climate. The white venations, the striking features observed in both UC and MZ, are caused by localized weathering due to abundant vegetation (vegetation cover > 75%) (Fookes, 1997) in the San Juan area. Three types of venation have been identified:

(1) White venations along shrinkage cracks (gleying)

This is a kind of localized weathering caused by organic acids released from dead plants and has been observed only in the shallow UC layer (Figure 6-2 (a)-(b)). Under the hot tropical climate, the evaporation rate is high and during dry period, strong desiccation (drying) causes shrinkage cracks near the ground surface. After cracking, subsequent

rainfall brings water flow along the shrinkage cracks and soil swells to fill them. In the mean time, alteration is caused by percolating surface water charged with organic acids (from the decomposed dead plants) which can dissolve and remove iron oxides, leaving white veins in the red soil matrix (Figure 6-2 (a)-(b)). This process is called "gleying" by geologists (Kaye, 1959).

(2) White venations along collapsing cracks

White venations in the MZ layer (Figure 6-1 (c)) are formed through the same mechanism, but may have a different cracking origin. It is possible that cracks in MZ are caused by (1) faulting and collapsing caused by the dissolution of the underlying middle Tertiary limestone; and (2) tectonic movements (Kaye, 1959); and (3) unloading and rebounding of the old alluvium which are caused by weathering, since basically weathering is a process of leaching cations and losing mass, as evidenced by the decreased density of a weathered rock in tropical wet areas.

(3) White venations along root paths

This kind of venation is caused by live root of plants, as the pattern of reticulations not uncommonly suggested (Figure 6-2 (c)-(d)). As described previously in Section 2.3.2, live roots release acids and help dissolve iron oxides, leaving white clays in place.

In summary, the white veins are the results of dissolving and leaching of Fe-oxides from the red soil by acid water, in which H^+ is released by either live roots or the decomposition of dead plants (another example why vegetation promotes rapid weathering and alteration of rock minerals). With Fe-oxides dissolved and removed, the white clay is more plastic than the red and, according to standard hydrometer tests,

contains a greater percentage of material of colloidal dimensions (Kaye, 1959). Furthermore, the result from XRF tests performed on both the bulk UC sample and the white veins further verifies that the white-vein clay is higher in silicon and aluminum and much lower in iron than the red clay (Table 6-1).

Table 6-1. Comparison of the chemical constituents by XRF between the air-dried bulk UC and white vein in UC. All date have a unit of wt.%.

Major elements	Bulk UC	White vein in UC
Na	0.10	0.07
Mg	0.87	0.57
Al	8.54	13.66
Si	22.34	27.01
K	1.15	1.10
Ca	0.16	0.20
Ti	0.5	0.67
Fe	9.24	3.70

The network of venations introduces heterogeneity to the deposit. Moreover, due to its alluvial origin, the non-uniformity is further strengthened by the variations of the historical depositing process. Therefore, it is challenging to characterize the heterogeneity and how to measure the deformation and strength properties in laboratory.

6.4 Microstructure

6.4.1 Introduction

Generally "microstructure" is used to describe the soil structure at the particle size level. The term "microstructure" or simply "structure", which is also adopted in this

thesis, is used to take both soil fabric and its stability into account (Mitchell, 1993, p.190). Therefore, the structure of a soil is determined by both the fabric, including particle associations and arrangements, and interparticle forces (e.g., cementation, aggregation, and bonding).

6.4.2 Materials and Methods

Methods utilized to determine the microstructure of the old alluvium consist of direct visual observations, examination with the aid of an environmental scanning electron microscope (ESEM), and a series of indirect methods, including slaking, cation exchange capacity (CEC) measurements, and selective chemical dissolutions (SCD) accompanied with particle size analysis.

Selective Chemical Dissolution

Selective chemical dissolution (SCD) is one indirect way to identify positively the bonding agents present in the old alluvium, which could be one or more of the following substances: carbonates, silica, organic matter, and Fe or Al oxides. The basic approach of SCD is to treat the disturbed bucket samples with some specific chemicals which selectively dissolve and remove one kind of bonding mineral, if any is present in the sample. Subsequent particle size analysis can measure the change of particle size characteristics and hence gives some quantitative comparison with the initial sample.

The amount of calcium carbonate ($CaCO_3$) equivalent was determined by treating the air-dried samples ground to pass a #325 (<44μm) mesh with 1.0N hydrochloric acid (HCl) solution (SSL, 1996; ASTM D4373, 1997). For complete dissolution of all Fe oxides (e.g., hematite) and oxyhydroxides (e.g., goethite), air-dried samples were treated 4-5 times with 1.0g sodium dithionite in 70-80°C 0.3M sodium citrate solution buffered with 1.0N sodium bicarbonate solution (DCB) (Schwertmann and Taylor, 1989; Smith, 1994; SSL, 1996); Silica and organic matter can be dissolved and removed by treating samples with 0.1N sodium hydroxide (NaOH) solution and 30 wt.% hydrogen peroxide (H_2O_2) solution, respectively (SSL, 1996). Particle size analyses were performed on untreated and all SCD treated samples, following the procedures given by ASTM D422 (ASTM, 1997).

ESEM

Observations on soil microfabric, including particle size and shape, particle associations or arrangements, and pore spaces, were performed under a FEI/Philips XL30 FEG ESEM featured with an energy dispersive X-ray spectrometer (EDXS). Both intact block samples and DCB-treated bucket samples were examined to look at the intact soil structure and to compare the changes of soil structure and micromorphology of clay particles caused by the removal of iron oxides. For all intact samples examined under the ESEM, the surfaces chosen for study should reflect the original fabric of the soil and not the preparation methods. Therefore, fresh surfaces were obtained by breaking a soil block (i.e., fracturing instead of cutting), and using an adhesive tape to peel off the surface several times to remove any loose grains and to expose the original intact fabric. DCB-

treated samples were directly examined wet after washing and concentrating in a centrifuge.

Slaking

Slake tests were performed to examine the stability of intact soil structure in five different solutions:

(1) distilled and de-ionized water;

(2) glycerol solution at a 1:7 glycerol/water volume ratio. This is generally used to solvate and expand smectites for X-ray diffraction analysis (Novich and Martin, 1983; SSL, 1996)

(3) 40g/L sodium hexametaphosphate ($(NaPO_3)_6$) (NaHMP) solution. This is recommended for dispersing soils by ASTM D422 (ASTM, 1997);

(4) DCB solution, which consists of 40ml 0.3M sodium citrate solution, 5ml 1.0M sodium bicarbonate buffer solution, and 1g sodium dithionite (SSL, 1996); and

(5) 1.0N hydrochloric acid (HCl) solution.

After immersion in these solutions, the disintegration response of an intact piece of soil taken from block samples was observed and recorded over time. In addition, slake tests were performed with water on soil pieces taken from block samples which have been air-dried or oven-dried.

Cation Exchange Capacity (CEC)

The determination of CEC was performed on disturbed natural samples with initial water content, and on disturbed samples treated with DCB to remove iron oxides. The procedures of Hendershot and Duquette (1986) and Martin (2000) were followed here. First, samples were washed 4 times with 0.5N barium chloride ($BaCl_2$) solution (pH = 8.0) and shaken in a mechanical shaker to accelerate cation exchange, washed again twice with distilled water, and finally washed twice with 0.0007N $BaCl_2$ solution. The difference of Ba concentrations measured by X-ray fluorescence in samples before and after cation exchange is quoted as the average CEC of clays in the old alluvium.

6.4.3 Results

Preliminary Visual Observations

Without the help of an optical microscope, the UC and MZ samples both appear to comprise aggregates of silt to sand sized particles. Interconnected macropores can be seen in the UC samples. Furthermore, aggregates or grains are not loosely grouped. In fact, intact block samples are all quite stiff and brittle, and the MZ samples are denser and stiffer than UC. There is a significant change in appearance and behavior as a piece of intact soil was pressed and remolded by hand. First, when a small force was applied, a brittle failure occurred, i.e., the soil matrix just broke down into smaller pieces. Continuous pressing and remolding gave a feeling that the soil consists of strong aggregates or grains. At this stage, the soil seems to be granular. However, with further pressure and remolding, the sample becomes sticky and highly plastic, and can be rolled

into small threads, indicating that these much strong grains actually consist of clays. In fact, quantitative mineralogical analysis found that UC and MZ samples contain 62.8% and 38.6% clays and oxides, respectively (Table 5-10). In summary, the intact soil behaves as a stiff and brittle matrix at low stress; with increasing stress and further remolding, it changes from granular grains to cohesive and highly plastic clays.

Observations under ESEM

Intact samples

Particles and their associations. With the high magnification (usually 0.1-1μm scale) provided by ESEM, the clay particles in the micrometer scale should become visible, and the size and shape of clay particles should be observed. However, careful examination of ESEM images taken from intact samples found no distinct boundaries between two particles (Figure 6-3). In fact, although mineralogical analysis has found kaolinites and smectites in this deposit, no individual hexagonal platy kaolinite particles were observed under the ESEM on either the UC or MZ intact samples. On the contrary, all platy-shaped particles seem to be stacked into thick or thin platelets/grains with face to face associations, which look like to be covered by a very thin layer (film) of coating (Figure 6-3). In other words, the outer surface, which includes both basal planes and edges, of thick clay platelets is coated, leaving no clear shapes and edges of individual clay particles. Furthermore, these thick or thin platelets are also connected by bridges with edge to face associations to form big aggregates, i.e., aggregates consist of some or many thick or thin clay platelets, which in turn are made of individual clay particles.

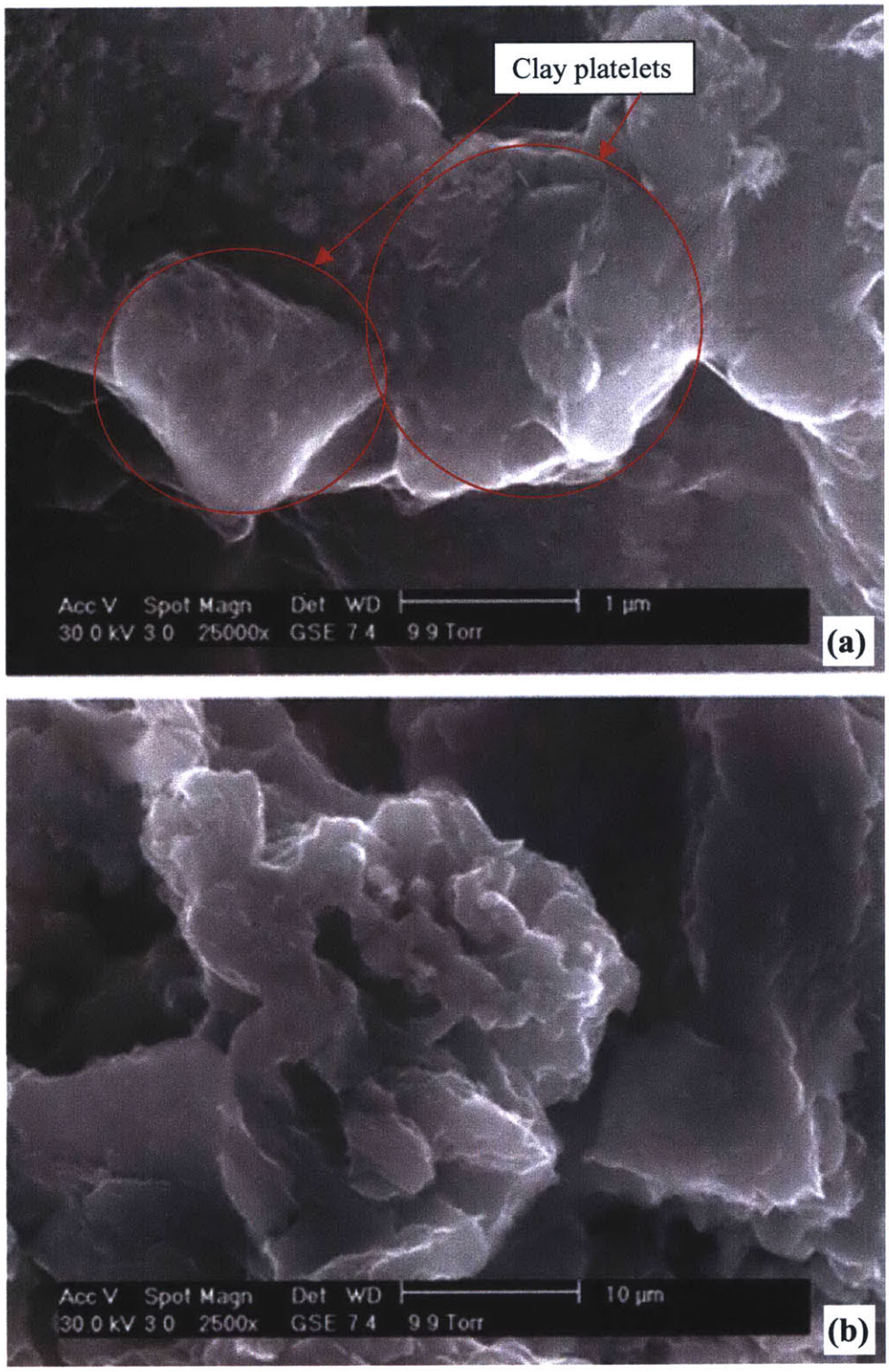

Figure 6-3. ESEM micrographs of intact soil samples. (a) and (b), UC intact block samples.

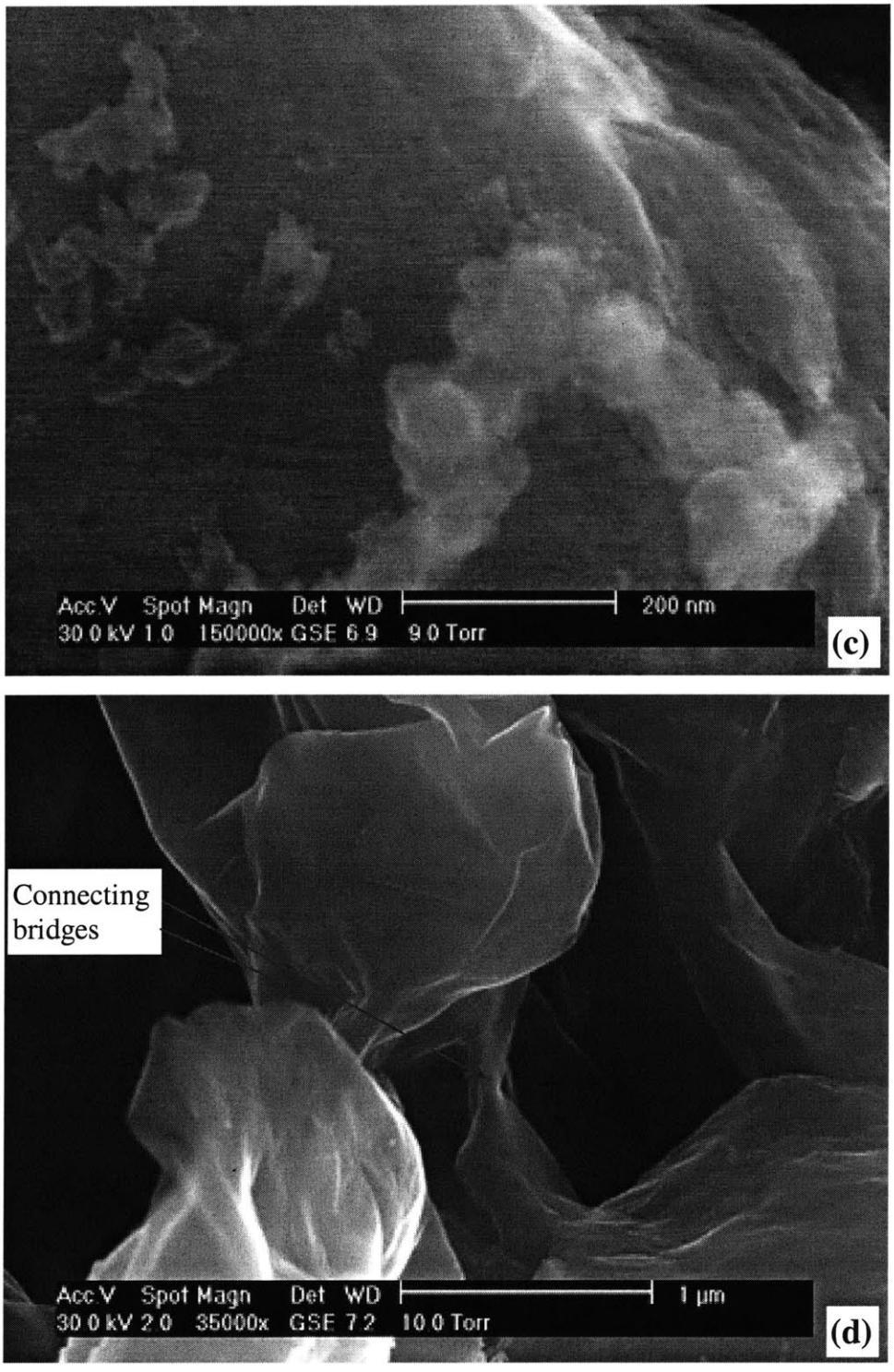

Figure 6-3 (continued). ESEM micrographs of intact soil samples. (c) UC intact sample at higher magnification; (d) MZ intact sample.

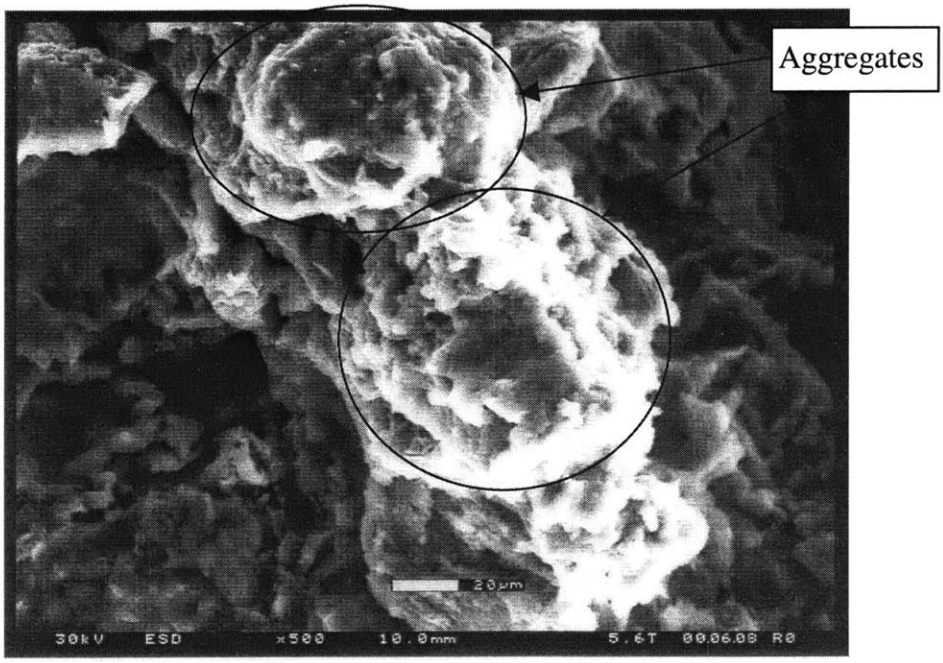

Figure 6-4. ESEM micrograph of intact UC sample showing the aggregates and connections between aggregates.

Aggregates are approximately spherical or semi-spherical in shape with characteristic dimension 80-100µm, and a surface texture resembling a cauliflower (Figure 6-4). Further observations found that aggregates are also connected and bridged together to form a stiff matrix with high porosity and certain stiffness, i.e., aggregates do not exist loosely or as individual separate grains. It appears that the thin layer of coating covers not only the particle groups/platelets, but also connects the platelets to form aggregates, which are further bridged to form a stiff matrix.

Pore Spaces. Since intact samples can be examined in wet mode under ESEM, the characteristics of the pore spaces in soils can be revealed with minimum distortion. For the old alluvium, attention was also paid to the observation of the features of pore space, which include pore size, shape, inter-connectivity, and distribution. As seen in Figure

6-5, the void spaces consist of two different types: inter-aggregate and intra-aggregate pores, i.e., the soil possesses a dual porosity, which is generally observed on many particulate materials with certain aggregation (Gens and Alonso, 1992; Mitchell, 1993; Righi and Meunier, 1995). Careful measurement shows that inter-aggregate pores are nearly 50-100μm, while intra-aggregate pores have sizes less than 10-20μm. Clearly, most inter-aggregate pores are connected to each other (Figure 6-5), resulting in a high in-situ hydraulic conductivity. Since SEM/ESEM can examine the sample at large depth of field (McHardy and Birnie, 1987), the pore shape can be roughly estimated in three dimensions. From Figure 6-5, most pores have irregular shapes and are connected to each other by channels at different directions. However, certain intra-aggregate pores are isolated from other void spaces and exist as individual separate pores, through which water may not flow.

EDXS analysis. Qualitative elemental analysis was performed by EDXS under ESEM on surfaces of aggregates and the bridge connections. It seems Fe exists everywhere (Figure 6-6 (a)). Since one of the clay minerals, nontronite contains Fe in its structure, and the penetration depth of the electron beam into the sample can be several micrometers (McHardy and Birnie, 1987), the measured Fe by EDXS could be from either Fe-oxides or nontronite. Therefore, a conclusion that Fe oxides act as coatings everywhere cannot be drawn at this time. However, a significant amount of Fe was also observed even on the surface of a sand (probably feldspar) particle (Figure 6-6 (b)), which was further verified by observing red grains with sand size during wet sieving analysis. Therefore, Fe-oxides precipitate as coatings over both sand particles and clay aggregates.

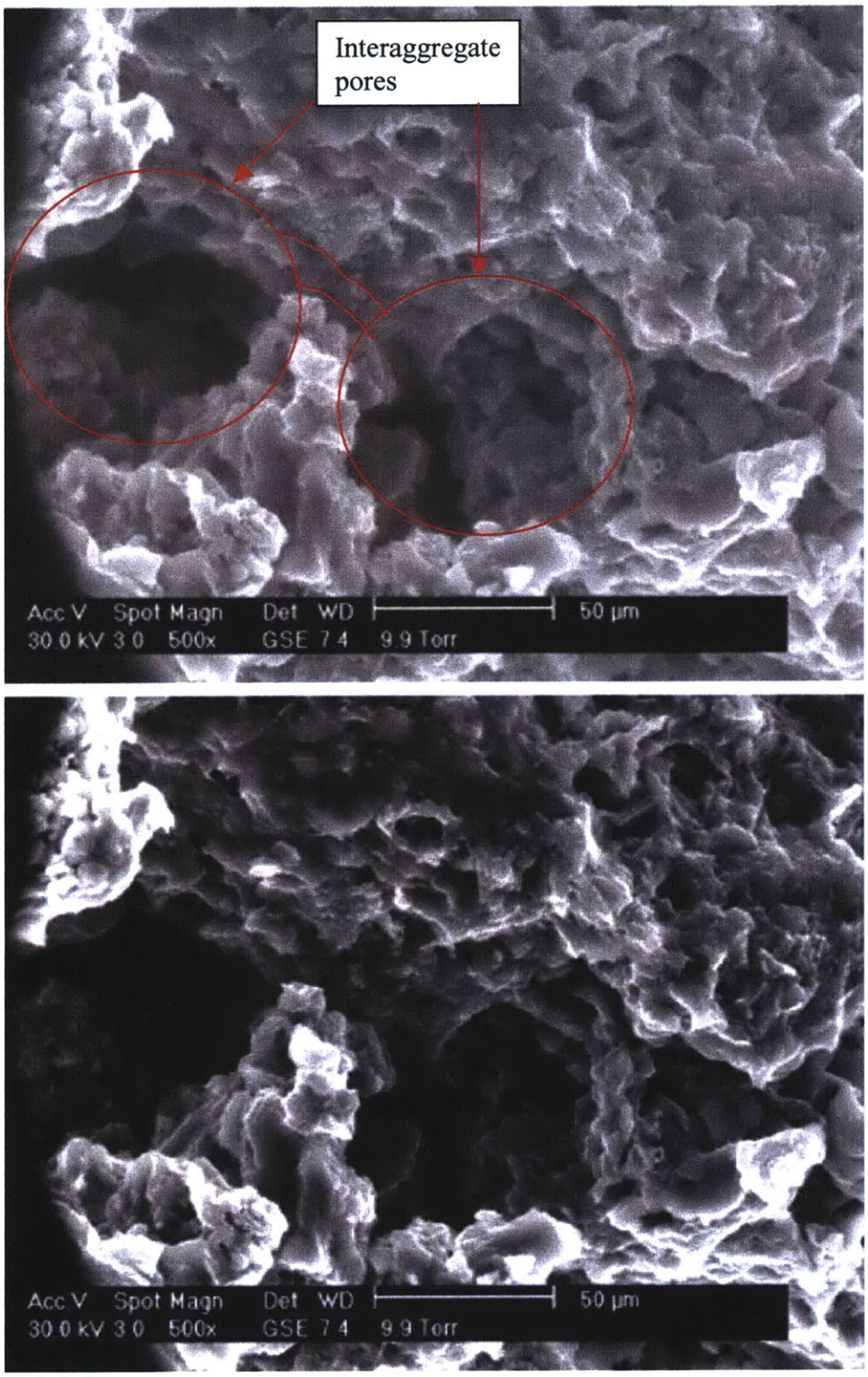

Figure 6-5. ESEM micrographs showing the features of void space with inter-aggregate pores and intra-aggregate pores.

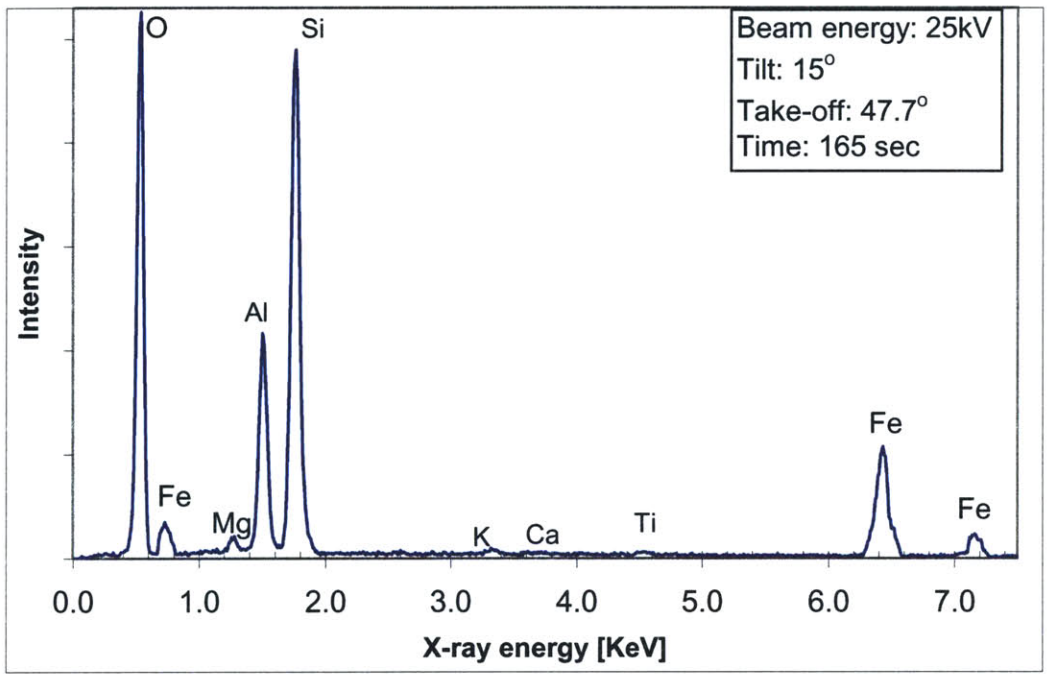

(a)

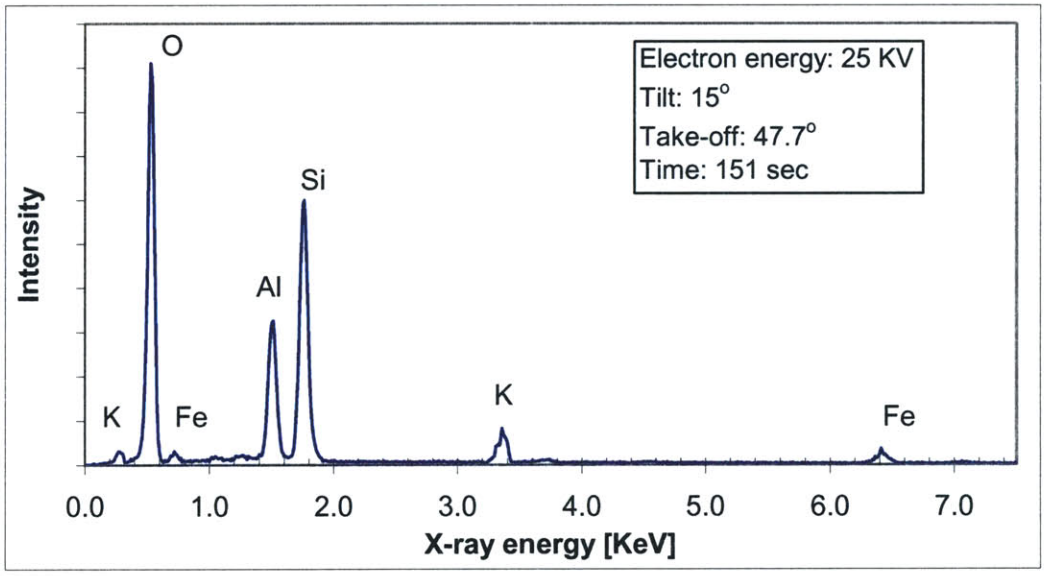

(b)

Figure 6-6. Spectra of EDXS analyses performed on (a) surface of a clay platelet; and (b) a sand particle (possibly feldspar) in intact UC sample.

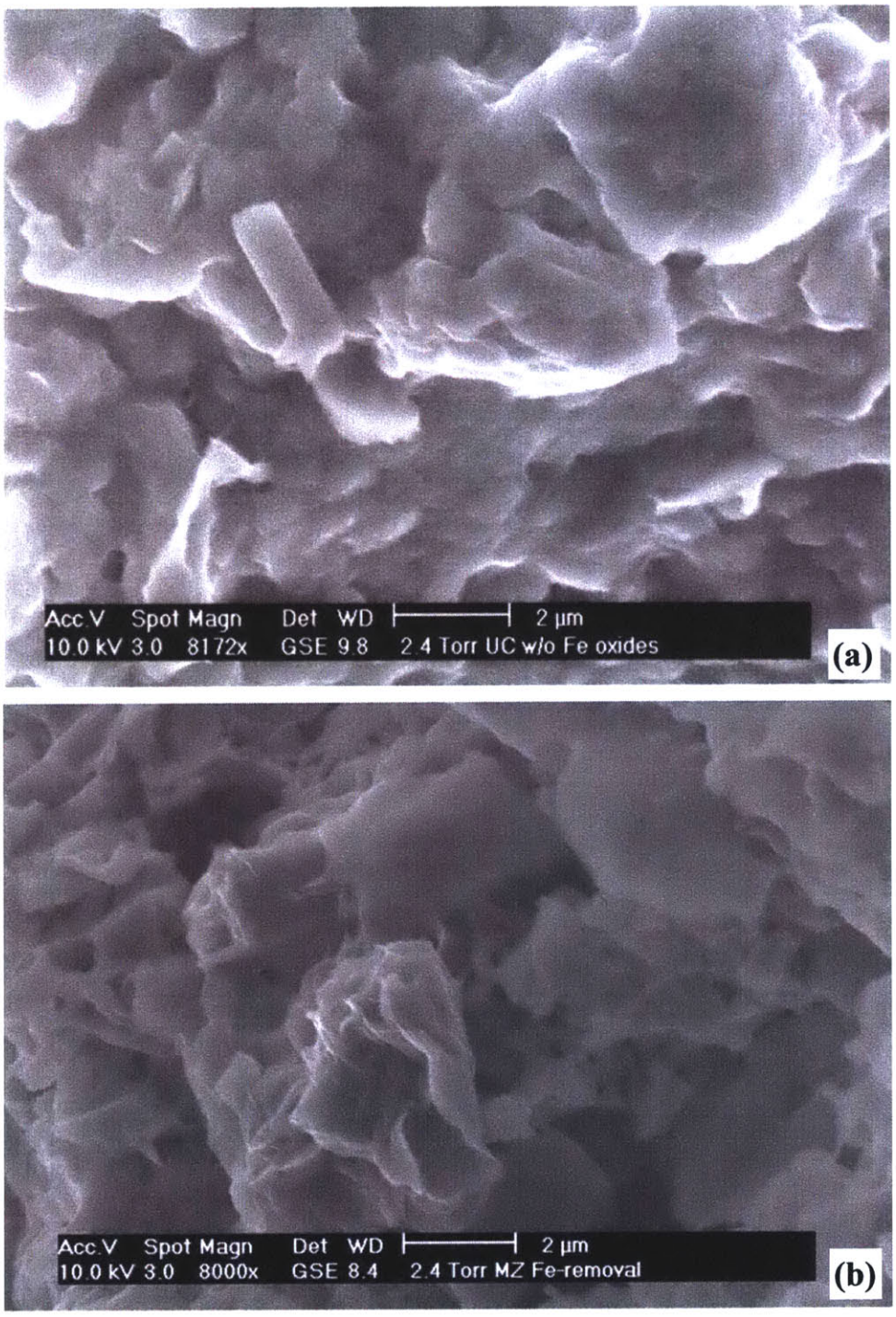

Figure 6-7. ESEM micrographs of DCB-treated samples. (a) UC; (b) MZ.

DCB-treated samples

Observations on the DCB-treated samples are useful for studying the fully dispersed and disintegrated individual clay particles. Figure 6-7 shows that clear particle shapes and boundaries are visible in DCB-treated samples. Particles of kaolinite exist as near hexagonal and flat plates with irregular shapes, while smectites are present as delicately thin and curved flakes (Borchardt, 1989). The imperfectness of the hexagonal shape reflects the low crystallinity of kaolinites. There are no thin coatings or connections in the ESEM micrographs on the dispersed samples.

Identification of Bonding Agents

Based on the above observations and examinations, it is quite clear that the intact soil of the old alluvium has cementation and aggregation in its structure. However, the bonding agents (causing either cementation or aggregation) are unknown. Table 6-2 lists the results of particle size analyses performed on the bucket samples which have been treated by various SCD techniques described above. The results show little difference in size fractions for the sample dispersed using NaHMP, the sample with organic matter dissolved, and the sample with silica dissolved (with clay fractions approximately 38%). However, the removal of Fe-oxides by DCB treatment increases the clay fraction by more than 15%. Notice that the clay fraction of the sample with no dispersant is much smaller than those prepared with dispersant NaHMP. Nevertheless, the removal of Fe-oxides significantly changes the characteristics of grain size distribution. This indicates that the removal of Fe oxides makes the soil particles more dispersed. Therefore, it can conclude that the cementing and aggregation agents are Fe oxides.

Table 6-2 Effect of various selective chemical dissolutions on the particle size distribution of UC sample.

Dissolution/dispersion	Clay fraction (wt.%)	Silt fraction (wt.%)	Sand fraction (wt.%)
No dispersion	18.8	63.7	17.5
NaHMP* only	38.1	49.0	12.9
Organic matter & NaHMP	37.5	50.5	12.0
Silica & NaHMP	39.7	46.7	13.6
Fe-oxides & NaHMP	54.8	34.8	10.4

* NaHMP = sodium hexametaphosphate.

It is also worthwhile to discuss the possible cementing agents in tropical residual soils from the point of view of the tropical weathering and soil formation mechanisms. Very small concentration of carbonates should be expected in tropical zones because of their low weathering resistance and quick dissolution in tropical wet climate. In fact, both UC and MZ samples contain no detectable carbonates (Table 3-2). On the other hand, soils of the warmer climatic zones generally have low organic matter, despite the large quantity of plant material produced and retuned to the soil. This is attributed to the high activity of microorganisms in the warmer temperatures, i.e., the transformation of organic molecules by microbes is rapid (Righi and Meunier, 1995). It is well known that goethite is the most widespread iron oxide in soils and mineral weathering environments. In warmer areas, it is most frequently associated with hematite; this association is a very common feature of the majority of soils of the tropical and subtropical regions (Schwertmann and Taylor, 1989). Therefore, it is not a surprise to find Fe oxides as

cementing agents in the old alluvium, which has been weathered under the tropical marine climate of Puerto Rico.

Slake Tests

The observed slaking responses of intact UC soil blocks in five different solutions are summarized in Table 6-3. Figure 6-8 also shows the final sample conditions after immersion unconfined in these solutions for 2 days. Although UC sample is unsaturated and contains significant amount of smectites, the intact soil block keeps its structure stable in water and glycerol solution for weeks, i.e., no dispersion slaking or swelling slaking are observed. If the smectites in the sample are fully hydrated, immersion in water will not cause noticeable swelling of smectites. However, access to glycerol should be able to expand the smectites and hence, destroy the structure, assuming glycerol can enter the interlayer space. The stable structure of the intact sample in water and glycerol solution indicates that water or glycerol cannot enter the interlayer space of smectites, which confirms that smectites are covered by a layer of Fe-oxides coating.

Immersion of the sample in DCB solution doesn't cause total disintegration of the block, but does cause it to split into smaller pieces. The most striking reaction is the change in the soil color starting from red or brown to dark gray, confirming the dissolution of Fe oxides. Although the color of the solution becomes yellow, it is still clear and transparent, which means that no dispersion slaking and swelling slaking occurred.

Table 6-3. Slaking responses of intact soil blocks of UC layer in five different solutions.

Solution	Slaking response	Final sample condition	Solution change
Water	No reaction	Same as intact	No change
Glycerol	No reaction	Same as intact	No change
DCB	Very slow cracking; but no swelling; no dispersion	Red color disappeared; sample become dark gray; fractured into big pieces	Become yellow, but still transparent
NaHMP	Quick self-peeling off; observable swelling; slight dispersion	Totally disintegrated into large aggregates; huge volume increasing	A little bit suspension; semi-transparent
HCl	Slow microcracking; but no swelling; no dispersion	Keep intact shape, but with microcracks	Light yellowish; still transparent

It is quite interesting to discuss the reaction processes of slaking in NaHMP solution. After immersion, it was observed that big and thick platy clumps peel off the surface immediately and settle down to the base with noticeable volume increase and slightly dispersion of very fine brown particles into suspension, changing the solution into light brown and semi-transparent. After two days, the block totally disintegrates into smaller pieces with the size of coarse sands. However, no significant amount of fines (e.g., clays) are found in the sedimented piles of grains. This slaking response confirms that the intact structure of the old alluvium which is stable in both water and glycerol solution can be partially dispersed by NaHMP. This kind of structure dispersible by dispersant NaHMP is related to aggregation. As the final dispersed coarse grains suggested, the old alluvium still possesses cementation after slaking in NaHMP solution.

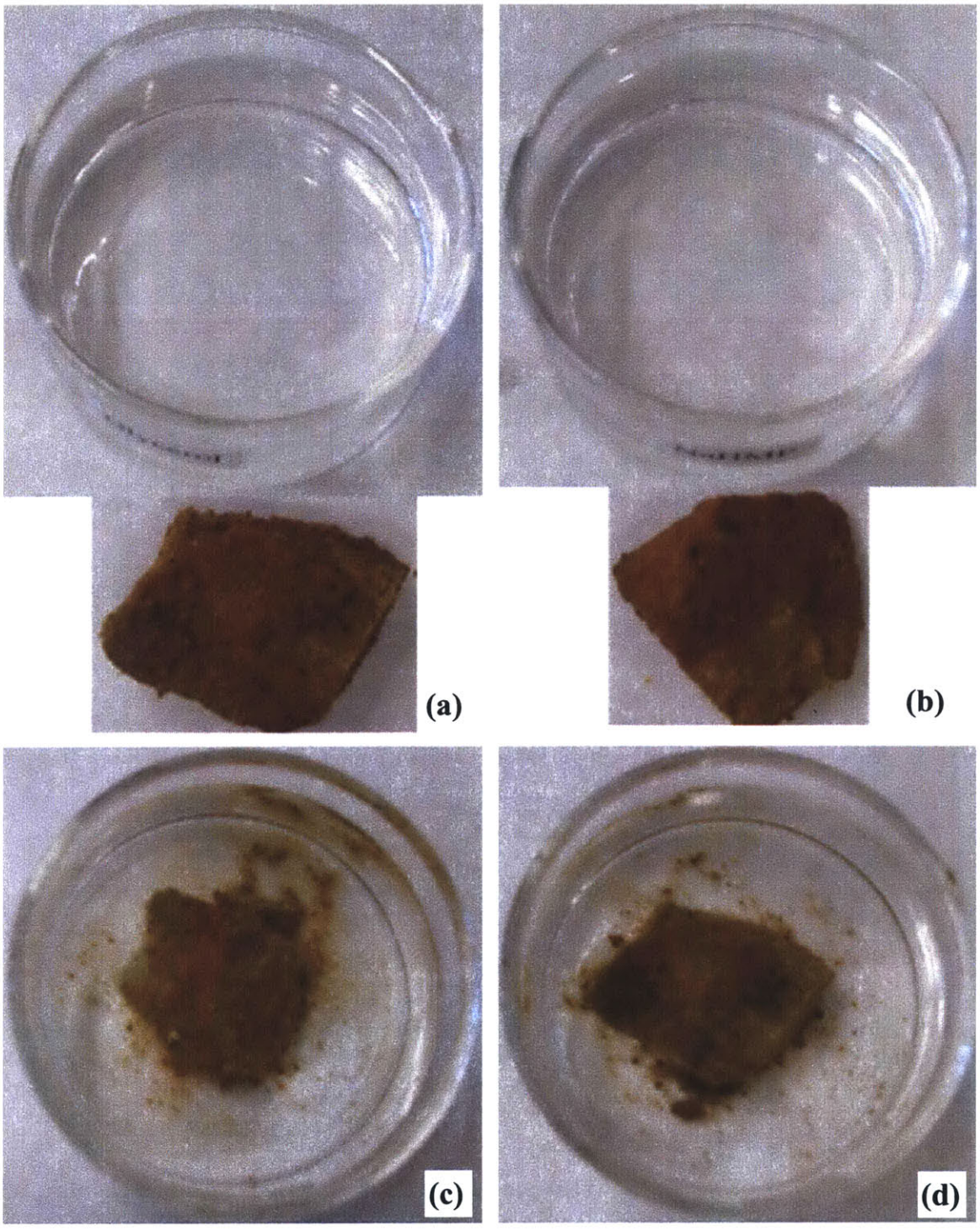

Figure 6-8. Slake tests performed on 5 different solutions. (a) and (b), initial intact soil pieces before immersion in glycerol and NaHMP solutions, respectively; (c) and (d), the soil state after immersion in water and glycerol solution for 2 days, respectively.

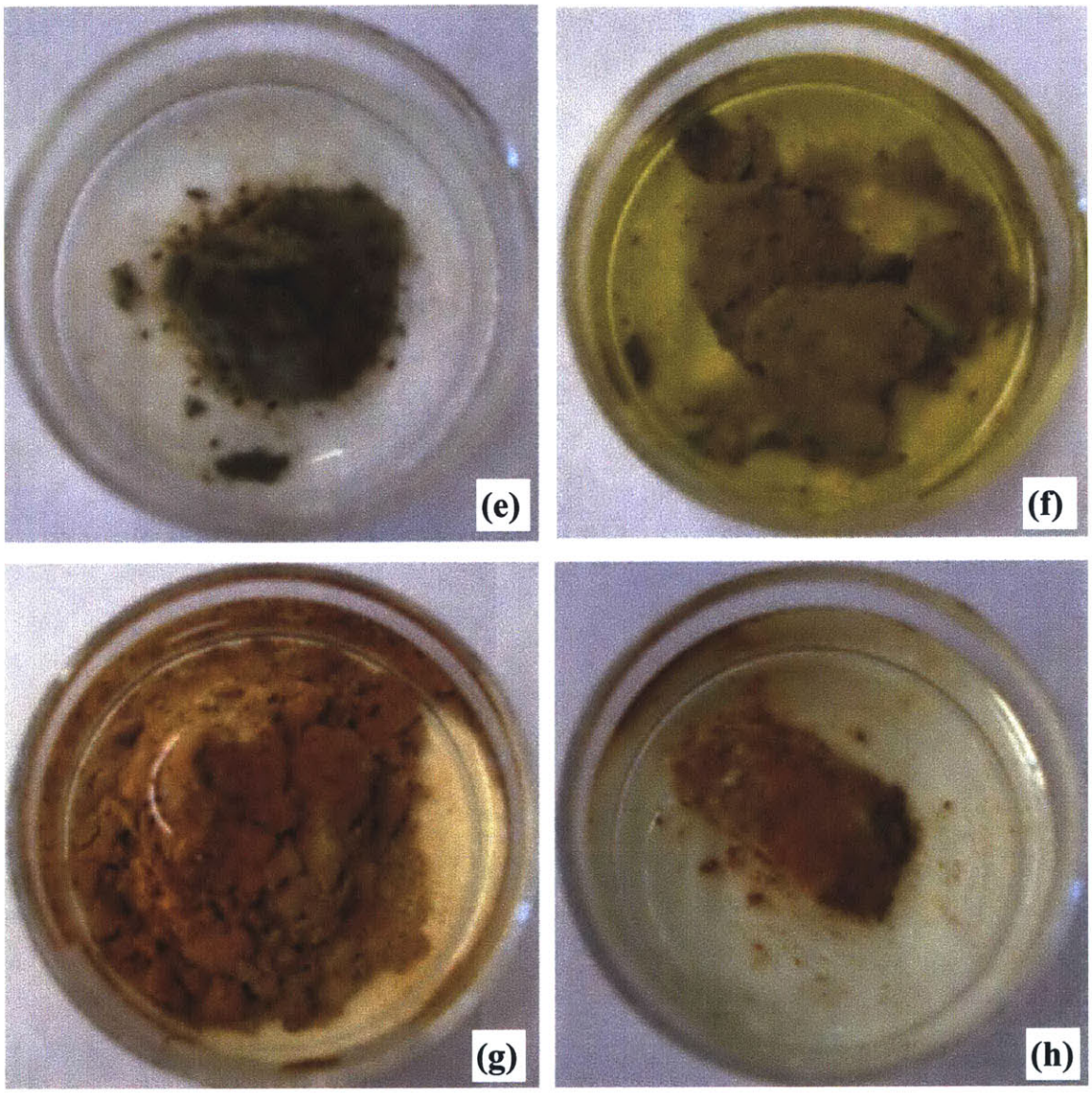

Figure 6-8 (continued). Slake tests performed on 5 different solutions. (e) and (f), the soil state after immersion in DCB solution for 1 and 7 days, respectively; (g), the slaked state of soil after immersion in NaHMP for 2 days; and (h), the soil state after immersion in HCl solution for 2 days.

The reaction of intact soil in HCl solution is very slow. After immersion for two days, only a few visible small cracks occurred, but the soil block remains stable. The solution became light yellow in color, indicating a very slow dissolution of Fe-oxides by acid.

One piece of sample was slaked again in glycerol solution after slaking in DCB solution for two days. This material swelled and peeled apart. Many fine particles (clay sized) were dispersed into solution and hence, the solution becomes cloudy. After one day, a stable and intact inner core was left with fresh red or brown outer surface exposed, indicating that the DCB solution dissolves Fe oxides at the outer surface while the inner core of the sample remains intact. This explains why an intact piece of soil does not disintegrate completely in DCB solution. However, the question why the outer shell of the soil piece does not disperse and swell in DCB solution after Fe oxides are dissolved by DCB still remains. One possible reason might be that the salt concentration in the DCB solution is sufficiently high to prevent swelling of the smectites.

CEC

Of all minerals present in the old alluvium, kaolinite, nontronite, illite, and montmorillonite have the ability to exchange cations. Iron oxides have a zero CEC (SSL, 1996). Since the total clay fraction in the bulk samples is known (Table 5-10), the CECs measured on total bulk samples which include sands were converted to milliequivalent charge per 100g of clays. Table 6-4 lists the CECs measured on natural and DCB-treated disturbed bulk samples. It is obvious that the CECs measured on natural samples are much smaller than these of DCB-treated samples. For example, after the removal of Fe-oxides, CEC of UC soil is almost doubled (from 29.13 to 52.12 meg/100g). Furthermore, even though UC sample has higher concentrations of kaolinite and nontronite than MZ, the CEC of natural UC is smaller than MZ, which is not possible if all clays are

dispersed. This is attributed to the higher Fe-oxides content in natural UC which means more clay particles or clay platelets in UC are covered. All these results indicate that the clays in the natural samples are covered or coated by iron oxides and hence the cation exchange sites of clays are not exposed to exchangeable cations in solution.

Table 6-4. Cation exchange capacities of natural and DCB-treated disturbed samples.

Samples	CEC (meq/100g clay)	Notes
Natural UC	29.13	With Fe-oxides cementation
DCB-treated UC	52.12	With Fe-oxides removed
Natural MZ	35.58	With Fe-oxides cementation
DCB-treated MZ	45.34	With Fe-oxides removed

6.4.4 Discussion

Based on the above discussions, it can be concluded that iron oxides act as coatings over clay platelets and bindings between clay aggregates. Indirect experimental approaches including slaking and CEC measurement show that intact soil is quite stable after immersion in water and glycerol and has smaller CECs than DCB-treated samples, indicating that the cation exchange sites and smectite interlayer spaces of intact soil are not available for water or exchangeable cations. The results confirm that smectites and kaolinites are covered or coated by iron oxides and hence the physical and chemical properties of clays become inactive. The higher concentrations of Fe-oxides, the more coverage of coating surfaces or cementation between surfaces of clay particles or platelets.

The slaking of an intact piece of soil in NaHMP solution into big peels or pieces but not into dispersed fine particles, suggests that the sample contains both cementation and aggregation, because only aggregation can be dispersed by NaHMP through edge or surface charge reversal and those big peels or pieces are still cemented by Fe oxides. In fact, Righi & Meunier (1995) pointed out that hematite doesn't coat or cement but groups together with itself or clays as aggregates, and probably goethite is the main oxide acting as coatings and cementing agents. Further discussion on cementation and aggregation will be discussed in Section 6.5.

The possible formation process of the current soil structure in the old alluvium should also be discussed. Clay minerals are first formed from the weathering of primary rocks, such as kaolinite from feldspar and smectite from muscovite. Then Fe oxides precipitate through crystal growth from solutions, and cover surfaces of clay particles or clay platelets and in the voids between aggregates, and hence act as coatings over platelets and connections between aggregates, respectively.

The special mineralogical composition and soil microstructure of the old alluvium give a complex macroscopic response to different stress levels and remolding. First, cementation and aggregation cause the soil to behave stiff and brittle at low stress, although the soil contains up to 60% clay fraction. With increasing stress and the degree of remolding or destructuring, it alters from a granular and frictional material into behavior typical of a highly plastic and cohesive clay.

The special microstructure gives many challenges to geotechnical engineers. These visible and sand-like aggregates often give a wrong impression for identification and classification. The special mineralogical composition (e.g., smectites and Fe oxides) and soil microstructure will cause a series of difficulties in engineering practice, including identification and classification, undisturbed sampling, and the correct measurement and interpretation of engineering properties.

6.5 Particle Size Analysis

6.5.1 Introduction

As pointed out by Lambe and Whitman (1969), "soil is inherently a particulate system". To quantitatively describe a soil – an assemblage of particles, particle size distribution is a parameter which is always measured for the purpose of soil classification and identification and of building certain empirical correlations linking particle size characteristics to engineering properties. In fact, ASTM D422 is the standard test method to perform particle size analysis for common sedimentary soils. This routine technique has the following specifications:

- Remolding energy: 1 min stirring in a specially designed blender;
- Dispersing agent: sodium hexametaphosphate ($(NaPO_3)_6$);
- Amount of dispersant: 5 g per 1 liter soil suspension, which is equivalent to 0.5 N in the final soil suspension;
- Initial sample condition: air-dried;
- Amount of sample: ~50 g dry solid mass.

However, a particle can be regarded as any coherent body bounded by a clearly recognizable surface. Particles may consist of one kind of material with uniform properties, or of smaller particles bonded together in some way (Loveland and Whalley, 1991). In the latter case, the particle size distribution may change with different degrees of disturbance or remolding. For example, if a soil is cemented by carbonate, the original material must be properly treated with acid to dissolve the bond in order to measure the true or intrinsic particle size distribution. In this case, different pre-processing or pretreatment techniques may result in variable particle size distributions. Therefore, particle size distribution of a soil can reflects the degree of destructuring or remolding, and the variation of particle size distribution can be an indicator for the alteration of initial intact soil structure.

In the literature, it has been reported that the particle size distributions of most residual soils are variable with different processing methods, consisting of different remolding energy or time, the type of dispersant used, the amount of dispersant, and the drying condition (Fookes, 1997). This section describes the particle size analysis of the old alluvium. The results can be used for the following purposes:

- Measuring the variability of particle size distribution;
- Evaluating different dispersants recommended in literature;
- Finding the best processing technique to measure the intrinsic particle size distribution;
- Providing recommendations for PSA in practice.

6.5.2 Materials and Methods

The materials used in all particle size analyses are the disturbed bucket samples, including both the UC and MZ. Following the specifications of ASTM D422, all tests use samples equivalent to 50g oven-dried solid mass. However, in order to investigate the variations of PSD, 4 different paths were designed by modifying the standard ASTMD422 procedures:

- Remolding energy: within this set of tests, the only parameter changed is the remolding energy, including two different stirring methods and various amounts of time. The change of remolding energy is achieved by different stirring time in the blender which is designated by ASTM D422, i.e., 0min, 1min, 5min, 15min, 20min. In addition, a mechanical shaker is also used to see the effect of different energy application modes. Other variables within this set of tests are the same as specified by ASTM, i.e., using 0.05N $(NaPO_3)_6$ dispersant and natural wet samples.
- Types of dispersant: the following dispersants suggested in literature have been used:
    - NaHMP specified by ASTM D422.
    - Polyphosphate ions, NaOH and NaF suggested by van Olphen (1987, p.210).
    - Na pyrophosphate ($Na_4P_2O_7$) is favored by Moore & Reynolds (1997, p.211).

- Trisodium phosphate (Na_3PO_4) is suggested by Fookes (1997) "as an occasional alternative dispersant".

All tests within this set used natural wet samples, 0.05N concentration in the final soil suspensions, and 1 min blending.

- Amount of dispersant: the concentration of dispersant in the final 1 liter soil suspension includes 0.0, 0.025, 0.05, 0.075, 0.1N.
- Sample drying condition: wet, air-dried, and oven-dried samples have been used.

After the hydrometer measurement, wet sieving was performed on the soil suspensions to measure the coarse fractions.

6.5.3 Results of Particle Size Analysis

The results of particle size analyses will be first presented individually within each set to clearly observe the effect of one variable. It is organized according to each of the variables listed in the previous section. Then comparisons will be made among different sets of measurements.

Effects of Remolding Energy

Within this set of tests, the only parameter changed is the remolding energy. Table 6-5 summarizes the results of particle size fractions, while Figure 6-9 plots the changes of different size fractions with the remolding time.

As seen from Figure 6-9, for both UC and MZ, clay fractions increase significantly with blending time, i.e., with increased remolding energy, while a large

reduction of silt fraction is observed, showing that the increasing of clay fractions is from the breakdown of silt-sized particles. It is interesting to notice only small decreases in the sand-sized fractions. The sand fraction in UC is almost constant, while MZ sand fraction decreases. Therefore, it can be concluded that the size of aggregates is mainly in the silt range and the bonds between these aggregates can be destroyed by increasing the remolding energy. Recall that the ESEM observations (see Section 6.4) did suggest the typical aggregate sizes in the range of 50-100μm, which agrees well with these results.

Table 6-5 Effect of remolding energy on particle size distribution of the old alluvium.

Sample	Remolding Energy	Test#	Clay [%]	Silt [%]	Sand [%]
UC	No energy	B2	40	46.2	13.8
	1min blending	P1	43.5	43.1	13.4
	1min blending	A1	44		
	1min blending	A2	44.5		
	5min blending	P17	53	33.5	13.5
	15hr shaking	P23	56.5	29.4	14.1
	15min blending	A7	62		
	20min blending	P19	61.5	27.2	11.3
MZ	No energy	B3	8.5	45.5	46
	1min blending	P2	12.5	41.7	45.8
	1min blending	A3	13	42.3	44.7
	1min blending	A4	14	42.1	43.9
	5min blending	P18	18	40	42
	15hr shaking	P24	35	24.3	40.7
	20min blending	P20	27	34.2	38.8

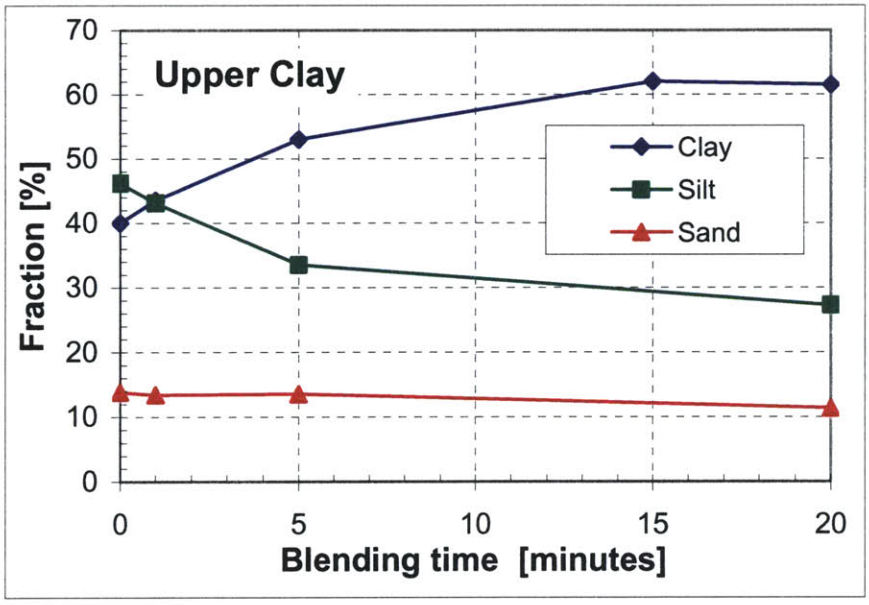

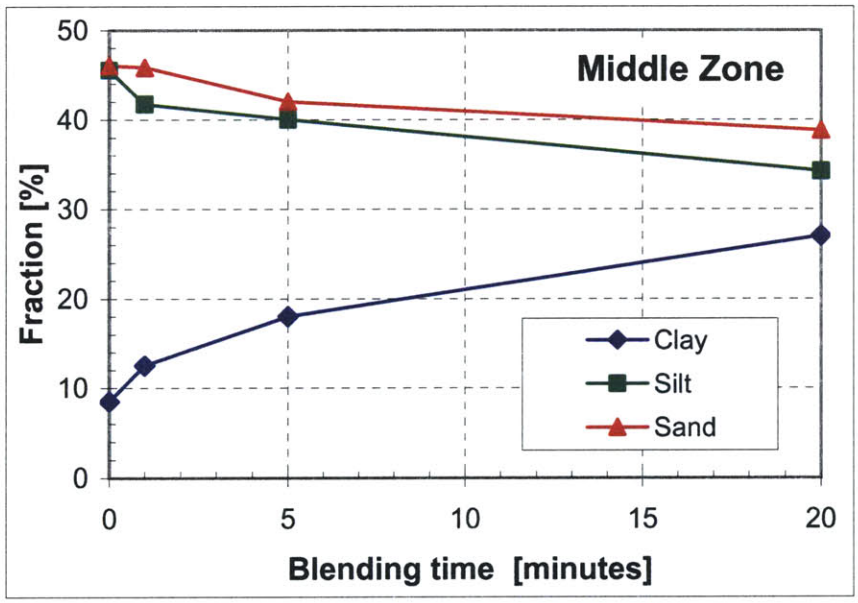

Figure 6-9. Effect of stirring time in the blender on the particle size distributions.

The next question of interest is to establish limits on the minimum energy required to breakdown all aggregates, and the maximum amount of clay fraction which can be obtained by increasing the remolding energy. The results in Figure 6-9 show no change in clay fraction of the UC obtained by 15min and 20min blending. It seems that

the remolding energy applied by 15min blending should be enough to destroy all aggregates in UC, then further increasing of remolding energy (e.g., 20min blending) will not contribute to the increasing of clay fraction. Therefore, it is possible to conclude that for this old alluvium, the intrinsic particle size distribution can be achieved by 20min of blending.

Table 6-6. Effect of different types of dispersants on the particle size distribution of the old alluvium.

Sample	Test#	Dispersant	Clay [%]	Silt [%]	Sand [%]
UC	P1	$(NaPO_3)_6$	43.5	43.1	13.4
	P5	NaOH	0	80.3	19.7
	P7	NaF	2	81.9	16.1
	P9	$Na_4P_2O_7$	42	44.4	13.6
	P11	Na_3PO_4	2	75.6	22.4
MZ	P2	$(NaPO_3)_6$	9.5	40.7	46.8
	P6	NaOH	0	32.9	67.1
	P8	NaF	0	53.4	46.6
	P10	$Na_4P_2O_7$	9.5	44	47
	P12	Na_3PO_4	0	47.5	52.5

Effects of Dispersant Type

Table 6-6 and Figure 6-10 shows the results of PSA obtained by using different types of dispersants suggested in the literature. All tests used 1 min blending energy, so the bonds were not fully broken. A zero percent of clay fraction simply means that no clay fraction has been measured. In fact, in these cases, unstable soil dispersions (i.e., clay particles are flocculated again) have been observed during hydrometer measurements. Nevertheless, for UC, the unstable clay suspensions give very high silt

fractions using NaOH, NaF, and Na_3PO_4 dispersants. The results of both UC and MZ consistently show that flocculates form in the silt size and these three sodium salts are not effective dispersing agents for the old alluvium.

It is interesting that $(NaPO_3)_6$ and $Na_4P_2O_7$ give almost the same results for both UC and MZ, which have highest clay fractions. Therefore, the selection of $(NaPO_3)_6$ by ASTM D422 does have a sound base. However, $Na_4P_2O_7$ can be used as an alternative effective dispersant for the old alluvium.

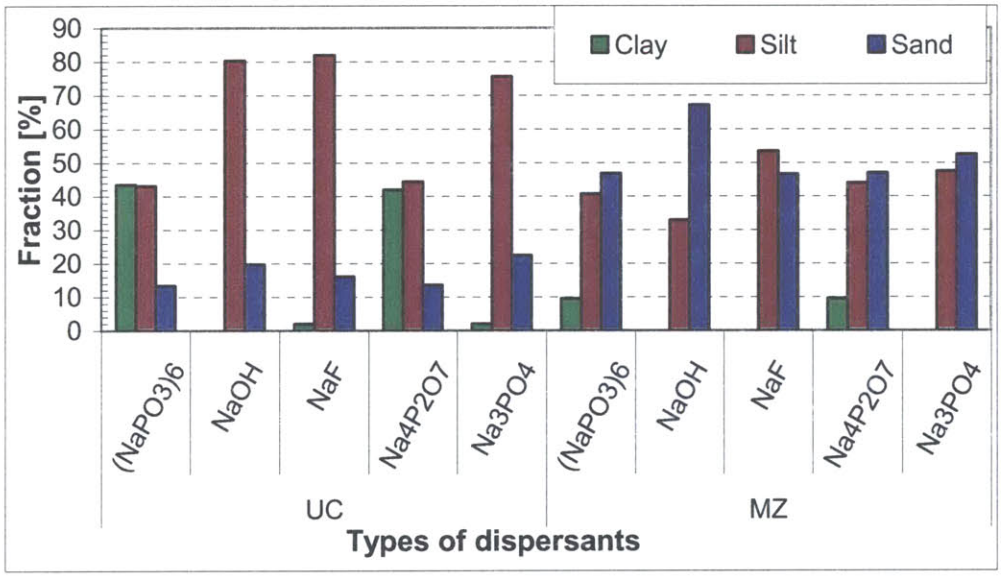

Figure 6-10. Effect of the types of dispersants on the particle size distributions.

Effects of the Amount of Dispersant

Based on the above discussion, $(NaPO_3)_6$ is one of the most effective dispersants for the old alluvium. Therefore, $(NaPO_3)_6$ is chosen to investigate the effect of the amount of dispersant on the particle size distributions. The results of this set of tests

(Table 6-7 and Figure 6-11) show no significant change in particle fractions for dispersants with concentrations above 0.025N. This especially holds true for MZ. In fact, even the amount of dispersant is increased, only ~10% clays are obtained for MZ.

However, without adding dispersant, the clay suspension is not a stable colloidal dispersion, as reflected by the result obtained from zero percent of dispersant concentration in UC. Therefore, even though mechanical energy (1min blending) has destroyed the bonds, the subsequent suspension in water without dispersant at low pH causes flocculation again since the electrical attraction forces between the negative charged clay faces and the positively charged surfaces of Fe-oxides have not been eliminated. This further confirms that chemical dispersion (i.e., adding dispersants to the suspension) is required in order to obtain a stable dispersion of the old alluvium.

Table 6-7. Effect of the amount of dispersant on the particle size distribution of the old alluvium.

Sample	Test#	Dispersant concentration	Remolding Energy	Clay [%]	Silt [%]	Sand [%]
UC	C3	0.0	3hr shaking	5	68.3	26.7
	P15	0.025N	1min blending	39	43.6	17.4
	P1	0.05N		43.5	43.1	13.4
	P13	0.075N		44	41.8	14.2
	P3	0.1N		45	40.8	14.2
MZ	P16	0.025N	1min blending	9	44.3	46.7
	P2	0.05N		9.5	40.7	46.8
	P14	0.075		11	42.7	46.3
	P4	0.10		8	43.8	48.2

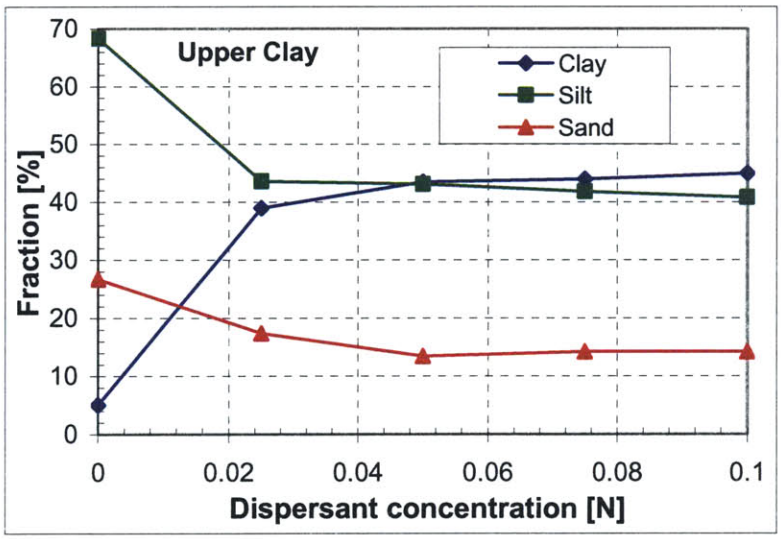

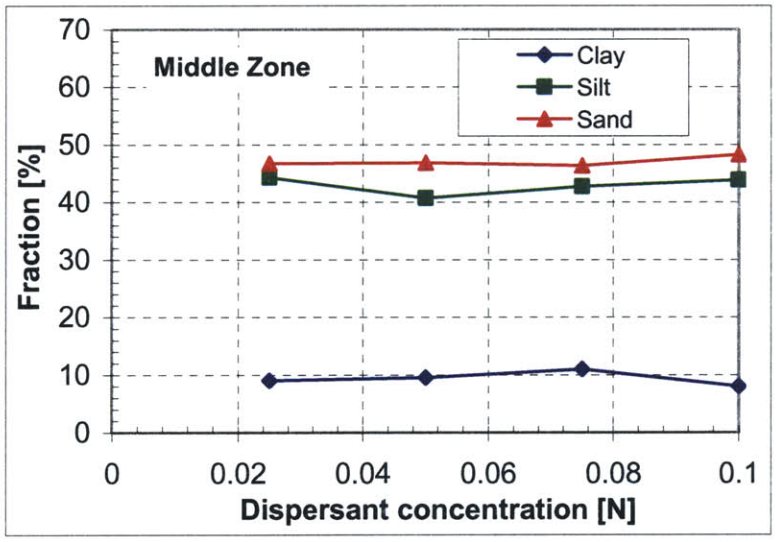

Figure 6-11. Effect of dispersant concentration on the particle size distributions.

Effects of Drying Conditions

Table 6-8 and Figure 6-12 show the results of particle size analysis performed on samples with different drying conditions. The clay fractions from both UC and MZ

increase from natural wet sample, oven-dried sample, and air-dried sample. Air-drying produces the highest clay fraction from both UC and MZ. As discussed previously, the natural (wet) samples keep their initial soil structure comprising mainly aggregates. Using only 1 min of blending may not be sufficient to breakdown all of the aggregates. The effectiveness of air-drying and oven-drying is dispersing the soil will be discussed later in Section 6.5.

It is also worthy to discuss the results of several tests which are shown in Table 6-8 but not in Figure 6-12. Notice the reproducibility is very good, i.e., the difference between Test# P25 and A8 and between Test# P28 and A9 is very small. Furthermore, the result of Test# B1 shows that remolding by 20 min blending on an oven-dried sample gives a clay fraction of 57%, which is higher than that obtained by 1 min blending (52%, Test# P27), but still lower than that obtained by either air-drying (63%, Test# P25) or 20 min blending of natural wet sample (61.5%, Test# P19, see Table 6-5). That means the effect of oven-drying can't be completely removed by longer remolding time.

In Table 6-8, the difference between Test# C1 and C2, both of which have been oven-dried, then blended for 20min, and then oven-dried again, is that C1 uses dispersant while C2 not. Test# C1 gives 56% clays which is the same as B1, which means if dispersant is used, oven-drying once more will not cause any changes. However, if no dispersant is used, the clay fraction drops to 9%. Therefore, the aggregates caused by oven-drying can be broken down by dispersant.

Table 6-8. Effect of drying on the particle size distribution of the old alluvium.

Sample	Drying condition	Test #	Remolding Energy	Clay [%]	Silt [%]	Sand [%]
UC	Natural	P1	1min blending	43.5	43.1	13.4
	Oven-dried	A6	No blending	45		
	Oven-dried	P27	1min blending	52	34.8	13.2
	Oven-dried	B1	20min blending	57	26.9	16
	Oven-dried	C1+	OD-BL-OD*	56	27.3	16.7
	Oven-dried	C2+	OD-BL-OD*	9	45.9	45.1
	Air-dried	P25	1min blending	63	24	13
	Air-dried	A8	1min blending	62	26	12
MZ	Natural	P2	1min blending	9.5	40.7	46.8
	Oven-dried	P26	1min blending	18	38.6	43.4
	Air-dried	P28	1min blend	29	28.3	42.7
	Air-dried	A9	1min blend	30	28	42

*** OD-BL-OD: oven-drying, then blending for 20 min, then oven-drying again.**

+ Test# C1 and C2: C1 uses 0.05N NaHMP, while C2 uses no dispersant.

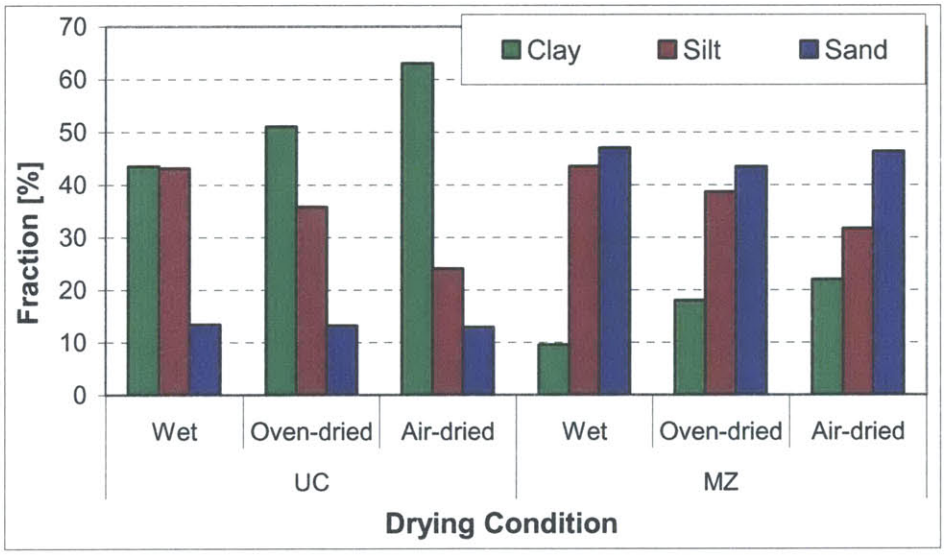

Figure 6-12. Effect of drying condition on the particle size distributions.

6.5.4 Discussion

Intrinsic Particle Size Distribution

Here the "intrinsic" means that all particles in a soil are fully dispersed, or no more two smaller particles in a soil are bound together to form bigger particles either by cementation or by flocculation/aggregation. The intrinsic particle size distribution reflects the upper bound of the remolding state and should define the maximum clay fraction.

The data in Table 6-9 are extracted from Table 6-5 and Table 6-8. It is quite clear from Table 6-9 that the maximum clay fractions are 63% and 30% for the UC and MZ, respectively, which are all obtained by air-drying. Notice that the clay fractions obtained by 20min blending are almost equal to those obtained by air-drying, reflecting that although different sample processing methods were used, it is possible to achieve the same remolded and dispersed state. Therefore, it can be concluded that the particle size distributions obtained either by air-drying or 20min blending are the intrinsic particle size characteristics.

Further confirmation of these results can be made from quantitative mineralogy described in Section 5.3 (see Table 5-10). The total clay size fractions including clay minerals and Fe-oxides (since particles of all Fe-oxides are much smaller than 2 μm, e.g., the size of goethite is 50-100 nm, hematite 20-50 nm) is 62.8% and 38.6% for UC and MZ, respectively. Therefore, the UC clay fraction 62.8% obtained by mineralogical analysis agrees well with that (63%) of the intrinsic particle size distribution. There is some error for the MZ clay fraction, which may be attributed to that some clay particles

in MZ may have a size greater than 2 μm. For example, it is possible that kaolinite particles with size ranging from 0.4 – 10 μm (Mitchell, 1993) are larger than the normal clay fraction.

Table 6-9. Maximum amount of clay fractions obtained by various methods.

Variable changed	Value	UC clay fraction	MZ clay fraction
Remolding energy	20min blending	61.5%	27%
Types of dispersant*	$(NaPO_3)_6$ (0.05N)	43.5%	9.5%
Amount of dispersant*	0.1N $(NaPO_3)_6$	45%	8%
Drying condition	Air-dried	63%	30%

* Methods do not completely destroy cementation bonds.

Evaluation of chemical and mechanical dispersion methods

It is also interesting to compare the difference between the chemical and mechanical methods of dispersion. As discussed in Section 6.2, dispersants basically reverse the positive edge charge of clays or the positive surface charge of Fe-oxides. Hence, they effectively separate particles connected by flocculation or aggregation, but do not effectively destroy cementation bonds. On the contrary, mechanical energy is required to break the cementation bonds for complete dispersion. Based on above experimental results (see Test# C3 in Table 6-7), for old alluvium, a soil suspension dispersed by mechanical energy may become flocculated again if no dispersant is used to cancel the attraction forces between clays and Fe-oxides.

From Table 6-9, the clay fraction obtained by changing either the type or the amount of dispersant is smaller than that by remolding energy or air-drying. Therefore,

using chemical dispersion alone can't achieve the fully dispersed state, and the mechanical energy must be applied to destroy cementation bonds to obtain the intrinsic particle size distribution.

In addition, there is a large increase in clay fraction for the MZ samples obtained by mechanical energy or drying, i.e., increasing from 8-9.5% to 27-30%. These results indicate that the majority of bonds in MZ are cementation caused by goethite, which is the only Fe-oxide present in MZ. This is consistent with other observations reported in the literature that goethite mainly acts as cementation agent (Righi and Meunier, 1995). Since the UC has both goethite and hematite which mainly causes aggregation, using dispersants in UC can disperse only the part of the bonds caused by aggregation. That is the reason why the maximum amount of clay fraction obtained by changing either the type or the amount of dispersant is ~45%, which is much less than that (~62%) obtained by using both dispersant and remolding energy which is sufficient to break all cementation bonds.

Effect of drying

Drying is a process of losing water by evaporation. Depending on the temperature, a soil may be air-dried or oven-dried (105-110°C). This section systematically summarizes the effect of drying on the soil fabric and particle size characteristics of the old alluvium. Further discussion on the effect of drying on Atterberg limits will be discussed in Section 6.6.

Essentially, there are three different mechanisms involved in the drying process to change the soil properties:

- Mechanical: due to loss of water, drying causes high suction and hence high effective stress applied on the intact soil structure. The stress induced by drying will cause the intact soil to shrink and hence break the cementation bonds. Therefore, the mechanical mechanism caused by drying will make a cemented intact soil more dispersed.
- Chemical: It is well known by clay scientists and geochemists that dried clay surfaces possess high acidity (pH = 2). The discussion of the theory of clay surface acidity is out of the scope of the thesis. More details can be found in Rupert et al. (1987), McBride (1989), Heimann (1993), Righi and Meunier (1995), and Moore and Reynolds (1997). As pointed by Righi and Meunier (1995), when the water films on the clay surfaces become increasingly thin during drying, water molecules dissociate more than in free water generating a very low pH<2. This strong surface acidity is responsible for the dissolution of Fe oxyhydroxides (FeOOH, goethite) and consequently the disintegration of the aggregates. Therefore, the chemical dissolution will contribute to the more dispersed soil characteristics.
- Physical: the physical mechanism includes the reprecipitation of salt from solutions and the loss of hydrated water on surfaces of clays and Fe-oxides and hydrated water in the interlayer spaces of smectites. If the pore water contains some soluble salts and cations, drying drives off water and causes reprecipitation of salts from solution between particle contacts which act as cementation bonding

particles together. Depending on the kind of solid salts or minerals formed, this process may or may not be reversible. If not, i.e., the reprecipitated salt cannot be dissolved in water at room temperature, then the aggregates form through drying.

- Drying at higher temperatures also drives off hydrated water adsorbed on clay and Fe-oxides surfaces and in the smectite interlayer. Much of the hydrated water on clay surfaces or in smectite interlayer is associated with the cations. As pointed out by Fookes (1997), the water of hydration in the sesquioxides of iron and aluminum may be driven off by oven-drying at 105 ^{O}C, the standard temperature for testing temperate region soils. Dehydration of the sesquioxides (Fe_2O_3, hematite) creates a stronger bond between the particles, which resists penetration by water. This process cannot be reversed by re-wetting. Furthermore, the process of dehydration of smectites with certain interlayered cations (e.g., Ca^{2+}, Fe^{3+}) may not be reversible and may bond more smectite layers to form a bigger particle. This is similar to the mechanism that the interlayered cation Ca^{2+} bonds more smectite layers to form bigger particles than Na^{+}. Therefore, both reprecipitation and dehydration tend to increase the particle size.

The effects of drying on the particle size characteristics of the old alluvium can now be summarized as follows: the old alluvium has a very low soluble salt concentration (see Table 3-2) due to the high rainfall in the tropical wet climate of San Juan, hence, drying will not produce noticeable mineral reprecipitation to bond particles. The effects of cementation by goethite and aggregation by hematite cause the intact soil to have a low apparent clay fraction. Air-drying is effective in driving off the free water in the soil

skeleton but probably will not cause loss of hydrated water at Fe-oxides surface or within the smectite interlayers. However, air-drying does break the cementation through either shrinkage stresses or the chemical dissolution of goethite by clay surface acidity. Therefore, a much higher clay fraction is obtained by air-drying. In addition to these same dispersing effects caused by air-drying, oven-drying causes dehydration of Fe-oxides and smectites which increases particle size and is not reversible, resulting in a clay fraction smaller than air-drying. In summary, the clay fraction obtained by oven-drying is a combined effect of: (1) disintegrating by shrinking; (2) disintegrating by dissolving the cementation through clay surface acidity; and (3) bonding particles together through the dehydration of Fe-oxides and smectites. Depending on the intensity of these three effects, oven-dried soil may have a higher or lower clay fraction than natural wet sample. However, for the old alluvium, it is certain that air-dried soil has a higher clay fraction than both natural wet and oven-dried samples.

6.6 Atterberg Limits

6.6.1 Introduction

In addition to the particle size distribution, the Atterberg limits and related indices (including plasticity index (PI) and liquidity index (LI)) provide very useful descriptions of the behavior of soil particle assemblages. In fact, the identification and classification of fine-grained soils in geotechnical engineering are solely done on the basis of Atterberg limits (ASTM D4318). They are also used extensively, either individually or collaterally,

with other soil properties in empirical correlations with engineering properties of compressibility, permeability, compactibility, shrink-swell, and shear strength.

The reactivity and behavior of soils are functions of the extent of the surface exposed to the equilibrium electrolyte in solution or water. The physical significance of the Atterberg limits is that a soil which has a greater tendency to attract water to the particle surfaces will have larger indices, i.e., the Atterberg limits are mainly a function of the available external surface area of the soil particles. Hammel et al. (1983) found very strong relationships (r^2>0.9) between Atterberg limits and the external surface areas of soils. Of course, other factors, such as the types of clay minerals and the amount of each type of clays, also affect the Atterberg limits. Since the conduct of the tests measuring these parameters inherently involves disturbance of the soil, they may not give a good indication of the behavior of the intact undisturbed soil. Therefore, a soil with cementation or aggregation may give different values of Atterberg limits if different sample preparation methods are used to expose the surface area. As discussed in the literature, most residual soils exhibit variable Atterberg limits which are affected by the reworking energy or time and by drying. It is well known that the index properties of most residual soils are variable and are affected by some factors, such as drying condition, remolding time and energy, and the method of remolding. To some extent, the variability of the index properties reflects the different degree of destructuring and remolding.

This section describes the measurement of the Atterberg limits of the old alluvium. Its objectives include: (1) providing an indirect way to assess the soil structure determined by those direct methods in Section 6.4; (2) measuring the maximum variability of these parameters; and (3) finding a proper sample preparation method to measure the parameters for a completely remolded sample. Furthermore, it is expected that a final classification and identification of the old alluvium can be recommended based on these experimental results.

6.6.2 Materials and Methods

All testing materials used to perform the Atterberg limits measurements are the processed disturbed bucket samples, as described in Section 3.7. The procedures of ASTM D4318 are followed explicitly but using different sample pre-processing procedures. For comparison, both Casagrande Cup and Fall Cone are used to measure the liquid limit (ω_L). Detailed descriptions of the Fall Cone method can be found in Wood (1982, 1985), Moon and White (1985), Leroueil and Bihan (1996), Farrell and Wassing (1997), and Feng (2000).

Based on the sample preparation methods, all tests are categorized 3 different groups, each of which represents a unique remolding path. Table 6-10 and Table 6-11 summarize the 3 different remolding paths for UC and MZ, respectively. Path 1 uses natural wet samples with variable remolding energy, while Path 2 and Path 3 start with air-dried and oven-dried samples, respectively. The different amounts of remolding energy are achieved through hand mixing, stirring in the blender specified in ASTM

D422, and shaking in a mechanical shaker. By varying the duration of the remolding time, the intensity of the mechanical energy is also changed.

Table 6-10. Atterberg limits of UC measured with various sample preparation methods.

Processing path	Test No.	Drying condition	Remolding energy	ω_L [%]	ω_P [%]	I_P [%]
Path 1	UC1	Natural Wet	~10min hand mixing*	72.9	40.7	32.2
	UC2		30min hand mixing	73.6	37.8	35.8
	UC3		5min blending	82.6	34.8	47.8
	UC6		20min blending	94.3	31.0	63.3
Path 2	UC1	Natural	~10min hand mixing	72.9	40.7	32.2
	UC5	Air-dried	~10min hand mixing	69.9	29.1	40.8
	UC11		3hr shaking	74.6	29.6	45.0
	UC7		20min blending	93.7	26.7	67.0
	UC8		20min blending, oven-dried, rewetted	81.2	28.2	53.0
Path 3	UC1	Natural	~10min hand mixing	72.9	40.7	32.2
	UC4	Oven-dried	~10min hand mixing	69.8	33.3	36.5
	UC9		20min blending	91.2	25.1	66.1
	UC10		20min blending, oven-dried, rewetted	76.1	25.7	50.4

*~10min hand mixing is equivalent to the mechanical energy specified by ASTM D4318.

Table 6-11. Atterberg limits of MZ measured with various sample preparation methods.

Processing path	Test No.	Drying condition	Remolding energy	ω_L [%]	ω_P [%]	I_P [%]
Path 1	MZ1	Natural	~10min hand mixing	44.7	22.5	22.2
	MZ2		30min hand mixing	44.9	21.4	23.5
	MZ3		5min blending	60	19.4	40.6
Path 2	MZ1	Natural	~10min hand mixing	44.7	22.5	22.2
	MZ4	Air-dried	~10min hand mixing	50.3	19.8	30.5
Path 3	MZ1	Natural	~10min hand mixing	44.7	22.5	22.2
	MZ5	Oven-dried	~10min hand mixing	46.7	18.2	28.5

*~10min hand mixing is equivalent to the mechanical energy specified by ASTM D4318.

Since the fraction of Fe-oxides is much smaller in the MZ than UC, only 5 representative tests are performed to measure the Atterberg limits of MZ, while more extensive testing were carried out on the UC samples.

6.6.3 Results and discussion

Table 6-10 and Table 6-11 also summarize the results of all Atterberg limits measured on the UC and MZ, respectively, while Figure 6-13 and Figure 6-14 present these result on the standard Casagrande plasticity charts. It should first be noticed that Atterberg limits of both UC and MZ do change with drying conditions and mechanical remolding energy.

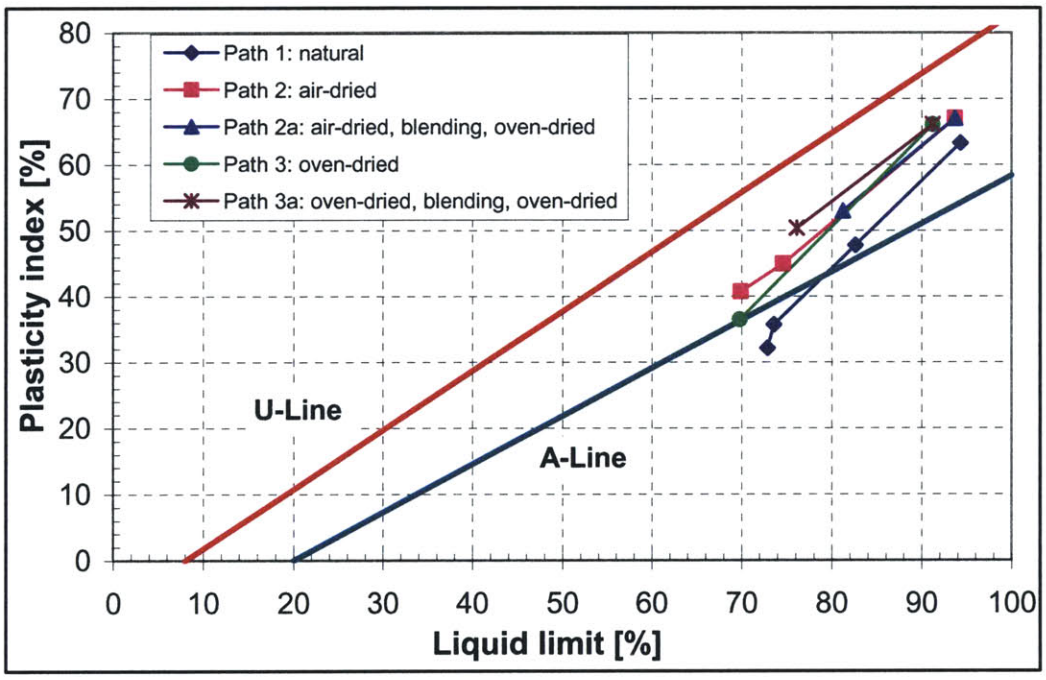

Figure 6-13. Effect of remolding and drying on the Atterberg limits of UC.

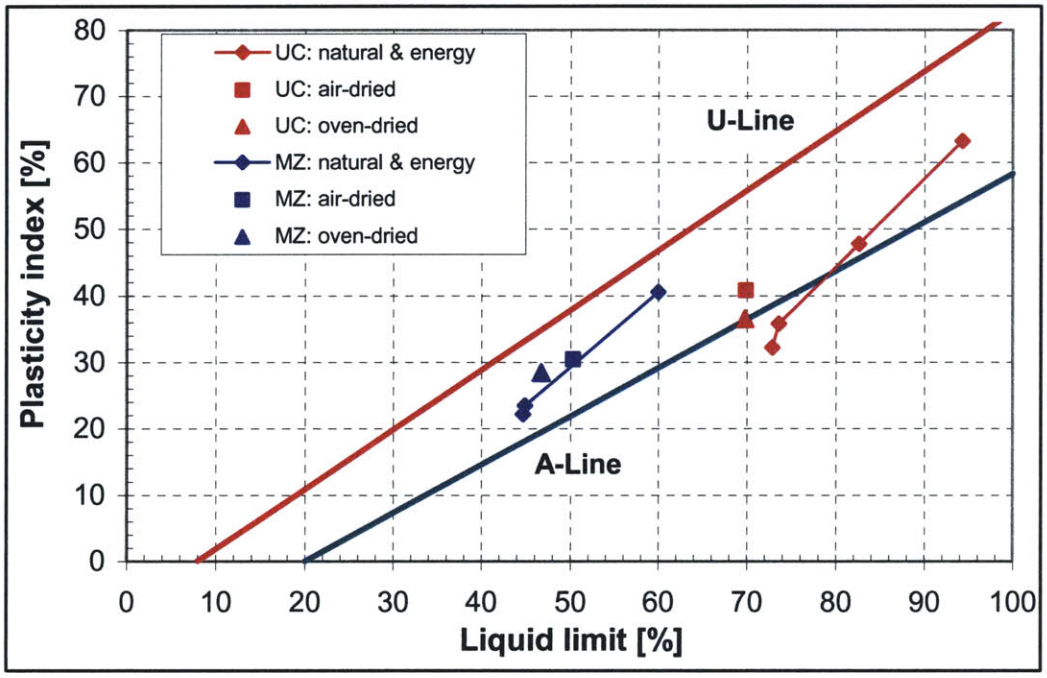

Figure 6-14. Comparison of Atterberg limits between UC and MZ.

Effect of Remolding Energy

By comparing the 3 paths shown in Figure 6-13, no matter what kind of drying process of the UC samples have subjected, i.e., either natural wet, air-dried, or oven-dried, the ω_L and I_P increase with remolding energy (except Paths 2a and 3a), while the plastic limit (ω_p) decreases with remolding energy (see Table 6-10 and Table 6-11). It is quite obvious that ω_L changes with remolding energy, as remolding breaks the bonds between particles and disperse the aggregates by mechanical forces, providing a dispersed soil and increasing the external surface area. In fact, notice that the three tests (i.e., UC6, UC7, and UC9, see Table 6-10), all of which have been blended for 20 min, have almost the same highest ω_L and I_P, indicating that after blending for 20 min, natural

wet, air-dried, and oven-dried samples have almost the same external surface area, while long-term blending tends to remove or mitigate the effect of drying on soil plasticity.

Although it is relatively easy to explain why ω_L increases with remolding energy, the variations of ω_p require more subtle interpretation. As shown in Table 6-10, ω_p decreases with increasing remolding energy. This is contrary to the conventional wisdom that ω_p should also increase with external surface area. This measured data can be explained by considering changes in Atterberg limits for montmorillonite with different exchangeable cations, as shown in Table 6-12. Since Na-montmorillonite can be dispersed as single smectite layers, it has the maximum external surface area and hence the largest ω_L. However, Na-montmorillonite has a smaller ω_p than Ca- or K-montmorillonite. This behavior can be explained by noticing that interlayer Ca^{2+} cations bond more smectite layers together to form a larger particle, while Na-montmorillonite comprises mainly single smectite layers as individual particles. Therefore, Na-montmorillonite has a much higher external surface area than Ca-montmorillonite and a much higher ω_L. On the other hand, ω_p defines the boundary water content which separates the plastic state of a soil from its semisolid state, i.e., the soil at ω_p doesn't contain too much water. Therefore, the ω_p is subjected to the effect of adsorbed water existing in the interlayer space of smectites, which can be driven off by oven-drying. The interlayered water in smectites exists in the internal surfaces of smectite particles and doesn't contribute to the soil plastic behavior, but the water content measurement at oven temperature still takes this amount of water into account. Therefore, the measured ω_p for Ca-montmorillonite is even higher than Na-montmorillonite though the latter has a much

higher external surface area than the former. Of course, the interlayered water also affects the ω_L, but compared to the free water and the water on the external surface, the interlayered water is such a small amount that its affect on ω_L can be neglected.

Table 6-12. Atterberg limits of montmorillonite with different exchangeable cations.

Exchangeable cation	Liquid Limit [%]	Plastic Limit [%]	Plasticity Index [%]
Na	710	54	656
K	660	98	562
Ca	510	81	429
Mg	410	60	350
Fe	290	75	215
Fe*	140	73	67

Data from Lambe and Whitman (1969, p.33).

* After 5 cycles of wetting and drying.

Based on the above discussion, it is not difficult to understand why the ω_p decreases with remolding energy. The intact aggregated soil contains intra-aggregate pores (see Section 6.4) which are filled with water. This water will not contribute to the soil plasticity, but it is recorded at oven temperature and taken into account for the ω_p. With increased degree of dispersion by remolding energy, more and more intra-aggregate pores are destroyed, resulting in less contribution of intra-aggregate water to the ω_p measurement. Therefore, ω_p decreases with increasing remolding energy. It should be pointed out here that the ω_p measured on the fully dispersed sample (i.e., 20 min blending) reflects the true soil plasticity. In addition, since smectites are present in the old alluvium, the interlayered water also affects the plastic limit measurement.

All three energy paths in Figure 6-13 are approximate parallel to each other and to the U-line in the plasticity chart. If Path 1 is considered and Test# UC1 (10min hand mixing) and UC2 (30min hand mixing) are compared, hand-mixing is not very effective in destroying the cementation caused by Fe-oxides, which is quite reasonable, while mechanical blending is effective in destroying the intact structure and disperse the cementation caused by Fe-oxides.

Effect of Drying

The effect of drying on Atterberg limits can be found by comparing the three lines corresponding to the 3 paths shown in Figure 6-13. For UC, with the same amount of energy (~10min blending), drying tends to decrease both ω_L and ω_p. The decrease of ω_p caused by drying is similar to that caused by remolding energy, since basically drying tends to destroy the bonds. However, for ω_L, even if drying disintegrate aggregates, without enough energy, dispersed soil can flocculate again and hence decrease ω_L. Therefore, the combined effect is that I_P increases with drying.

Moreover, Paths 2 and 3 which are for air-dried and oven-dried samples, respectively, are very close to each other, but they always lie above Path 1. This strongly implies that certain chemical reactions which may change the soil composition have happened during drying. As described in Section 6.5, goethite may be dissolved during drying by the strong surface acidity of extremely dried clays.

Attention should also be paid to Paths 2a and 3a, which represent a cycle of drying, blending for 20 min, and oven-drying again. They are parallel to each other and to the U-line. Even though the samples have been blended for 20min, another cycle of oven-drying does not change ω_p too much, but it decreases significantly ω_L, which means oven-drying of a fully dispersed soil with Fe-oxides does introduce certain bonds which can't be destroyed by simple rewetting. In fact, Fookes (1997) pointed out that the changes caused by drying of soils which contain hydrated oxides of iron and aluminum are irreversible and they become less plastic.

Comparison of liquid limits measured by Casagrande cup and Fall cone methods

Although there are only 6 liquid limits measured by both Casagrande cup and fall-cone, it is interesting to compare the results for the old alluvium (Table 6-13). Figure 6-15 compares the two sets of ω_L values and shows that there is a consistent bias between the two methods. The fall cone measures ω_L values that are 5-10% higher than those found using the Casagrande cup.

Table 6-13. Comparison of liquid limits measured by Casagrande cup and fall-cone.

Test No.	ω_L by Casagrande cup	ω_L by Fall-cone	Ratio
UC6	94.3	103.5	1.098
UC7	93.7	102	1.089
UC8	81.2	86.5	1.065
UC9	91.2	97.8	1.072
UC10	76.1	80.4	1.056
UC11	74.6	79.9	1.070

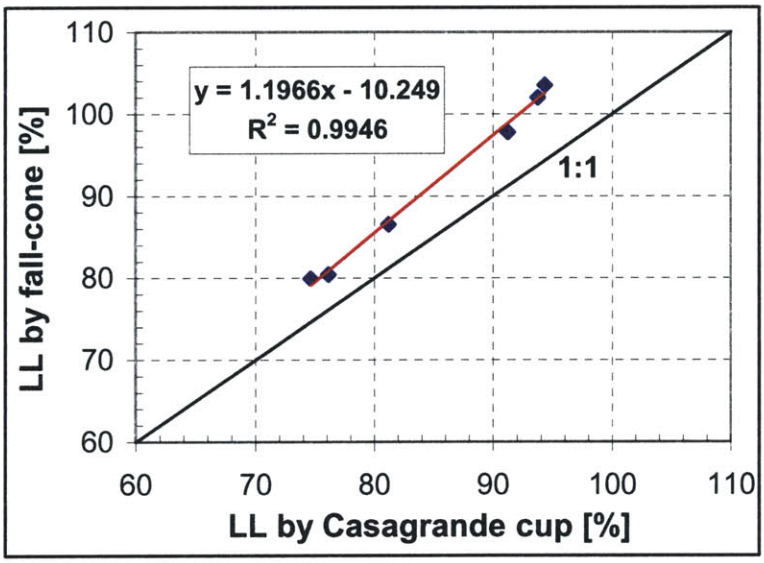

Figure 6-15. The relationship of the liquid limits measured by Casagrande cup and by fall cone.

It is also interesting to point out that Queiroz De Carvalho (1986), after making 27 measurements on 9 lateritic soils from Brazil, found that the fall cone method overestimates by 10% the values of ω_L determined by the Casagrande cup. This is quite consistent with the determination of ω_L of the old alluvium. The possible reason is that both the old alluvium from San Juan and the lateritic soils from Brazil contain significant amounts of Fe-oxides, which are finely particles with positive charges and quite often stick to steel. As the fall cone is made of stainless steel, the liquid limits measured by the fall cone method will have a greater value.

Comparison between UC and MZ

Figure 6-14 compares the Atterberg limits measured on both UC and MZ samples. Although their soil composition obtained by mineralogical analysis are different, the two lines corresponding to the natural wet samples and changing remolding energy are almost

parallel to each other, which further approves what the remolding energy can affect the Atterberg limits of the old alluvium cemented by Fe-oxides along the same path. For both UC and MZ, air-drying gives the highest I_P, while the I_P of oven-dried samples lies between these of natural wet and air-dried. However, both air-drying and oven-drying give a higher ω_L for MZ than natural wet samples, but lower ω_L for UC samples. This may be attributed to the different types of Fe-oxides present in the two layers, i.e., hematite is present in UC but not in MZ. As discussed in Section 6.5, dehydration of hematite may cause bonds between particles, while goethite cementation can be dissolved or broken by drying. Therefore, drying MZ which contains only goethite simply disperse the soil, whereas drying UC can cause both disintegration and bonds. The combined effect may give a smaller ω_L for air-dried UC than natural wet.

6.7 Conceptual soil structure model

The soil microstructure of the old alluvium was observed directly under ESEM, and indirectly investigated by a series of chemical approaches, consisting of slake tests, EDXS, and CEC measurements. The cementing or coating agents, iron oxides, were further positively identified by selective chemical dissolution and grain size analysis. In addition, the variation of index properties also confirms the intact soil structure determined by these techniques.

A systematic synthesis of all these experimental results show that the old alluvium is cemented and aggregated by iron oxides as a stiff and brittle material with big inter-aggregates pores, and these visible and "broccoli-like" aggregates with size of 80-100μm

are formed by cementing or bridging together many clay platelets (10-20μm), which in turn consist of many clay particles and are covered by iron oxides coatings. Although the sample contains up to 64% clays, due to Fe-oxides coating, cementation, and aggregation, no clay particles exist as separate individuals and thus the physical and chemical properties of clay minerals are relatively inactive.

So far, both the soil microstructure and index properties have been determined. As the variations of index properties also stem from the initial intact soil structure, it is possible to synthesize all information about soil microstructure and hence to build a conceptual soil structure framework for future constitutive modeling of the behavior and engineering properties of the old alluvium. This section discusses a conceptual soil structure model for the old alluvium.

Figure 6-16 shows the similarity between the real soil microstructure and the conceptual unit. Based on the above observations and determination of the soil structure, the steps listed below are followed to build the conceptual soil structure model:

- Individual clay particles are not discernible under ESEM observations on intact samples. Mineralogical analysis found that both kaolinites and smectites are present in this soil. Usually, kaolinites are thick-stacked flat platy particles and smectites are very thin and delicate curved flakes. However, careful ESEM observations only found thick or thin clay platelets with a thin film of coating and found no clear clay particle edges or particle boundary. Furthermore, clay flakes are most likely associated with face to face contact.

- Fe-oxides are very fine particles, i.e., goethite has a size of 50-100 nm and hematite 20-50 nm. It is generally believed that goethite cements soil grains or aggregates through the reprecipitation from solution, while hematite mainly acts as aggregation mineral between clay particles.

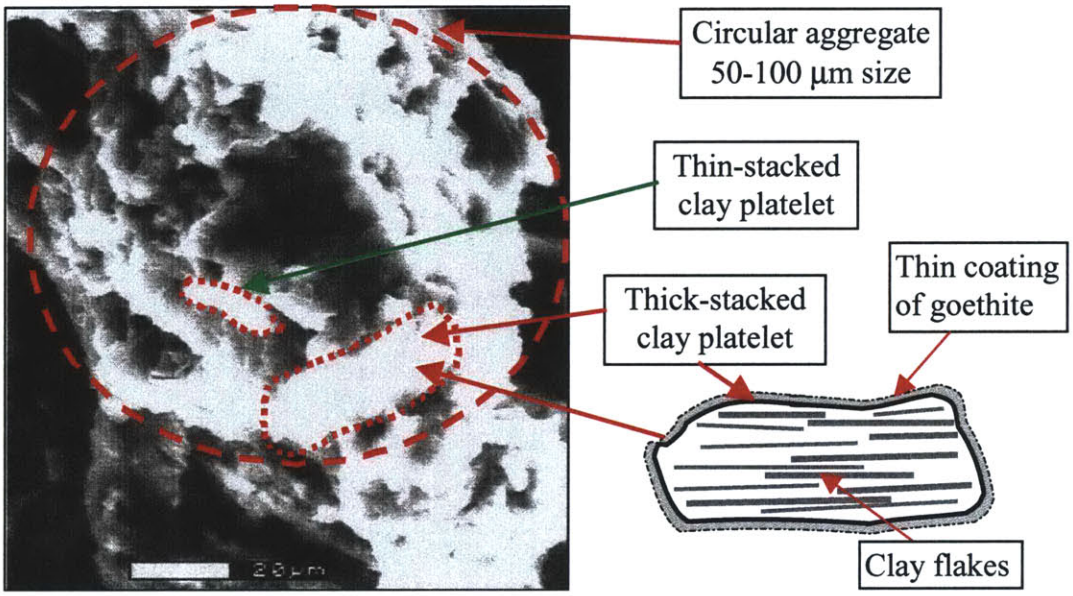

(a) Microstructure shown on real ESEM micrograph

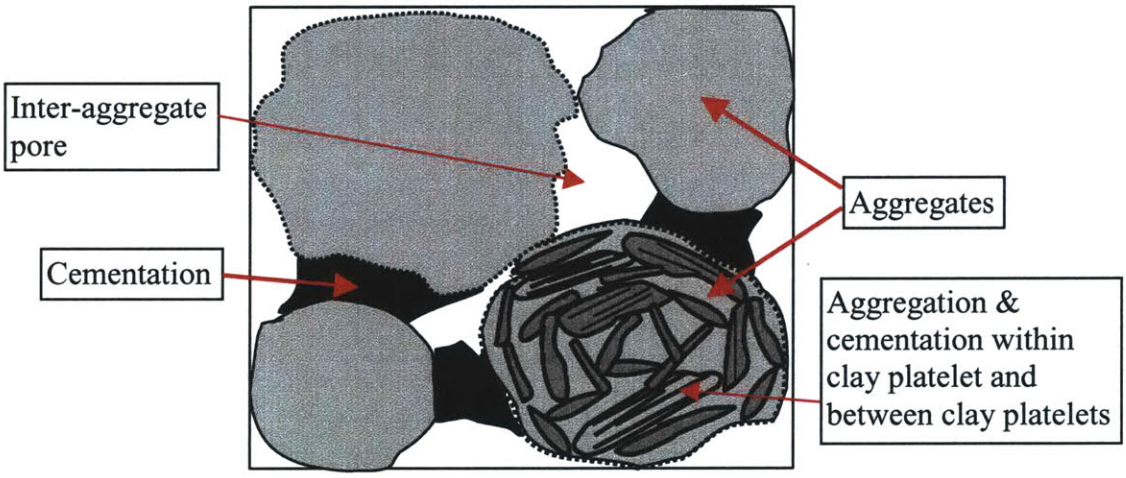

(b) Conceptual structure unit

Figure 6-16. A representative volume element showing the typical features of soil microstructure.

- After Fe-oxides are dissolved and removed by DCB treatment, the micromorphology of kaolinites and smectites is exposed.
- Single clay platelet, either thin or think, has a size of 10-20 mm and contains many clay particles with face to face associations.
- An aggregate with size of 50-100mm consists of many clay platelets cemented and coated by goethite. It seems that these clay platelets are mainly cemented by face to edge contact.
- Further reprecipitation of goethite may also cement two or more aggregates and hence the intact soil doesn't contain loose silt size aggregates.

It is also possible that neo-formed clays may recrystallize and grow at the contacts of existing aggregates, but these clay particles are either coated again by goethite or aggregated by hematite, which may attract more clay particles. Therefore, the cementation or "connection bridge" is broadened and strengthened, giving the intact soil a firm and stiff state.

At this point, a good and clear picture about the soil microstructure has been presented. As discussed in Chapter 4, soil behavior and properties in macroscopic level are determined by many factors, one of which is soil microstructure. By having in mind the conceptual soil structure, one can proceed to predict and investigate the macroscopic soil behavior. For example, the previous discussion on the variations of index properties

can be easily understood. The discussion on the dependence of engineering properties on soil composition and soil structure is left for the next chapter.

References

ASTM—American Society for Testing and Materials (1997) *Annual Book of ASTM Standards*. Volume 04.08, 970pp.

Borchardt, G. (1989) Smectites. In: J.B. Dixon and S.B. Weed (eds.), *Minerals in Soil Environments*, p.675-727. Published by the Soil Science Society of America, Madison, Wisconsin.

CSTC (Caribbean Soil Testing Co., Inc.) (1996) *Geotechnical Data Report –Rio Piedras Contract.*

Deere, D.U. (1955) Engineering Properties of the Pleistocene and Recent Sediments of the San Juan Bay Area, Puerto Rico. Ph.D. thesis, University of Illinois, Urbana.

Dixon, J.B. and Weed, S.B. (1989) Minerals in Soil Environments. 2nd Edition. Published by the Soil Science Society of America, Madison, Wisconsin. 1244pp.

Farrell, E. and Wassing, B. (1997) ETC 5 Fall-cone study. Ground Engineering, **30**, 33-36.

Feng, T.W. (2000) Fall-cone penetration and water content relationship of clays. *Geotechnique,* **50**, 181-187.

Fookes, P.G. (ed.) (1997) *Tropical Residual Soils*. Geological Society Professional Handbook. The Geological Society, London.

Gens, A. and Alonso, E.E. (1992) A framework for the behavior of unsaturated expansive clays. *Canadian Geotechnical Journal*, **29**, 1013-1032.

Hammel, J.E., Sumner, M.E., and Burema, J. (1983) Atterberg limits as indices of external surface areas of soils. *Soil Science Society of America Journal*, **47**, 1054-1056.

Heimann, R.B. (1993) Bronsted acidification observed during hydrothermal treatment of a calcium montmorillonite. *Clays and Clay Minerals*, **41**, 718-725.

Hendershot, W.H. and Duquette, M. (1986) A simple barium chloride method for determining cation exchange capacity and exchangeable cations. *Soil Science Society of America Journal*, **50**, 605-608.

Kaye, C.A. (1959) Coastal Geology of Puerto Rico: (A) Geology of the San Juan Metropolitan Area. Geological Survey Professional Paper 317. US Government Printing Office, Washington, D.C.

Lambe T.W. and Whitman, R.V. (1969) Soil Mechanics. John Wiley & Sons, Inc., 553pp.

Leroueil, S. and Bihan, J.L. (1996) Liquid limits and fall cone. *Canadian Geotechnical Journal*, **33**, 793-798.

Leroueil, S. and Vaughan, P.R. (1990) The general and congruent effects of structure in natural soils and weak rocks. *Geotechnique*, **40**, 467-488.

Loveland, P.J. and Whalley, W.R. (1991) Particle size analysis. In: K.A. Smith and C.E. Mullins (eds.), *Soil Analysis: Physical Methods*. Dekker.

Martin, R.T. (2000) Personal communications, together with his unpublished CEC determination method.

McBride, M.B. (1989) Surface chemistry of soil minerals. In: J.B. Dixon and S.B. Weed (eds.), *Minerals in Soil Environments*, 35-88. Published by Soil Science Society of America, Madison, Wisconsin.

McHardy, W.J. and Birnie, A.C. (1987) Scanning electron microscopy. In: M.J. Wilson (ed.), *A Handbook of Determinative Methods in Clay Mineralogy*, 174-208. Blackie & Son Limited, London.

Mitchell, J.K. (1993) Fundamentals of Soil Behavior. 2nd Edition. John Wiley & Sons, Inc., 437pp.

Mitchell, J.M. and Sitar, N. (1982) Engineering properties of tropical residual soils. *Engineering and Construction in Tropical and Residual Soils*. Proceedings of the ASCE Geotechnical Engineering Division Special Conference, 30-57.

Monroe, W.H. (1980) Geology of the Middle Tertiary Formations of Puerto Rico. Geological Survey Professional Paper 953. US Government Printing Office, Washington, D.C.

Moon, C.F. and White, K.B. (1985) A comparison of liquid limit test results. Geotechnique, 35, 59-60.

Moore, D.M. and Reynolds, R.C., Jr. (1997) *X-Ray Diffraction and the Identification and Analysis of Clay Minerals*. Oxford University Press, 378pp.

Morgenstern, N.R. and Eigenbrod, K.D. (1974) Classification of argillaceous soils and rocks. Journal of the Geotechnical Engineering Division, ASCE, **11**, 1137-1156.

Novich, B.E. and Martin, R.T. (1983) Solvation methods for expandable layers. *Clays and Clay Minerals*, **31**, 235-238.

Pease, M.H., Jr. and Monroe, W.H. (1977) Geologic Map of the San Juan Quadrangle, Puerto Rico. US Geological Survey.

Queiroz De Carvalho, J.B. (1986) The applicability of the cone penetrometer to determine the liquid limit of lateritic soils. *Geotechnique*, **36**, 109-111.

Righi, D. and Meunier, A. (1995) Origin of clays by rock weathering and soil formation. In: B. Velde (ed.), *Origin and Mineralogy of Clays*, 43-161. Springer-Verlag Berlin.

Rupert, J.P., Granquist, W.T., and Pinnavaia, T.J. (1987) Catalytic properties of clay minerals. In: A.C.D. Newman (ed.), *Chemistry of Clays and Clay Minerals*, 275-318. Published by the Mineralogical Society, London.

Schwertmann, U. and Taylor, R.M. (1989) Iron oxides. In: J.B. Dixon and S.B. Weed (eds.), Minerals in Soil Environments. 2nd Edition. 379-465. Published by the Soil Science Society of America, Madison, Wisconsin.

Shadfan, H., Dixon, J.B., and Calhoun, F.G. (1985) Iron oxide properties versus strength of ferruginous crust and iron glaeblues in soils. *Soil Science*, **140**, 317-325.

Shirlaw, J.N., Hencher, S.R., and Zhao, J. (2001) Design and construction issues for excavation and tunneling in some tropically weathered rocks and soils.

Smith, B.F.L. (1994) Characterization of poorly ordered minerals by selective chemical methods. In: M.J. Wilson (ed.), Clay Mineralogy: Spectroscopic and Chemical Determination Methods, p.333-357. Chapman & Hall, UK.

SSL—Soil Survey Laboratory (1996) Soil Survey Laboratory Method Manual. Soil survey investigation report No.42, Version 3.0, 693pp.

Townsend, F.C., Manke, P.G., and Parcher, J.V. (1971) The influence of sesquioxides on lateritic soil properties. *Highway Research Record*, **374**, 80-92.

Van Olphen, H (1987) Dispersion and flocculation. In: A.C.D. Newman (ed.), *Chemistry of Clays and Clay Minerals*, 203-224. Mineralogical Society of Monograph No.6, Mineralogical Society, London.

Velde, B. (ed.) (1995) *Origin and Mineralogy of Clays*. Springer-Verlag Berlin. 334pp.

Wilson, M.J. (ed.) (1994) *Clay Mineralogy: Spectroscopic and Chemical Determinative Methods*. Chapman & Hall, UK.

Wood, D.M. (1982) Cone penetrometer and liquid limit. *Geotechnique*, **32**, 152-157.

Wood, D.M. (1985) Some fall-cone tests. *Geotechnique*, **35**, 64-68.

Chapter 7 ENGINEERING PROPERTIES

7.1 Introduction

Engineering properties are the primary interest of the geotechnical engineer. The previous chapters have provided detailed information on geological origin, soil formation, soil composition, structure, and index properties of the old alluvium. These data can now assist in interpreting the results of the engineering properties. On the other hand, measurements of the mechanical behavior can help understand the effects of the soil mineralogy and micro and macro-structure. This chapter presents results of more conventional engineering property tests and discusses the fundamental mechanical behavior based on its composition and structure of the old alluvium. These test results also provide the first direct evidence of effects of the micro-characteristics of the material (soil composition and structure) on macroscopic behavior.

Generally speaking, compressibility, hydraulic conductivity, and shear strength are the three most important engineering parameters in geotechnical engineering practice. Therefore, this chapter will discuss these parameters as they are measured through laboratory consolidation tests and triaxial shear tests. Section 7.2 describes experimental program, materials and test methods. Section 7.3 focuses on consolidation behavior, including compressibility and rate of consolidation. A special subsection considers the importance of an expansive clay mineral (smectites) and its effect on soil compressibility and swelling behavior. Finally, Section 7.4 presents the triaxial shear behavior of the

intact material and the strength and stiffness characteristics are interpreted according the soil composition and microstructure of the old alluvium.

7.2 Materials and Methods

The general testing procedure for measuring properties of undisturbed soils includes four phases: (1) selection of high quality undisturbed samples, (2) specimen preparation (cutting and trimming), (3) applied stress history and experimental measurements (flow, deformation, etc.), (4) data processing. Since this chapter focuses only on the measurement of consolidation and triaxial shear behavior, which are routine types of test with well developed and published techniques (e.g., Lambe, 1951; Germaine and Ladd, 1988; Sheahan et al., 1990; Santagata, 2000), this section only discusses the special techniques which have been developed especially for the old alluvium and are different from routine testing of sedimentary soils.

7.2.1 Testing Materials

In order to obtain engineering properties of intact materials, high-quality large block samples were used for all the laboratory tests described in this section. Section 3.7 describes the evaluation of sample quality by X-ray photography. Only those block samples showing no cracks or detectable disturbance were selected. Special attention has also been paid to the macrostructure in selecting test specimens (using the more homogeneous parts of each sub-block with minimal white venations in the macrostructure) of the soil block.

It should be pointed out that the physical orientation of the block samples was not recorded during field sampling and hence, it is not possible to investigate anisotropic properties of the old alluvium. There is minimal data on anisotropic properties of residual soils (Fookes, 1997). Therefore, the current experiments inevitably assume isotropic properties in interpreting the measured data.

7.2.2 Specimen Preparation

Not only do soil composition and soil structure give unusual behavior and engineering properties to the old alluvium, but also they present challenges in laboratory testing. For example, it is difficult to cut and trim the block samples to make specimens for oedometer or triaxial tests. In fact, it has been found that, due to the presence of quartz which has high hardness (even higher than steel), the teeth of the bandsaw blade used to cut Shelby steel sample tubes were worn down quickly during cutting a block sample from the MZ layer. Therefore, significant efforts have been made to develop special testing procedures for preparing specimen for the old alluvium. Experience gained through a series of preliminary trial tests has led to the following procedures to prepare specimens from block samples:

- *Subdividing*: cut a big block sample into pieces with adequate size (4″x 5″) by using a handsaw with a carbide-tipped blade. Due to the brittleness of the intact soil, manual cutting which can better control the force applied to the specimen is preferred over a motor-operated bandsaw;
- *Preliminary trimming*: trim each subdivided piece with a vertical bandsaw with a carbide-tipped blade. By turning the soil piece very carefully (which requires

some practice and experience) as the extra part is cut away, a cylinder can be formed for an oedometer or a triaxial specimen. In order to avoid fracturing by the forces applied to the soil block through the fast-moving blade, stop trimming when the cylinder is typically 1.5-2.0 cm larger than the final specimen;

- *Fine trimming*: Move the cylinder for a triaxial specimen or a disk for an oedometer specimen to the conventional specimen trimming frames which are used to trim soft sedimentary soils. Hand trimming is again required. For the triaxial specimen, a sharp straight-edged knife (not a wire saw) longer than the width of the trimming frame is used to trim off the excess diameter by scrapping while the specimen is rotated. This step produces a smooth circumferential surface for the final triaxial specimen. For the oedometer specimen, a short blade with a small tip is used to scratch off the excess soil outside the cutting rim;
- Surface smoothing: since the material, especially for the MZ layer, contains angular sand or silt-sized quartz or feldspar particles, the two thin rubber membranes encasing the triaxial specimens can be easily pierced under high cell pressure if the circumferential surface is not smooth enough. Therefore, a thin layer of silt paste is patched onto the irregular and sharp surface of the specimen in order to prevent the membranes from puncturing.

Although this technique takes more time and efforts and requires great patience, it has been found to be the most effective and successful specimen preparation method.

7.2.3 Consolidation Tests

The consolidation behavior of the old alluvium was measured using mainly two different devices, one is the traditional oedometer, and the other a newly designed consolidometer modified from a Baldwin high force universal loading frame, which is generally used for testing concrete or other materials at MIT. This new hybrid consolidometer includes more sophisticated computer feedback control of the loading system which has a smart mechanical structure using two load cells to control small and large stress ranges separately. The motivations for the development of this consolidometer are listed as follows:

- The traditional oedometer loading frame has a stress limit of 30 ksc, while the old alluvium (especially MZ) requires much higher stresses to reach the virgin compression line. Therefore, a high stress loading frame, such as Baldwin, is necessary to obtain the consolidation behavior;
- After evaluating several trial consolidation tests, it was found that some discrepancy in the strain measurement exists between different loading frames used to test a single specimen, i.e., oedometer low stress loading frame and Baldwin high stress loading machine. This was caused while transferring the oedometer with no stress on specimen between two loading frames, which may introduce disturbance to the fully soaked and unloaded specimen, or by the lost datum for the displacement measurement, or both;
- The incremental loading of an oedometer test requires a constant static load on specimen. The original Baldwin loading frame was not automated and the applied load drifts and changes with time, which has a very profound effect on the strain

measurement of the secondary compression, therefore automation and control was implemented for the Baldwin loading frame. This also includes adding a 500 lbs load cell into the machine to control small load and keep higher resolution at small stresses.

The final modified high stress consolidometer can automatically apply and control stress and most importantly keep a constant load on the specimen with high resolution even on small load. For example, it can control load from 1 lb to 64,000 lbs. Evaluation tests have been performed to verify the capability of controlling small and large constant loads, its long-time stability, and its workability.

Here it seems redundant to give detailed procedures for the incremental loading and measurement of a conventional oedometer test. However, it should be pointed out that during oedometer testing, attention was paid to the swelling when water was added to the specimen. As the consolidation behavior of the intact samples is concerned, any disturbance introduced through testing should be minimized. If swelling was observed during inundation (water was added to the bath), the vertical consolidation stress was increased to the next load increment without waiting for the end of primary consolidation. This was done to keep the soil structure intact before the actual measurement of consolidation behavior.

7.2.4 Triaxial Shear Tests

The MIT automated triaxial system is used to perform shear tests on the old alluvium. Since this pilot apparatus was first developed in the MIT Geotechnical Laboratory in 1990 (Sheahan et al., 1990), it has been modified several times. The key features of current device are as follows (Figure 7-1):

- It is fully automated with closed-loop feedback control;
- Data are recorded using the central data acquisition system;
- K_0 consolidation can be performed continuously with computer control;
- Axial load is measured inside pressure chamber;
- It has internal on-specimen small strain measurement (Figure 7-2), which was developed by Santagata (1998) and Da Re (2000).

It is unnecessary here to provide a complete introduction to this automated triaxial system. Detailed description can be easily found in publications and recent students' theses, such as Sheahan at al. (1990), Santagata (1998), and Da Re (2000).

It should be pointed out that the main objective of this chapter is to present the engineering properties of the intact samples, all tests were not K_0 consolidated to certain high stress, since consolidating the intact soil to a high stress inevitably causes destructuring (or disturbance) of the intact soil structure.

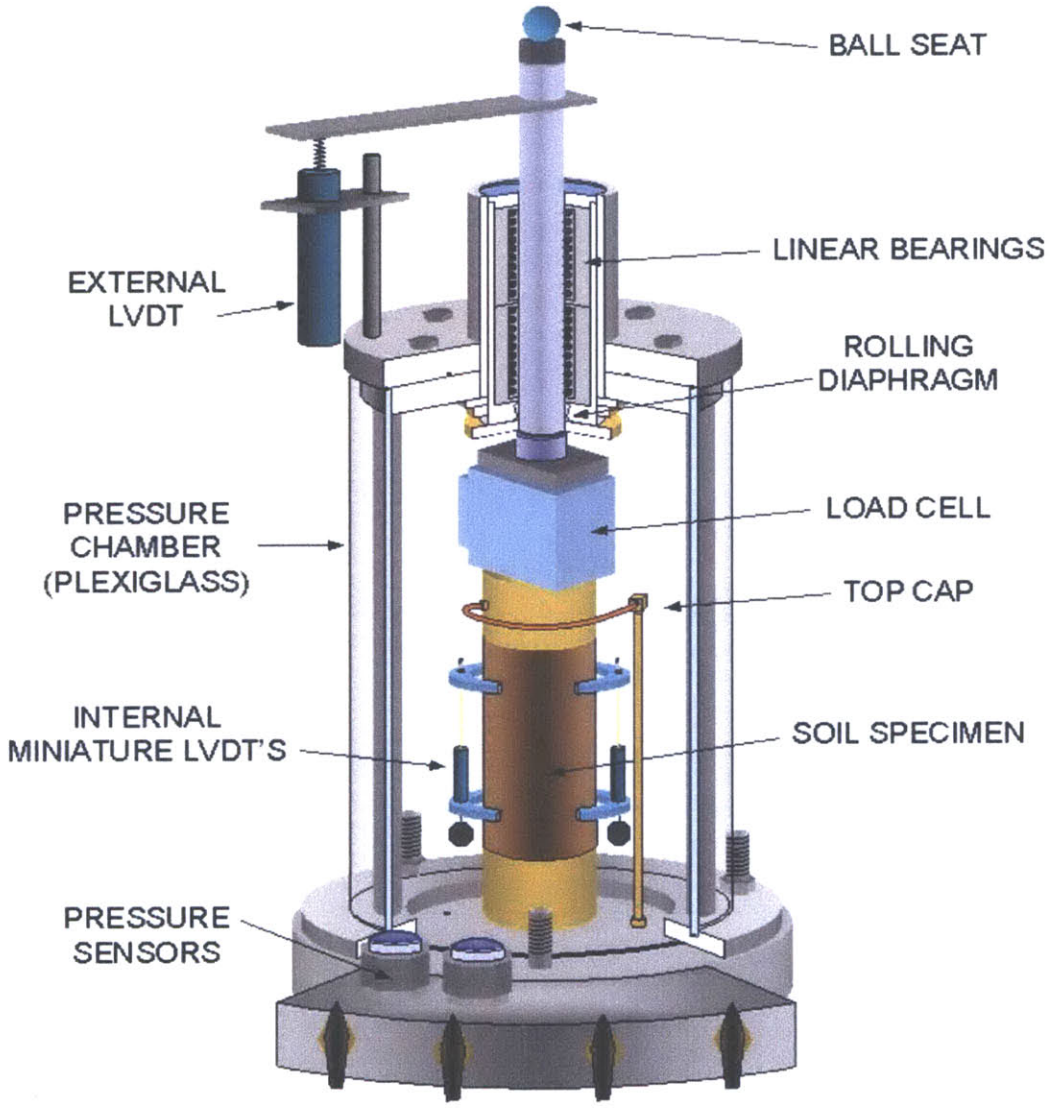

Figure 7-1. The MIT triaxial cell system (Da Re, 2000).

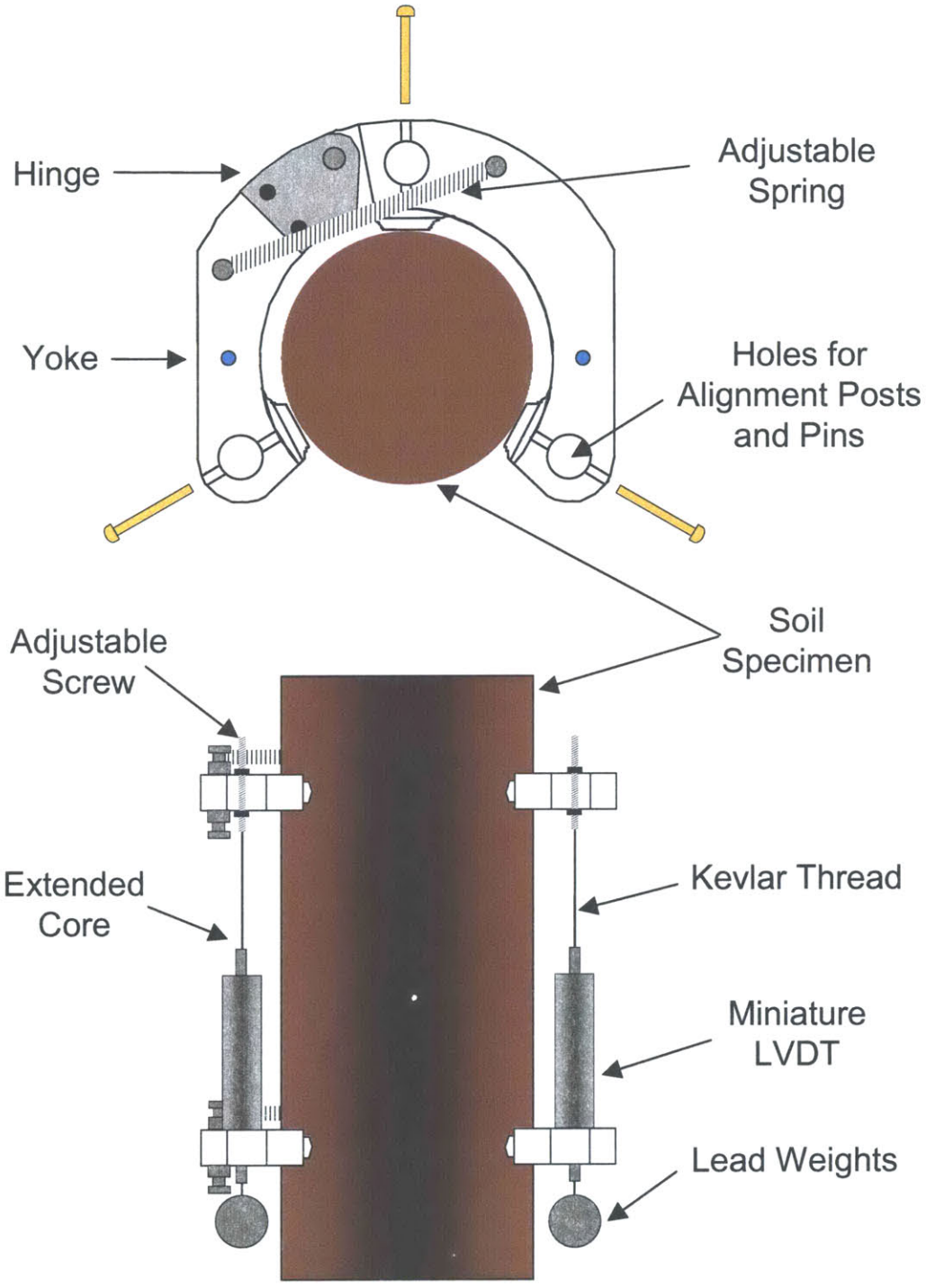

Figure 7-2. The internal on-specimen small strain measurement system (Da Re, 2000).

The general procedures of a triaxial test include specimen setting up, saturation, consolidation, and drained or undrained shearing. No details are given here about the routine procedures, since most of them are controlled by a computer and the techniques are well published, except some special and important precautions, which are listed as follows:

- *Dry setup method*: since swelling was observed during oedometer tests, the dry setup method is required to prevent the specimen from swelling. This requires dry porous stones, dry filter paper and filter strips, and no water left on the top cap and bottom pedestal in the triaxial cell.
- *Initial pressure-up stress*: based on the results of oedometer tests, an initial confining pressure, σ_c = 1.8-2.0 ksc is applied to prevent the specimen from swelling during the subsequent saturation phase. Such a high initial stress needs to be subdivided into several steps to be applied to the specimen.
- *Saturation*: back pressure is applied to saturate the specimen. Generally, this step takes a long time (several days) because the initial specimen is not saturated. Since the soil is stiff, the measured B value may not be very close to 1.00. However, the volumetric strain was recorded over time during saturation phase in order to check the final degree of saturation, i.e., when the volumetric strain becomes constant, the specimen is approximately fully saturated.
- *K_0 consolidation*: due to the stress limit of the triaxial cells used, only one K_0 consolidated undrained shear test was performed. In fact, the test doesn't consolidate the soil to the virgin compression line, so no preconsolidation pressure or K_0 value are obtained from triaxial testing.

- *Strain rate of shearing*: As discussed later, oedometer tests show that coefficient of consolidation decreases dramatically with consolidation stress increasing. Therefore, a small strain rate 0.1%/hour is adopted for drained or undrained shearing.
- *Drained shearing*: Since only the shear strength of intact samples is of interest, drained sharing along different paths can provide a failure envelope for the old alluvium. Therefore, most triaxial shear tests were carried out using drained shear.

7.3 Consolidation Behavior

7.3.1 Introduction

As described above, the consolidation behavior of the intact old alluvium was measured by the incremental loading tests using both conventional oedometers and a hybrid consolidometer. Table 7-1 summarizes the four consolidation tests with reliable data. Although several more tests, which include the two tests for the measurement of the intrinsic compressibility of the soil material of the old alluvium, have been performed, their data are not reliable either due to the incompatibility of the two apparatus or the mistakes in the preliminary trial measurement to development suitable procedures and techniques, therefore, their results are not presented here. Also included in Table 7-1 is the K_0 constant rate of strain consolidation phase of TX506 performed in the triaxial cell Prior to shear.

Table 7-1. Summary of the initial sample conditions for the consolidation tests.

Test ID#	Sample ID#	Sample depth [m]	Initial density [g/cm^3]	Initial water content	Initial void ratio	Initial degree of saturation
Oed07	UC, B3-S1	1.22	1.82	27.00%	0.86	83.0%
Oed08	MZ, B1-S2	10.67	2.08	15.63%	0.48	86.2%
Oed11	UC, B3-S2	1.22	1.90	27.18%	0.80	91.1%
Oed13	UC, B3-S6	1.22	1.71	26.86%	0.90	80.0%
TX506	MZ, B2-S1	8.84	1.98	13.68%		

7.3.2 Compressibility and Swelling Behavior

This section presents the results of the soil compressibility and the swelling behavior measured by consolidation tests. Figure 7-3 shows the consolidation curves (vertical strain ε at the end of primary verse consolidation stress σ'_{vc}) of the four consolidation tests with unloading/reloading cycles. The following key features of behavior can be seen in these data:

- All specimens behave as over-consolidated and the apparent preconsolidation stress is very high, compared to the initial in situ overburden stress. Table 7-2 summarizes the apparent over-consolidation ratios (OCR) for each of the consolidation tests, all of which are very high.
- After the soil is loaded to certain vertical consolidation stress, e.g., σ'_{vc}=30 ksc, subsequent unloading produces large swelling such that the net strain at zero stress is very small or negative (net swelling of sample) strain, indicating that the soil is able to recover all strain induced by loading and to swell back to a larger final volume than the initial volume.

- The swelling ratio, defined by the slope of the unloading part of the consolidation curves, is not a constant in successive cycles of unloading and reloading. In fact, the swelling ratio increases with the maximum past consolidation stress imposed in the tests.
- The compression ratio, i.e., CR, defined by the slope of the virgin compression line of the consolidation curves, is also a constant value. In fact, it seems that there is only one virgin compression line even if a sample has subjected to multiple unloading/reloading cycles. For Oed08 (Figure 7-3 (b)). The discrepancy between the two virgin compression lines is possibly caused by the shifting movement of the specimen from a conventional oedometer loading frame to the Baldwin loading frame.
- At high stress, the virgin compression line tends to be concaved or S-shaped. In fact, this is typical of some structured soils, such as the Canadian Champlain sea clays (Leroueil et al., 1985).

Also in Figure 7-3 (b) is shown the consolidation curve of the K_0 constant rate of strain (CRS) consolidation of a MZ sample measured in a triaxial cell (TX506). Due to the limitation of the stress level being applied in a triaxial cell, the CRS curve is just a short part in the recompression line. Nevertheless, it is exactly parallel to the recompression line of Oed08 measured from a MZ sample too. With respect to the apparent over-consolidation ratio, the possible mechanisms which give the old alluvium such high OCR are: (1) the cementation and aggregation caused by Fe-oxides, and (2) the weathering is basically an unloading process due to the leaching of cations and hence

reduction in mass. However, the high apparent preconsolidation stresses may actually be the yield stress introduced to the old alluvium through cementation, since cementation increases yield stress significantly.

Table 7-2. The measured over-consolidation ratios of the old alluvium.

Test ID#	Sample	σ'_{v0} [ksc]	σ'_{p} [ksc]	OCR
Oed07	UC	0.25-0.40	8	20
Oed08	MZ	1.60-1.80	60	35
Oed11	UC	0.25-0.40	8	20
Oed13	UC	0.25-0.40	8	20

Figure 7-4 shows the e ~ $\log\sigma'_{vc}$ and loge ~ $\log\sigma'_{vc}$ curves for the four consolidation tests. It is clearly shown that the three tests performed on UC samples are quite consistent, and MZ sample has a smaller initial void ratio, due to MZ sample has higher density and more coarse fractions. Furthermore, both the recompression line and virgin compression line are approximately linear in log-log plot, as depicted by the MIT-S1 Model (Pestana and Whittle, 1995). The slope of the loge ~ $\log\sigma'_{vc}$ is defined as ρ_c by Pestana (1994). Table 7-3 lists the calculated ρ_c values. By comparison, it is quite clear that the ρ_c of the UC layer is in the range of typical clays, while that of the MZ layer is in the range of typical sands.

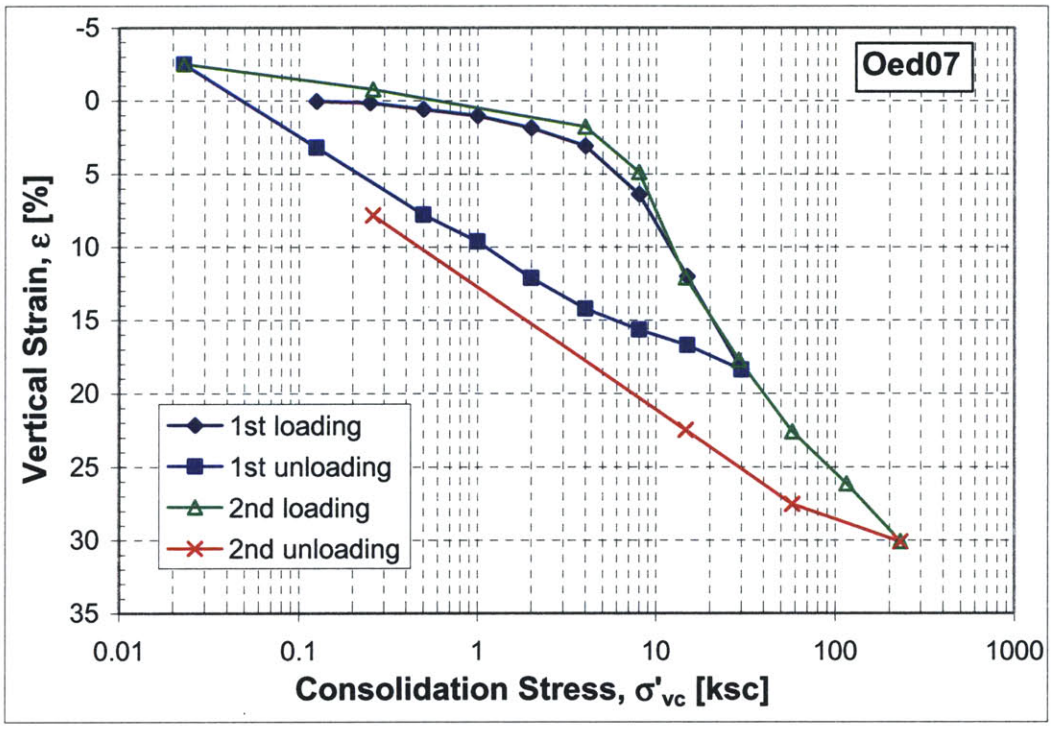

(a)

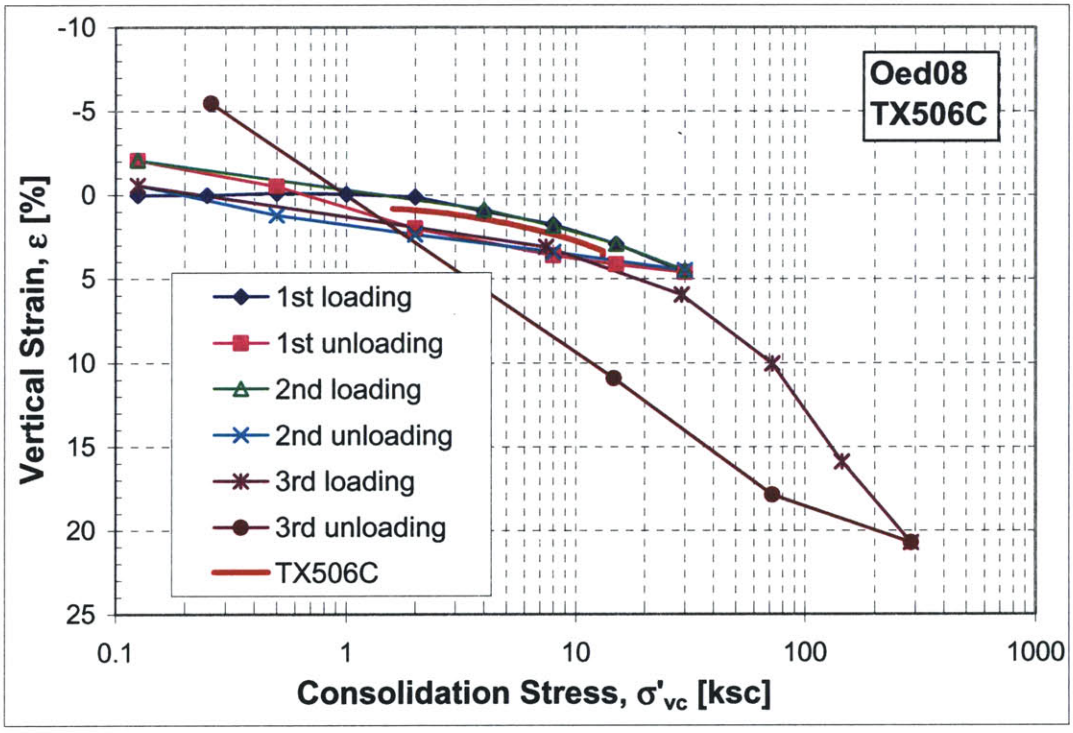

(b)

Figure 7-3. Consolidation curves for the intact old alluvium. (a) Oed07, UC; (b) Oed08 and TX506C, MZ.

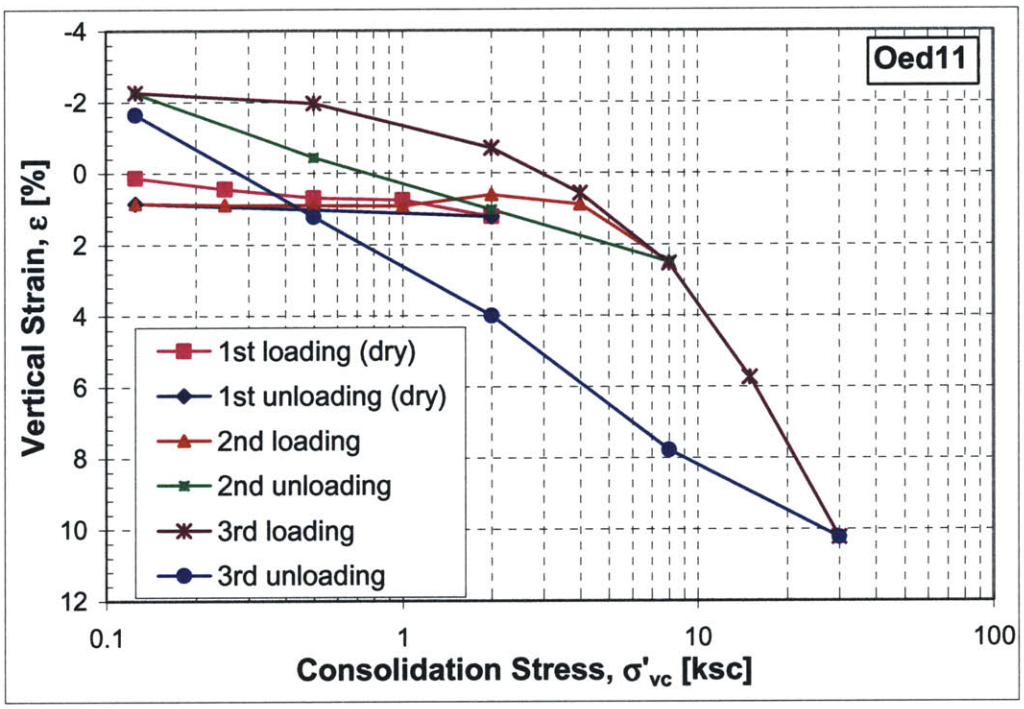

(c)

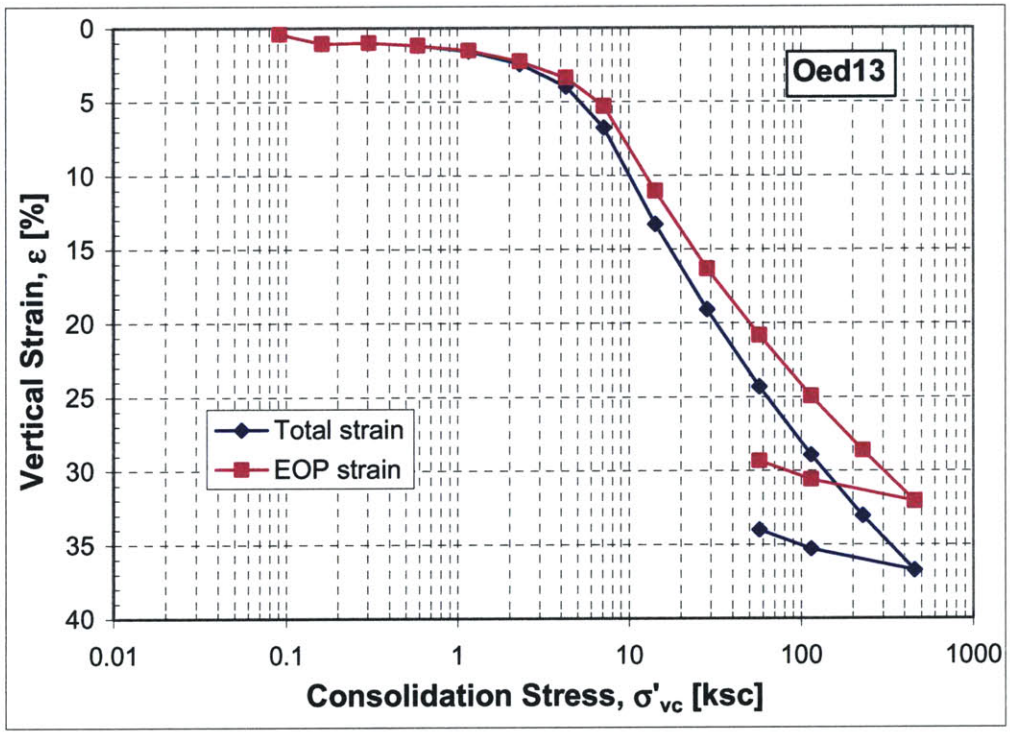

(d)

Figure 7-1 (continued). Consolidation curves for the intact old alluvium. (c) Oed11, UC; (d) Oed13, UC.

Table 7-3. Comparison of ρ_c values of the old alluvium and other soils.

Soil sample	Test ID#	ρ_c	Other soil samples*	ρ_c^*
UC	Oed07	0.26	Argille Plastique	0.25
			Bothkennar	0.26
UC	Oed13	0.27	Empire Clay	0.29
			London Clay	0.24
MZ	Oed08	0.46	Ottawa Sand	0.45
			Ground Dolomite	0.425
			Glauconite	0.43
			Mol	0.46

* Data are from Pestana (1994).

Table 7-4 summarizes the compression ratio (CR) and swelling ratios (SR) at different stress levels of the consolidation curves shown in Figure 7-3 and Figure 7-4. A simple comparison shows that CR ranges from 0.151-0.179, which is almost a constant for the old alluvium. However, the SRs have some variations. It is also quite clear that SR increases with the maximum past consolidation stress imposed during testing, as observed in the above figures.

Table 7-4. Summary of compression ratios of all four consolidation tests.

Test ID#	Sample	CR	SR at σ'_{vc}= 8ksc	SR at σ'_{vc}=30ksc	SR at σ'_{vc}=300ksc
Oed07	UC	0.179		0.066	0.083
Oed08	MZ	0.177		0.035	0.093
Oed11	UC	0.151	0.0271	0.055	
Oed13	UC	0.152			

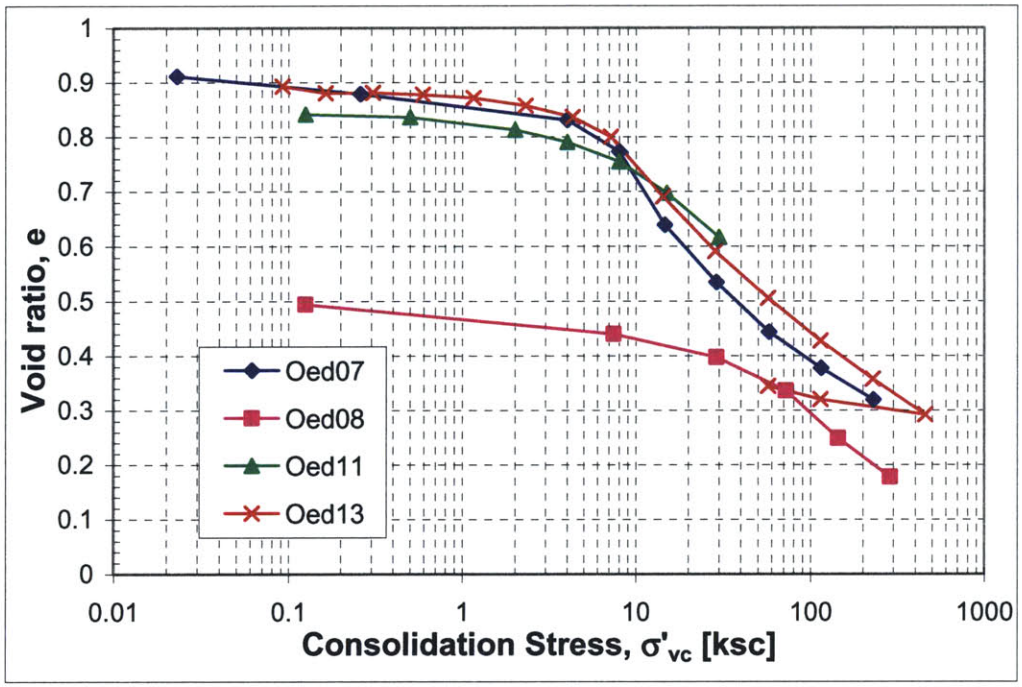

(a)

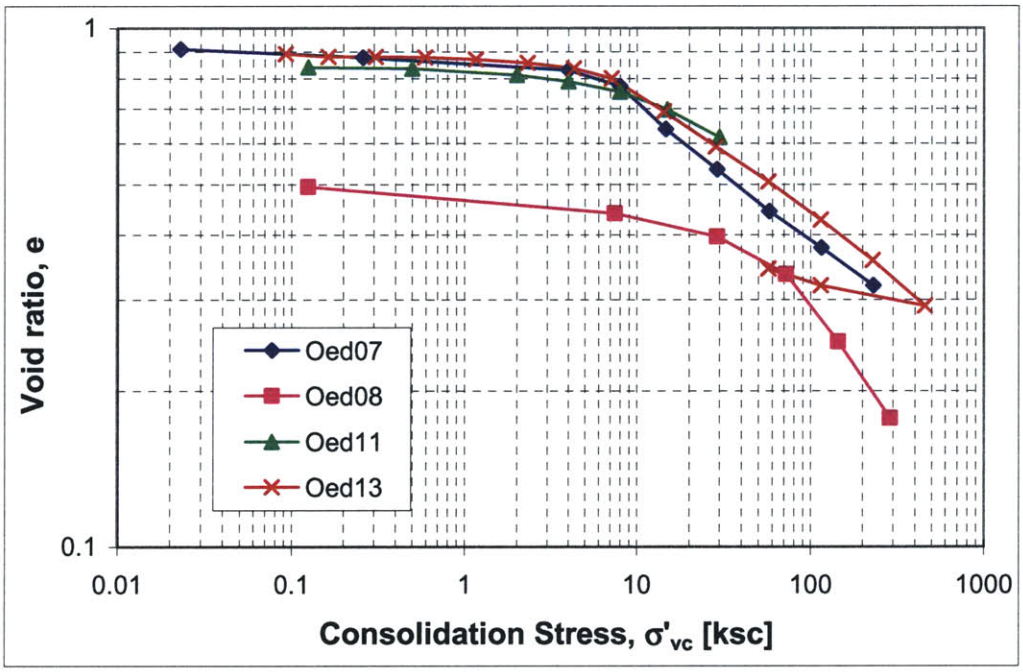

(b)

Figure 7-4. Consolidation curves e ~ logσ'_{vc} for the intact old alluvium.

It is now reasonable to conclude that the compressibility and swelling behavior of the old alluvium, as discussed above, are quite different from those of common sedimentary soils, such as Boston Blue Clay. This special behavior of the old alluvium is consistent with the characteristics of the soil microstructure and soil composition. In fact, it has been shown previously that the intact old alluvium contains expandable minerals of smectites which are cemented and aggregated by Fe-oxides. The Fe-oxides most probably consists of both a thin coating on clay mineral surfaces and bridge connections between clay particles or clay platelets. Therefore, the highly over-consolidated behavior (i.e., high OCR) of the old alluvium is caused by the strong cementation. As the soil is compressed, the cementation bonds are broken and the coatings can be cracked by the increased consolidation stress providing water access to the smectites. Subsequent unloading of the compressed samples allows expansion of the exposed smectite minerals and the soil swells. Furthermore, the higher stress the soil has subjected to, the more Fe-oxide bonds are destroyed and the greater the swelling of the soil exhibits. Therefore, the macroscopic response corresponding to these changes in the soil microstructure is that the soil can recover all the consolidation strain and even have a negative final strain. With the increased vertical consolidation stress, the magnitude of the swelling is increased even with reduced void ratio, showing an increasing in the swelling ratio.

7.3.3 Rate of Consolidation

Consolidation is the transient response of a soil subjected to a change in stress and describes the process of changes in deformation, effective stress and pore pressure over time. In the last section, the magnitude of compression or swelling was discussed without

taking into account of time. This section focuses on the transient process of the deformation or the rate of consolidation, which can be described by the coefficient of consolidation (c_v). The rate of consolidation is a function of the hydraulic conductivity and the compressibility (Lambe and Whitman, 1969). Therefore, the compressibility of the old alluvium and c_v will be used to investigate the hydraulic conductivity.

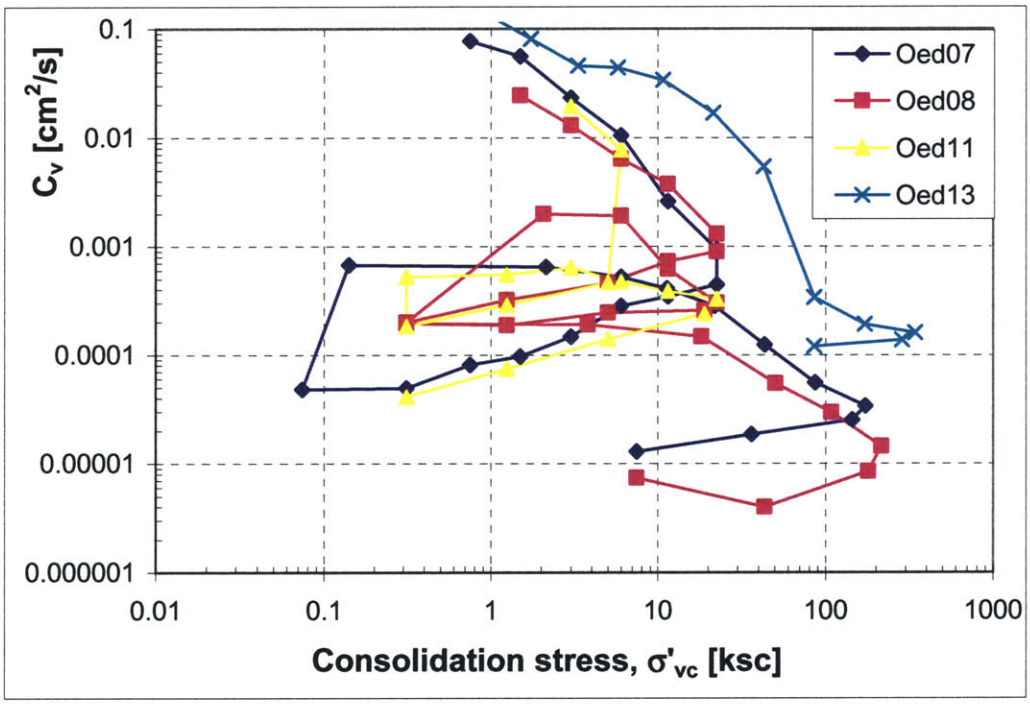

Figure 7-5. Coefficient of consolidation of the old alluvium measured by the 4 tests.

Coefficient of Consolidation (c_v)

Figure 7-5 summarizes the coefficient of consolidation of the old alluvium for the four consolidation tests. This figure contains the results from loading and unloading cycles. In order to clearly see the trends of c_v with consolidation stress, Figure 7-6 only plots the results of Oed07 performed on the UC sample. It should be pointed out that the

following discussion of results assumes that the sample is 100% saturated during the consolidation process after the specimen is inundated with water.

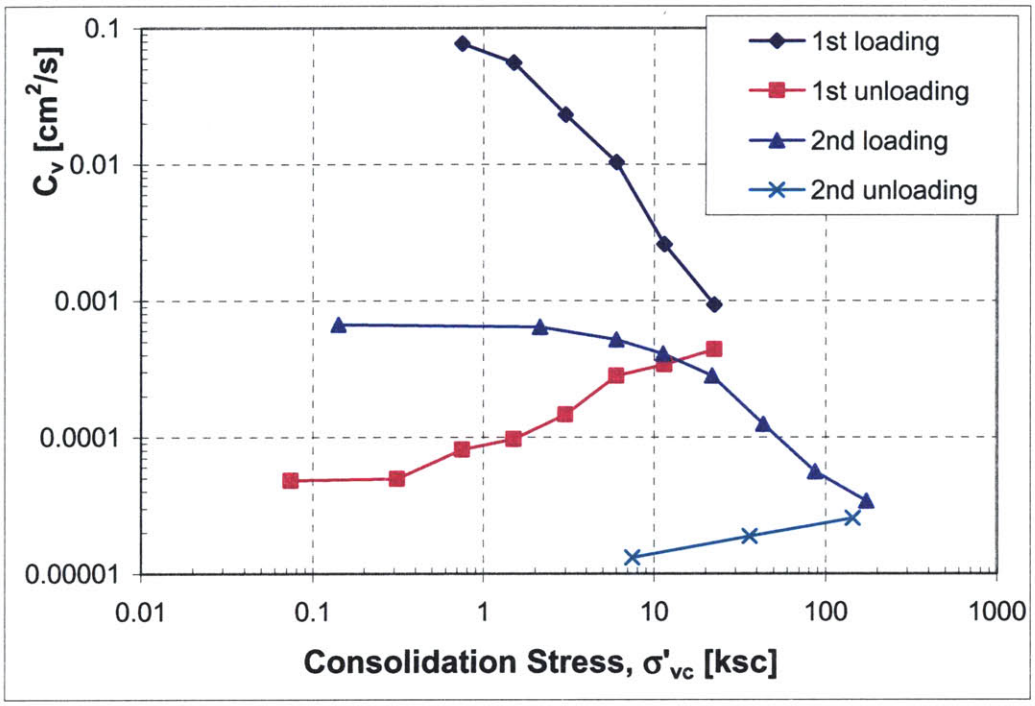

Figure 7-6. Coefficient of consolidation of the UC measured by Oed07.

The coefficient of consolidation, c_v shown with a logarithmical scale decreases dramatically with increasing consolidation stress. In fact, after the two unloading/reloading cycles with maximum consolidation stress of 200 ksc, the c_v of the intact UC sample has decreased by 4 orders of magnitude, compared to the first loading condition. Furthermore, each unloading sequence causes further decreasing in c_v. For the second unloading phase, c_v is not equal to the first unloading. In addition, after the soil is subjected to a cycle of unloading and reloading, c_v in the virgin compression line becomes even smaller than the extrapolation of the first loading trend in the virgin

loading stress. Therefore, c_v depends on both the consolidation stress and the imposed cyclic stress history.

Figure 7-5 compares the measured c_v from different tests. Clearly, Oed07 and Oed11 have similar results since they are followed the same loading stress path. Oed08 which was performed on MZ and started with a smaller initial void ratio, so Oed08 shows a smaller c_v than Oed07 at higher stresses. Nevertheless, the general trend of the changes of c_v is the same for all three tests except Oed13.

It is worthy pointing out the difference of the c_v measured by Oed13, which does not have unloading/reloading cycles. The values of c_v measured by Oed13 are always much higher than these by other tests with unloading/reloading cycles. Therefore, the results of Oed13 further approve that the changes of c_v significantly depend on the stress history.

The above observation on c_v is very different from that of common sedimentary soils. For a common sedimentary soil, c_v is almost a constant for the normally consolidated soils. Certain peats and highly organic soils may exhibit such behaviors (Ladd, 2001), but the mechanisms lying behind these macroscopic behaviors may be totally different.

Hydraulic Conductivity

As pointed out previously, c_v depends on both the compressibility and the hydraulic conductivity. To investigate the mechanisms which control the c_v changes during the loading cycles, it seems appropriate to examine the changes of hydraulic conductivity. The hydraulic conductivity (k) presented here is back calculated from c_v, based on the assumption that the soil is completely saturated. To date, there was no direct measurement on the hydraulic conductivity at various consolidation stresses and loading cycles to provide direct confirmation of the hydraulic conductivity.

Figure 7-7 shows the calculated hydraulic conductivity from the four tests plotted in e-logk space. The log hydraulic conductivity – void ratio is almost perfectly linear (constant slope, C_k) for Oed13 (Figure 7-7 (d)), which has no unloading – reloading cycles. For other 3 tests, unloading causes changes in the slope (C_k) of the e~logk curves. However, the C_k for loading, unloading, and reloading at the same stress level (i.e., with the same maximum past consolidation stress) is almost constant, as reflected by the parallel lines corresponding to loading, unloading, and reloading (see Figure 7-7 (b)). For example, in Figure 7-7 (a), at low stresses (σ'_{vc}<30ksc), the three lines corresponding to loading, unloading, and reloading are more or less parallel to each other (except one data point). The unloading line has the smallest C_k values, while reloading lies in the middle between the loading and unloading line; after this unloading and reloading cycle, subsequent loading changes the slope of the e~logk curves. This phenomenon is more apparent in Figure 7-7 (b), where the C_k parameter at high stresses is much greater than these at low stresses. The C_k values of the four tests are summarized in Table 7-5.

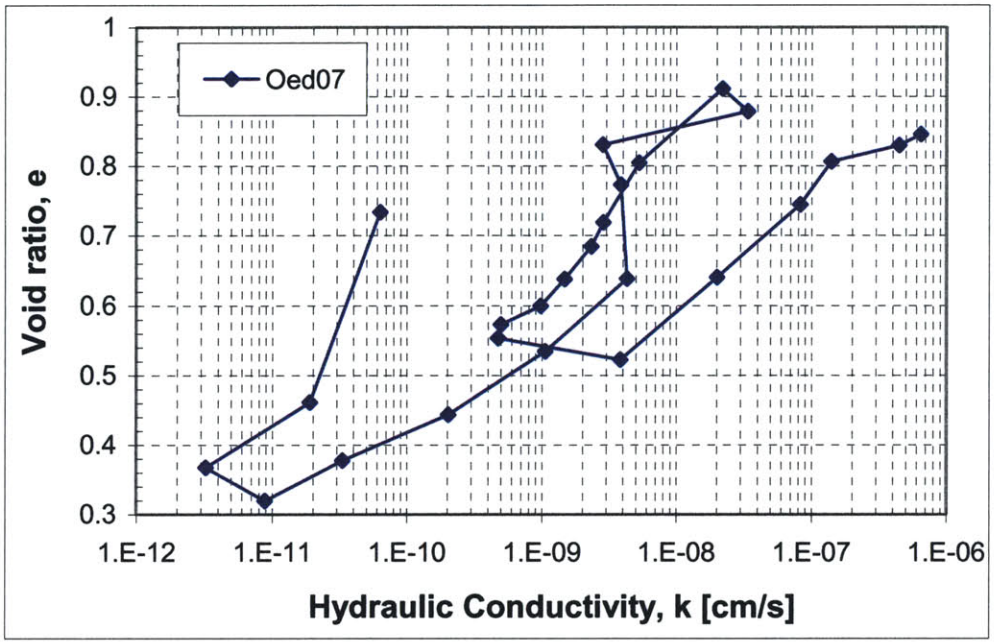

(a)

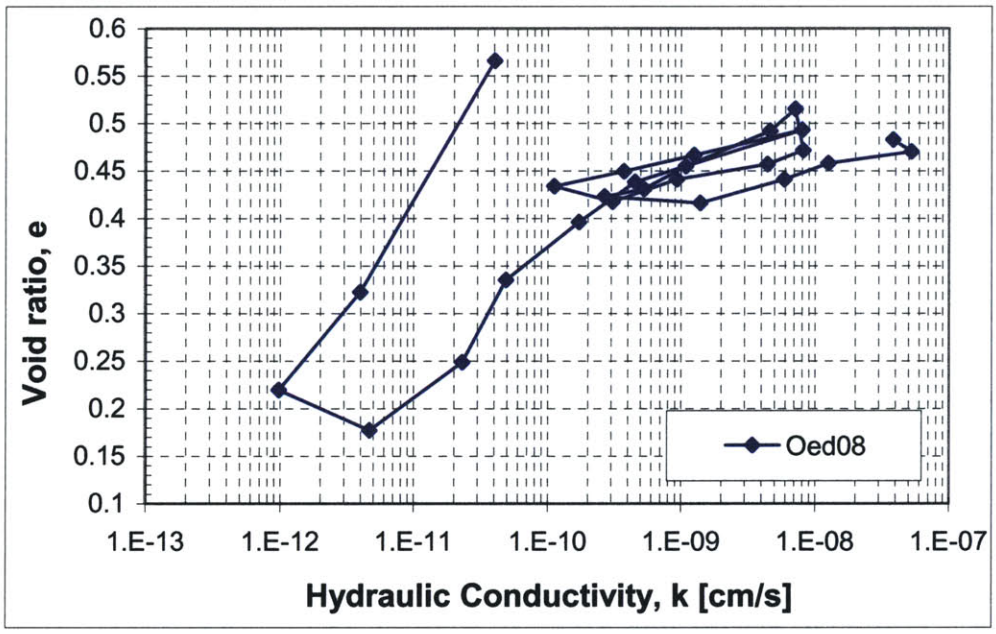

(b)

Figure 7-7. Hydraulic conductivity of the old alluvium calculated from the consolidation tests. (a) Oed07, UC; (b) Oed08, MZ.

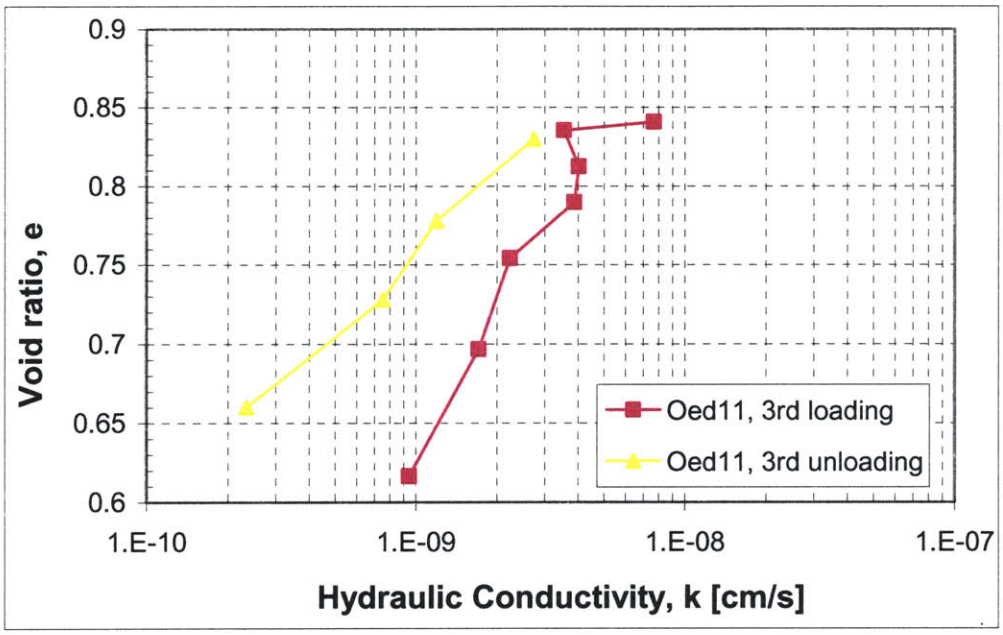

(c)

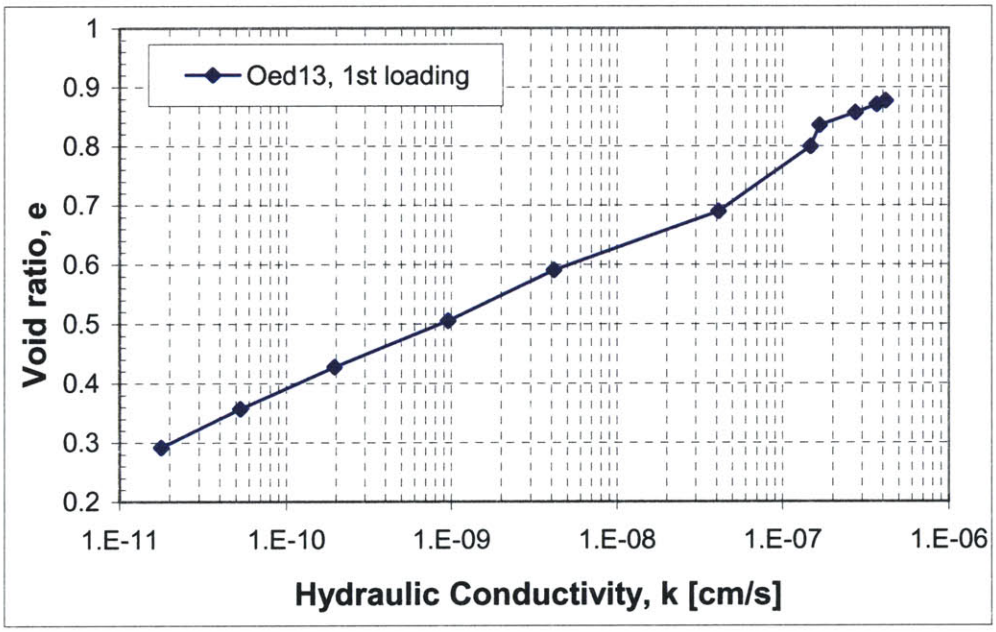

(d)

Figure 7-5. (continued) Hydraulic conductivity calculated from the four consolidation tests. (c) Oed11, UC; (d) Oed13, UC.

Table 7-5. The variations of C_k with different loading cycles.

Test ID#	Unloading cycles	C_k at 1st loading to σ'_{vc}=30ksc	C_k at 1st unloading σ'_{vc}<30ksc	C_k at 2nd loading to σ'_{vc}=30ksc	C_k at reloading to σ'_{vc}>30ksc
Oed07	Yes	0.17	0.175	0.17	0.095
Oed08	Yes	0.04	0.032	0.04	0.13
Oed11	Yes	0.283	0.162	No data	No data
Oed13	No	0.13	No unloading	No reloading	0.13

The hydraulic conductivity (k) decreases from $1.0x10^{-6}$ to $1.0x10^{-10}$ cm/s, with four orders of magnitude reduction. Furthermore, the cycles of unloading and reloading cause further reduction of the hydraulic conductivity. Table 7-6 summarizes the hydraulic conductivity at various stress levels. Clearly, the hydraulic conductivity depends on both the stress level and the stress history.

Table 7-6. The calculated hydraulic conductivity of the old alluvium at different stress levels.

Test ID#	K at 1st loading to 30 ksc [cm/s]	K at 2nd loading to 30 ksc [cm/s]	K at loading to 300 ksc [cm/s]
Oed07	$3.82x10^{-9}$	$1.06x10^{-9}$	$8.84x10^{-12}$
Oed08	$1.39x10^{-9}$	$1.71x10^{-10}$	$4.68x10^{-12}$
Oed11	$9.44x10^{-10}$		
Oed13	$4.17x10^{-7}$		$1.78x10^{-11}$

Discussion

So far, this section has presented the results about the rate of consolidation, including the coefficient of consolidation and the hydraulic conductivity. Although the behavior of the rate of consolidation of the old alluvium is different from that of sedimentary soils, the calculated permeability index C_k is a constant for the normal consolidation lines without the unloading cycles.

To explain the trends of the rate of consolidation, it is once again necessary to consider the possible changes in the soil microstructure during the consolidation tests with multiple unloading cycles. First of all, recall the features of the void space of the intact soil samples of the old alluvium. It has been found that the intact soil possesses a double porosity structure with interaggregate pores of 80-100μm. This larger interaggregate pores account for the higher in situ hydraulic conductivity and the initial high coefficient of consolidation.

During loading in the consolidation test, the increased stress destroys the cementation bonds between aggregates and breaks the coatings over smectite platelets, allowing access of water to smectite interlayer space and swelling of smectites. At this stage, a new force equilibrium is achieved between the applied consolidation stress and the swelling pressure of the smectites. If the former is greater than the latter, there is no swelling deformation observable macroscopically. However, the swelling of smectites tends to fill more or less the interaggregate pores and hence decreases the void ratio. In addition, the average grain size is decreasing significantly due to the breakdown of aggregates. Therefore, the hydraulic conductivity is decreasing dramatically. Without unloading, the interlocking between particles prevents smectites from swelling further and from filling all void space, since the smectite particles can not totally reorient under the applied stress due to the interlocking between particles or aggregates. Therefore, there is still some void space leaving unfilled and the soil still has potential for further reduction of the coefficient of consolidation.

The unloading process decreases the vertical consolidation stress and a new force equilibrium should be built under the decreased consolidation stress. The smectites tend to swell more and have more free degree of movement, and hence swelling fills more void space, which further decreases the hydraulic conductivity. Therefore, after unloading, the soil sample possesses a different microstructure with a great reduction of the void space and an expanded smectite interlayer space due to access to water. Subsequent reloading can break more cementation, reduce pore space more, and reorient the clay particles, resulting in further reduction of the hydraulic conductivity.

In addition, due to the finely divided particle size of Fe-oxides, the high gradient caused by the stress increment probably mobilizes the Fe-oxides particles which may stay in a new void space through the attraction forces between Fe-oxides and clays and clog the channels of water flow. The mobilization of Fe-oxides further decreases the hydraulic conductivity.

7.4 Triaxial Shear Behavior

7.4.1 Introduction

This section presents the triaxial shear behavior of the old alluvium. As pointed out previously, the measurement of triaxial shear behavior is not the main focus of this thesis. Furthermore, since all the triaxial tests presented in this section were performed before the characterization of the soil composition and soil structure, little attention was

paid to design a comprehensive triaxial testing program to measure the strength and deformation characteristics of the old alluvium. However, the main objective of these tests is to measure the strength and deformation characteristics of the *intact* soil of the old alluvium, i.e., the intact soil structure should be kept undisturbed or unchanged until actual shearing. These preliminary tests can provide basic strength and deformation parameters for the intact samples and give some rational basis for the future design of a systematic experimental program to investigate the strength and deformation characteristics. Table 7-7 lists all the triaxial tests performed on block samples of both UC and MZ, including 7 tests for MZ (with 2 unconfined compression) and 14 tests for UC.

Also listed in Table 7-7 are the initial water content and density of the block samples. These tests were performed on block samples taken from two boring sites (boring site B2 for MZ and site B7 for UC). The average water contents for boring sites B7 and B2 are 39.03±2.50% and 13.65±0.80%, respectively, while the average densities are 1.73±0.04 g/cm^3 and 1.98±0.03 g/cm^3. Therefore, as both the density and the initial water content are concerned, these block samples are quite homogeneous, and the variation in MZ (site B2) is even smaller than UC (site B7), though MZ is denser than UC and has much lower water content than UC. However, as seen later, the heterogeneity in macrostructure features discussed previously affects the strength measurement, but this is not reflected in density and water content measurements.

Table 7-7. Summary of all triaxial tests performed on both UC and MZ block samples.

Test ID#	Sample	Block sample ID#	Initial Water content [%]	Initial Density [g/cm^3]	Triaxial Cell#	Test type
TX510	UC	B7-U14	38.81	1.75	MIT05	CIUC(L)
TX511		B7-U12, sub1	38.72	1.73	MIT05	CIDC(U)
TX512		B7-U2, sub3	38.53	1.77	MIT05	CIDE(U)
TX513		B7-U2, sub2	38.20	1.77	MIT01	CIDC(L)
TX514		B7-U12, sub2	40.10	1.76	MIT05	CIDE(L)
TX516		B7-U9, sub1	39.96	1.72	MIT01	CIDE(U)
TX517		B7-U9, sub2	41.27	1.70	MIT01	CIDC(L)
TX518		B7-U9, sub3	40.23	1.67	MIT05	CIDC(U)
TX519		B7-U8, sub1	40.51	1.69	MIT01	CIDC(L)
TX520		B7-U8, sub2	39.02	1.68	MIT05	CIDE(L)
TX521		B7-U4, sub3	41.01	1.72	MIT01	CIDE(U)
TX522		B7-U4, sub2	42.31	1.69	MIT05	CIDE(L)
TX524		B7-U1, sub3	39.15	1.77	MIT05	CIDC(L)
TX525		B7-U1, sub1	35.10	1.77	MIT01	CIDC(L)
TX526		B7-U1, sub2	32.53	1.70	MIT01	CIDC(L)
		Average	39.03±2.5	1.73±0.04		
TX503	MZ	B2-S3, sub1	13.06	2.04	--	UC
TX504		B2-S3, sub2	13.06	1.96	--	UC
TX505		B2-S3, sub3	13.15	1.94	MIT01	CIUC(L)
TX506		B2-S1, sub5	13.68	1.98	MIT01	$CK_0UC(L)$
TX507		B2-S1, sub4	13.38	1.97	MIT01	CIDC(U)
TX508		B2-S1, sub3	13.90	1.96	MIT01	CIDE(U)
TX509		B2-S1, sub2	15.30	2.00	MIT05	CIDE(L)
		Average	13.65±0.80	1.98±0.03		

* The location of these block samples can be found in Table 3-3.

Table 7-8. Summary of control parameters for all triaxial tests.

Test ID#	Sample	Test Type	Back Pressure [ksc]	Pre-shear B Value	Pre-shear Effective Stress [ksc]	Post-shear Water Content [%]
TX505	MZ	CIUC(L)	2.2	0.65	1.8	16.20
TX506		$CK_0UC(L)$	2.97	0.69	13.1*	16.82
TX507		CIDC(U)	2.78	0.51	1.68	17.90
TX508		CIDE(U)	2.77	0.63	1.73	17.68
TX509		CIDE(L)	2.50	0.62	1.90	17.89
TX510	UC	CIUC(L)	2.95	0.84	1.85	41.85
TX511		CIDC(U)	2.80	0.87	2.00	43.96
TX512		CIDE(U)	2.80	1.02	2.00	40.20
TX513		CIDC(L)	2.55	0.87	1.95	38.35
TX514		CIDE(L)	2.96	0.77	1.84	39.61
TX517		CIDC(L)	2.55	0.92	1.95	40.74
TX518		CIDC(U)	2.76	0.74	2.04	44.31
TX519		CIDC(L)	2.10	0.94	1.90	40.91
TX520		CIDE(L)	2.74	0.82	2.06	43.05
TX521		CIDE(U)	2.06	0.92	1.94	41.53
TX522		CIDE(L)	2.70	0.84	1.80	45.33
TX524		CIDC(L)	2.44	0.97	1.96	34.64
TX525		CIDC(L)	2.53	1.01	1.87	36.31
TX526		CIDC(L)	2.59	0.89	1.81	38.47

* Vertical consolidation stress for CK_0UC.

In addition to special procedures for specimen preparation, special attention was also paid to control the triaxial tests in order to prevent the intact specimen from any possible disturbance or destructuring before shearing. Table 7-8 lists all the testing conditions to preserve the intact soil structure.

Generally, the strength measurement of common sedimentary soils requires the K_0 consolidation to certain stress level. For the structured soils with high sensitivity, the recompression technique is preferred, while for most soft sedimentary soils with low sensitivity, the SHANSEP has more advantages than the recompression method. It has been shown in Chapter 6 that this old alluvium possesses a high degree of cementation, i.e., this soil is structured. Therefore, all tests were performed unconsolidated drained in order to investigate the failure envelope, except two undrained shear tests and one K_0 consolidated undrained shear test. If the soil is consolidated to a stress level which is greater than the yielding stress, then the intact soil structure will be destroyed and the subsequent shearing will give a much lower strength measurement.

In addition, it has been found from the only one K_0 consolidated undrained shear test TX506 that the stress level required to K_0 consolidate the specimen to the virgin compression line exceeds the stress limits of the MIT low-stress triaxial cells, which can also be seen from the consolidation test results. Therefore, to measure the shear strength of the intact soil, no K_0 or isotropic consolidation beyond the yielding stress is preferred before shearing.

From Table 7-8, all tests have a pre-shear effective stress around 1.8-2.0 ksc. The following lists the reasons why such effective stress was chosen:

- As the protection of the intact soil structure is concerned, a pre-shear effective stress should not be too high in order to avoid destroying the cementation in the soil structure;
- Due to the presence of smectites and small disturbance to the outer surface layer of the specimen caused by cutting and trimming, smaller pre-shear effective stresses are unable to prevent swelling of smectites and hence, the effect of swelling on the shear strength measurement cannot be minimized.
- Based on the results of consolidation tests discussed in Section 7.3, it has been found that the stress which can prevent the swelling (only limited swelling) of the oedometer specimens is 1.8 ksc for MZ and 2.0 ksc for UC. Therefore, the pre-shear effective stress is chosen as 1.8-2.0 ksc for both layers.

Nevertheless, for each test, attention was paid to the observation of the initial axial deformation (swelling) of the triaxial specimen when the back pressure saturation was started. If any noticeable swelling occurred, then the saturation process was stopped and the pre-shear effective stress was increased until no further swelling was noticed. Therefore, slightly variations in the pre-shear effective stress of these triaxial tests may exist, as shown in Table 7-8.

Another important point is the measured B value. As shown in Table 7-8 and Figure 7-8, the B values are quite low for MZ and erratic for UC. It is reasonable to measure a low B value if the high stiffness and density of the MZ layer are considered. Since B-value is mainly a function of the stiffness of the soil skeleton, the smoothness of

the specimen surface (also known as membrane penetration effect), it is not surprising that B-value for UC is quite erratic. However, if drained shearing is considered, a B-value greater than 0.8 should suffice.

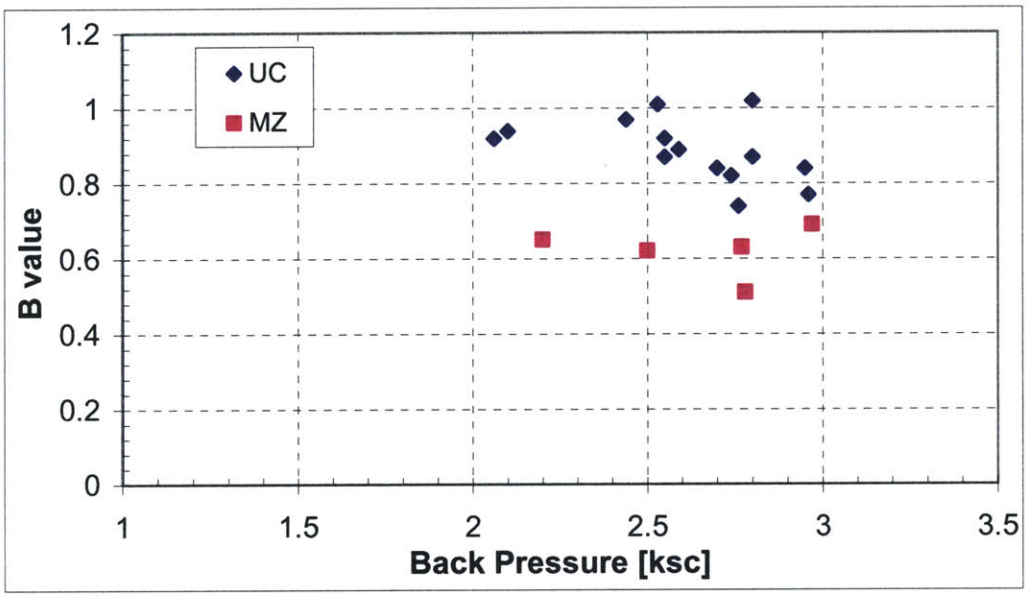

Figure 7-8. Relationship between back pressure and B value.

7.4.2 UC test results

Failure Envelope

Figure 7-9 shows the stress paths of all 14 triaxial tests performed on the intact UC samples. It is first noted that variations exist between measurements on different specimens. For example, TX513, TX517, and TX519 follow the same stress path of drained compression loading, but they fail at different shear stress. Careful examination of the specimens after the testing found that the lowest shear strength obtained by TX513 is caused by the coincidence of a plane with white veins with the failure plane. Nevertheless, discarding tests where preferred failure occurred due to macrostructure

heterogeneity, the failure envelope for both compression and extension seems quite reasonable.

Table 7-9. The strength measurements of the intact UC samples.

Test ID#	p′ [ksc]	q [ksc]
TX518	1.06	0.67
TX511	1.46	0.83
TX510	2.13	1.24
TX525	2.34	1.18
TX524	3.97	1.98
TX512	1.28	-0.75
TX520	1.43	-0.70
TX522	1.51	-0.97
TX521	3.51	-1.49
TX514	3.63	-1.74

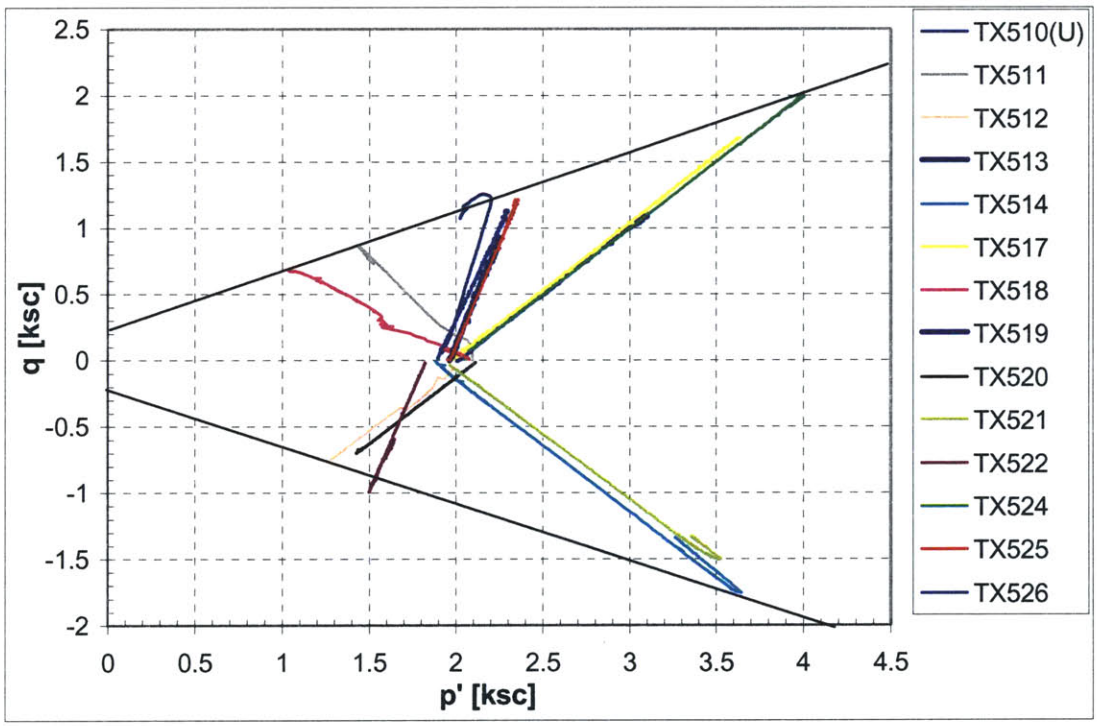

Figure 7-9. Stress paths for 14 triaxial tests performed on intact UC Samples.

Table 7-9 lists all the reasonable failure strength measurements. From Figure 7-9, it appears that the intact UC soil has isotropic strength parameters, as indicated by the nearly equal friction angles and cohesions for compression and extension shear modes. This isotropy may be attributed to effects of cementation introduced to the old alluvium through tropical weathering. Therefore, according to these data shown in Table 7-9, a simple linear regression gives the failure envelop as $q = a' + p' \tan\alpha'$, where $a' = 0.24$ and $\alpha' = 22.3^{\circ}$ with $r^2 = 0.95$. Table 7-10 lists the measured Mohr-Coulomb parameters of the UC layer.

Although the heterogeneity is one possible reason for the variations of the shear strength, there are maybe other factors affecting the measurement of the shear strength, such as the possible disturbance introduced from sampling, cutting, and trimming; the possible anisotropy in the macrostructure; and the inappropriate testing procedures (e.g., saturation).

Table 7-10. Mohr-Coulomb parameters of the intact samples of the old alluvium.

Samples	a′ [ksc]	c′ [ksc]	α′ [°]	ϕ' [°]
UC	0.24	0.26	22.3	24.2
MZ	0.175	0.24	32.5	39.5

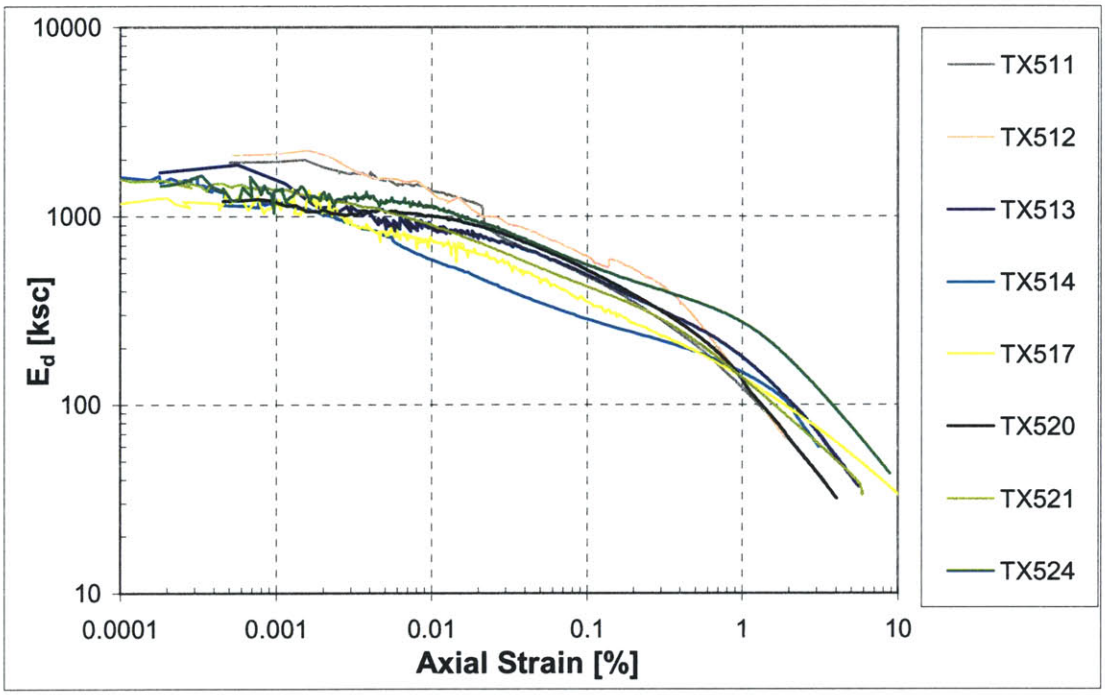

Figure 7-10. The Young's modulus of intact UC samples.

Deformation Chatacteristics

Figure 7-10 plots the measured Young's modulus of the intact UC sample. For the small strain levels (ε = 0.001% to 0.01%), variations between different stress paths are very small. The average small-strain modulus is about 1800 ksc, while the range is from 1100 ksc to 2000 ksc. Since the sample orientation is lost, the variation between compression and extension is unknown. The results also show that the yielding strain is approximately 1% for all tests, indicating that yielding may be controlled by cementation. Furthermore, for the strain level from 0.01% to 1%, the modulus is decreasing approximately linearly.

Figure 7-11 shows the stress-strain relationship of the intact UC. There are significant variations between tests following the same stress path. For example, both TX517 and TX524 follow the path of drained compression loading, but the difference of the stress-strain curves between these two tests cannot be neglected, which is possibly caused by the heterogeneity of the intact soil sample.

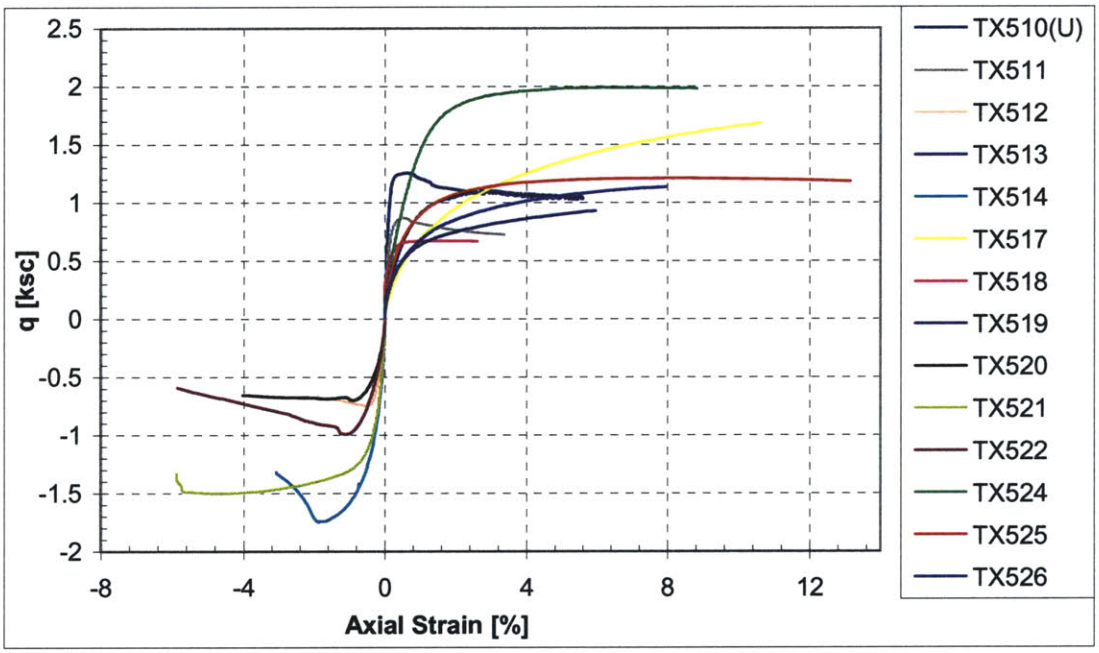

Figure 7-11. The stress-strain relationship of UC samples.

For the volume change behavior, as shown in Figure 7-12, there is no observable dilation for the stress paths of both compression loading and extension loading. Since the effective confining stress, which was chosen to protect the initial soil structure is very low, and the failure is brittle due to cementation in microstructure and is only localized along the failure plane, the drained shearing will not destroy the majority of the cementation and coatings in the soil. Therefore, no observable swelling from smectites

occurs, resulting in a measured contraction for these loading tests and a small amount of dilation for these unloading tests.

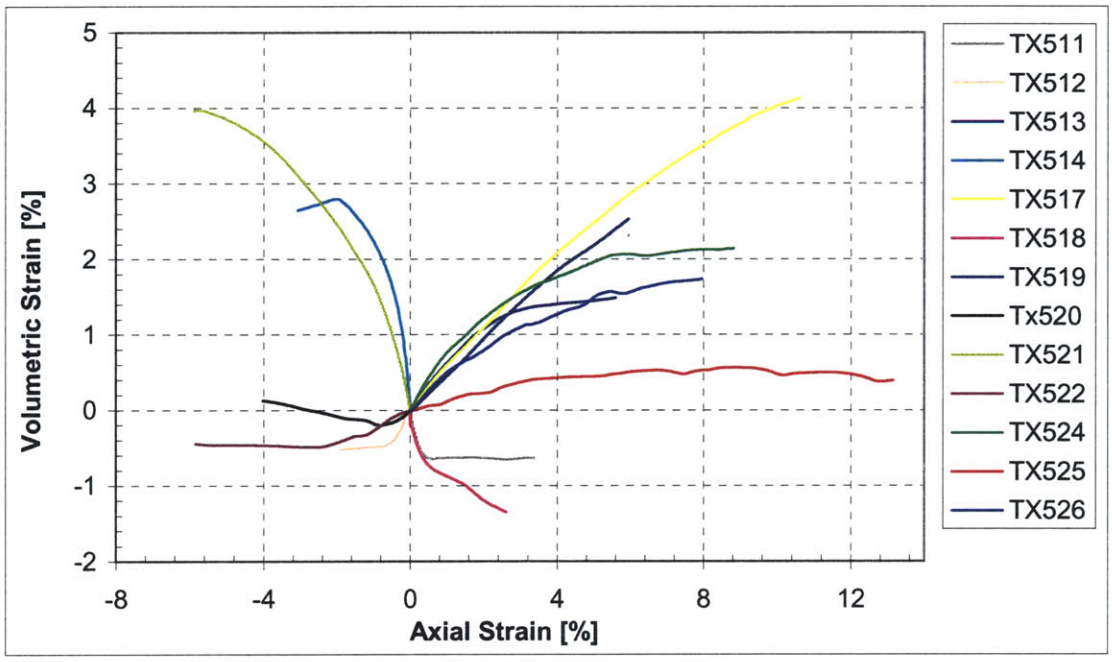

Figure 7-12. Volumetric strain following different stress paths.

7.4.3 MZ test results

Failure Envelope

Figure 7-13 plots the stress paths for the five triaxial tests performed on intact MZ. The test TX506 should be excluded in the consideration of the intact shear strength of the MZ layer, since the Ko consolidation implemented in TX506 significantly destroy the intact soil structure. With only three drained test results available, it is surprising that the failure envelope in the compression mode is almost symmetrical about the p′ axis to the extension mode. Table 7-11 summarizes the strength parameters at failure. A simple linear regression of these data shown in Table 7-11 gives the isotropic failure envelop as

$q = a' + p' \tan\alpha'$, where $a' = 0.175$ and $\alpha' = 32.5^{\circ}$ with $r^2 = 0.99999$. The corresponding Mohr-Coulomb parameters are also listed in Table 7-10. Therefore, it can be concluded that both the UC and MZ have isotropic strength parameters.

Table 7-11. Strength parameters of the intact MZ samples measured by drained shear.

Test ID#	p′ [ksc]	q [ksc]
TX507	1.89	1.38
TX508	1.11	-0.88
TX509	3.78	-2.58

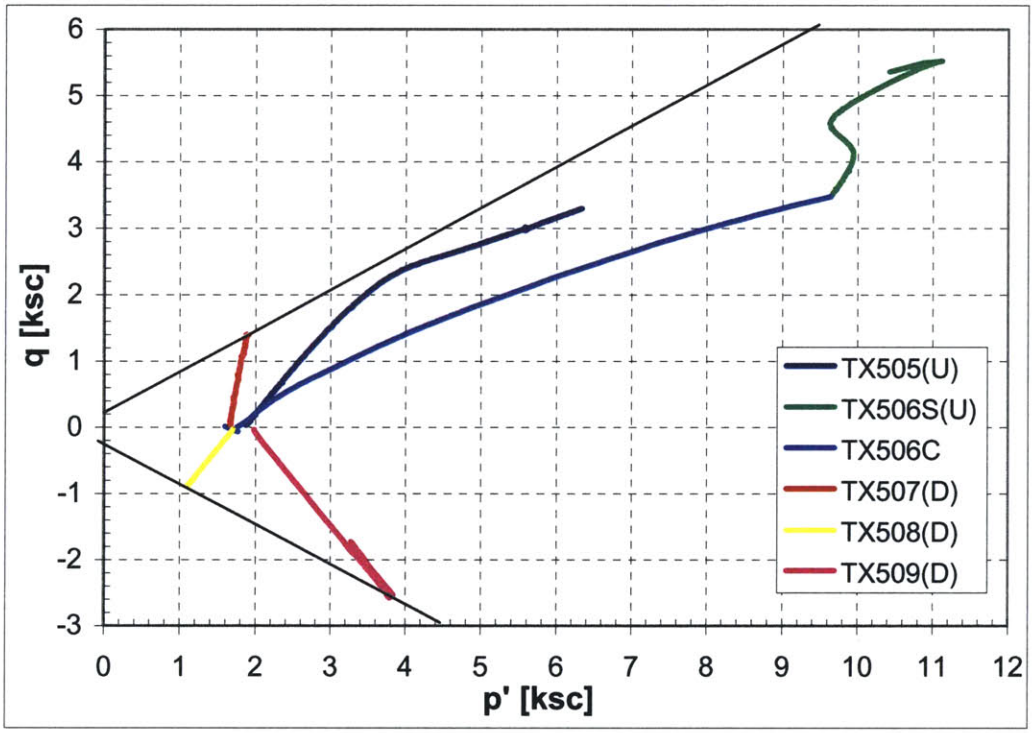

Figure 7-13. Stress paths for MZ soil.

It is interesting to compare the shear strength parameters between the UC and MZ. For compression, the intact UC and MZ have approximately the same cohesion, while the MZ soil has a much higher friction angle (39.5°) than that (24.2°) of the UC.

The approximately equal cohesion for both UC and MZ is caused by the same Fe-oxide cementation. In fact, the UC layer has more Fe-oxides than the MZ, which may give a little bit higher cohesion. The MZ is much denser than UC (see Table 7-7 for the densities of UC and MZ samples), and contains a greater percentage of coarse-grained particles, it is certain that MZ soil should have a higher friction angle than UC. Therefore, It can be concluded that the two layers have approximately the same apparent cohesion (although UC may have a little bit higher cohesion) and the MZ have a higher friction angle than UC. Furthermore, both layers have isotropic strength parameters.

Deformation Characteristics

The measured Young's modulus of intact MZ is summarized in Figure 7-14. Except the CK_0UC test TX506, all other three tests have almost the sample initial stiffness until the strain reaches 0.1%. Of course, the intact soil structure is destroyed by the K_0 consolidation to σ'_{vc}=13.11 ksc. Although the initial modulus of TX506 is much higher than others, the normalized modulus E/σ'_{vc} is 385 ksc, which is much smaller than that of normalized modulus of other tests, i.e., E/σ'_c = 1500ksc/1.8= 833 ksc. Since consolidating the intact soil to a higher stress destroys the cementation in the intact soil structure, it is reasonable to expect a lower initial stiffness than the intact soil. This is quite different from sedimentary soils, which generally give higher stiffness after K_0 consolidation.

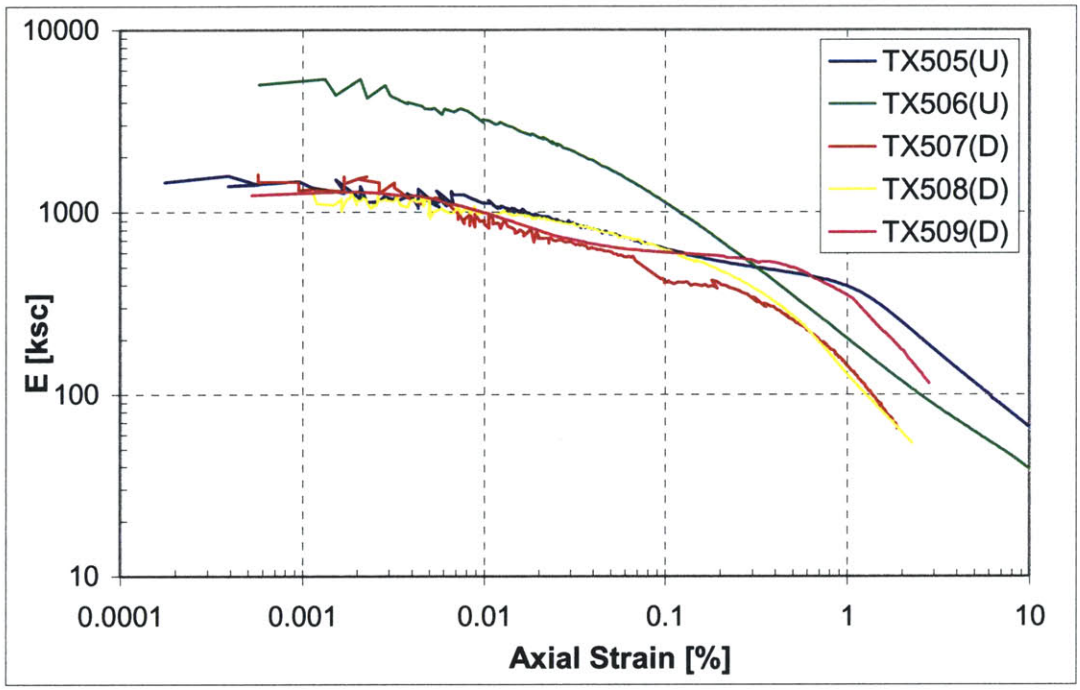

Figure 7-14. Young's modulus of the intact MZ soil.

After the axial strain reaches 0.1%, the brittle cementation may be broken down and hence the soil behaves as a particulate material or common sedimentary soils. Therefore, the Young's modulus starts to show difference in the plot, which means that the mean effective stress or the stress path starts to influence the stiffness. In addition, Figure 7-14 does show the correct trend of the modulus change when the axial strain is greater than 0.1%, i.e., TX509 has a higher modulus than both TX507 and TX508. It should be pointed out that the initial stiffness of intact MZ is almost the same as that of intact UC, despite MZ has higher density than UC.

There are not too many things new about the stress-strain relationships, as shown in Figure 7-15. Basically, due to the brittle cementation, drained shearing gives the soil brittle failure, and failure planes were also observed on undrained shearing.

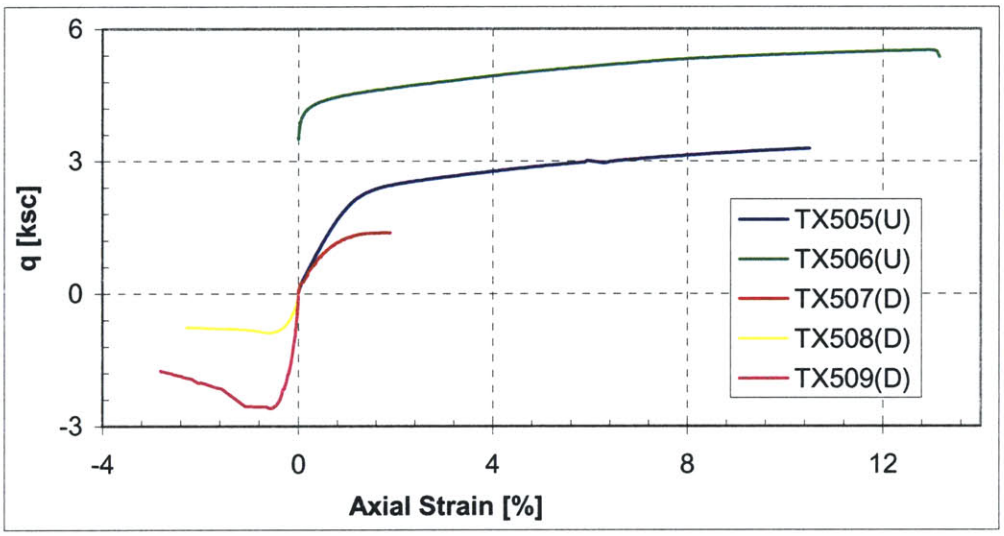

Figure 7-15. Stress-strain relationship of MZ soil.

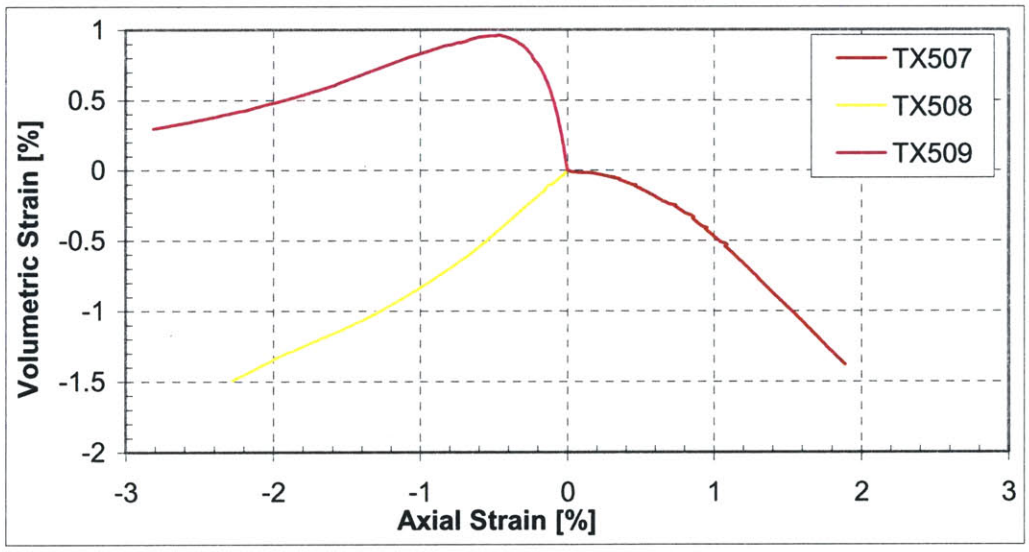

Figure 7-16. The volumetric strain measured by the drained triaxial tests.

The volume change behavior is presented in Figure 7-16 for the drained tests. It is expected that dilation occurs in the unloading tests, such as TX507 and TX508. For the extension loading test TX509, the specimen starts to dilate after the strain reaches –0.5%. As discussed for the volume change of the UC, the low confining stress will not break down too much coatings, the dilation may only be caused by the higher density of MZ sample and not from the swelling of smectites.

For the two undrained shear tests, TX505 and TX506, Figure 7-17 shows the pore pressure response during undrained shearing. Since TX506 has a much higher consolidation stress than TX505, the negative pore pressure increasing rate of the former is much smaller than the latter. In TX506, the negative pore pressure may not generate too much through the swelling of smectites, but largely through the shearing induced dilation. It is important to notice that the stress level is not high enough to obtain the normally consolidated behavior.

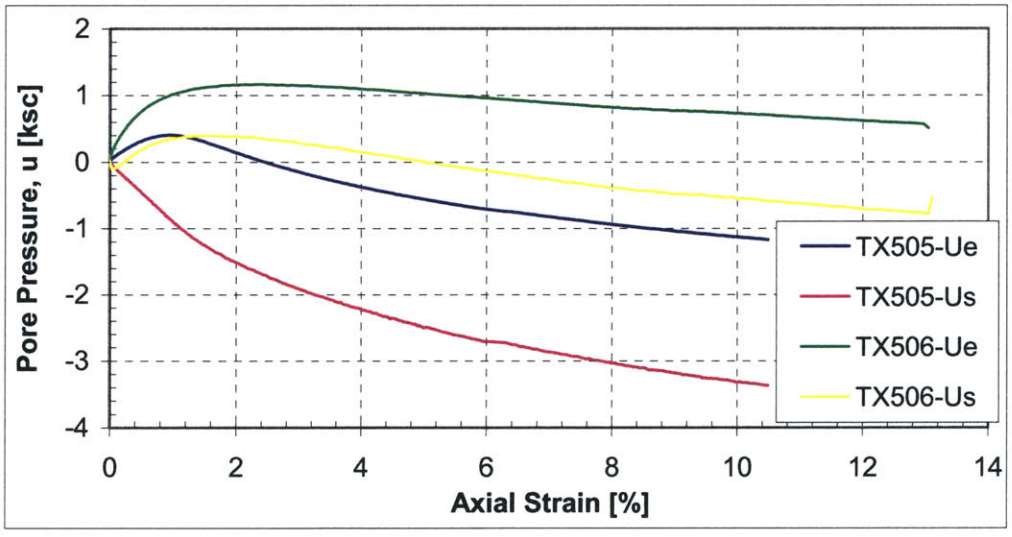

Figure 7-17. The pore pressure measured by the two undrained shear tests on MZ samples.

References

Da Re, G. (2000) *Physical Mechanisms Controlling the Prefailure Stress-Strain Behavior of Frozen Sand.* Ph.D. Thesis, MIT, Cambridge, MA.

Germaine, J.T. and Ladd, C.C. (1988) Triaxial testing of saturated cohesive soils. In: R.T. Donaghe, R.C. Chaney, and M.L. Silver (eds.), *Advanced Triaxial Testing of Soil and Rock, ASTM STP 977*, 421-459.

Ladd, C.C. (2001) *Soil Behavior Class Notes.*

Lambe, T.W. (1951) *Soil Testing for Engineers.* John Wiley & Sons, Inc., New York. 165pp.

Lambe T.W. and Whitman, R.V. (1969) *Soil Mechanics.* John Wiley & Sons, Inc., 553pp.

Leroueil, S., Kabbaj, M., Tavenas, F., and Bouchard, R. (1985) Stress-strain-strain rate relation for the compressibility of sensitive natural clays. *Geotechnique*, **35** (2), 159-180.

Santagata, M.C. (1998) Factors Affecting the Initial Stiffness and Stiffness degradation of cohesive soils. Ph.D. Thesis, MIT, Cambridge, MA.

Sheahan, T.C., Germaine, J.T., and Ladd, C.C. (1990) Automated triaxial testing of soft clays: an updated commercial system. ASTM Geotechnical Testing Journal, 13(3), 153-163.

Pestana, J.M. (1994) *A Unified Constitutive Model for Clays and Sands.* D.Sc. Thesis, MIT, Cambridge, MA, USA.

Pestana, J.M. and Whittle, A.J. (1995) Compression model for cohesionless soils. *Geotechnique*, **45** (4), 611-631.

Chapter 8 SUMMARY, CONCLUSIONS, AND RECOMMENDATIONS

8.1 Summary

The main goal of this research was to characterize the highly weathered old alluvium in San Juan and to provide better understanding of its unusual engineering properties. This has been achieved through an extensive experimental research program to investigate its soil mineralogy, structure, index properties, and engineering behavior.

The present-day old alluvium of San Juan deposited in early Pleistocene has undergone intensive post-depositional weathering under the tropical marine climate of Puerto Rico. This original coarse-grained deposit derived from volcanic rocks, intrusive rocks, and sedimentary rocks in the central mountainous province of the Puerto Rico island has decomposed through tropical weathering, and the old alluvium now consists dominantly of clayey or silty soils with red or brown mottling and white inclusions. Therefore, this deposit is a residual soil with an alluvial origin.

Geotechnical site investigations found that the old alluvium is stiff and brittle and contains quart sand grains. Simple visual observation indicated that the material consists mainly of sand or silt grains, which is misleading for identification. In addition, remolding the material between fingers causes a textual change and the material feels like a plastic clay. The deposit has a depth of 25-30m and is underlain by limestone. The basic subdivision of the deposit based on engineering site investigation reports consists of three

main layers: Upper Clay (UC), Middle Zone (MZ), or Lower Sand (LS). The striking characteristics of the deposit is that the soil color is bright red or brown in UC while yellowish brown or gray in MZ.

For this weathered old alluvium, it is necessary to analyze the soil composition and soil microstructure in order to obtain a thorough appreciation of its engineering properties. Therefore, both qualitative and quantitative mineralogical analyses have been performed using a series of analytical techniques, consisting of X-ray diffraction, thermal analysis, and chemical analysis by X-ray fluorescence, and other approaches of soil analysis, such as cation exchange capacity, pH, dissolution of Fe-oxides, etc. Results show that the old alluvium contains both primary minerals and neoformed secondary ones. The former, inherited mainly from the parent rocks, are weathering resistant so that they can exist in the old alluvium. They are quartz, muscovite, and orthoclase (a K-feldspar). The latter include mainly kaolinite and smectites as clay minerals and Fe-oxides (including hydroxides) as special fine-grained minerals. The MZ also contains illite and pyrophyllite, two other clay minerals in minor fractions. The presence of smectites (not previously detected in this material) - an expandable clay mineral, is the major concern of geotechnical engineers. Nontronite (Fe-rich) is the principal species of smectites in UC while MZ has both nontronite and montmorillonite. The soil color is mainly caused by two Fe-oxides, i.e., the red color is from hematite while the brown and yellowish from goethite.

Following the qualitative analysis, the main mineral phases were further quantified. The results of quantitative analysis yield a reasonably high accuracy for both the UC and MZ layers, i.e., all individual phases sum up to 94.3% and 95.4% of the bulk UC and MZ samples, respectively. In addition, the two major primary minerals, quartz and orthoclase, are more abundant in the MZ than UC, while the UC has more kaolinites, smectites, and Fe-oxides than the MZ, indicating that UC is more weathered than MZ. The results also prove that various methods can be combined to quantify a soil mixture of various mineral phases and to provide enough accuracy for the analysis.

Features of the intact soil structure have been characterized in both macroscopic and microscopic levels. The macrostructure was determined mainly through visual observations. First of all, the material looks like granular in texture if observed with the naked eye. The stratification, typical of alluvial deposits, gives the old alluvium heterogeneity at large scale. Even though the long-term weathering and alteration tend to homogenize the deposit by converting sands and gravels into clays and oxides, depositional stratification and sand pockets and lenses can still be observed on the soil profile. In addition, the soil formation processes introduce reticulated white venations to the deposit, which strengthen the heterogeneity of the soil. These white venations are caused by localized weathering with surface acid water percolation along shrinkage or collapsing cracks, and root paths. Therefore, difficulties arise with the identified heterogeneity of macrostructure in strength measurement and large scale characterizations.

The microstructure of the old alluvium was characterized with both direct and indirect methods. The former consists of SEM/ESEM and simple visual observations, while the latter include slaking, CEC, and selective chemical dissolution with particle size analysis. The results positively show that those visually looked-like sand or silt grains are indeed aggregates (50-100μm), which are made of clay platelets (10-20μm), which in turn are groups of clay particles (~2μm) associated with face to face contacts. The cementation and aggregation agents were identified as Fe-oxides by selective chemical dissolution and subsequent particle size analysis. Furthermore, by ESEM observations, Fe-oxides act as both coatings over clay platelets and aggregates and bridge bonding between aggregates. This was further proved by slake tests in water and glycerol, the stiff behavior of the soil mass, and CEC measurement. The Fe-oxides cementation and coatings hide the physical and chemical properties of the clay particles and hence, the smectites cannot swell and the intact soil is stable when inundated with water. In addition, the large (50-100μm) interaggregate pore spaces were observed directly under ESEM, accounting for the high in situ hydraulic conductivity.

Index properties, including particle size analysis (PSA) and Atterberg limits, were determined with various pretreatment methods, e.g., remolding energy, drying, and chemical dispersants (for PSA only). The results showed that Fe-oxides cause both cementation and aggregation, whose corresponding disintegration methods resemble both mechanical and chemical dispersions, respectively. For both UC and MZ, a completely dispersed suspension can only be obtained by a combination of chemical dispersions (i.e., adding dispersants) and mechanical energy (to break interparticle bonds). On the other

hand, a stable colloidal suspension cannot be obtained by only using mechanical energy either, since the electrical attraction forces between Fe-oxides and clay minerals cannot be canceled without dispersants. The experiments also showed that ($NaPO_3$) and $Na_4P_2O_7$ are the most effective dispersants and function equally well for this old alluvium. Furthermore, drying significantly changes the soil structure and some physical-chemical properties. Air-drying causes complete mechanical dispersion, while chemical dispersion is still needed to achieve a stable dispersion of the old alluvium. However, oven-drying results in re-generation of interparticle bonds and is not an effective method to disperse the soil.

In addition to particle size distribution, the variation of Atterberg limits was also evaluated by varying remolding energy and drying conditions. Results show that the liquid limit increases significantly with remolding energy, while the plastic limit decreases slightly, resulting in increasing in plasticity index and toughness. The increasing of liquid limit with remolding energy is due to the increased external surface area of the dispersed soil, while the decreasing of plastic limit is caused by the release of water entrapped inside the aggregates and the water absorbed in the smectite interlayer. The changes of both limits caused by air-drying or oven-drying are the combined effect of disintegration/dispersion, losing interlayered water (thus less bias on W_p), decreased plasticity of smectites (certain smectites are not easily rehydrated after oven-drying), and the dehydration of Fe-oxides (which causes stronger bond between clay particles).

The engineering properties of the old alluvium are the great interests of engineers. Both consolidation and triaxial shear behavior were investigated for the intact material. During consolidation, some rather uncommon results were obtained, which include: (1) exceptionally high apparent preconsolidation pressures for both the UC and MZ layers; (2) the consolidation strain can be completely recovered after unloading; (3) the swelling ratio is not constant for multiple unloading/reloading cycles and increases with maximum past consolidation pressures; (4) c_v decreases by 4 orders of magnitude; and (5) permeability index C_k is constant for monotonic loading but changes with unloading/reloading cycles. All these uncommon consolidation behavior reflects the alteration of soil microstructure caused by loading or unloading. These macroscopic engineering properties can also be used to interpret the characteristics of microstructure explored by other direct methods.

Finally, the triaxial shear behavior of the old alluvium was studied on intact soils, i.e., soils with intact structure just before shearing. Results found that cementation gives a constant cohesion c' for both UC and MZ and the old alluvium has isotropic strength and deformation characteristics. However, due to the fact that the MZ layer has more sand fraction than UC and the size of these sand particles in MZ is greater than UC, MZ has a much higher effective friction angle than UC. In addition, the strong cementation gives the soil high stiffness and brittle failure mode. On the other hand, the white venations along old cracks have weaker cementation and cause difficulty in obtaining consistent measurement on shear strength and stiffness, especially for the UC layer.

8.2 Practical Engineering Implications

Based on above analyses, the old alluvium is a residual soil with alluvial origin, possessing unusual combination of soil mineralogy and structure. The former includes expandable clay mineral smectites, mineral quartz with high hardness, and iron oxides as cementing and aggregation agents. The latter includes white venations and layering in macroscopic scale and cementation and aggregation in microscopic scale. It is quite different from common sedimentary soils by its color, mineralogy, and structure, and thus provides challenges to geotechnical engineers ranging from classification and identification, to undisturbed sampling, to laboratory testing, to the interpretation of engineering properties, to soil modeling, and to field construction. As discussed below, it has some important engineering implications for geotechnical engineers.

Identification and Classification

Iron oxides cause cementation of all particle sizes and aggregation of clay particles. Fe-oxide aggregation causes difficulty in field identification and classification, since the aggregated clay particles look like sand or silt grains and are quite stable and rigid. That is why this kind of residual soil is called pseudo-silt /sand by soil scientists. Moreover, as Kaye (1959) stated, in many places within the deposit, the original sand and gravel texture and their outer grain boundaries are still apparent to the eye in spite of the advanced state of alteration. As a result of aggregation and originally granular texture of the deposit, a classification and identification based on only simple visual observations may be misleading.

In practice, such soil structure requires special techniques to break down the cementation and aggregation bonds during field identification and laboratory classification. If the intrinsic behavior of the material is desired, air-drying or long-time blending is recommended for the Atterberg limits measurements and particle size analysis (which also requires a proper dispersant).

Undisturbed Sampling

The stiff and brittle consistency of the intact soil and the quartz grains cause difficulty in sampling. It is hard to obtain undisturbed samples for this material. Only large block samples are recommended for strength testing, which can be obtained by using the casing method (Fookes, 1997). Sample disturbance appears to break inter-aggregate cementation, causing the material to flow like cohesionless loose sands. Field tube sampling has found low recovery and extreme disturbance to the samples, which was confirmed by using X-ray radiography on samples recovered. In addition, quartz causes problems of sampling due to its high hardness and hence, a good cutting tool with carbide-tipped blade is required to take samples.

Laboratory Testing

Since drying causes destructuring, dried sample swells when water is available. Therefore, during sample preparation, drying should be minimized. As for cutting and trimming, careful attention should be paid to the disturbance due to its structural brittleness. However, the presence of quartz requires carbide-tipped blades to cut the large block samples into small pieces. Moreover, the membrane used in triaxial cell can

easily be pierced by sharp quartz sands. Some remediation methods, such as patching a thin layer of silt paste have been used.

Soil Properties

The soils with iron oxides generally posses a double porosity, which consists of larger inter-aggregate pores (in μm scale) and smaller intra-aggregate pores (in 0.1 μm scale). Thus, the in situ hydraulic conductivity of residual soils rich in iron oxides is generally very high. For the old alluvium, the field-measured coefficient of hydraulic conductivity is 4~10 x 10^{-4} cm/s (USDA, 1978; CSTS, 1996) even if it consists mostly of clay particles. This is attributed to the aggregation caused by iron oxides.

As for the soil plasticity, intensive remolding of the soils breaks down aggregates and coatings, thus increases soil plasticity. This is important when relating laboratory testing procedures to construction operations. Field operations of excavation, transport, and placement are unlikely to break down completely all aggregates to the extent that plasticity is affected. The degree of working required to prepare laboratory specimens for Atterberg limits determination is, by comparison, very much greater. The plasticity of the construction material may thus be lower than would appear from the standard Atterberg or other laboratory tests in remolded samples.

Design and Construction

The heterogeneity of the old alluvium introduced by the alluvial deposition and the localized weathering along the cracks and root paths presents the most challenging work

on how to take the heterogeneity into account and to determine soil parameters for engineering design. It has been found that the material has a weak strength if failure occurs along the white veins during triaxial testing. The variability is furthered strengthened by the depositional variation, both vertically and horizontally. Therefore, for this soil, geotechnical engineers must be cautious to the weak bands associated with the white venations formed by localized weathering along previous cracks.

Regarding the tunneling methods used in the construction of Tren Urbano, open cut and cover is not recommended for tunnel construction, since drying is more serious in open excavation. For any other methods, excessive drying should be avoided. Besides, any destructuring by machine disturbance or stress changes should be minimized. Therefore, it is critical to choose the best construction method in field.

The presence of quartz sands with very high hardness also causes problems of construction, since construction tools can be quickly worn down during excavation. In addition, iron oxides introduce construction problems. After remolding, wet soils rich in iron oxides are very sticky and may adhere to steel plate or tools and the bodies of dump trucks, thus making excavation and transportation difficult and ineffective. This special property is attributed to the very fine crystalline particles (10-100nm) and the surface properties of iron oxides (Stucki et al, 1985).

8.3 Conclusions and Contributions

In summary, the following conclusions can be drawn:

- The old alluvium has undergone intensive post-depositional weathering, as reflected by its composition and structure, and can be classified as a special residual soil – either transported residual soil with alluvial origin or highly weathered old alluvium. The soil has a very unusual combination of mineralogy and soil structure.
- The geologic origin and soil formation process have great influences on the behavior and properties of the old alluvium since special soil minerals and structure are formed during weathering process.
- soil composition,
    - Soil minerals in two layers of the old alluvium were determined both qualitatively and quantitatively;
    - One smectite species, nontronite, is present in the UC, while both nontronite and montmorillonite are present in the MZ;
    - Only three most weathering resistant primary minerals are left after weathering;
    - Special colorful Fe-oxides give the soil red, brown, and yellowish colors.
- Soil structure
    - Heterogeneity existing in macroscopic structure has great influence to engineering concerns such as design and construction, soil modeling, and laboratory measurements;
    - Fe-oxides act as both cementation and aggregation agents, most likely, hematite causes aggregation, while goethite cementation;
    - Fe-oxide coatings hide swelling and CEC of clays, and prevent complete dispersion of the soil mass

- Index properties
    - Intrinsic particle size distribution can only be obtained by using both a suitable dispersant and high mechanical energy;
    - Atterberg limits change with drying and remolding energy, W_p is biased by the water inside the aggregates and the water in the smectite interlayer.
- Consolidation behavior
    - Cementation gives a high preconsolidation stress;
    - Swelling ratio increases with maximum past pressure;
    - C_v decreases rapidly if the soil is destructured and compressed and water is available for smectite swelling
    - C_v depends on stress history and unloading/reloading cycles
- Triaxial shear behavior
    - Intact soil has very high stiffness;
    - The shear strength can be reasonably represented by the Mohr-Coulomb strength envelope.
    - The two layers (UC and MZ) have similar apparent effective cohesion, c', but MZ has a higher effective friction angle;
    - Strength and deformation behavior are affected by heterogeneity in macrostructure.
- The soil minerals and structure formed during the weathering process present much difficulty to engineering practice, ranging from sampling, identification and classification, laboratory testing, modeling, engineering design to construction activities.

- Integration of origin, formation, mineralogy, and soil structure should be able to give a clear appreciation to the soil behavior and engineering properties. In turn, the measurement on engineering properties can also be used to deduct information about the soil structure.

The following simply lists the contributions the thesis can provide by conducting this experimental research:

- Completely characterized a highly weathered old alluvium by using materials microcharacterization techniques, soil analyses, and geotechnical laboratory;
- Accumulated a coherent set of direct and indirect approaches for soil microstructure characterization;
- Proposed a conceptual soil fabric model which is developed from real soil mineralogy and soil microstructure;
- Developed new laboratory techniques for trimming and testing of such intact materials with quartz grains;
- For the first time, applied simple experiments (such as slaking and grain size analysis) to evaluate and separate the effects of cementation and aggregation by Fe-oxides;
- The effect of drying and the difference between air-drying and oven-drying were systematically summarized and rationalized;
- Evaluated a series of chemical and mechanical dispersion methods and recommended a method to obtain the intrinsic particle size distribution;

- Provided a clear interpretation of the unusual consolidation properties of the soil based on its composition and microstructure;
- Explained the isotropic strength and stiffness of an residual soil based on its microstructure cementation.

8.4 Recommendations for Future Research

Although this thesis has conducted an extensive experimental study on the material characteristics and engineering properties of the old alluvium in San Juan and has contributed fundamentally to the understanding of its behavior and engineering properties, the effort and time on these two aspects are not well balanced since, of course, much more knowledge on the consolidation and shear behavior could be obtained if more measurements had been performed and more data were available. In addition, more approaches and experiments could be conducted to achieve more information on the microcharacteristics. Due to the time limit, it is not possible to investigate all problems and to answer every question which may arise from this old alluvium. Definitely, there is a need for further research on this old alluvium in order to broaden and deepen the current understanding, which can be divided into three directions: soil composition and structure; index and physico-chemical properties; and engineering properties.

Soil Composition and Soil Structure

Nothing much can be done to gain more data on the soil mineralogy, since the results presented in this thesis are quite comprehensive, at least for engineering practice. Adding one or two more techniques to the soil mineralogical analysis will only improve

the accuracy. Therefore, no further new research is recommended to analyze the soil composition. However, all data presented in this thesis only focuses on two depths in the soil profile. By following the same experimental program and applying similar techniques, future research can perform such mineralogical analysis on samples from other depths or other sites in the old alluvium so that the variation of soil composition along depth or at different locations can be evaluated.

Although the soil microstructure is conceptually well understood in this thesis, much more can still be done to confirm the current understanding. These include: (1) measurements of the effective specific surface area (SSA) on intact and disturbed samples, which can be used to assess the effect of Fe-oxides coatings over clay surfaces; (2) using different selective chemical dissolution techniques to dissolve and remove one phase (i.e., either hematite or goethite) each time, to better understand which one causes cementation and which one causes aggregation. The DCB treatment presented in this thesis removes both phases; (3) examining with ESEM the samples which has been previously consolidated to a high stress to approve the microstructure alteration and swelling caused by mechanical destructuring; and (4) direct measurement of porosity on intact and destructured samples.

Index and Physical-Chemical Properties

For particle size analysis, there is no need to evaluate other dispersants. However, other mechanical dispersion methods, such as compaction with varying efforts, ultrasound vibration, etc., merit investigation. Especially, the results obtained from

compaction have significant practical implications for the old alluvium when it is used as fill or earth dam construction material.

All Atterberg limits measured in this study reflect the effect of mechanical dispersion. Therefore, future research can try to change the chemistry of pore water simply by adding some salts or dispersants (with varying concentrations). The alteration of pore water chemistry has a sound practical basis. For instance, if this old alluvium is to be used as the foundation soil or the barrier for a waste repository, leaching of chemicals from the waste will change the pore water chemistry, and thus the Atterberg limits.

Engineering Properties

As mentioned previously, a thorough investigation into the engineering properties of the old alluvium is not the main objective of this thesis. Therefore, more results are desired on the engineering properties of the old alluvium and for building a constitutive model for this soil in the future.

For compressibility, more incremental loading tests can be performed to measure the variations. In addition, more complex loading histories can be applied to examine the possible particle reorientation after destructuring and swelling, since the particle reorientation is a key factor for understanding the mechanism that permeability changes between unloading and reloading at the same stress level. Furthermore, an important experiment is the direct measurement of the hydraulic conductivity during the process of

consolidation. The results can be used to interpret the significant decreasing of c_v with increasing consolidation stress and with unloading/reloading cycles.

The verification of the degree of saturation during incremental loading is critical for understanding the dramatic decrease of c_v during consolidation. It is highly recommended to acquire the direct evidence of the complete saturation of oedometer specimens. The constant rate of strain (CRS) consolidation can provide a complete saturation to the speciment, but only a small strain rate is applicable.

For shear strength and deformation characteristics, a systematic experimental program needs to be designed to investigate both the intact and destructured soils. For example, strength can be measured on samples either having the same consolidation stress but different vertical strains (on virgin compression line, swelling line, or recompression line); or having the same vertical strain but different stresses on different part of the consolidation curves. By comparing the variations of strength on intact and partially destructured soils, the strength loss caused by construction disturbance in field or sampling disturbance can be evaluated. Furthermore, destructuring can also be introduced by pre-shearing the specimen to different strain levels.

References

Bain, D.C. and Smith, B.F.L. (1987) Chemical analysis. In: *A Handbook of Determinative Methods in Clay Mineralogy* (edited by M. J. Wilson). Blackie & Son Limited.

Blight, G.E. (ed.) (1997) *Mechanics of Residual Soils*. A. A. Balkema, Rotterdam.

CSTC (Caribbean Soil Testing Co., Inc.), 1996. *Geotechnical Data Report* – Rio Piedras Contract.

Deere, D.U. (1955) *Engineering properties of the Pleistocene and recent sediments of the San Juan Bay area, Puerto Rico*. Ph.D. thesis, University of Illinois Urbana.

Fookes, P.G. (ed.) (1997) *Tropical Residual Soils*. Geological Society Professional Handbooks. The Geological Society, London.

Kaye, C.A. (1959) *Coastal Geology of Puerto Rico: (A) Geology of the San Juan metropolitan area.* Geological Survey Professional Paper 317. US Government Printing Office, Washington.

Martin, R.T. (2000) Personal communication.

Mitchell, J.K. (1993) *Fundamentals of Soil Behavior*. 2nd edition. John Wiley & Sons, Inc.

SSL – Soil Survey Laboratory (1996) *Soil Survey Laboratory Methods Manual*. Soil survey investigations report No. 42, Version 3.0.

WCC (Woodward Clyde Consulting, Inc.) (1997) *Geotechnical Data Report* – Rio Piedras Contract.

Wilson, M.J. (ed.) (1987) *A Handbook of Determinative Methods in Clay Mineralogy*. Blackie & Son Ltd.

Wilson, M.J. (1999) The origin and formation of clay minerals in soils: past, present and future perspectives. *Clay Minerals*, **34**, 7-25.

APPENDIX

A NOVEL SAMPLE MOUNTING METHOD FOR RANDOM POWDER X-RAY DIFFRACTION

Guoping Zhang, John T. Germaine*, R. Torrence Martin[+], Andrew J. Whittle**
*Department of Civil and Environmental Engineering,
Massachusetts Institute of Technology, Cambridge, MA 02139, USA
[+]Ardaman & Associates, Inc., Orlando, FL 32809, USA

ABSTRACT -- This paper describes a novel sample mounting method for random powder X-ray diffraction (XRD), namely the Razor Tamped Surface (RTS) method, which involves tamping the loose powder using the sharp edge of a razor blade on a sample holder modified to fit to a vertical axis diffractometer. The RTS method was evaluated experimentally using four kaolinites with different crystallinity and a quartz powder (<44μm) by comparing with other published sample mounting methods which do not require addition of foreign minerals or adhesives to the sample powder, including front-loading, back-loading, and side-loading. XRD patterns show that the RTS method produces minimum packing density in the powder mount and always has minimum preferred orientation for both kaolinites and quartz, as exhibited by the orientation indices, I(002)/I(020), I(001)/I(060), and I(002)/I(060) for kaolinites and I(100)/I(101) for the quartz powder. In addition, the reproducibility of the RTS method was evaluated using one of the four kaolinites. The mechanism by which the RTS method reduces preferred orientation is explained by showing that the width of the blade edge is smaller than or in the same range as the size of clay particles and hence the platy particles are seldom orientated perpendicularly to the compression direction. The quartz powder used

in this study does exhibit a tendency for preferred orientation which can be minimized by RTS method. The advantages and disadvantages of RTS method over side-loading are also discussed.

Key Words --- Crystallinity, Kaolinite, Preferred Orientation, Quartz, Random Powder, X-Ray Diffraction.

INTRODUCTION

In mineralogical analysis, X-ray diffraction (XRD) is a very basic and powerful technique for both qualitative phase identification and quantitative estimation of mineral fraction. Though oriented aggregates, which enhance the basal reflection of platy clay minerals, are the most effective method to identify clay minerals, in many cases, random powder is still needed for both qualitative and quantitative characterization of detailed mineralogy, such as measurement of crystal unit cell dimensions and quantification of certain minerals. For example, random powder must be used to differentiate completely dioctohedral from trioctohedral subgroups of clay minerals by (060) reflections (Brown & Brindley, 1980; Moore & Reynolds, 1997). In fact, achieving true random orientation has been a long-term goal in powder XRD practice and "one of the long-standing problems" (Bish & Reynolds, 1989). However, just as perfect orientation can never be

obtained, complete randomness in a powder mount is equally elusive, especially for platy shaped particles prone to preferential orientation.

Significant research effort has been devoted to develop robust and simple techniques to achieve random orientation in a powder mount. The various methods can be divided into two broad categories: (1) techniques without the need for pretreatment of the powder itself; and (2) techniques requiring either pretreatment of the powder or adding foreign minerals or adhesives to the powder or the sample holder. The former consists of several mounting methods, including front-loading, back-loading, and side-loading, in which the powder is pressed into a cavity from various directions referenced to the examined surface. The latter includes: (a) pretreating the sample powder to form small agglomerates containing randomly oriented particles, such as freeze-drying (Moore & Reynolds, 1997) and spray-drying (Jonas & Kuykendall, 1966; Hughes & Bohor, 1970; Calvert *et al.*, 1982; Hillier, 1999); (b) adding adhesives to the sample holder so that particles stick to the surface with random orientation, such as adding gelatin solution to the sample holder (Barwood, 2000) or smearing grease on the slide (Brown & Brindley, 1980); (c) adding different filling materials to the sample powder to reduce preferred orientation, *e.g.*, embedding the sample in a thermoplastic organic cement (Brindley & Kurtossy, 1961; Hinckley, 1963) or mixing clay with powdered cork (Wilson, 1987), corundum (Hillier, 1999), or glass beads; and (d) making a clay suspension in acetone instead of water to reduce preferred orientation by decreasing the surface tension of the suspension fluid for small amount (10-15 mg) of sample (Paterson *et al.*, 1986). As

pointed out by Brown & Brindley (1980, p.311), these more elaborate methods are tiresome for routine work. Certain methods require special equipment which may not be available commercially. Again, as one problem is solved, another problem arises. For example, embedding clay in an organic cement contaminates the sample and reduces the mass absorption coefficient of the mixture resulting in significant shifts of peak position in a thick sample which is known as "transparency effects" (Klug & Alexander, 1974; Bish & Reynolds, 1989).

Without doubt, the front-loading achieved by pressing powder into a cavity in the sample holder will produce preferred orientation of particles with platy shape or pronounced cleavage parallel to the surface of the sample holder. Back-loading and side-loading have been shown to reduce preferred orientation. Klug & Alexander (1974, p.372-374) described a back-loading method in detail. For side-loading, McMurdie *et al.* (1986) and Moore & Reynolds (1997, p.222) provided much detail on how to pack a powder mount from the side. After reviewing a series of techniques for preparing a random powder mount, Brindley (1980, p.427) concluded that the side-packed holder is probably the best simple technique available.

However, though all sorts of sample preparation techniques were reviewed in literature, *e.g.*, Brindley (1980) and Bish & Reynolds (1989), there is no publication which provides quantitative comparison and qualification of all techniques. This study

focuses only on these simple techniques without any pretreatment or contamination to the powder itself.

Kaolinites have platy-shaped particles with size ranging from 0.1 to 4 μm (Mitchell, 1993) and generally tend to have preferred orientation during sample packing. Therefore, they are good materials for evaluation of a sample preparation method for random orientation. In fact, Brindley & Kurtossy (1961) found in a quantitative analysis that the degree of orientation of kaolinites is high for well-crystallized samples and diminishes for the poor-crystallized. To quantify the degree of preferred orientation, they proposed an orientation index (OI) for clay minerals as

$$\text{OI} = \frac{\text{Intensity of a suitable basal reflection, } 00l}{\text{Intensity of a non-basal, prism reflection, } 060}$$

in which l = 1 or 2. Orientation increases I(001) and I(002), but reduces I(060). As basal plane orientation increases, the OI ratio increases rapidly. Therefore, the ratios of I(001)/I(060) and I(002)/I(060) give a quantitative measurement of the degree of orientation. Though another prism reflection, (020), gives diffuse scattering for kaolinites with layer stacking disorder (Brindley & Kurtossy, 1961), it occurs in the same angular range as the (001) and (002) reflections, and the ratio of I(002)/I(020) can still be used as an indicator of the degree of preferred orientation for kaolinites with less disorder.

Quartz grains generally exhibit conchoidal fracture and occur as anhedral particles. It is commonly believed that quartz shows little or no tendency for preferred orientation. Therefore, quartz is seldom used as a material to assess a sample preparation method for random orientation. However, Eslinger *et al.* (1973) found that the ratio of the intensities of the two strongest peaks (100) and (101), *i.e.*, I(100)/I(101), obtained from thin suspensions sedimented onto glass slides varies from 0.12 to 28.5. They attributed the difference to preferred orientation of authigenic quartz, which tends to form well-developed (100) prism faces. Furthermore, Krinsley & Smalley (1973) showed that the relative magnitude of fracture and cleavage in quartz is a function of grain size. For grains >500 μm, fracture predominates over cleavage, while cleavage is dominant on those <50 μm in diameter. Therefore, some quartz powder with certain grain size and origin may have tendency for preferred orientation, though it is much less prone to have preferred orientation than kaolinite.

This paper presents a novel simple mechanical technique to prepare random powder for XRD analysis, and assesses this method experimentally by comparing the degree of orientation with front-loading, back-loading, and side-loading methods using the OI defined above. Both kaolinite, a mineral inclined to preferred orientation, and quartz which is much less susceptible to preferential orientation were chosen to prepare random powder to verify that the new method does produce random orientation more effectively than other methods. Since a razor blade is used to tamp the powder to form a special packing surface, it is named the Razor Tamped Surface (RTS) method. Indeed,

this method has been used in a horizontal axis diffractometer at MIT for more than 20 years by one of the authors, R. T. Martin. This paper presents the newest technique applicable to a diffractometer with vertical axis.

EXPERIMENTAL

Materials

Both platy-shaped kaolinite and anhedral quartz were selected to perform XRD analysis. Four essentially pure kaolinites with different crystallinity were used for random powder diffraction, including two from the Clay Minerals Society Source Clay Repository, namely KGa-1b (Washington, Georgia) and KGa-2 (Warren, Georgia), and two with unknown origin from the MIT Geotechnical Laboratory which are labeled as Peerless #2 and Grim Calibration, respectively. Since KGa-1b and KGa-2 are widely used in practice, the results from this research can be compared with others in literature. Due to its low crystal defect, KGa-1b is chosen to measure the reproducibility of the RTS method. Also, a pure quartz powder (<44 μm) with unknown origin was used to prepare both random powder and oriented aggregates for XRD analysis.

Sample Mounting Methods

Samples were prepared for random powder XRD, using the three widely used sample mounting methods (front-loading, back-loading, and side-loading) and the novel RTS method. Here front-loading means simply pressing the powder into the cavity with a glass slide by applying a normal force and shear motion to make smooth and flat the

surface of the powder mount. The back-loading method described in Klug & Alexander (1974, p.372-274) was adopted here. For side loading, one side of the window in the holder is removed so that powder can be loaded from that side. The procedures of McMurdie *et al.* (1986) and Moore and Reynolds (1997, p.222) were followed to load the powder from the side. During this investigation, it was found that side-packing the powder into the holder in 3 to 4 layers helps to make a more homogeneous mount, therefore, the sample was packed with several layers. It is worth pointing out that, during this investigation, a frosted glass slide is placed facing the powder mount for both side-loading and back-loading to prevent the platy clay particles from orientating against the smooth surface of the glass slide.

The "standard" specimen holder provided by the manufacturer is used by the RTS method. It is a rectangular aluminum plate with dimensions 50.2 X 32.2 X 1.6 mm containing a rectangular window having size 20.0 X 18.0 X 1.6 mm which holds the powder. Preliminary examination found that the powder mount is relatively loose and tends to fall out of the cavity in whole in a diffractometer with vertical axis if a clean glass slide is used on the back of the holder to support the powder. To give the powder more adhesion to the holder, a piece of double-sided sticky tape was used to glue the glass slide to the sample holder and to provide certain adhesion to the powder. Furthermore, it has been found that the RTS-prepared powder mount gains more stability if the four sides of the cavity are tapered toward the back surface (Figure 1).

The procedures of mounting the powder by the RTS method are as follows:

1. Cut from a microscope slide a piece of glass having size slightly larger than the empty window in the aluminum holder. Cover it with a piece of double-sided sticky tape, and then stick it to the back of the window to form a cavity with front surface open (Figure 1).
2. After mixed on a clean glass plate with a razor blade to remove any pre-existed orientation, the powder is transferred without any free falling height into the cavity with a razor blade. Add more powder until it piles up 3-5 mm above the holder surface.
3. Tamp gently the powder (40-50 times) in random directions with a razor blade to cause initial compaction and more uniform packing in the cavity. Pay attention to hold the blade totally vertical (in both up and down motion) to eliminate any shearing motion along the holder surface (Figure 2(a)).
4. Tamp gently the powder once again along one direction, but follow a different motion path, in which the blade is moved downward straight and lifted upward at an angle of 30-45 degrees to the vertical (Figure 3). Some excess powder can be removed by moving the blade across the cavity from the center toward the two edges (Figure 2(b)-(c)).
5. Blow across the surface of the holder to remove the loose surplus by keeping the holder horizontal with a distance of half a meter away. Do not try to remove all loose surplus at one time. Never try to slice off the surplus powder with a razor blade.

6. Repeat steps 4 and 5 in alternate directions to remove all loose surplus until a flat and relatively smooth surface appears on the powder mount (Figure 2(d)).

In addition to the random powder prepared by these mounting methods, two oriented aggregates of quartz powder (<44 μm), one thin and one thick, were prepared by drying a dilute quartz suspension (0.5g powder in 50 ml water) onto a glass slide. The thin layer aggregate was obtained by drying a few drops of suspension on a slide, while the thick one was prepared by dropping suspension 3 times on a slide after the former drops were totally dried.

X-ray Powder Diffraction

XRD patterns were obtained in a Rigaku Rotaflex 180mm diffractometer with a graphite diffracted beam monochromator, using CuKα radiation generated at 18 kW (60kV, 300mA), a continuous scanning range of 2-64° 2θ, 1° DS and SS, 0.3mm RS, scan speed 1° 2θ/min, and a step size of 0.02° 2θ. All peak positions of kaolinite were identified with a commercial software (JADE) and compared to PDF#14-0164 (JCPDS, 1993), while PDF#33-1161 was used to check the peak positions of quartz. It should be pointed out that the background of peaks was determined manually with the help of JADE to calculate all net peak intensities.

Environmental Scanning Electron Microscope

To investigate the mechanism by which RTS method reduces preferred orientation, the sharp edge of a razor blade was examined microscopically by using an FEI/Philips XL30 FEG environmental scanning electron microscope (ESEM). The micrographs were obtained by both back-scattered electrons and secondary electrons and the dimension of the blade edge was measurement under ESEM.

RESULTS AND DISCUSSION

Sample Packing Density

As shown in Tables 1 and 2, compared to other sample loading methods, the RTS method always produces a powder mount with the smallest packing density for the four different kaolinites and a quartz powder, while front-loading gives the highest packing density. For example, the density of the powder mount by front-loading is 2.5 times greater than that by RTS method for Peerless#2 and 2 times larger for quartz. It is obvious that as the powder is compressed from one direction, the platy-shaped clay particles tend to orientate perpendicular to the compression direction. The more the powder is compressed, the higher degree of orientation the particles have. Therefore, the packing density of the powder mount is an indirect indicator for preferred orientation. As a result, the RTS method gives minimum preferred orientation in a powder mount.

Evaluation of Orientation

The diffraction patterns for the four kaolinites and a quartz powder are presented in Figures 4 and 5. Since the sample surface is aligned on the diffractometer axis, there is no detectable difference in peak positions among different methods. Notice the difference in peak intensities. Table 1 summarizes all orientation indexes of the four kaolinites together with these estimated from publications in literature.

First, it is noticed that the kaolinites OIs, I(002)/I(020), I(002)/I(060), and I(001)/I(060), have the smallest values by the RTS method for all four different kaolinites. The only exception is that for KGa-2, I(002)/I(060) gives almost the same values for both RTS method (3.67) and side-loading (3.66). The reason is that KGa-2 which is a poor-crystallized kaolinite tends to have less preferred orientation.

Table 1 also gives the measured crystallinity index (CI) proposed for kaolinites by Hinckley (1963). It appears that the CI of each kaolinite is relatively independent on sample loading technique. However, as CI decreases from Grim Calibration (CI=1.22) to KGa-2 (CI=0.16), OI generally decreases. This is consistent with the results shown by Brindley & Kurtossy (1961). Peerless #2 (CI=0.77) is the exception which may be attributed to the effect of particle size. Moreover, for each kaolinite, the difference in OI between the RTS method and others (side-loading and back-loading) increases with increasing CI. Hence, the RTS method reduces the preferred orientation more effectively for well-crystallized minerals. It also indicates that back-loading and side-loading do not effectively reduce the preferred orientation of well-crystallized kaolinites.

Just for comparison, Table 1 also shows that OI=14.16 of Peerless#2 obtained by front-loading is nearly 5 times higher than other loading methods. It is well known that the pressed powder will produce a large degree of preferred orientation for platy particles.

In an attempt to provide independent verification, the new method is compared to published data. Table 1 also lists OI estimated from the published diffraction patterns in the literature for the two source clays KGa-1b (or KGa-1) and KGa-2. For KGa-1b (or KGa-1), the RTS method has a minimum I(002)/I(020)=2.12, compared to OI by side-loading (2.67 for particles <44μm, Pruett & Webb, 1993) and OI by freeze-drying (3.73, Wang *et al.*, 1998). For KGa-2, RTS method gives I(002)/I(020)=1.95, while spray-drying (Hillier, 1999) gave 1.86. However, since the latter was obtained from a 1:1 mixture of KGa-2 and corundum which is used as a non-orientating filler material to reduce preferred orientation of clay particles, the reduction of orientation by corundum needs to be separated out of the effect of spray-drying. Nevertheless, the RTS method gives OI much closer to 1.86.

Though Brindley & Kurtossy (1961) gave the calculated OI for kaolinite as I(001)/I(060)=3.90, which is greater than that of KGa-1b (3.51) and KGa-2 (3.80) obtained by the RTS method, and I(002)/I(060)=2.12, which is smaller than that obtained by the RTS method, they also pointed out that "the importance of the calculated ratios must not be over-exaggerated". In fact, the structure of kaolinites is highly complex as a

result of the large number of stacking defects introduced during crystal growth or formation. Therefore, a single calculated diffraction pattern based on the ideal structure is not representative to all kaolinites with different structural disorder and particle size.

Table 2 lists the results for quartz. The ratio of I(100)/I(101) decreases from 0.271 obtained by the RTS method to 0.181 by oriented thin aggregates. Definitely, if the quartz powder tends to have preferred orientation, the highest degree of orientation must exist in the thin layer of aggregates sedimented onto a glass slide from dilute suspension. This also means that the RTS method has the highest reduction of the preferred orientation. Moreover, the orientation index I(100)/I(101) decreases monotonically for all methods listed in Table 2. This agrees with the general belief that side-loading is better than back-loading which in turn is better than front-loading. The difference of OI I(100)/I(101) between this quartz powder and PDF#33-1161 may be attributed to the different origin and particle size distribution of this quartz powder.

Discussion of the Method

To assess the reproducibility of the RTS method, 10 random powder mounts were prepared using KGa-1b. Their statistical data on OI and density is shown in Table 3. The standard deviation for density and OI is small.

To help explain the experimental results, the shape and width of the sharp edge of the razor blade was measured under ESEM (Figure 6). Careful measurement under

ESEM gives the edge tip a thickness of 0.5μm, though theoretically it has a zero thickness. A typical kaolinite particle has size ranging from 0.1 to 4 μm. When the sharp edge is compressing a platy clay particle with diameter greater than the tip of the blade edge, the particle will not move vertically and will not orientate perpendicular to the compressing direction. Therefore, the sharp razor tip is capable of causing rotation of platy clay particles. Just for comparison, imagine a tool having a flat surface and dimension much greater than the size of the particles, then all particles tend to orientate parallel to the surface of the compressing tool. Smaller clay particles with size <0.5μm have less tendency to develop preferred orientation (Bish & Reynolds, 1989).

With respect to the surface of powder mount and compaction direction caused by razor tamping, the tip of razor blade introduces complex localized two dimensional particle motion (Figure 7), resulting various compaction directions around the blade tip and hence a significant reworking of the surface of powder mount. Since the powder is first packed randomly by tamping along various directions with a blade, a theoretically true random orientation is produced in the sample powder mount.

In addition to improving random orientation in a powder mount, the RTS method solves several practical problems encountered by side-loading. They are listed as follows: First of all, RTS method is simple and requires no special pretreatment of the sample powder and equipment. No special practice is required to be familiar with the technique. Indeed, the powder mount prepared by RTS method has repeatable packing density even

for different operators since the powder can't be compressed further when the blade hits the surface of the aluminum holder. However, it requires some practice to control the packing effort for side-loading, as pointed out by Moore & Reynolds (1997). Different compressing force results in different packing density. Moreover, if the powder is compressed too hard, the surface of the powder may bulge upward after the glass slide is removed, making it impossible to align a flat surface with the diffractometer axis.

RTS method gives more homogeneous density than side-loading in a powder mount. Generally the bottom part of the powder prepared by side-loading is looser than the upper part due to side friction. If the powder is packed up with one layer, the density is not homogeneous at all. This defect can't be eliminated even if the powder is side packed with several layers. Furthermore, based on the authors' experience, it is very difficult to obtain a powder mount with smooth surface if it is side packed up with several layers. When the cover glass is removed, the contact surface between adjacent layers tends to lose some particles, which becomes more severe for loose-packed powder.

As the shape of the cavity in the sample holder is considered, RTS method has more flexibility than side-loading. A rectangular cavity is required by side-loading, while RTS method can pack the powder into a cavity with any shape.

Though particles in a side-loaded powder mount do not orientate parallel to the holder surface, they have a significant preferred orientation perpendicular to the side-packing direction. Therefore, reflections from certain plane may have excessively high intensity.

One major disadvantage for RTS method is that the powder is very loose and hence is not very stable in a diffractometer with vertical axis. However, with the modified sample holder shown in Figure 1, this problem can be eliminated if care is taken to prevent any shaking or disturbance to the powder mount before examination.

CONCLUSIONS

The novel RTS method for making a random powder mount for XRD analysis was evaluated by comparison with other mounting methods, published data, and theoretical values. Orientation indices indicate that a minimum preferred orientation and a minimum packing density exist in the powder prepared by this method. Experimental results also show that the RTS method has a very good reproducibility and is more effective in reducing preferred orientation for well-crystallized and large platy particles than those poor-crystallized and small particles. Furthermore, the modified sample holder can be used in a diffractometer with vertical axis even the sample powder is loosely packed. The results also show that the quartz powder used in this study has tendency for preferred orientation, as exhibited by the difference of orientation index I(001)/I(101) between oriented aggregates and random powder by various methods. Moreover, it proves that RTS method is also effective to minimize preferred orientation in a powder with less tendency for preferred orientation, such as quartz.

As pointed out by Brindley (1980), a near-random orientation can be achieved, but strictly random orientation is probably unattainable in practice. It is clear that the RTS method produces less preferred orientation than side-loading, which was claimed by Brindley (1980, p.427) as "the side-packed holder is probably the best simple technique to use". Therefore, RTS method should be considered as a significant improvement toward perfect randomness from side-loading, as far as the randomness and other advantages are concerned.

ACKNOWLEDGEMENTS

This study was supported by the KKZ/CMA Consortium in conjunction with the underground construction of Tren Urbano in Rio Piedras, Puerto Rico. The Shared Experimental Facility (SEF), sponsored by NSF, in the Center for Materials Science and Engineering (CMSE) at MIT is gratefully acknowledged for use of XRD and ESEM equipment.

REFERENCES

Aparicio, P. and Galan, E. (1999) Mineralogical interference on kaolinite crystallinity index measurements. *Clays and Clay Minerals*, 47, 12-27.

Artioli, G., Bellotto, M., Gualtieri, A., and Pavese, A. (1995) Nature of structural disorder in natural kaolinites: a new model based on computer simulation of powder diffraction data and electrostatic energy calculation. *Clays and Clay Minerals*, 43, 438-445.

Barwood, H.L. (2000) Personal communication

Bish, D.L. and Reynolds, R.C. Jr. (1989) Sample preparation for x-ray diffraction. In *Modern Powder Diffraction,* D.L. Bish and J.E. Post, eds., Reviews in Mineralogy, Mineralogical Society of America, 20, 73-99.

Brindley, G.W. (1980) Quantitative x-ray mineral analysis of clays. In *Crystal Structure of Clay Minerals and Their X-Ray Identification*, G.W. Brindley and G. Brown, eds., Mineralogical Society Monograph No. 5, Mineralogical Society, London, 411-438.

Brindley, G.W. and Kurtossy, S.S. (1961) Quantitative determination of kaolinite by x-ray diffraction. *The American Mineralogist*, 46, 1205-1215.

Brindley, G.W. and Kurtossy, S.S. (1962) Quantitative determination of kaolinite by x-ray diffraction, a reply to H.W. Van der Marel. *The American Mineralogist*, 47, 1213-1215.

Brindley, G.W., Kao, C., Harrison, J.L., Lipsicas, M., and Raythatha, R. (1986) Relation between structural disorder and other characteristics of kaolinites and dickites. *Clays and Clay Minerals*, 34, 239-249.

Brown, G. and Brindley, G.W. (1980) X-ray diffraction procedures for clay mineral identification. In *Crystal Structures of Clay Minerals and Their X-Ray Identification*, G.W. Brindley and G. Brown, eds., Mineralogical Society Monograph No. 5, Mineralogical Society, London, 305-359.

Calvert, L.D. and Sirianni, A.F. (1980) A technique for controlling preferred orientation in powder diffraction samples. *Journal of Applied Crystallography*, 13, 462.

Calvert, L.D., Sirianni, A.F., and Gainsford, G.J. (1982) A comparison of methods for reducing preferred orientation. *Advances in X-ray Analysis*, 26, 105-110.

Dollase, W.A. (1986) Correction of intensities for preferred orientation in powder diffractometry: application of the March model. *Journal of Applied Crystallography*, 19, 267-272.

Eslinger, E.V., Mayer, L.M., Durst, T.L., Hower, J., and Savin, S.M. (1973) An x-ray technique for distinguishing between detrital and secondary quartz in the fine-grained fraction of sedimentary rocks. *Journal of Sedimentary Petrology*, 43, 504-543.

Hillier, S. (1999) Use of an air brush to spray dry samples for x-ray powder diffraction. *Clay Minerals*, 34, 127-135.

Hinckley, D.N. (1963) Variability in "crystallinity" values among the kaolin deposits of the coastal plain of Georgia and South Carolina. *Clays and Clay Minerals*, 11, 229-235.

JCPDS (1993) *Mineral Powder Diffraction File Databook.* Joint Committee on Powder Diffraction Standards, Swarthmore, PA.

Jenkins, R., Fawcett, T.G., Smith, D.K., Visser, J.W., Morris, M.C., and Frevel, L.K. (1986) Sample preparation methods in x-ray powder diffraction. *Powder Diffraction*, 1.

Jonas, E.C. and Kuykendall, J.R. (1966) Preparation of montmorillonites for random powder diffraction. *Clay Minerals*, 6, 232-235.

Krinsley, D.H. and Smalley, I.J. (1973) Shape and nature of small sedimentary quartz particles. *Science*, 180, 127-129.

Klug, H.P. and Alexander, L.E. (1974) *X-Ray Diffraction Procedures.* 2nd Edition. John Wiley & Sons.

Lambe, T.W. and Whitman, R.V. (1969) *Soil Mechanics.* John Wiley & Sons.

McCreery, G.L. (1949) Journal of American ceramic society, 32, 141.

McMurdie, H.F., Morris, M.C., Evans, E.H., Paretzkin, B., Wong-Ng, W., and Hubbard, C.R. (1986) Methods of producing standard x-ray diffraction powder patterns. *Powder Diffraction*, 1.

Mitchell, J.K. (1993) *Fundamentals of Soil Behavior.* 2nd Edition. John Wiley & Sons.

Moore, D.M. and Reynolds, R.C., Jr. (1997) *X-Ray Diffraction and the Identification and Analysis of Clay Minerals.* 2nd Edition, Oxford University Press, 378 pp.

Paterson, E., Bunch, J.L., and Duthie, D.M.L. (1986) Preparation of randomly-oriented samples for x-ray diffractometry. *Clay Minerals*, 21, 101-106.

Pruett, R.J. and Webb, H.L. (1993) Sampling and analysis of KGa-1b well-crystallized kaolin source clay. *Clays and Clay Minerals*, 41, 514-519.

Taylor, R.M. and Norrish, K. (1966) The measurement of orientation distribution and its application to quantitative x-ray diffraction analysis. *Clay Minerals*, 6, 127-142.

Wang, W., Yeh, H., Chen, P., and Wang, M. (1998) Kaolin mineralogy of clays in paleosol profiles on the late-miocene sediments in Penghu Islands (Pescadores), Taiwan. *Clays and Clay Minerals*, 46, 1-9.

Wilson, M.J. (1987) X-ray powder diffraction methods. In *A Handbook of Determinative Methods in Clay Mineralogy*, M.J. Wilson, ed., Blackie & Son Limited.

Table 1. Orientation indexes for 4 kaolinites obtained by different mounting methods.

Kaolinite Sample	Mounting Method	Packing Density [g/cm^3]	Orientation Indexes			Crystallinity Index (CI)
			I(002)/I(020)	I(002)/I(060)	I(001)/I(060)	
Grim Calibration	RTS method	0.19	2.44	5.07	6.32	1.22
	Side-loading	0.64	3.29	5.53	6.63	1.30
	Back-loading	0.76	3.96	6.55	7.06	1.31
KGa-1b	RTS method	0.45	2.12	3.38	3.51	0.94
	Side-loading	0.55	2.15	3.56	3.97	0.94
	Back-loading	0.64	2.15	3.65	3.76	0.95
	Side-loading[1]		2.67	4.36	4.55	1.09
KGa-1	Side-loading[1]		4.48	6.28	8.57	1.03
	Freeze-drying[2]		3.73			1.11
Peerless #2	RTS method	0.37	2.79	4.72	5.47	0.77
	Side-loading	0.67	2.88	4.77	5.62	0.75
	Back-loading	0.67	3.15	5.53	5.81	0.73
	Front-loading	0.96	14.16			0.64
KGa-2	RTS method	0.34	1.95	3.67	3.80	0.16
	Side-loading	0.41	2.00	3.66	4.00	0.15
	Back-laoding	0.48	2.08	3.79	3.97	0.18
	Side-loading[3]		2.36			
	Side-loading[4]		2.36			
	Freeze-drying[5]		3.02			
	Spray-drying[5]		1.86			

[1] Pruett and Webb (1993), for <44μm fraction; [2] Wang *et al* (1998); [3] Artioli *et al.* (1995); [4] Aparicio & Galan (1999) (may not be KGa-2); [5] Hillier (1999).

Table 2. Orientation Index for quartz.

Mounting Method	Packing Density [g/cm3]	Orientation Index I(100)/I(101)
RTS method	0.73	0.271
Side-loading	0.97	0.268
Back-loading	1.15	0.257
Front-loading (pressed)	1.35	0.256
Oriented aggregate (thick)		0.228
Oriented aggregate (thin)		0.181
PDF#33-1161		0.22
PDF#5-490*		0.35

*This old file has been replaced by PDF#33-1161

Table 3. Orientation indices and packing density of KGa-1b by the RTS method

Test No.	Density [g/cm^3]	Net peak intensity [counts]				Orientation indices		
		I(001)	I(002)	I(020)	I(060)	I(002)/I(020)	I(002)/I(060)	I(001)/I(060)
1*	0.514	22582	21740	10249	6425	2.121	3.384	3.515
2	0.512	21199	20986	9804	6110	2.141	3.435	3.470
3	0.489	20526	20514	6591	5911	2.139	3.470	3.473
4	0.480	21258	20609	9695	6074	2.126	3.393	3.500
5	0.462	20865	20528	9635	5753	2.131	3.568	3.627
6	0.450	21106	19871	9440	5911	2.105	3.362	3.571
7	0.450	20672	19861	9380	5637	2.117	3.523	3.667
8	0.515	21510	20310	9576	5976	2.121	3.399	3.599
9	0.544	21395	20794	9718	6020	2.140	3.454	3.554
10	0.549	21506	20752	9821	6212	2.113	3.341	3.462
Mean	0.496					2.125	3.433	3.544
S.D.	0.0361					0.012	0.072	0.072

* Test No.1 was performed 6 months before Test No.2-10.

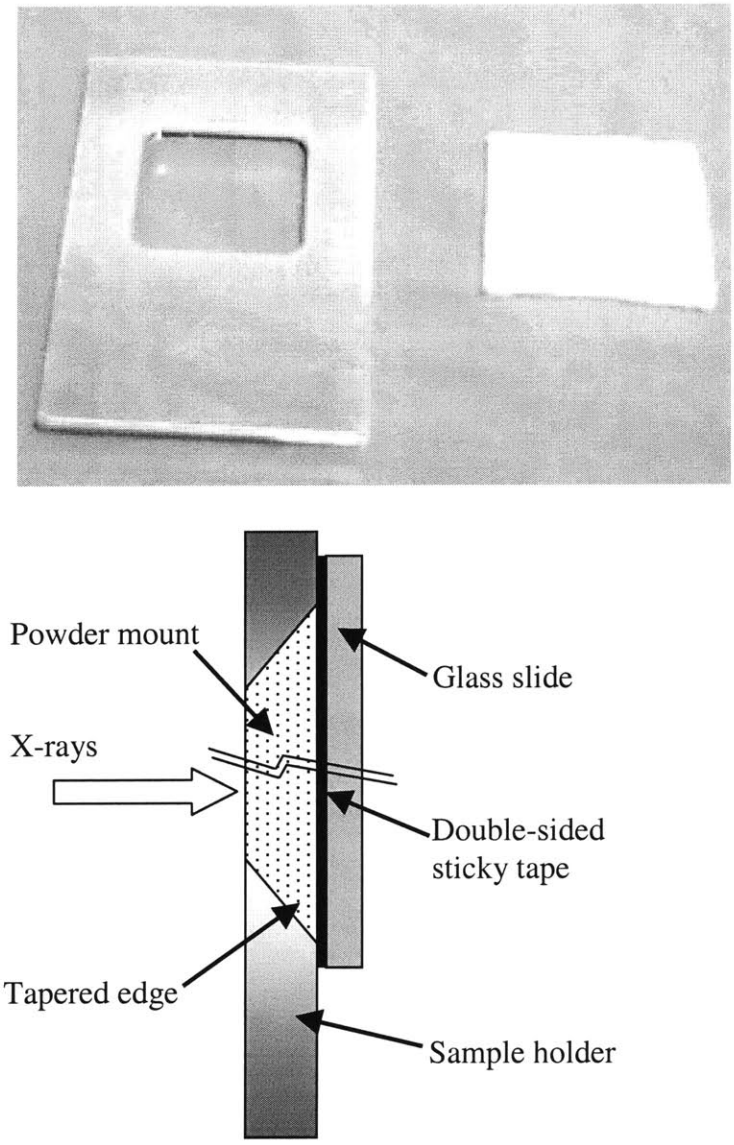

Figure 1. The modified sample holder (not to scale).

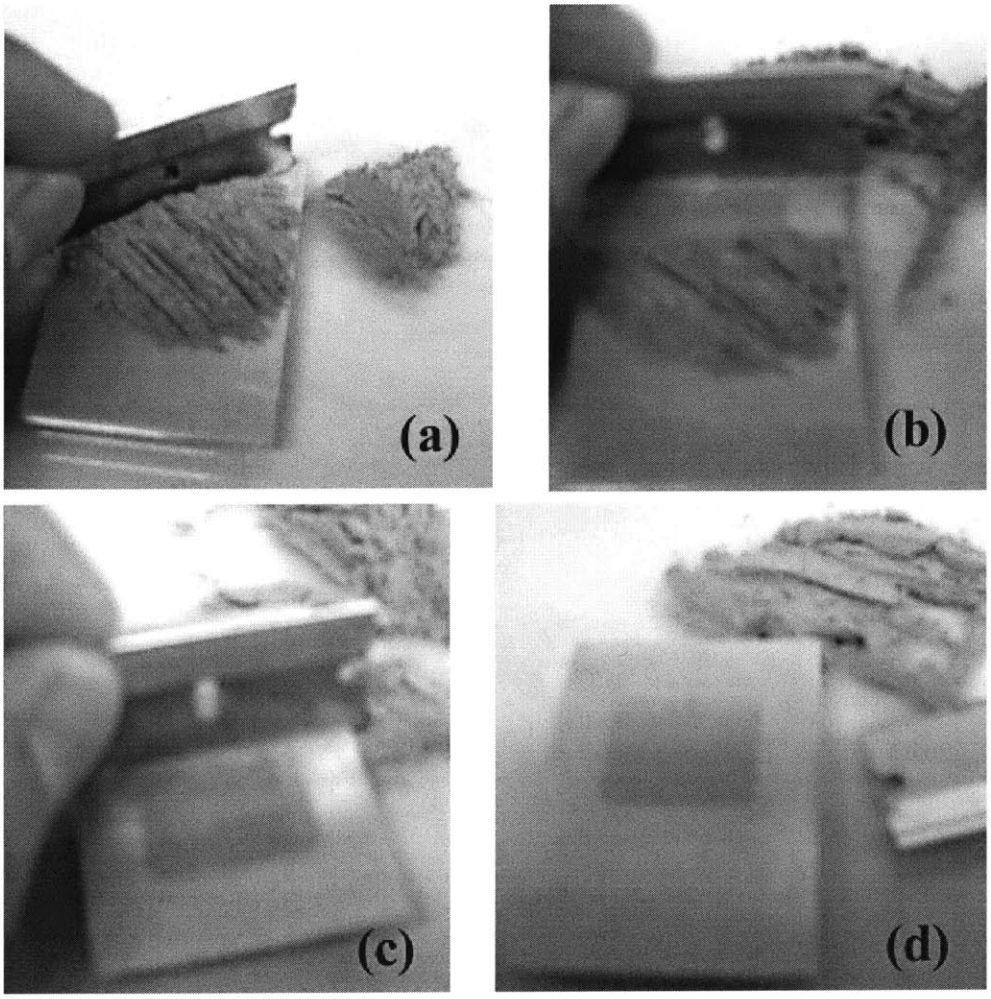

Figure 2. Procedures of the RTS method to make a random powder mount.

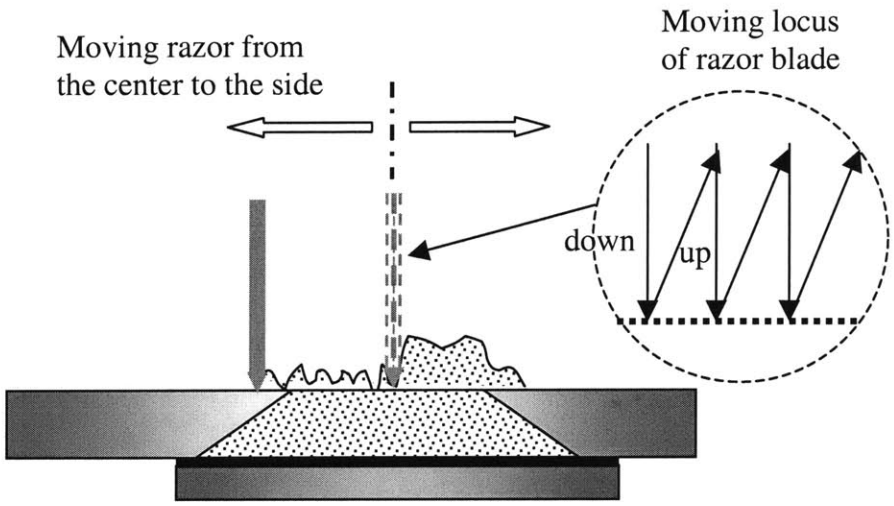

Figure 3. Moving direction and locus of the razor blade during tamping to remove the excess powder (not to scale).

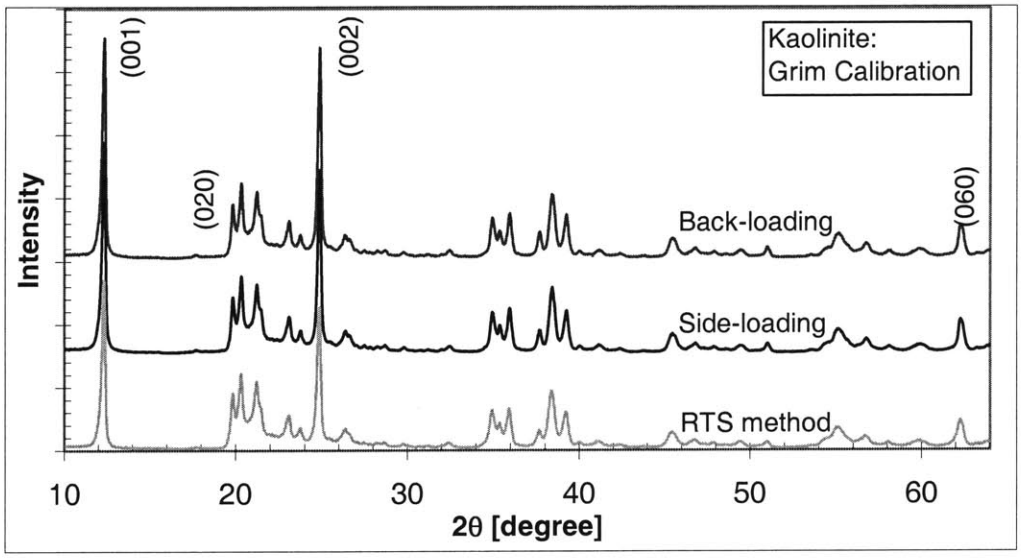
Kaolinite:
Grim Calibration
(001)
(002)
(020)
(060)
Back-loading
Side-loading
RTS method
Intensity
10
20
30
40
50
60
2θ [degree]

(a)

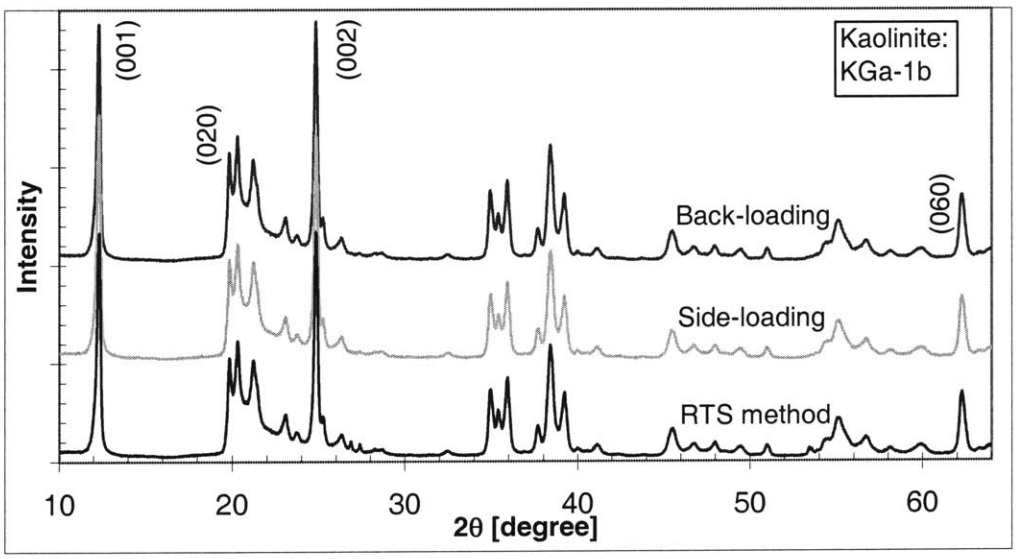
Kaolinite:
KGa-1b
(001)
(002)
(020)
(060)
Back-loading
Side-loading
RTS method
Intensity
10
20
30
40
50
60
2θ [degree]

(b)

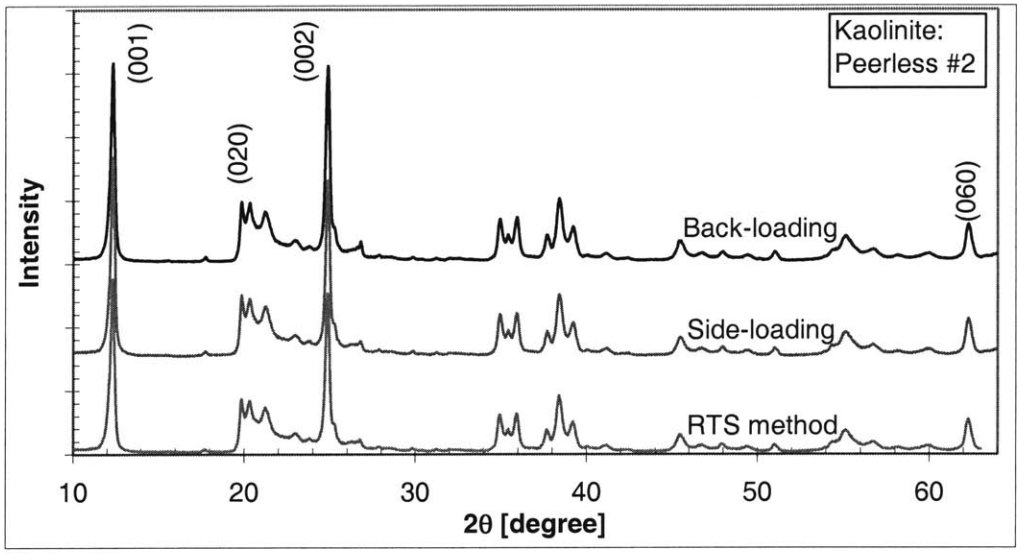
Kaolinite:
Peerless #2
(001)
(020)
(002)
(060)
Back-loading
Side-loading
RTS method
Intensity
10
20
30
40
50
60
2θ [degree]

(c)

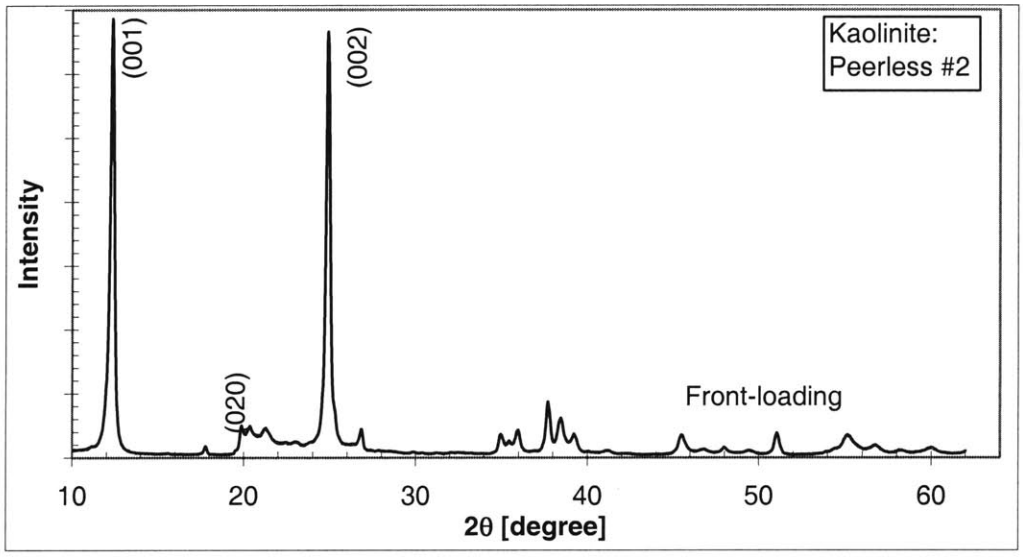
Kaolinite:
Peerless #2
(001)
(020)
(002)
Front-loading
Intensity
10
20
30
40
50
60
2θ [degree]

(d)

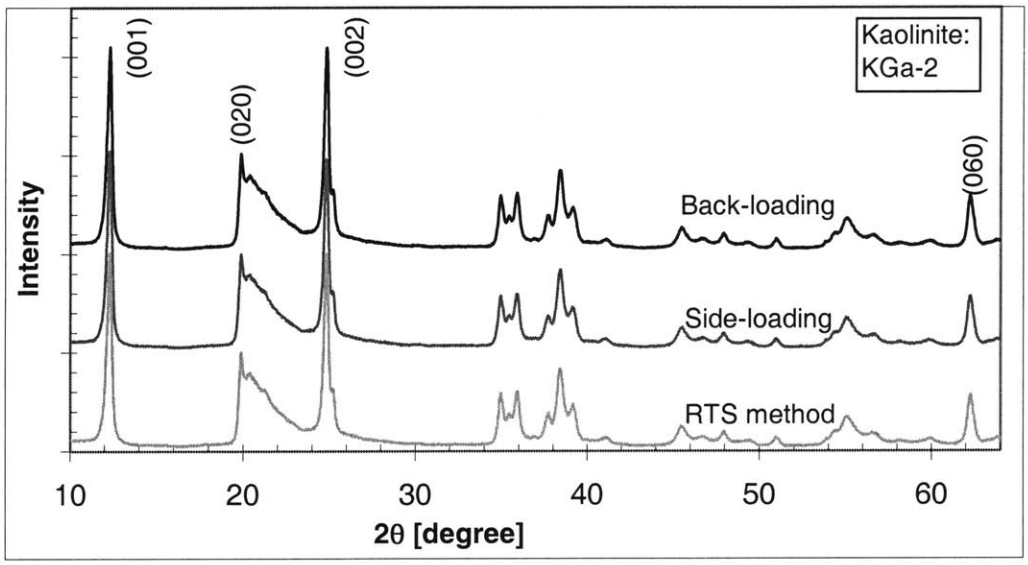

(e)

Figure 4. Diffraction patterns for 4 kaolinites packed by different methods.

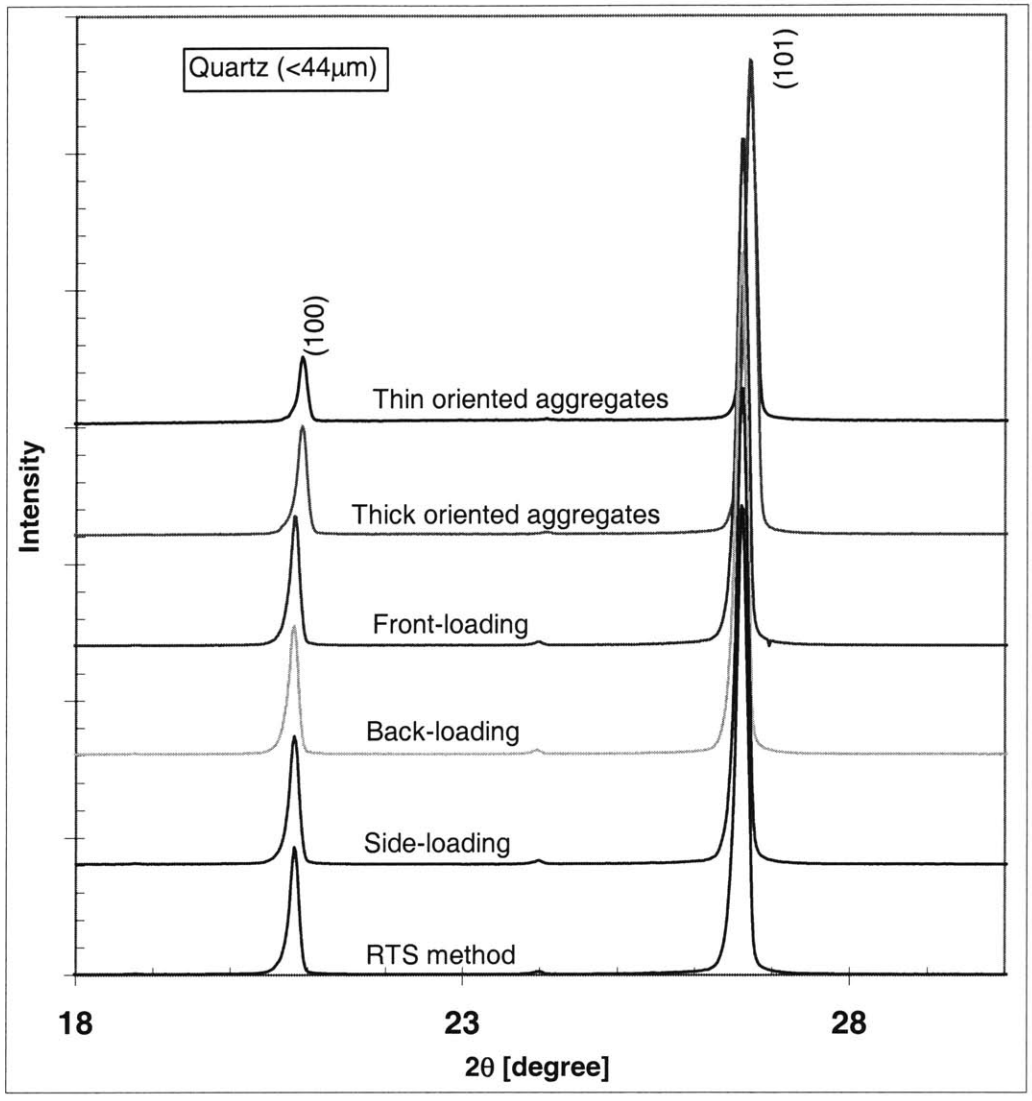

Figure 5. Diffraction patterns of quartz powder prepared by different methods.

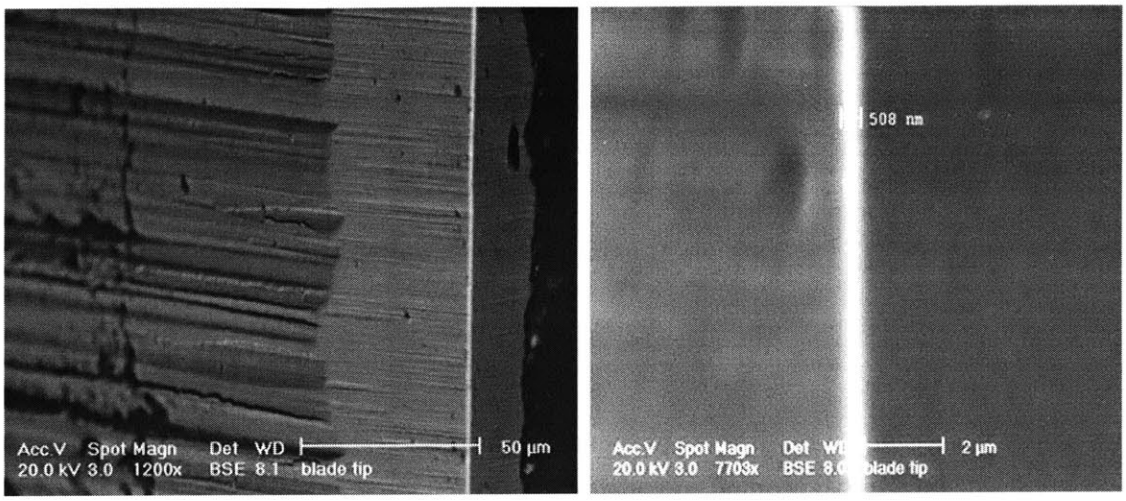

Figure 6. Electron micrographs of the sharp edge of the razor blade.

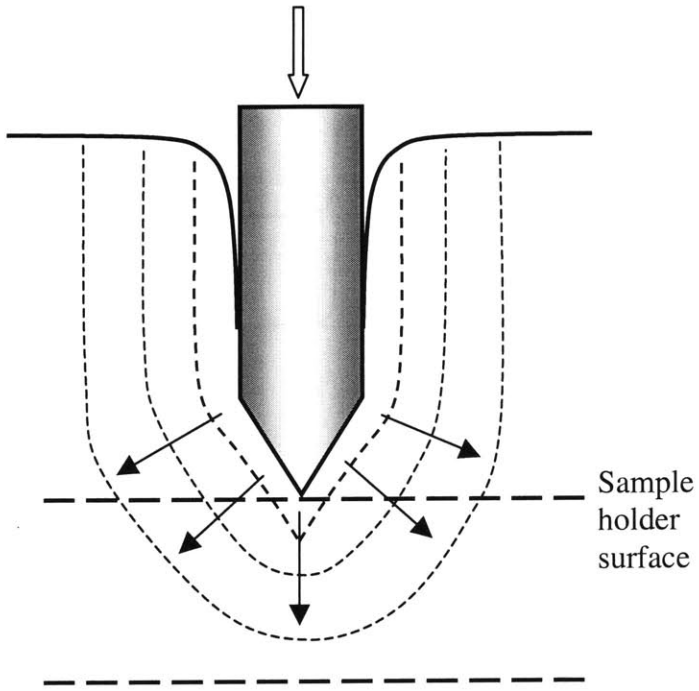

Figure 7. Compaction directions caused by the sharp edge of a razor blade.